

**Interfacial Water Organization and Ion Distributions Investigated with Vibrational
Sum Frequency Spectroscopy: Answering Fundamental Questions for
Environmental Chemistry**

DISSERTATION

Presented in Partial Fulfillment of the Requirements for the Degree Doctor of Philosophy
in the Graduate School of The Ohio State University

By

Wei Hua

Graduate Program in Environmental Science

The Ohio State University

2013

Dissertation Committee:

Professor Heather C. Allen, Advisor

Professor Anne E. Carey

Professor Barbara E. Wyslouzil

Professor Lingying Zhao

Copyrighted by

Wei Hua

2013

Abstract

Knowledge of interfacial water organization and ion distributions is necessary to elucidate questions regarding atmospheric aerosol chemistry, thundercloud electrification, geochemistry, and ocean surface processes, among others. Water organization at air/aqueous interfaces is strongly influenced by inorganic ions, specifically, ion distributions that exist in the interfacial region, where the molecular environment changes from three-dimensions to two-dimensions. Over the past century, the study of water has been a major focus of experimental and theoretical work. Although much progress has been made, interfacial water behavior and ion distributions are still incompletely understood.

Here, interface-specific nonlinear optical spectroscopies, conventional vibrational sum frequency generation (VSFG) and heterodyne-detected vibrational sum frequency generation (HD-VSFG), are employed to probe interfacial water molecules at the molecular level. HD-VSFG spectroscopy allows for direct interrogation of the average orientation of the transition dipole moment of interfacial water molecules that is intrinsically contained in the sign of the second-order nonlinear susceptibility, $\chi^{(2)}$. The water organization and ion distributions at air/aqueous interfaces of inorganic salt solutions are inferred from $\text{Im } \chi^{(2)}$ spectra obtained by HD-VSFG spectroscopy.

It is shown here that salt purity grade and/or pretreatment have a tremendous impact on the interfacial water spectrum of aqueous salt solutions. It is determined that the presence of trace organic contamination is primarily responsible for spectral distortion for the bare air/ aqueous interfaces of salt solutions while the presence of trace polyvalent cations proves to be critical in exploring the alkali cation-carboxylate binding and comparing relative binding affinity of different cations at the air/aqueous surfactant interfaces. A standard pretreatment procedure for inorganic salts and their solutions is established for VSFG spectroscopy via a series of systematic studies.

Results indicate that the ion-induced interfacial electric field is in the opposite direction for solutions containing sulfate and carbonate salts relative to solutions of chloride, nitrate and perchlorate salts. It is found that bicarbonate and its counterion do not significantly perturb the interfacial water organization. These findings are attributed to charge separation, or lack thereof, arising from ion distributions within the air/aqueous interfaces tested. It is also suggested that the cation identity (lithium, sodium, ammonium, magnesium) as well as the concentration changes result in the partial reversal of the net direction of the interfacial electric field in the nitrate salt solutions.

These findings have great significance for understanding the differences observed in aerosol reactivity as a function of aerosol salt composition. In addition, we now have a better understanding of cloud droplet electrification and ocean surface properties. Moreover, a fundamental appreciation of ions at aqueous surfaces has been gained such that we now know that monovalent anions exist in the interfacial region and on average above their counterions. However, high valency anions exist below their counter cations,

causing a reversal in electric field direction. Although various specific ion properties such as polarizability, size, charge (surface charge density), geometry (shape) have been suggested to account for interfacial ion distribution, it is indicated here that charge effect exerts a greater impact than the other factors in the case of oxyanions.

This dissertation is dedicated to my parents

谨以此文献给我的父亲母亲

Acknowledgments

First and foremost, I am greatly indebted to my advisor, Prof. Heather C. Allen, for her continuous support and mentorship in the past five years. Her integrity and enthusiasm in science as well as her optimism and diligence in life are the qualities that I hope to cultivate in my future endeavors. I would like to show my appreciation to Profs. Yuen-Ron Shen and Mary J. Shultz for their inspirational comments and encouragement. I would like to thank the Dale Fay Fellowship provided by Environmental Science Graduate Program and the Presidential Fellowship provided by The Ohio State University. I would also sincerely acknowledge Dr. Xiangke Cheng, Dr. Cheng Y. Tang and Zishuai Huang for their generous help in both research and life. I would also express my gratitude to Dr. Dominique Verreault and Dr. Aaron M. Jubb for their illuminating scientific discussions and remarkable efforts made during our collaboration. Special thanks to Dr. Christine E. Lemon for an enjoyable time in and out of the office during my graduate studies. I would also like to extend my best wishes to previous and current Allen group members and friends. Last, but not least, I would like to dedicate my PhD degree to my parents for their endless love and support throughout my life, in joyful as well as in adverse times. I sincerely wish them a healthy and happy life every day.

Vita

2005.....B.S. Chemistry, Peking University, China

2008.....M.Sc. Environmental Science, Peking
University, China

2008 to 2009Dale Fay Fellowship, Environmental
Science Graduate Program, The Ohio State
University

2009 to 2011Graduate Teaching Associate, Department
of Chemistry and Biochemistry, The Ohio
State University

2011 to 2012Graduate Research Associate, Department
of Chemistry and Biochemistry, The Ohio
State University

2012 to presentPresidential Fellowship, The Ohio State
University

Publications

1. **W. Hua**, D. Verreault, E. M. Adams, Z. Huang, H. C. Allen; Impact of Salt Purity on Interfacial Water Organization Revealed by Conventional and Heterodyne-Detected Vibrational Sum Frequency Generation Spectroscopy, *Journal of Physical Chemistry C*, **2013**, 117, 19577-19585.
2. **W. Hua**, A. M. Jubb, H. C. Allen, Electric Field Reversal of Na₂SO₄, (NH₄)₂SO₄, and Na₂CO₃ relative to CaCl₂ and NaCl at the Air/Aqueous Interface revealed by Phase-Sensitive Sum Frequency, *Journal of Physical Chemistry Letters*, **2011**, 2, 2515-2520.
3. **W. Hua**, X. K. Chen, H. C. Allen; Phase-Sensitive Sum Frequency Revealing Accommodation of Bicarbonate Ions, and Charge Separation of Sodium and Carbonate Ions within the Air/Water Interface, *Journal of Physical Chemistry A*, **2011**, 115, 6233-6238.
4. **W. Hua**, D. Verreault, H. C. Allen; Surface Prevalence of Perchlorate Anions at the Air/Aqueous Interface, *Journal of Physical Chemistry Letters*, **2013**, accepted.
5. X. K. Chen, **W. Hua**, Z. S. Huang, H. C. Allen; Interfacial Water Structure Associated with Phospholipid Membranes Studied by Phase-Sensitive Vibrational Sum Frequency Generation Spectroscopy, *Journal of the American Chemical Society*, **2010**, 132 (32), 11336-11342.

6. A. M. Jubb, **W. Hua**, H. C. Allen; Environmental Chemistry at Vapor/Water Interfaces: Insights from Vibrational Sum Frequency Generation Spectroscopy, *Annual Reviews of Physical Chemistry*, **2012**, 63, 6.1-6.24.
7. A. M. Jubb, **W. Hua**, H. C. Allen, Organization of Water and Atmospherically Relevant Ions and Solutes: Vibrational Sum Frequency Spectroscopy at the Vapor/Liquid and Liquid/Solid Interfaces, *Accounts of Chemical Research*, **2012**, 45(1), 110-119.
8. D. Verreault, **W. Hua**, and H.C. Allen. From Conventional to Phase-Sensitive Vibrational Sum Frequency Generation Spectroscopy: Probing Water Organization at Aqueous Interfaces. *Journal of Physical Chemistry Letters*, **2012**, 3(20), 3012-3028.
9. Z. Huang, **W. Hua**, D. Verreault, H. C. Allen; Influence of Salt Purity on Na⁺ and Palmitic Acid Interactions, *Journal of Physical Chemistry A*, **2013**, accepted.
10. Z. Huang, **W. Hua**, D. Verreault, H. C. Allen; Salty Glycerol versus Salty Water Surface Organization: Bromide and Iodide Surface Propensities, *Journal of Physical Chemistry A*, **2013**, 117, 6346-6353.
11. X. Chen, Z. Huang, **W. Hua**, H. Castada, H. C. Allen; Reorganization and Caging of DPPC, DPPE, DPPG, and DPPS Monolayers Caused by Dimethylsulfoxide Observed Using Brewster Angle Microscopy, *Langmuir*, **2010**, 26 (24), 18902-18908.
12. A. G. F. de Beer, J. S. Samson, **W. Hua**, Z. Huang, X. Chen, H. C. Allen, S. Roke; Direct Comparison of Phase-Sensitive Vibrational Sum Frequency

generation with Maximum Entropy Method: Case Study of Water, *Journal of Chemical Physics*, **2011**, 135, 224701.

Fields of Study

Major Field: Environmental Science

Table of Contents

Abstract	ii
Dedication	v
Acknowledgments.....	vi
Vita.....	vii
Publications	viii
Fields of Study	x
Table of Contents.....	xi
List of Tables	xvi
List of Figures	xvii
Chapter 1 Introduction	1
1.1 Motivation	1
1.2 Dissertation Highlights.....	8
Chapter 2 Vibrational Sum frequency Generation Theory.....	13
2.1 Principle of VSFG Spectroscopy	13
2.2 Heterodyne-Detected VSFG (HD-VSFG)	19

Chapter 3 Instrumentation of Broad Bandwidth VSFG.....	28
3.1 Conventional VSFG Instrumentation.....	28
3.2 HD-VSFG instrumentation	31
3.3 Infrared and Raman Spectroscopy	34
Chapter 4 Heterodyne-Detected Sum Frequency Revealing Accommodation of Bicarbonate Ions, and Charge Separation of Sodium and Carbonate Ions within the Air/Water Interface	38
4.1 Introduction	38
4.2 Experimental	42
4.3 Results and Discussion.....	43
4.4 Conclusions	50
Chapter 5 Electric Field Reversal of Na_2SO_4 , $(\text{NH}_4)_2\text{SO}_4$, and Na_2CO_3 relative to CaCl_2 and NaCl at the Air/Aqueous Interface revealed by Heterodyne-Detected Sum Frequency Spectroscopy	54
5.1 Introduction	54
5.2 Experimental	56
5.3 Results and Discussion.....	57
5.4 Conclusions	62

Chapter 6 Impact of Salt Purity on Water Organization at Bare Air/Aqueous Solution Interfaces and Influence of Salt Purity on the Interactions between Na ⁺ Ions and Carboxylate Headgroup of Palmitic Acid Monolayers.....	68
6.1 Impact of Salt Purity on Interfacial Water Organization at Bare Air/Aqueous Solution Interfaces.....	68
6.1.1 Introduction	68
6.1.2 Experimental.....	70
6.1.3 Results and Discussion	72
6.1.4 Conclusions	80
6.2 Influence of Salt Purity on the Interactions between Na ⁺ Ions and Carboxylate Headgroup of Palmitic Acid Monolayers.....	94
6.2.1 Introduction	94
6.2.2 Experimental.....	95
6.2.3 Results and Discussion	96
6.2.4 Conclusions	100
Chapter 7 Surface Prevalence of Perchlorate Anions at the Air/Aqueous Interface	104
7.1 Introduction	104
7.2 Experimental	107
7.3 Results and Discussion.....	108
7.4 Conclusions.....	115

Chapter 8 Cation Effects on Water Organization at the Air/Aqueous Nitrate Solution	
Interfaces.....	123
8.1 Introduction.....	123
8.2 Experimental.....	127
8.3 Results and Discussion.....	129
8.4 Conclusions.....	141
Chapter 9 Conclusions, and Specific Ion Properties and Potential Driving Forces	
Dictating Interfacial Distributions of Oxyanions (ClO_4^- , NO_3^- , SO_4^{2-} , and CO_3^{2-}).....	154
9.1 Introduction.....	154
9.2 Results and Discussion.....	156
9.2.1 Surface Propensity of Oxyanions Inferred from HD-VSFG spectra.....	156
9.2.2 Hofmeister Series and Driving Forces for Oxyanions.....	158
9.2.3 Examination of Specific Ion Properties.....	165
9.3 Conclusions.....	170
Chapter 10 Implications and Future Work.....	175
10.1 Implications.....	175
10.2 Future Work.....	179
References.....	182
Appendix B Performance Test of the Broad Bandwidth VSFG Spectrometer.....	205

Appendix C Permissions..... 212

List of Tables

Table 6.1 Comparative list of purity of salts used in previously published SHG, conventional VSFG and HD-VSFG studies at the air/solution interface.	91
Table 6.2 Standardized pretreatment procedure for inorganic salts purification.....	93
Table 6.3 Salts with different purities and pretreatment used among research groups in studies of alkali cation-carboxylate interactions.....	103

List of Figures

Figure 2.1 Energy level diagram of the sum frequency generation process. $v = 0$ is the ground state, $v = 1$ is a vibrationally excited state, and dash line indicates a virtual state.	26
Figure 2.2 Schematic of the reflected VSG signal generated at the air/aqueous solution interfaces.	26
Figure 2.3 Upper panel: Raw interferogram of z-cut quartz with GaAs. Middle panel: Time domain real (black) and imaginary (red) signals. The cross term at ~ 2.6 ps (ΔT) is extracted to yield the heterodyne frequency spectra. Lower panel: Real (black) and imaginary (red) parts of heterodyne frequency spectra of z-cut quartz with GaAs. Phase information (φ) is therefore obtained.	27
Figure 3.1 Schematic of the heterodyne-detected PS-SFG optical configuration. Filters and polarizer denote two short-pass filters, a notch filter (770~805 nm filtered out), and a Glan-Thompson polarizer respectively from left to right. The first short-pass filter has a cutoff ~ 770 nm and the second is a 785 nm Razor Edge ultrastep short-pass edge filter.	36
Figure 3.2 Reproducibility testing: $\text{Im } \chi^{(2)}$ spectra of neat water, 1.1 M Na_2CO_3 , 1.8 M CaCl_2 and NaCl salt solutions measured on different days.	37

Figure 4.1 HD-VSFG and conventional VSFG spectra of neat water. $\text{Im } \chi^{(2)}$ VSFG spectra (bottom panel), deduced power spectrum (middle panel), conventional VSFG spectra (top panel). The inset in the top panel is full conventional VSFG spectrum from 3000 to 3800 cm^{-1} 51

Figure 4.2 HD-VSFG and conventional VSFG spectra of water molecules at different vapor/aqueous salts solution interfaces: a) 1.1 M Na_2CO_3 , b) 0.8 M NaHCO_3 salt solution. $\text{Im } \chi^{(2)}$ SFG spectra (bottom panel), deduced power spectrum (middle panel), conventional VSFG spectra (top panel). Neat water spectra are shown as a reference (black circles). The insets in the top panels are conventional VSFG spectra showing the full 3000 to 3800 cm^{-1} region..... 52

Figure 4.3 Illustration of water orientation at the air/aqueous salt solution interface of (a) 1.1 M Na_2CO_3 and (b) 0.8 M NaHCO_3 . Carbon and oxygen in carbonate and bicarbonate ions are bluish-gray and yellow spheres respectively, while sodium ions are green..... 53

Figure 5.1 Conventional VSFG $|\chi^{(2)}|^2$ and HD-VSFG $\text{Im } \chi^{(2)}$ spectra of water molecules at vapor/aqueous solution interfaces of 1.8 M CaCl_2 and 1.8 M NaCl salt solutions. a) $|\chi^{(2)}|^2$ spectra of full 3000 to 3800 cm^{-1} region (top panel), b) $\text{Im } \chi^{(2)}$ spectra (bottom panel). Neat water spectra are shown as a reference (light grey line). 63

Figure 5.2 Conventional VSFG $|\chi^{(2)}|^2$ and HD-VSFG $\text{Im } \chi^{(2)}$ spectra of water molecules at vapor/aqueous solution interfaces of 1.1 M Na_2CO_3 , 1.1 M Na_2SO_4 , and 1.1 M $(\text{NH}_4)_2\text{SO}_4$ salt solutions. a) $|\chi^{(2)}|^2$ spectra of full 3000 to 3800 cm^{-1} region (top panel),

b) Im $\chi^{(2)}$ spectra (bottom panel) to 3500 cm^{-1} . Neat water spectra are shown as a reference (light grey line).....	64
Figure 5.3 HD-VSFG Re $\chi^{(2)}$ spectra of water molecules at vapor/aqueous solution interfaces of neat water, 1.8 M CaCl_2 , 1.8 M NaCl , 1.1 M Na_2CO_3 , 1.1 M Na_2SO_4 , and 1.1 M $(\text{NH}_4)_2\text{SO}_4$ salt solutions.	65
Figure 5.4 Difference HD-VSFG Im $\chi^{(2)}$ spectra (Im $\chi^{(2)}$ salt spectrum minus Im $\chi^{(2)}$ water spectrum) for the indicated salts. These spectra represent qualitative differences between the Im $\chi^{(2)}$ solution spectra and neat water's Im $\chi^{(2)}$ response.	66
Figure 5.5 Illustration of water orientation at the air/aqueous salt solution interface of (a) 1.8 M CaCl_2 and (b) 1.1 M Na_2SO_4 solutions.....	67
Figure 6.1 (a) Raman spectra of 0.4 M, 0.7 M, 1.0 M, 1.3 M, 1.6 M Na_2SO_4 , as well as ACS and UP grade pretreated Na_2SO_4 stock solutions, (b) Calibration curve of Na_2SO_4 solutions using the height of the vibrational symmetric stretch ion mode of each individual Raman spectrum. The concentrations of other sulfate, carbonate, and nitrate stock solutions were determined in the same manner.....	82
Figure 6.2 Conventional VSFG spectra in the CH stretching region (2800–3000 cm^{-1}) of neat water and all stock salt solutions studied after filtering 2 to 4 times.	83
Figure 6.3 Stability of SFG system shown by the GaAs profile, conventional VSFG and HD-VSFG Im $\chi^{(2)}$ spectra of neat water in the OH stretching region (3000–3800 cm^{-1}). (a) GaAs profile and (b) conventional VSFG spectra in the OH stretching region, and (c) Im $\chi^{(2)}$ spectra in the OH stretching region from 3000 to 3600 cm^{-1}	84

Figure 6.4 Deduced power spectra $|\chi^{(2)}|^2$ from HD-VSFG results of ACS and UP grade salt solutions in the OH stretching region (3000–3600 cm^{-1}). (a) 1 M Na_2CO_3 , (b) 1 M Na_2SO_4 , (c) 1 M $(\text{NH}_4)_2\text{SO}_4$, and (d) comparison of all 1 M salt solutions. Neat water spectra are shown as reference..... 85

Figure 6.5 Comparison between conventional VSFG spectra from ACS and UP grade salt solutions in the OH stretching region (3000–3800 cm^{-1}) after pretreatment. (a) 1 M Na_2CO_3 , (b) 1 M Na_2SO_4 , (c) 1 M $(\text{NH}_4)_2\text{SO}_4$, and (d) 1.5 M NaCl . The VSFG spectrum of neat water is also shown as reference by a grey line. 86

Figure 6.6 Conventional VSFG spectra of neat water and ACS grade 2 M LiNO_3 solution in the OH stretching region (3000–3800 cm^{-1}) before and after filtration..... 87

Figure 6.7 Comparison between HD-VSFG spectra from ACS and UP grade salt solutions after pretreatment. (a) 1 M Na_2CO_3 , (b) 1 M Na_2SO_4 , (c) 1 M $(\text{NH}_4)_2\text{SO}_4$, and (d) comparison of all 1 M salt solutions. The VSFG spectrum of neat water is also shown as reference..... 88

Figure 6.8 (a) Comparison between conventional VSFG spectra of untreated and pretreated 1 M $(\text{NH}_4)_2\text{SO}_4$ solutions made from ACS and UP grade salts. (b) Comparison between conventional VSFG spectra of untreated 1 M $(\text{NH}_4)_2\text{SO}_4$ solutions made from ACS and UP grade salts. 89

Figure 6.9 (a) Comparison between conventional VSFG spectra of baked or filtered 1.5 M NaCl solutions made from ACS and UP grade salts. (b) Comparison between conventional VSFG spectra of pretreated and untreated 1.5 M NaCl solutions made from ACS and UP grade salts. 90

Figure 6.10 VSFG spectra of PA monolayers on neat water and NaCl salt solutions in the OH stretching region ($3000\text{--}3800\text{ cm}^{-1}$) up to about 1 h after spreading. (a) PA on neat water, (b) UP grade 0.6 M NaCl solution, and (c) ACS grade 0.6 M NaCl solution. Spectra were taken every 7 min on average approximately 10 min after spreading. 102

Figure 7.1 Conventional VSFG spectra in the CH stretching region ($2800\text{--}3000\text{ cm}^{-1}$) of the air/aqueous interface of neat water and filtered NaClO_4 stock salt solution. 117

Figure 7.2 Stability of SFG system shown by the GaAs profile, conventional VSFG and HD-VSFG $\text{Im } \chi^{(2)}$ spectra of neat water in the OH stretching region ($3000\text{--}3800\text{ cm}^{-1}$). (a) GaAs profile and (b) conventional VSFG spectra, and (c) $\text{Im } \chi^{(2)}$ spectra in the OH stretching region from 3000 to 3600 cm^{-1} 118

Figure 7.3 (a) Deduced power spectra $|\chi^{(2)}|^2$ and (b) $\text{Re } \chi^{(2)}$ spectra from HD-VSFG results of 1 M and 1.7 M NaClO_4 salt solutions in the OH stretching region ($3000\text{--}3600\text{ cm}^{-1}$). Neat water spectra are shown as reference. 119

Figure 7.4 (a) Raman spectra and (b) IR spectra of 1.0 M and 1.7 M NaClO_4 salt solutions. Neat water spectrum is shown as a reference. 120

Figure 7.5 (a) Conventional VSFG $|\chi_{\text{eff}}^{(2)}|^2$ spectra of the air/aqueous interfaces of neat water and 1.0 M NaClO_4 salt solutions across the entire OH stretching region ($3000\text{--}3800\text{ cm}^{-1}$). (b) HD-VSFG $\text{Im } \chi^{(2)}$ spectra of air/aqueous interfaces of 1.0 and 1.7 M NaClO_4 salt solutions. Neat water spectrum is shown as a reference. Inset: $\text{Im } \chi^{(2)}$ difference spectra ($\text{Im } \chi^{(2)}$ salt spectrum minus $\text{Im } \chi^{(2)}$ neat water spectrum) of the same salt solutions found in (b). 121

Figure 7.6 Diagram qualitatively demonstrating the salt concentration dependence of the magnitude and direction of the overall electric field as exemplified by NaClO_4 and Na_2SO_4 salt solutions. 122

Figure 8.1 (a) Raman spectra of 0.6, 1.4, 2.2, 3.0, and 3.6 M unfiltered NH_4NO_3 , as well as filtered SFG stock solution (1.6 M), (b) Calibration curve of NH_4NO_3 solutions using the height of each individual Raman spectra. The concentrations of other nitrate SFG stock solutions were determined in the same manner..... 143

Figure 8.2 Conventional VSFG spectra of neat water, 1.7 M NaNO_3 , 1.6 M NH_4NO_3 , and 1.0 M $\text{Mg}(\text{NO}_3)_2$ salt solutions in the CH stretching region ($2800\text{--}3000\text{ cm}^{-1}$)..... 144

Figure 8.3 SFG spectra at the air/water interface in the OH stretching region ($3100\text{--}3800\text{ cm}^{-1}$). (a) $|\chi_{\text{eff}}^{(2)}|^2$ spectra, (b) deduced $|\chi^{(2)}|^2$ power spectra from HD-VSFG, and (c) $\text{Im } \chi^{(2)}$ spectra. 145

Figure 8.4 Deduced $|\chi^{(2)}|^2$ power spectra from HD-VSFG at air/aqueous solution interfaces of (a) 1.0 M and 2 M LiNO_3 , (b) 1.0 M and 1.7 M NaNO_3 , (c) 1.0 M and 1.6 M NH_4NO_3 , and (d) 1.0 M and 2.3 M $\text{Mg}(\text{NO}_3)_2$ salt solutions. Neat water spectrum is shown as a reference. 146

Figure 8.5 HD-VSFG $\text{Re } \chi^{(2)}$ spectra at air/aqueous solution interfaces of neat water, 2.0 M LiNO_3 , 1.7 M NaNO_3 , 1.6 M NH_4NO_3 , and 1.0 M $\text{Mg}(\text{NO}_3)_2$ salt solutions. Neat water spectrum is shown as a reference..... 147

Figure 8.6 Raman spectra of (a) 1.0 M and 2 M LiNO_3 , (b) 1.0 M and 1.7 M NaNO_3 , (c) 1 M and 1.6 M NH_4NO_3 , and (d) 1.0 M and 2.3 M $\text{Mg}(\text{NO}_3)_2$ salt solutions. Neat water

spectrum is shown as a reference. The ~2 M NO ₃ ⁻ spectra reveal a relatively constant Raman transition moment strength.	148
Figure 8.7 IR spectra of (a) 1.0 M and 2.0 M LiNO ₃ , (b) 1.0 M and 1.7 M NaNO ₃ , (c) 1.0 M and 1.6 M NH ₄ NO ₃ , and (d) 1.0 M and 2.3 M Mg(NO ₃) ₂ salt solutions. Neat water spectrum is shown as a reference. The ~2 M NO ₃ ⁻ spectra reveal a relatively constant IR dipole moment strength.....	149
Figure 8.8 Conventional VSFG $ \chi_{\text{eff}}^{(2)} ^2$ spectra of air/aqueous interfaces of (a) 1.0 M and 1.7 M NaNO ₃ , (b) 1.0 M and 2.3 M Mg(NO ₃) ₂ , (c) 1.0 M and 1.6 M NH ₄ NO ₃ , and (d) 1.0 M and 2.0 M LiNO ₃ salts solutions over the entire OH stretching region (3000–3800 cm ⁻¹). Neat water spectrum is shown as a reference. Legend colors in this figure will be followed in all subsequent figures.	150
Figure 8.9 HD-VSFG Im $\chi^{(2)}$ spectra of air/aqueous interfaces of (a) 1.0 M and 1.7 M NaNO ₃ , (b) 1.0 M Mg(NO ₃) ₂ , (c) 1.0 M and 1.6 M NH ₄ NO ₃ , and (d) 1.0 M and 2.0 M LiNO ₃ salt solutions. Neat water spectrum is shown as a reference.....	151
Figure 8.10 HD-VSFG Im $\chi^{(2)}$ difference spectra (Im $\chi^{(2)}$ salt spectrum minus Im $\chi^{(2)}$ water spectrum) for the indicated salts.	152
Figure 8.11 (a) Illustration of the relative location for NO ₃ ⁻ and its counter cations at the air/aqueous interface of NH ₄ NO ₃ and Mg(NO ₃) ₂ salt solutions. (b) Diagram qualitatively demonstrating the salt concentration dependence of the magnitude and direction of the overall electric field.	153
Figure 9.1 Conventional VSFG $ \chi_{\text{eff}}^{(2)} ^2$ spectra of air/aqueous interfaces of (a) 1 M Na ₂ SO ₄ and 1 M NaClO ₄ , (b) 1 M Na ₂ CO ₃ , and 1 M and 1.7 M NaNO ₃ salts solutions	

over the entire OH stretching region (3000–3800 cm^{-1}); HD-VSFG $\text{Im } \chi^{(2)}$ spectra of air/aqueous interfaces of (c) 1 M Na_2SO_4 , and 1 M and 1.7 M NaClO_4 , (d) 1 M Na_2CO_3 , and 1 M and 1.7 M NaNO_3 salt solutions. Neat water spectrum is shown as a reference.

..... 172

Figure 9.2 HD-VSFG $\text{Im } \chi^{(2)}$ difference spectra ($\text{Im } \chi^{(2)}$ salt spectrum minus $\text{Im } \chi^{(2)}$ water spectrum) for the indicated salts. Neat water spectrum is shown as a reference (zero line).

..... 173

Figure 9.3 (a) Illustration of the relative location for oxyanions ($\text{ClO}_4^- > \text{NO}_3^- > \text{CO}_3^{2-} > \text{SO}_4^{2-}$) and its counter Na^+ ions at the air/aqueous interfaces. (b) Diagram qualitatively demonstrating the salt concentration dependence of the magnitude and direction of the overall electric field. 174

Figure 10.1 Illustration of the molecular-level charge transfer mechanism in thundercloud electrification. (a) Smoke rich in NO_3^- and Cl^- ions results in enhanced positive lightning. (b) Negative lightning under normal conditions. 181

Figure A.1 Stability of the VSFG system shown by the GaAs profile and the conventional VSFG spectrum of neat water in the OH stretching region (3000–3800 cm^{-1}) before and after infrared energy attenuation. 207

Figure A.2 (a) GaAs profile and (b) conventional VSFG spectra of neat water in the OH stretching region measured using different visible energy. 208

Figure A.3 GaAs profiles measured with original infrared energy ($\sim 9 \mu\text{J}$), attenuated infrared energy ($\sim 6.9 \mu\text{J}$), and attenuated infrared energy with timing adjustment. 209

Figure A.4 Raw and normalized final conventional VSFG spectra of neat water, 1.6 M NH_4NO_3 and 2.3 M $\text{Mg}(\text{NO}_3)_2$ salt solutions before and after energy attenuation.	210
Figure A.5 An example showing that the relative spectral differences between various samples are not affected by the incident energy utilized.	211

Chapter 1 Introduction

1.1 Motivation

The work presented in this dissertation is focused on elucidating the interfacial water organization and ion distributions for various environmentally relevant air/aqueous salt solution interfaces. The ubiquity of water and the vital role it plays in all aspects of life motivates scientific inquiry into its properties beyond sheer fascination. “God made the bulk; the surface was invented by the devil.”¹ Wolfgang Pauli used this famous sentence to express his frustration towards studies on solid surfaces due to the broken symmetry in that region. If one attempts to investigate the molecular-level information at air/aqueous interfaces, the level of complexity would even deepen due to the presence of solute and capillary fluctuations at such surfaces.

Water organization at air/aqueous interfaces is strongly influenced by the presence of various inorganic ions, specifically ion distributions that exist in the interfacial region where the molecular environment changes from the bulk to the surface. It has been recognized that both the kinetics and mechanisms of interfacial reactions differ from those in the isotropic bulk phase.²⁻⁵ For instance, the molecules residing in the interfacial region play critical roles in the heterogeneous chemistry of atmospheric aerosols.^{2,6,7} Hence, elucidating interfacial water organization and ion distributions would shed light

on atmospheric aerosol chemistry,⁶⁻¹¹ in addition to ice/snowpack chemistry,¹²⁻¹⁵ thundercloud electrification,¹⁶ geochemistry,¹⁷⁻²¹ and ocean surface processes,²² among others. Beyond these practical interests in environmental, atmospheric and oceanic chemistry, the study of specific ion effects would also facilitate a better understanding of some ambiguous fundamental questions in physical chemistry.

Traditionally, it was accepted that aqueous surface are devoid of ions on the basis of surface tension measurement interpretation.^{9,23-26} However, molecular dynamics (MD) simulation results from Jungwirth and Tobias gave rise to a rethinking of ion surface depletion.²⁷ They proposed that large halide ions, such as bromide and iodide, have a strong propensity for the surface, although the integrated ionic distribution in the interfacial region still maintains a negative surface excess. This prediction was subsequently confirmed by numerous experiments using various techniques.²⁸⁻³² However, molecular-level information regarding the interfacial behavior of more complicated polyatomic anions is relatively limited. In this subsection, the significance of the inorganic ions studied in this work will be presented and the relevant published experimental and theoretical accounts will be summarized, followed by a discussion on the current incomplete understanding of ion distributions and water organization at air/aqueous interfaces.

It is well known that polyatomic anions, particularly oxyanions, exert a significant impact on atmospheric and oceanic chemistry. For example, sulfate (SO_4^{2-}) and nitrate (NO_3^-) anions are two of the most abundant anions in atmospheric aerosols.³³ The concentration of sulfuric acid in tropospheric aerosols is typically greater than 40 wt.%

and can be neutralized by gaseous ammonia to form $(\text{NH}_4)_2\text{SO}_4$ and NH_4HSO_4 .³⁴ Sulfate aerosols are intimately involved in acid rain, radiative balance, nucleation of polar stratospheric clouds and heterogeneous reactions.^{6,35,36} An example of heterogeneous reactions is the hydrolysis and oxidation of dinitrogen pentoxide (N_2O_5) on the surface of sulfate aerosols.³⁷⁻⁴⁰ Nitrate ions are commonly found in atmospheric aerosols, sea ice, and snowpacks through heterogeneous reactions and direct deposition.^{6,41-44} As an important semi-volatile component in aerosols, NH_4NO_3 can be formed via reaction of gaseous ammonia with nitric acid in the atmosphere, a product of the heterogeneous hydrolysis of NO_2 . In marine regions, NaNO_3 and $\text{Mg}(\text{NO}_3)_2$ are generated by the heterogeneous reaction of sea salt aerosols.^{45,46} Sulfate- and nitrate-containing aerosols play significant roles in global climate.⁴⁷ These particles scatter incoming solar radiation (direct effect) and act as cloud-condensation nuclei, thus altering cloud properties and the associated impact on radiation (indirect effect).⁶ Moreover, sulfate and nitrate ions and their distributions in the interfacial region are suggested to be strongly associated with charge transfer in the thundercloud electrification.¹⁶

Carbonate (CO_3^{2-}) ions are also of great significance in environmental chemistry, particularly in the uptake and the chemical transformation of atmospheric carbon dioxide (CO_2) by atmospheric aerosol and ocean surfaces. Currently, oceans serve as the largest sustained sink of anthropogenic CO_2 where it can readily undergo hydration and chemical reaction when in the presence of water and be converted into the form of bicarbonate (HCO_3^-) and CO_3^{2-} which further lower the pH of the oceans.⁴⁸⁻⁵² Therefore, the knowledge of their distributions at the air/aqueous interface may facilitate a better

understanding of the process of CO₂ absorption into the ocean.

Finally, in recent years, the perchlorate (ClO₄⁻) ion has also drawn much attention as an emerging environmental pollutant leading to widespread contamination of groundwater, particularly in the southwestern United States.^{53,54} To develop a potentially viable remediation technology, such as selective extraction of contaminants from air/aqueous interface, insight of interfacial behavior of ClO₄⁻ ions is essentially required. Furthermore, the presence of surface-active ClO₄⁻ ion may affect the evaporation mechanism and kinetics at the vapor/liquid interfaces.⁵⁵

Numerous computational studies have been implemented to explore the behavior of oxyanions at the air/aqueous interface. Jungwirth and co-workers proposed that SO₄²⁻ ions clearly prefer bulk over surface solvation and are strongly repelled from the surface, which further increase the thickness of the interfacial region.⁵⁶⁻⁵⁸ Morita and co-workers utilized MD simulations to explore the ion distributions of Na₂SO₄ and sulfuric acid (H₂SO₄) in the interfacial region.⁵⁹⁻⁶¹ Their analysis confirmed that all the ionic species are repelled from the surface in the case of Na₂SO₄. Pegram and Record applied a surface-bulk partitioning model to predict the exclusion of Na₂SO₄ and Na₂CO₃ from the surface region and the accumulation of ClO₄⁻ ion there.^{62,63} For NO₃⁻ ions, Salvador et al. and Dang et al. demonstrated somewhat contradictory results with respect to NO₃⁻ interfacial solvation by treating polarizability differently in the polarizable MD simulations.^{64,65} More recently, MD simulations conducted by Thomas et al. and Minofar et al. have considered the effect of counter cations on the interfacial NO₃⁻ ion distribution. Thomas et al. predicted that NO₃⁻ anions reside primarily in the bulk and only a small

concentration exists at the air/aqueous interface of NaNO_3 solution.⁶⁶ Simulation results from $\text{Mg}(\text{NO}_3)_2$ solution studies also indicated a very weak surface propensity for NO_3^- .⁶⁷ These somewhat conflicting results regarding the surface propensity of NO_3^- ions need to be further studied. Nevertheless, it is clear that the introduction of a counter cation plays a significant role in the outcome of the simulation. Very recently, the importance of cation effects in the interfacial ion distributions has drawn much attention,^{68,69} and will be illustrated by using the results of sulfate and nitrate salts as discussed in Chapter 5 and 8. With regard to CO_3^{2-} ions, the MD simulation results from Du et al. proposed that in the aqueous Na_2CO_3 solution CO_3^{2-} ions are excluded from the interfacial region which is extended in depth.⁷⁰ By utilizing MD simulations, the enhancement of ClO_4^- ion at the interface was predicted by Baer et al. using both first principles as well as polarizable classical force field.⁷¹

To unravel the behavior of SO_4^{2-} , CO_3^{2-} , NO_3^- , and ClO_4^- ions at air/aqueous interfaces, various experimental techniques have been adopted. In addition to the mass spectrometric/electrospray study,⁷² the glancing-angle Raman study,⁷³ the infrared spectroscopy work,⁷⁴⁻⁷⁶ the photoelectron spectroscopy (PES)/electrospray work,⁷⁷ and the X-ray photoemission spectroscopy (XPS) work,^{71,78} many experiments concerning the interfacial oxyanion distributions and their impact on water hydrogen-bonding network have been carried out utilizing interface-specific nonlinear optical techniques such as second harmonic generation (SHG) and vibrational sum frequency generation (VSFG) spectroscopy. In recent years, these two techniques have become indispensable tools for many interfacial studies because of their high surface specificity. In particular, VSFG

spectroscopy is the only technique available to probe the vibrational structures of a host of different interfaces. For instance, with the help of resonant SHG, Otten et al. showed the existence of NO_3^- ions in the interfacial region of aqueous solution but no strong enhancement in its concentration,⁷⁹ while Fordyce et al. demonstrated that the nature of surface changes as a function of acid concentration at the air/ H_2SO_4 solution interface.⁸⁰ Similarly, numerous experiments have been conducted by VSFG spectroscopy regarding oxyanions because of its interface specificity and molecular sensitivity. Radüge et al. and Baldelli et al. first reported about water organization at the air/ H_2SO_4 solution interface independently with different interpretation.^{81,82} Later, Baldelli et al. further studied interfacial water hydrogen-bonding network for a series of alkali metal $\text{SO}_4^{2-}/\text{HSO}_4^-$ salt solutions.⁸³ The hydrogen bonding of interfacial water molecules in the presence of Na_2SO_4 and $(\text{NH}_4)_2\text{SO}_4$ was investigated by Gopalakrishnan et al.,⁵⁷ while the former one was examined by Tarbuck and Richmond as well.⁸⁴ More recently, Miyamae et al. and Jubb and Allen confirmed the existence of HSO_4^- ions in the interfacial region by directly interrogating their vibrational signature (in the S-O stretching region) at the air/aqueous interfaces of sulfuric acid and alkali bisulfate salt solutions, respectively.^{85,86} With regard to CO_3^{2-} ions, Tarbuck and Richmond and Du et al. explored the impact of Na_2CO_3 on the interfacial water organization.^{70,84} In the case of NO_3^- ions, Schnitzer et al. revealed changes to the hydrogen-bonding network and to the “free” (non-hydrogen-bonded) OH at the air/aqueous nitrate solution interface in the presence of Na^+ cations.⁸⁷ The perturbation of NO_3^- ions on the interfacial water hydrogen-bonding network in the presence of divalent cations was determined as well by Xu et al.⁸⁸ They further

demonstrated the presence of NO_3^- ions in the interfacial region by directly probing their vibrational symmetric stretch mode, and found unique behavior for aqueous $\text{Mg}(\text{NO}_3)_2$ compared to $\text{Sr}(\text{NO}_3)_2$ and $\text{Ca}(\text{NO}_3)_2$.⁸⁹ The NO_2 group of nitric acid has also been studied in different spectral regions using VSFG spectroscopy by Soule et al.⁹⁰

Despite the emergence of these computational and experimental studies, the organization of SO_4^{2-} , CO_3^{2-} , NO_3^- , and ClO_4^- ions and their counter cations at the air/aqueous interfaces, and how these ions alter the interfacial water hydrogen-bonding network, still remains elusive. Recently, the emergence of heterodyne-detected vibrational sum frequency generation (HD-VSFG) spectroscopy, a variant of conventional VSFG spectroscopy based on an interference method, has provided additional information.^{29,91-93} The main advantage of HD-VSFG spectroscopy is that it provides the imaginary part of the nonlinear susceptibility $\chi^{(2)}$ ($\text{Im } \chi^{(2)}$) which is related directly to the net transition dipole orientation of interfacial water molecules. The sign of $\text{Im } \chi^{(2)}$ then gives an idea of the net orientation of the interfacial electric field from which ion distributions may be inferred. Hitherto, no HD-VSFG contribution has systematically investigated interfacial distributions of cations and polyatomic anions and analyzed critical ion properties (size, geometry, charge, and polarizability) and potential driving forces that may dictate their surface propensity.

In addition, water organization and ion distribution at air/aqueous interfaces investigated by nonlinear vibrational spectroscopy and other surface-sensitive techniques depend critically on the purity grade and purification processing of the chosen salts. A possible explanation for the observed discrepancy from different VSFG research groups

could come from the use of commercial salts of different grades and/or from salts and salt solutions that have undergone different processing. However, aside from sporadic reports regarding halide salts,^{28,94} no study using conventional VSFG and HD-VSFG spectroscopy has so far systematically compared the influence of salt purity and/or different prior treatments of salts and their solutions on the spectrum in the water OH stretching region for a variety of salts, particularly molecular ion-based ones. Moreover, the impact of salt purity grade and purification processing on binding affinity of different cations to monolayers of amphiphilic macromolecules (e.g. fatty acids, phospholipids) at the air/aqueous surfactant interfaces is not yet clear.

1.2 Dissertation Highlights

Chapter 2 begins by discussing the basic theory necessary for the application of the VSFG spectroscopy followed by a brief introduction of a new variant of conventional VSFG, the heterodyne-detected vibrational sum frequency generation (HD-VSFG) spectroscopy, which enables to provide the information about the net dipole orientation of interfacial species that is lost in the conventional VSFG method. Chapter 3 describes instrumentation of both conventional and heterodyne-detected VSFG spectrometers. Supplementary details are given about the key points that play critical roles in improving the performance of systems and infrared profiles.

Chapter 4 reports on the behavior of HCO_3^- and CO_3^{2-} at the air/aqueous interfaces and their perturbation to the water hydrogen-bonding network investigated by conventional VSFG and HD-VSFG spectroscopy. The net orientation of water molecules at air/aqueous interfaces of Na_2CO_3 and NaHCO_3 salts are inferred from the direct

measurement of the averaged direction of transition dipole moment of the interfacial water molecules. It is found that HCO_3^- ions and their Na^+ counter ion do not significantly perturb the interfacial water organization, whereas CO_3^{2-} ions strongly orient water so that water's hydrogens point down toward the bulk solution. This is consistent with the picture of CO_3^{2-} anions residing many layers below the water surface with a preference for the Na^+ cations to be above the anions and thereby closer to the topmost layer of the water surface.

Chapter 5 details on the water organization at the air/aqueous interfaces of various inorganic salts (CaCl_2 , NaCl , Na_2SO_4 , $(\text{NH}_4)_2\text{SO}_4$, and Na_2CO_3) using the same approach as in Chapter 3. The findings are attributed to the net charge separation arising from the ion distributions at the air/water interface, assuming similar ion distribution widths for all systems studied. This is most evident for the $(\text{NH}_4)_2\text{SO}_4$ solution where the electric field has a greater magnitude relative to the other salt solutions studied. The magnitude of the electric field in the interfacial region decreases in the order: $(\text{NH}_4)_2\text{SO}_4 > \text{Na}_2\text{SO}_4 > \text{Na}_2\text{CO}_3 \geq \text{CaCl}_2 > \text{NaCl}$. The electric field is opposite in direction for the sulfate and carbonate salts relative to the chloride salts.

Chapter 6 discusses the impact of salt purity on interfacial water organization at bare air/aqueous solution interfaces and the influence of salt purity on Na^+ interactions with the headgroup of palmitic acid monolayers at the air/aqueous interfaces. It is shown here by means of conventional VSFG and HD-VSFG spectroscopy that salt purity grade and/or pretreatment has a tremendous impact on the interfacial water spectrum of aqueous salt solutions after a series of systematic comparison. To avoid spectral distortion

introduced by the presence of organic contamination, a standardized pretreatment procedure is established here for salts and their solutions before being used by VSFG spectroscopy and most likely by any other surface-sensitive spectroscopic studies of water organization at bare air/ aqueous interfaces. In the case of palmitic acid monolayers, it is found that alkali salt grade (even after pretreatment) is critical as the presence of polyvalent cations even in trace amounts in the salt of interest may largely influence the results of alkali cation-carboxylate interactions and comparison of relative binding affinity of different cations.

Chapter 7 presents results on the surface prevalence of perchlorate anions at the air/aqueous interface investigated by means of conventional VSFG and HD-VSFG spectroscopy. It is found that perchlorate (ClO_4^-) ions exist in the interfacial region and prefer to reside on average above their counterions. These findings can be inferred from the averaged orientation of dipole moment of interfacial water molecules governed by the direction of the net electric field arising from the interfacial ion distributions. At the air/aqueous interface of NaClO_4 salt solutions, hydrogen-bonded water molecules are oriented preferentially towards the vapor phase. Contrary to some other salts (e.g. sulfates), the presence of ClO_4^- causes a full reversal in the direction of the interfacial electric field in the concentrated regime relative to neat water. This effect becomes even more pronounced with increasing salt concentration.

Chapter 8 reports on the cation effects on water organization at the air/aqueous nitrate solution interfaces. The water organization at air/aqueous interfaces of NaNO_3 , $\text{Mg}(\text{NO}_3)_2$, NH_4NO_3 , and LiNO_3 salts was inferred from $\text{Im } \chi^{(2)}$ spectra obtained by HD-

VIS-SFG spectroscopy. It is found that nitrate (NO_3^-) ions exist in the interfacial region and prefer to reside on average above their counter cations. These findings can be derived from the degree of charge separation arising from the ion distributions at the air/aqueous interface in which the cation identity plays a significant role. The varying ion distributions and their concentrations, dictate the magnitude of the electric field in the interfacial region, which decreases in the order of $\text{Mg}^{2+} > \text{Na}^+ \approx \text{Li}^+ > \text{NH}_4^+$ on the basis of higher concentration (~ 2 M for nitrate ions) data. This trend generally follows the decrease of the ion's surface charge density with the exception of Na^+ and Li^+ ions. It is suggested here that the cation identity as well as the concentration changes give rise to the partial reversal of the net direction of the interfacial electric field. The relative location of these cations in the interfacial region still remains speculative. The presence of NO_3^- ions in the interfacial region proposed here may facilitate a better understanding of atmospheric aerosol chemistry. This is the first systematic HD-VIS-SFG study revealing the counter cation effect.

Chapter 9 concludes by preliminarily discussing the impact of critical ion properties (size, geometry, charge, and polarizability) on their interfacial surface propensity based on the HD-VIS-SFG results present in this dissertation. To the author's best knowledge, this is the first systematic demonstration of the polyatomic anion effect employed by HD-VIS-SFG spectroscopy. It is noteworthy that specific ionic properties, such as polarizability and size, which successfully explained the relative surface propensity of halide ions, cannot solely account for the interfacial distribution of oxyanions studied herein. The other two ionic properties, charge (surface charge density)

and geometry (shape) is also examined. Although these properties all play a role in determining interfacial ion distributions, our results indicate that charge exerts a greater impact compared to the others. On the basis of literature review, a brief discussion is also presented to analyze the potential contributions from series of driving energy/forces and some other factors, including dehydration energy, electrostatic energy, cavitation energy, dispersion forces, anisotropic solvation, as well as interfacial flexibility, to the interfacial solvation of oxyanions. The proposed order of oxyanions' surface propensity agrees well with their dehydration free energy and with predictions from the current surface-bulk partitioning models.

In closing, Chapter 10 highlights environmental implications of the work presented here and a future outlook for subsequent studies covered by this dissertation is included.

Chapter 2 Vibrational Sum frequency Generation Theory

2.1 Principle of VSFG Spectroscopy

Detailed theoretical description of VSFG spectroscopy and other related nonlinear optical techniques has been presented in depth in abundant literature.^{8,95-98} Hence, only a brief introduction of the theoretical background of VSFG spectroscopy will be given here. VSFG spectroscopy is based on sum frequency generation (SFG), a second-order nonlinear optical process that is induced by the coupling of two incident oscillating electric fields of different frequencies (ω_1 and ω_2) and which results in the generation of a signal at the sum of these frequencies ($\omega_3 = \omega_1 + \omega_2$). A SFG signal is generated from the second-order nonlinear polarization in a medium ($P^{(2)}(\omega_{SF})$) induced by the coupling two electric fields at different frequencies (ω_1 and ω_2), respectively, as shown in Equation 2.1:

$$P^{(2)}(\omega_{SF}) = \epsilon_0 \chi^{(2)} : E(\omega_1)E(\omega_2) \quad (2.1a)$$

where $\chi^{(2)}$ is the macroscopic hyperpolarizability (also known as the surface nonlinear susceptibility in VSFG spectroscopy), ϵ_0 is the vacuum permittivity. In the specific case of VSFG spectroscopy, a visible and an infrared incident beams at frequencies ω_{vis} and ω_{IR} , respectively, are used to generate SF signal, then $\omega_1 = \omega_{vis}$ and $\omega_2 = \omega_{IR}$. Nonlinear effects only become significant when the magnitude of the applied electromagnetic field

is comparable to the atomic electric field experienced by the electrons in a molecule. Typically, such intense fields are only achievable by the use of pulsed lasers. Under the electric-dipole approximation (refer to the interaction of light with matter),⁹⁸ the effects of optical magnetic fields and of multipoles (e.g., quadrupoles) are neglected. Therefore, a lack of inversion symmetry becomes an imperative criteria for the generation of second-order optical processes.⁹⁹ In other words, any surface or interface that separate two adjacent isotropic bulk media meets this requirement, leading to an SFG response that is essentially interface-specific.^{8,100-105}

The VSFG process can be viewed as a coherent anti-stokes Raman process over an IR excited surface (Figure 2.1). This gives rise to the VSFG selection rule that a vibrational mode must be both Raman and infrared active to generate a surface SFG signal; the origin of this rule will be discussed below. In most VSFG experiments, including those in the current work, only the reflected SFG beam is detected (Figure 2.2), even though both reflected and transmitted SFG beams are generated by the two co-propagating visible and infrared beams. The direction of the reflected SFG signal can be calculated using the conservation of momentum of all three beams parallel to the interface (known as the phase-matching condition), as shown in Equation 2.2:

$$n_{SF}\omega_{SF} \sin \theta_{SF} = n_{vis}\omega_{vis} \sin \theta_{vis} + n_{IR}\omega_{IR} \sin \theta_{IR} \quad (2.2)$$

$$\frac{\sin \theta_{SF}}{\lambda_{SF}} = \frac{\sin \theta_{vis}}{\lambda_{vis}} + \frac{\sin \theta_{IR}}{\lambda_{IR}} \quad (2.3)$$

where ω_i is the frequency of the pulse, $n_i(\omega_i)$ is the refractive index of the bulk medium through which the beam propagates at frequency ω_i . θ_i is the angle of the indicated beam

(incident or generated) relative to the surface normal, and λ is the wavelength of each pulse. Equation 2.3 is commonly used in preference to Equation 2.2.

Conventional VSG intensity is proportional to the absolute square of the effective second-order nonlinear susceptibility, $\chi_{eff}^{(2)}$, and then to the visible and infrared pulse intensities:

$$I_{SF} \propto |\chi_{eff}^{(2)}|^2 I_{vis} I_{IR} \propto \left| \chi_{eff,NR}^{(2)} + \sum_v \chi_{eff,v}^{(2)} \right|^2 I_{vis} I_{IR} \quad (2.4)$$

$$I_{SF} = \frac{8\pi^3 \omega_{SF}^2 \sec^2 \theta_{SF}}{c^3 n_1(\omega_{SF}) n_1(\omega_{vis}) n_1(\omega_{IR})} |\chi_{eff}^{(2)}|^2 I_{vis} I_{IR} \quad (2.5)$$

where I_{SF} , I_{vis} and I_{IR} are the intensities of the output SFG, incident visible, and infrared beams respectively, and $\chi_{eff,NR}^{(2)}$ and $\chi_{eff,v}^{(2)}$ refer to the effective non-resonant and resonant components of the second-order nonlinear susceptibility, respectively. The effective second-order susceptibility $\chi_{eff}^{(2)}$ is related to the macroscopic second-order susceptibility $\chi^{(2)}$ by the Fresnel factors $L(\omega)$ and the unit electric field vector of a laser beam at frequency ω , $\hat{e}(\omega)$.

$$\chi_{eff}^{(2)} = [L(\omega_{SF}) \cdot \hat{e}(\omega_{SF})] \cdot \chi^{(2)} : [L(\omega_{vis}) \cdot \hat{e}(\omega_{vis})] \cdot [L(\omega_{IR}) \cdot \hat{e}(\omega_{IR})] \quad (2.6)$$

In experiment, $\chi_{eff}^{(2)}$ is directly probed and it depends on the VSG experimental setup, i.e. input beam geometry and polarization.

$\chi^{(2)}$ is a third-ranked tensor that has a maximum of 27 components in the laboratory coordinate system, $\chi_{ijk}^{(2)}$. Under the symmetry constraints, the number of non-zero components can be reduced. In a centrosymmetric environment, the value of $\chi_{ijk}^{(2)}$ for two opposing directions should be identical since all directions are equivalent:

$$\chi_{ijk}^{(2)} = \chi_{-i-j-k}^{(2)} \quad (2.7)$$

However, as a third rank tensor, a change in the sign of the three subscripts is equivalent to the reversing of axis system:

$$\chi_{-i-j-k}^{(2)} = (-1)^3 \chi_{ijk}^{(2)} = -\chi_{ijk}^{(2)} \quad (2.8)$$

To satisfy both Equations 2.7 and 2.8, $\chi_{ijk}^{(2)}$ can only equal 0. This is the intrinsic explanation of surface specificity of VSFG since the centrosymmetry is naturally broken at the surface. For instance, an isotropic interface with C_∞ symmetry has only 7 non-vanishing components. Because the interface is defined to be in the xy plane, x and y axes become equivalent. Hence, only four independent non-zero components contribute to a SF signal: $\chi_{xxz}^{(2)} = \chi_{yyz}^{(2)}$, $\chi_{xzx}^{(2)} = \chi_{zyy}^{(2)}$, $\chi_{zxx}^{(2)} = \chi_{zyy}^{(2)}$, $\chi_{zzz}^{(2)}$.

Four most common beam polarizations utilized in VSFG experiments are: ssp, sps, pss, and ppp, where the first letter represents the output VSFG beam, the second letter corresponds to the input visible beam, and the last letter refers to the input infrared beam. Among these, the ssp combination is the most widely used. The s-polarized light has its electric field vector perpendicular to the plane of incidence, while the p-polarized light has its electric field vector parallel to the plane of incidence. The relationship between $\chi_{eff}^{(2)}$ and the actual non-linear susceptibility, $\chi_{ijk}^{(2)}$ under these polarization combinations is given by Equation 2.9.

$$\begin{aligned}
\chi_{\text{eff},ssp}^{(2)} &= L_{yy}(\omega_{SF})L_{yy}(\omega_{vis})L_{zz}(\omega_{IR})\sin\theta_{IR}\chi_{yyz} \\
\chi_{\text{eff},sps}^{(2)} &= L_{yy}(\omega_{SF})L_{zz}(\omega_{vis})L_{yy}(\omega_{IR})\sin\theta_{vis}\chi_{zyy} \\
\chi_{\text{eff},pss}^{(2)} &= L_{zz}(\omega_{SF})L_{yy}(\omega_{vis})L_{yy}(\omega_{IR})\sin\theta_{SF}\chi_{zyy} \\
\chi_{\text{eff},ppp}^{(2)} &= -L_{xx}(\omega_{SF})L_{xx}(\omega_{vis})L_{zz}(\omega_{IR})\cos\theta_{SF}\cos\theta_{vis}\sin\theta_{IR}\chi_{xxz} \\
&\quad - L_{xx}(\omega_{SF})L_{zz}(\omega_{vis})L_{xx}(\omega_{IR})\cos\theta_{SF}\sin\theta_{vis}\cos\theta_{IR}\chi_{zxx} \\
&\quad + L_{zz}(\omega_{SF})L_{xx}(\omega_{vis})L_{xx}(\omega_{IR})\sin\theta_{SF}\cos\theta_{vis}\cos\theta_{IR}\chi_{zxx} \\
&\quad + L_{zz}(\omega_{SF})L_{zz}(\omega_{vis})L_{zz}(\omega_{IR})\sin\theta_{SF}\sin\theta_{vis}\sin\theta_{IR}\chi_{zzz}
\end{aligned} \tag{2.9}$$

where L_{ii} denotes the non-linear Fresnel factor associated with ω_i , and θ_i is the input or output angle versus surface normal for the associated beam.^{95,97} The Fresnel factor acts as a local-field correction factor of each electric field when a beam propagates across the boundary that separates the interface and the adjacent isotropic medium. Fresnel factors can be written as functions of the refractive indices of the beam in different media, the incident (reflection) angle and the refractive angle. A detailed derivation of all three tensorial Fresnel factors has been presented by Shen.¹⁰⁶ Therefore, the Fresnel factors affect VSFG intensity and spectral lineshape and should be considered in spectral normalization. Recently, Feng et al. have illustrated that for the water spectra at the vapor/liquid interface originating from many research groups that the spectral contributions arising from experimental geometry could be removed by correcting for the nonlinear Fresnel coefficients.¹⁰⁷ It is noteworthy that for the simplicity of data processing, numerous VSFG studies including this dissertation only report $\chi_{\text{eff}}^{(2)}$, indicating that the presented VSFG spectra are only normalized to the visible and IR intensities.

$\chi_{ijk}^{(2)}$ is the macroscopic orientational average of microscopic molecular hyperpolarizability tensorial element, $\beta_{lmn}^{(2)}$, of all the interfacial molecules in the

molecular coordinate system. It can be understood as the ensemble average of the Euler angle transformation between the molecular and laboratory coordinate systems.

$$\chi_{ijk}^{(2)} = N \sum_{lmn} \langle \mu_{ijk:lmn} \rangle \beta_{lmn}^{(2)} \quad (2.10)$$

where N is the number density of VSFG active oscillators, $\langle \mu_{ijk:lmn} \rangle$ is the orientationally averaged Euler angle transformation. The molecular hyperpolarizability, $\beta_{lmn}^{(2)}$, is proportional to the Raman polarizability tensor for the transition moment $\langle g | \alpha_{lm} | v \rangle$ and the infrared transition moment $\langle v | \mu_n | g \rangle$. This explains the origin of the VSFG selection rule according to which a vibrational active mode must be both Raman and infrared active in order to be VSFG allowed.

$$\beta_{lmn} = \frac{\langle g | \alpha_{lm} | v \rangle \langle v | \mu_n | g \rangle}{\omega_{IR} - \omega_v + i\Gamma_v} \quad (2.11)$$

In SFG, for discrete vibrational mode, both $\chi^{(2)}$ and $\beta^{(2)}$ can be generally expressed into two terms, a non-resonant and a sum of resonant term, as follows:

$$\begin{aligned} \chi^{(2)} &= \chi_{NR}^{(2)} + \sum_v \frac{A_v}{\omega_{IR} - \omega_v + i\Gamma_v} \\ \beta^{(2)} &= \beta_{NR}^{(2)} + \sum_v \frac{\beta_v}{\omega_{IR} - \omega_v + i\Gamma_v} \end{aligned} \quad (2.12)$$

Here, $\beta_{NR}^{(2)}$ represents the non-resonant component, A_v is the transition moment strength, ω_{IR} is the incident infrared frequency, ω_v is the frequency of the vibrational transition, and Γ_v is the line width of the vibrational transition, also known as the half-width at the half maximum (HWHM). Equations 2.12 reveal the Lorentzian lineshape character of the collected VSFG signal. More generally, for continuous modes (e.g., collective OH

vibrational modes of interface water molecules), the summation in Equation 2.12 can be replaced by an integration over the density of modes at that frequency $\rho(\omega_v)$:

$$\chi^{(2)} = \int \frac{A_v \rho(\omega_v)}{\omega_{IR} - \omega_v + i\Gamma_v} d\omega_v \quad (2.13)$$

The impact of non-resonant component can vary dramatically depending on the nature of the medium. For dielectric medium, such as water, $\chi_{NR}^{(2)}$ is usually very small,¹⁰⁸ and hence a resonant enhancement in the VSFG signal primarily originates from the resonant terms when the incident IR matches the vibrational transition frequencies of molecules, yielding the smallest denominator. In contrast, the contribution of $\chi_{NR}^{(2)}$ becomes significant in metals or semiconductors when electronic transitions become accessible.⁹⁹

2.2 Heterodyne-Detected VSFG (HD-VSFG)

Reproduced in part with permission from Hua, W; Jubb, A.M.; and Allen, H.C. “Electric Field Reversal of Na_2SO_4 , $(\text{NH}_4)_2\text{SO}_4$, and Na_2CO_3 relative to CaCl_2 and NaCl at the Air/Aqueous Interface revealed by Phase-Sensitive Sum Frequency” *J. Phys. Chem. Lett.*, **2011**, 2, 2515-2520. Copyright 2011 American Chemical Society.

In this dissertation, the term VSFG refers to conventional VSFG spectroscopy, while the heterodyne-detected vibrational sum frequency generation that provides the orientation (phase) information of the transition moment of the vibrational modes will be referred as HD-VSFG for clarification.

In conventional VSFG spectroscopy, all of the molecular information is folded in the factor $|\chi^{(2)}(\omega_{IR})|^2$, where $\chi^{(2)}$ is a complex number and be expressed as (with $\chi_{NR}^{(2)}$ being constant)

$$\chi^{(2)}(\omega_{IR}) = |\chi^{(2)}| e^{i\varphi(\omega_{IR})} = \text{Re } \chi^{(2)} + i \text{Im } \chi^{(2)} \quad (2.14)$$

where $|\chi^{(2)}|$ and φ denote the amplitude (modulus) and phase of $\chi^{(2)}$, respectively.

Following Equations 2.12 and 2.13, the imaginary part of $\chi^{(2)}$ can be been written in the form of:

$$\begin{aligned} \text{Im } \chi^{(2)} &= -\sum_{\nu} \frac{A_{\nu} \Gamma_{\nu}}{(\omega_{IR} - \omega_{\nu})^2 + \Gamma_{\nu}^2} \\ \text{Im } \chi^{(2)} &= -\int \frac{A_{\nu} \Gamma_{\nu} \rho(\omega_{\nu})}{(\omega_{IR} - \omega_{\nu})^2 + \Gamma_{\nu}^2} d\omega_{\nu} \end{aligned} \quad (2.15)$$

It is clear that the sign of the complex second-order nonlinear susceptibility, $\chi^{(2)}$, inherently contains the orientation information, as shown in Equations 2.12 and 2.13. For instance, the net polar orientation, either up or down, at the isotropic air/water interface (with C_{∞} symmetry), dictates the relative sign of A_{ν} . However, the information of the sign of the second-order nonlinear susceptibility is lost in conventional VSFG response because its intensity is proportional to the absolute square of the $\chi_{eff}^{(2)}$, as depicted in Equation 2.4. In other words, it becomes impossible to unambiguously obtain the net orientation (phase) information of the transition moment that is intrinsically contained in the $\chi^{(2)}$ of the VSFG response. In principle, for discrete resonances, the phase information can be derived from fitting of the experimental data. Nevertheless, for the focus of this dissertation, the broad OH stretching region (3000—3800 cm^{-1}), the overall spectral shape arises from a continuous band of OH stretch resonances of interfacial water

molecules that are hydrogen-bonded to their neighbors with a wide variety of geometries and strengths.^{29,93} Without knowledge of the resonant frequencies and in particular the respective sign of their amplitudes, fitting these spectra becomes somewhat arbitrary. This has led to different and often contradictory structural interpretations of the VSFG spectra of the air/water interface.^{93,96} Additionally, coupling between water modes also plays a role in the spectral shape.^{109,110} As a result, despite the similarity of VSFG spectra obtained by different groups, detailed interpretation of the spectra often varies.^{111,112}

More recently, the emergence of novel computational methods that enables determination of the phase information has alleviated the limitations of conventional VSFG spectroscopy somehow.^{113,114} Phase retrieval algorithms based on the maximum entropy method (MEM) could reconstruct the absolute phase of the SF signal directly from VSFG intensity spectra. However, phase retrieval method also suffers from a certain number of weaknesses that would lead to drastic discrepancies between reconstructed and directly measured $\text{Im } \chi^{(2)}$ spectra without sufficient prior knowledge.¹¹³ For instance, our $\text{Im } \chi^{(2)}$ spectra of the phospholipid/water interfaces are opposite with the calculated $\text{Im } \chi^{(2)}$ results obtained by Bonn et al.^{114,115}

The inability of losing inherent orientation (phase) information has been recognized for years as a weakness of the homodyne detection based conventional VSFG technique. This issue is mostly remedied by using a phase-resolved VSFG method that enables direct determination of the imaginary part of $\chi^{(2)}$ ($\text{Im } \chi^{(2)}$ spectra). In fact, as early as 1986, the first direct measurement of the phase of $\chi^{(2)}$ was completed using SHG by Kemnitz et al.¹¹⁶ It was not until 1990 that Shen and co-workers directly measured the

phase of a pentadecanoic acid monolayer on water with VSFG;¹¹⁷ however, this method received limited adoption due to the added experimental complexity.

Until recently, a widely applicable phase-resolved VSFG technique was pioneered by Shen and co-workers on their pico-second (in reference to the pulse width of the incident infrared beam) scanning laser system,^{29,93,109,118,119} known as phase-sensitive sum-frequency spectroscopy (PS-SFVG or PS-SFG). Later, Benderskii and co-workers¹²⁰ and Tahara and co-workers^{91,121} developed this technique for their femtosecond broad bandwidth (non-scanning) VSFG systems, respectively. It is notable that to date the nomenclature of this phase-resolved SFG approach is still controversial. Tahara and co-workers pointed out that these multiplex broadband interferometric measurements using ultrafast laser spectroscopies should be named as heterodyne-detected vibrational SFG method (HD-VSFG), while the term PS-VSFG should only be used for scanning single-channel phase-sensitive measurements.¹²² However, it is argued by Bonn and co-worker that the method of Tahara and co-workers is technically a homodyne technique since heterodyning implies interference with a local oscillator of a different frequency to frequency-shift the detected signal but the two frequency used in Tahara's method are the same.¹²³ In my previous publications, both terms have been adopted to name this phase-resolved method on broad bandwidth VSFG system.^{68,113,115,124-130} In this dissertation, to avoid confusing readers and being consistent through the entire text, only the term HD-VSFG will be utilized for my own results presented in later chapters.

The HD-VSFG (or PS-SFVG) method is based on interference of the sample sum frequency response with an additional signal from a phase reference (called local

oscillator) at the same frequency, and hence provides the imaginary part of nonlinear susceptibility $\chi^{(2)}$, $\text{Im } \chi^{(2)}$, which directly reveals the net dipole orientation of surface species. The experimental setup of our HD-VSFG system used here is similar to the one reported by Nihonyanagi et al.¹³¹ Briefly, the sum frequency signal of a target sample is interfered with the signal of a local oscillator delayed by a time ΔT , and hence the electric field of total sum frequency can be expressed as follows:^{91,132}

$$E_{total}(t) = E_{sample}(t - \Delta T) + E_{LO}(t) \quad (2.16)$$

E_{sample} denotes the sum frequency beam from samples or quartz and E_{LO} denotes the sum frequency beam from the local oscillator (GaAs crystal). Equation (2.16) can be converted into the frequency domain by Fourier transform which is written as:

$$E_{total}(\omega) = \int_{-\infty}^{+\infty} dt E_{total}(t) \exp(i\omega t) = E_{sample}(\omega) \exp(i\omega\Delta T) + E_{LO}(\omega) \quad (2.17)$$

The total detected intensity of the raw HD-VSFG spectra can be described as:⁹¹

$$\begin{aligned} I_{HD-VSFG} \propto |E_{tot}|^2 &= |E_{sample} + E_{LO}|^2 \\ &= |E_{sample}|^2 + |E_{LO}|^2 + E_{sample} E_{LO}^* \exp(i\omega\Delta T) + E_{sample}^* E_{LO} \exp(-i\omega\Delta T) \end{aligned} \quad (2.18)$$

The cross-terms which contains the imaginary and real parts information can be retrieved from the fringe pattern seen in the detected VSFG intensity spectrum under HD-VSFG setup.

The data processing of the raw HD-VSFG spectra (interferograms) to retrieve the real and imaginary $\chi^{(2)}$ spectra is shown in Figure 2.3. The raw interferograms were first inverse Fourier transformed to the time domain using OriginPro software (version 7.5). The $|E_{sample}|^2$ and $|E_{LO}|^2$ signals at $t = 0$ in the time domain which is the envelope in the

raw interferogram were filtered out and only the cross-terms were kept and followed by Fourier transform back to the frequency domain. The resulting frequency spectrum contains the phase information (φ) of the complex $E_{sample}E_{LO}^* \exp(i\omega\Delta t)$ (Figure 2.3). The phase of z-cut quartz was used as a reference because quartz does not have any apparent resonance in this infrared region and hence its phase can be regarded as a constant. Therefore, the real and imaginary $\chi^{(2)}$ spectra can be obtained by dividing the sample interferogram by the quartz reference spectrum through which the contribution from E_{LO} is completely removed. The final spectra were normalized to the reflectivities of the incident visible and IR beams on quartz and on the samples. The expression of the Im $\chi^{(2)}$ spectrum is as follows:

$$\text{Im } \chi^{(2)} \propto \frac{r_{vis,quartz} r_{IR,quartz} |E_{sample} E_{LO}|}{r_{vis,sample} r_{IR,sample} |E_{quartz} E_{LO}|} \sin(\phi_{sample} - \phi_{quartz}) \quad (2.19)$$

r is the reflectivity of the incident visible or IR beams on quartz or the sample. The phases of the quartz and sample (φ) were obtained directly from the Fourier transformation.

Considering that this dissertation is focused on the HD-VSFG study at the air/salt solution interfaces, the relationship of the sign of Im $\chi^{(2)}$ spectra and the net orientation of interfacial water transition dipole will be briefly illustrated below. For example, for water OH symmetric stretch with C_{2v} symmetry, the macroscopic second-order susceptibility $\chi^{(2)}$ can be expressed as follows:⁹¹

$$\chi_{yz}^{OH,SS} = \frac{1}{2} N_s \{ (\langle \cos^2 \psi \rangle \beta_{aac} + \langle \sin^2 \psi \rangle \beta_{bbc} + \beta_{ccc}) \langle \cos \theta \rangle + \langle \sin^2 \psi \rangle \beta_{aac} + \langle \cos^2 \psi \rangle \beta_{bbc} - \beta_{ccc} \} \langle \cos^3 \theta \rangle \quad (2.20)$$

where θ is the orientational angle between the water dipole (along the C_{2v} axis from oxygen to hydrogen) and the outwards surface normal, and ψ is the twist angle. The relative $\beta^{(2)}$ values (assuming $\beta_{ccc} = 1$) for the water OH symmetric stretch has been given by Gan et al. as follows $\beta_{aac} = 1.296$, $\beta_{bbc} = 0.557$ and $\beta_{ccc} = 1$.¹³³ By introducing these values into Equation 2.20, it can be expressed as:

$$\chi_{yz}^{OH,SS} = \frac{1}{2} N_s \beta_{ccc} \left\{ (1.296 + 0.557 \frac{\langle \cos^3 \theta \rangle}{\langle \cos \theta \rangle}) \langle \cos^2 \psi \rangle + (0.557 + 1.296 \frac{\langle \cos^3 \theta \rangle}{\langle \cos \theta \rangle}) \langle \sin^2 \psi \rangle + (1 - \frac{\langle \cos^3 \theta \rangle}{\langle \cos \theta \rangle}) \right\} \langle \cos \theta \rangle \quad (2.21)$$

Clearly, as shown by Equation 2.21, $\chi_{yz}^{OH,SS}$ becomes positive when $\cos\theta > 0$, that is, $0^\circ < \theta < 90^\circ$. It can be understood as a positive OH stretch band observed in $\text{Im } \chi^{(2)}$ spectrum indicates a net orientation of interfacial water molecules in the spectral region having their hydrogens on average pointing up towards the vapor phase.

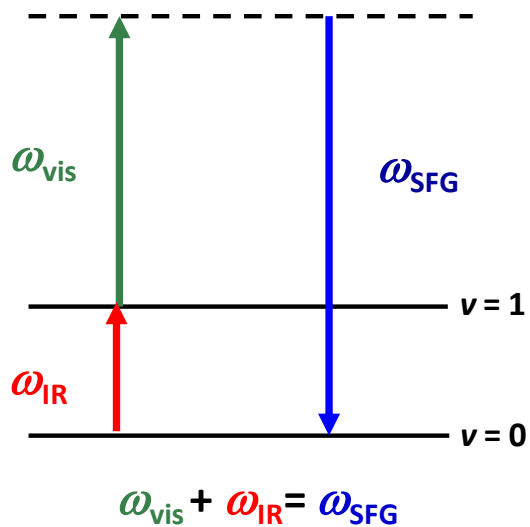


Figure 2.1 Energy level diagram of the sum frequency generation process. $v = 0$ is the ground state, $v = 1$ is a vibrationally excited state, and dash line indicates a virtual state.

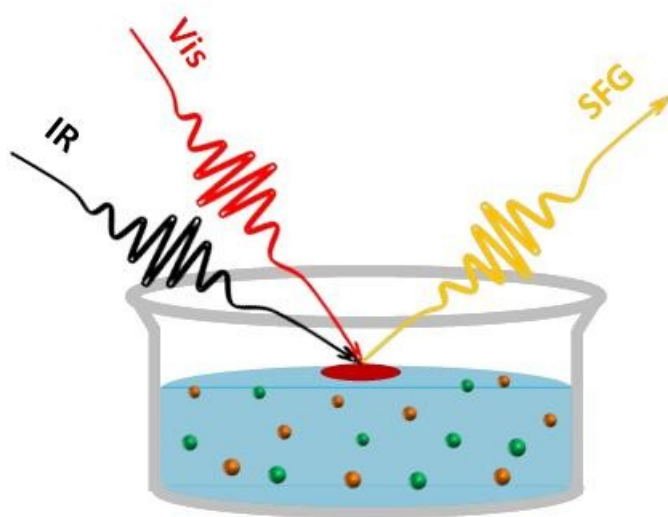


Figure 2.2 Schematic of the reflected VSG signal generated at the air/aqueous solution interfaces.

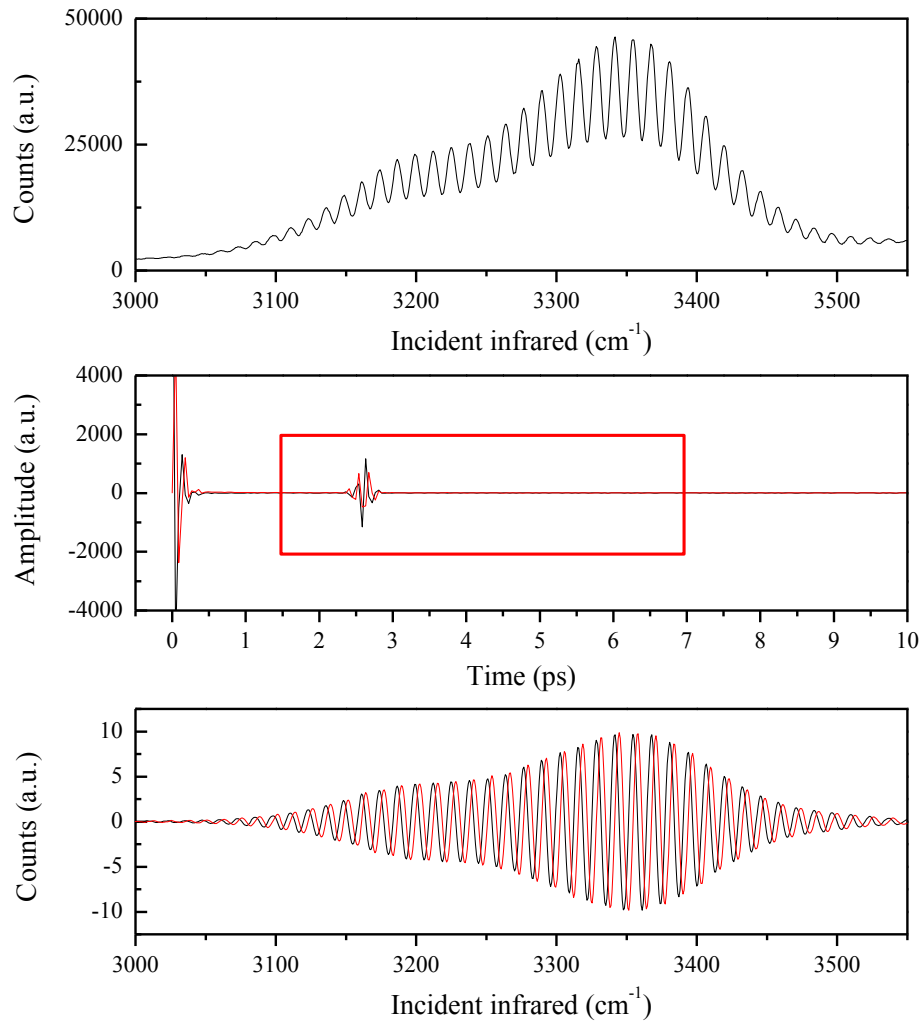


Figure 2.3 Upper panel: Raw interferogram of z-cut quartz with GaAs. Middle panel: Time domain real (black) and imaginary (red) signals. The cross term at ~ 2.6 ps (ΔT) is extracted to yield the heterodyne frequency spectra. Lower panel: Real (black) and imaginary (red) parts of heterodyne frequency spectra of z-cut quartz with GaAs. Phase information (φ) is therefore obtained.

Chapter 3 Instrumentation of Broad Bandwidth VSG

Reproduced in part with permission from Hua, W; Jubb, A.M.; and Allen, H.C. “Electric Field Reversal of Na_2SO_4 , $(\text{NH}_4)_2\text{SO}_4$, and Na_2CO_3 relative to CaCl_2 and NaCl at the Air/Aqueous Interface revealed by Phase-Sensitive Sum Frequency” *J. Phys. Chem. Lett.*, **2011**, 2, 2515-2520. Copyright 2011 American Chemical Society.

3.1 Conventional VSG Instrumentation

The broad bandwidth VSG spectrometer setup has been described elsewhere.¹³⁴⁻
¹³⁷ For the visible and infrared light generation, a titanium:sapphire oscillator (Spectra-Physics, Tsunami) with an optimal center-wavelength at 785 nm and a sub-50 fs pulse-width seeds two 1-kHz regenerative amplifiers (Spectra-physics, Spitfire, femtosecond and picosecond versions) that are pumped by a solid state Nd:YLF laser (Spectra-physics, Evolution 30) at 527 nm. The amplifiers generate ~85 fs pulses at 785 nm (22 nm bandwidth, > 1 W) and 2 ps pulses at 785 nm (17 cm^{-1} bandwidth, > 800 mW, used as the visible beam), respectively. The broadband femtosecond laser pulses (~85 fs, > 1 W) are used to generate amplified parametric waves (signal and idler) in an optical parametric amplifier (Light Conversion, TOPAS C). The amplified signal and idler beams are then used to create a tunable broadband infrared laser beam in the nonlinear difference-

frequency generation system (Light Conversion, NDFG connected to the TOPAS). The full spectral bandwidth of the generated broadband infrared beam is $\sim 800\text{ cm}^{-1}$ in the OH stretching region ($3000\text{-}3800\text{ cm}^{-1}$) under investigation. The average power of the visible beam and the infrared beam were $\sim 300\text{ }\mu\text{J}$ and $\sim 10\text{ }\mu\text{J}$, respectively. The visible beam (*s*-polarized, 785 nm) and the infrared beam (*p*-polarized, OH stretch region) were spatially and temporally overlapped on the sample stage to generate the sum frequency beam (*s*-polarized). To minimize an energy loss of the infrared beam and an overwhelming spectral interference arising from water vapor absorption, most part of the infrared beam path ($\sim 90\%$) was purged with dry nitrogen gas (in-house). The SF signal detection will be detailed in the HD-VSFG instrumentation section.

All the spectra shown in this dissertation were obtained under the *ssp* (*s*-SFG; *s*-visible; *p*-infrared) polarization combination. Spectral resolution was $\sim 8\text{ cm}^{-1}$. A raw VSFG spectrum needs to be processed before final presentation. First, a background spectrum needs to be subtracted from its corresponding raw sample spectrum after removal of all sharp peaks introduced by cosmic rays. Second, the background-subtracted VSFG spectrum is normalized against a non-resonant VSFG spectrum from a GaAs(110) crystal (Lambda Precision Optics, Inc) to eliminate the spectral distortion caused by the uneven infrared beam energy distribution at different frequency in the spectral region of interest. Third, the VSFG spectrum is calibrated by comparing it with a non-resonant GaAs profile obtained from a polystyrene thin film positioned in the infrared beam path (right after the output port of NDFG). The VSFG peak positions reported in this work are accurate to 1 cm^{-1} . All the VSFG spectra presented here were averaged over two

consecutive runs with a integration time of 5 min for each sample. Each VSG spectrum demonstrated in this dissertation was reproduced at least three times to ensure reproducibility.

To achieve a broad IR profile that allows probing the entire OH stretching region ($3000\text{-}3800\text{ cm}^{-1}$) in a single shot measurement with sufficient signal-to-noise ratio, several criteria had to be met: (i) the energy of the pulse at the output of the fs regenerative amplifier must be over 1 mJ, and the sum of signal and idler energy in the OH stretching region must be over 220 μJ ; (ii) the angle between the signal and idler beams on the AgGaS crystal in NDFG is critical. By varying this angle, the energy of the generated infrared beam varies substantially in a certain frequency range. However, the width of the IR profile is not always positively correlated with the infrared energy. In fact, the IR profile sometimes shows a sharp triangular or trapezoidal shape when the infrared energy approaches the upper limit achievable at that center frequency; (iii) the beam size of the infrared pulse after the NDFG stage, controlled by the position of IR focal lens, also plays an important role. If the size of the IR beam is equal or larger than that of the visible beam, the low and high frequency edges of the IR beam cannot be efficiently upconverted on the sample surface to generate a sum frequency signal; (iv) the compressor length in the fs amplifier is of paramount importance for improving the infrared energy distribution over the broad IR profile. In order to increase IR energy distributed at the two edges of the profile, it is often necessary to sacrifice some portion of the SFG peak intensity at the central spectral wavenumber by fine tuning the fs compressor length.

3.2 HD-VSFG instrumentation

The HD-VSFG system used here is similar to the design reported by Tahara and co-workers,⁹¹ which is based on heterodyne detection of broad band intensities and Fourier transform analysis. The important part of the optical configuration in our SFG system was redesigned for the HD-VSFG application as is illustrated in Figure 3.1.^{115,124}

As described above, the visible beam and the infrared beam were spatially and temporally overlapped on the sample stage (for samples and phase reference z-cut quartz) with incident angles of $\sim 50^\circ$ and $\sim 60^\circ$, respectively, to generate sum frequency signal. After reflection from the sample/reference, the incident visible, infrared, and the generated sum frequency (s-polarized) beams were refocused by a gold concave mirror ($f = 100$ mm) onto a GaAs (Lambda Precision Optics) surface to generate another sum frequency beam (local oscillator, LO). The two sum frequency beams from different stages generated an interference fringe in the frequency domain by passing the sum frequency beam generated from the sample (or quartz reference) through a 1 mm thick silica plate positioned before the gold concave mirror, resulting in a time delay of ~ 2.6 ps. The interferogram was stretched in a monochromator (Acton Research, SpectraPro SP-500 monochromator with a 1200 g/mm grating blazed at 750 nm) and detected by a liquid-nitrogen cooled charge-coupled device (CCD) (Roper Scientific, 1340×400 pixel array, Spec-10:400B: LN400EB back illuminated CCD). Special attention was given to the shape of image on the CCD array. In order to generate a good interferogram with a well-resolved fringe pattern, the response of the local oscillator (GaAs) needs to be attenuated somewhat (by changing the orientation of GaAs) to avoid an overwhelming

signal from the envelope. If the image was slightly tilted, data points need to be consistently shifted relative to the central pixel line on the image to avoid integrated signal attenuation during data processing. The height of the sample surface was checked by the image on the CCD. Retaining the same height is extremely critical for accurate phase determination. During the experiments, the height of the reference surface (quartz) and the sample surface were identical, within our measurement ability. Neat water was used as a reference for the pixel height. Height accuracy was better than 3 μm , where each CCD pixel is 20 x 20 μm . Final resulting $\text{Im } \chi^{(2)}$ spectra were averaged over the two consecutive runs with 5 min integration times for each sample. The measured reproducibility of the intensity when the sample was changed was within 5%.

During the completion of the work presented herein, part of the VSFG system was upgraded and efforts were constantly made to improve our HD-VSFG measurement, so the system setup and the quality of $\text{Im } \chi^{(2)}$ spectra differs somewhat in Chapters 6 to 9 compared to Chapters 4 and 5. Here, only the modifications made to the experimental setup and calculated parameters are presented. Briefly, the full spectral bandwidth of the generated broadband infrared beam has been expanded from 3000 to 3600 cm^{-1} in the latest HD-VSFG setup (3000 to 3500 cm^{-1} in Chapters 4 and 5) in the OH stretching region. The average incident energy of the visible (*s*-polarized, 800 nm) and infrared (*p*-polarized, OH stretching region) beams prior to the sample stage was reduced to $\sim 260 \mu\text{J}$ and $\sim 8 \mu\text{J}$, respectively. The primary SF beam was time-delayed from its previous value of 2.6 ps to 1.7 ps. The phase resolution (uncertainty) was thus improved from $20 \pm 5^\circ$ to $15 \pm 5^\circ$.

To discuss the delicate spectral changes at the air/aqueous interface the phase stability and accuracy need to be carried out with extreme care. As mentioned above, in the course of data processing, the $\text{Im } \chi^{(2)}$ spectrum of neat water is calculated by normalizing the phase of neat water (ϕ_{sample}) with the phase of quartz reference (ϕ_{quartz}). However, during the experimental operation, the way that the quartz reference was mounted on the sample stage was imperfect, so the phase (angle) of the z-cut quartz might vary slightly for different days. This may result in an uncertainty when assigning the *absolute* phase of our quartz reference; work is underway in our laboratory to improve this. Therefore, a phase drift of the quartz reference could be observed occasionally. Our spectral resolution (and reproducibility) is less than optimal. This is also a possible reason for the inconsistency of the zero-crossing point in the $\text{Im } \chi^{(2)}$ spectrum for neat water in literature^{29,91,93,115,124-126,138} (varying from $\sim 3150 \text{ cm}^{-1}$ to $\sim 3270 \text{ cm}^{-1}$) and among chapters within this dissertation.

Neat water spectra were used as a reference for salt comparison to assess reproducibility during the entire experimental period. The reproducibility for both conventional VSFG and HD-VSFG spectra of neat water will be demonstrated in the following chapters. Note that the zero-crossing point of $\text{Im } \chi^{(2)}$ spectra shown in this study was adjusted to match that published by Shen and co-workers,^{29,93} although critical here is that all $\text{Im } \chi^{(2)}$ spectra of salt solutions are compared to the same neat water $\text{Im } \chi^{(2)}$ spectrum. Thus our interpretation is based on the *relative* spectral difference between neat water and salt solutions. To check the validity of the $\text{Im } \chi^{(2)}$ spectra, the $|\chi^{(2)}|^2$ power spectra of each salt solutions deduced from the HD-VSFG data were compared to that

measured directly by conventional VSFG spectroscopy. A high similarity in their spectral shape is a necessary but insufficient criterion to prove the validity of the $\text{Im } \chi^{(2)}$ spectra. To avoid spectral clutter, only every fourth data point is plotted in all the $\text{Im } \chi^{(2)}$ spectra.

During daily operation, the quartz reference was never moved when measuring the spectra for neat water and all the salt solution samples, and the neat water sample was re-measured around every one to two hours to ensure the stability and reproducibility of the phase of the neat water $\text{Im } \chi^{(2)}$ spectrum obtained in the same day. This supplementary precaution ensured reliable phase reproducibility between measured neat water and salt solutions $\text{Im } \chi^{(2)}$ spectra. Although fine spectral line shape may change slightly, the general shape of $\text{Im } \chi^{(2)}$ spectra on different days for the same sample agree well within experimental error. The relative difference observed between a certain sample and neat water in the $\text{Im } \chi^{(2)}$ spectra can be reproduced on different days. Examples of $\text{Im } \chi^{(2)}$ spectra reproducibility are illustrated in Figure 3.2.

3.3 Infrared and Raman Spectroscopy

Attenuated total reflection Fourier transform infrared (ATR-FTIR) spectroscopy for bulk solution measurements were done using a FTIR spectrometer (Spectrum 100 FTIR Spectrometer, Perkin-Elmer) with a 45° incident geometry and a ZnSe crystal. For each solution, a volume of about 1 mL was deposited on the crystal surface. Spectra were collected using Spectrum Software (version 6.3.4) with a spectral resolution of 4 cm^{-1} and 128 scans at room temperature.

Raman spectroscopy measurements were performed on custom-built setup

consisting of a 532 nm continuous wave laser (Millennia Vs, SpectraPhysics), a Raman probe (RPS532/12-15, InPhotonics), a monochromator (SR-303I-A, Andor Technology; 1200 g/mm grating), and a CCD camera (Newton EM, DU970N-BV, Andor Technology). Raman spectra were collected in the 0° backscattered direction using a fiber optic, which was coupled to the entrance slit of the monochromator. The output power of the 532 nm beam exiting the Raman probe was ~95 mW. Prior to data collection, the Raman system was calibrated with a USB NeAr source (Princeton Instrument) and further fine-calibrated by taking the Raman spectrum of naphthalene powder. All samples were measured in 2 mL pyrex glass vials and the spectra were collected using Andor SOLIS software (version 4.15).

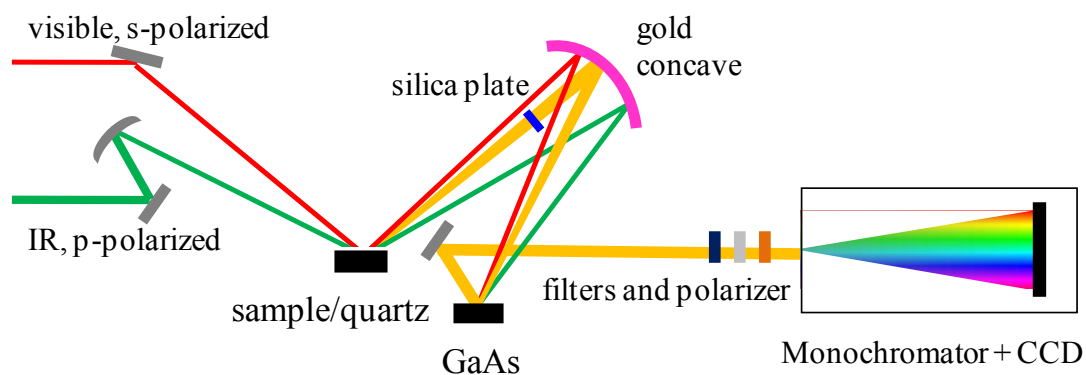


Figure 3.1 Schematic of the heterodyne-detected PS-SFG optical configuration. Filters and polarizer denote two short-pass filters, a notch filter (770~805 nm filtered out), and a Glan-Thompson polarizer respectively from left to right. The first short-pass filter has a cutoff ~ 770 nm and the second is a 785 nm Razor Edge ultrasteep short-pass edge filter.

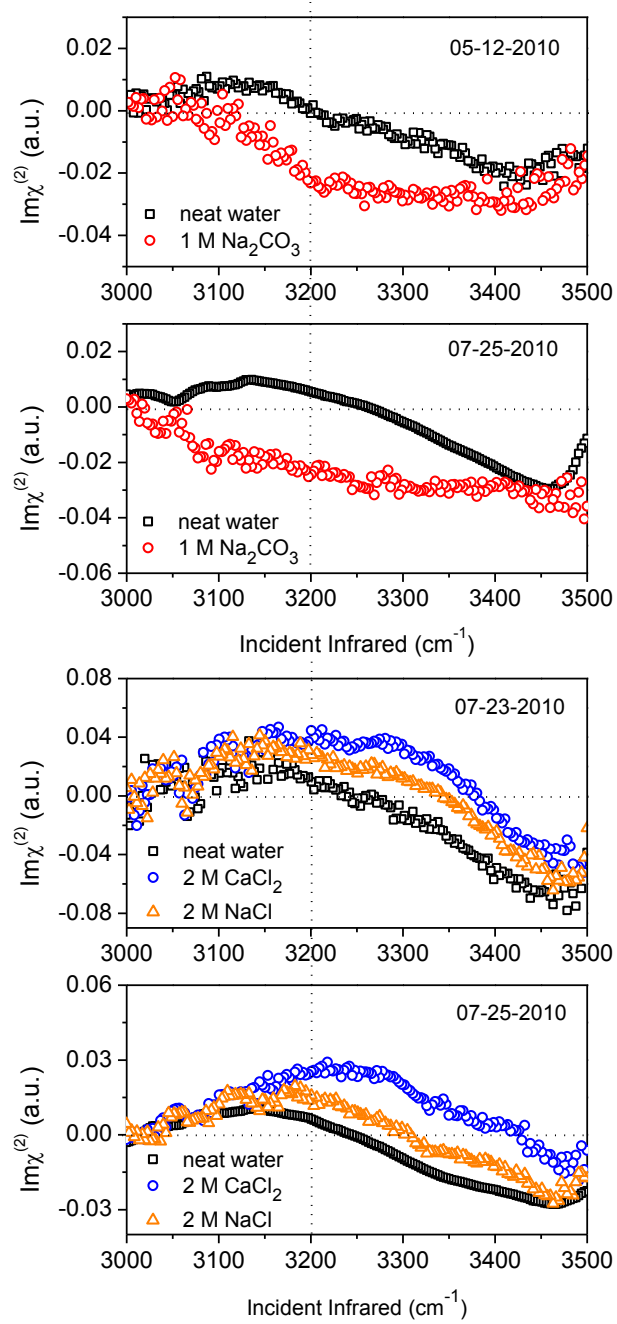


Figure 3.2 Reproducibility testing: $\text{Im } \chi^{(2)}$ spectra of neat water, 1.1 M Na_2CO_3 , 1.8 M CaCl_2 and NaCl salt solutions measured on different days.

Chapter 4 Heterodyne-Detected Sum Frequency Revealing Accommodation of Bicarbonate Ions, and Charge Separation of Sodium and Carbonate Ions within the Air/Water Interface

Reproduced in part with permission from Hua, W.; Chen, X.K.; and Allen, H.C. "Phase-Sensitive Sum Frequency Revealing Accommodation of Bicarbonate Ions, and Charge Separation of Sodium and Carbonate Ions within the Air/Water Interface" *J. Phys. Chem. A*, **2011**, 115, 6233-6238. Copyright 2011 American Chemical Society.

4.1 Introduction

Understanding interfacial water structure of ubiquitous air/aqueous interfaces at the molecular level is of prime importance in environmental chemistry and atmospheric aerosol science.^{2,9} The orientations and hydrogen bonding arrangements of water molecules may influence the surface properties and hence surface processes and surface reactivity of these systems. Many studies have revealed that it is the properties of the interfacial region that drive the heterogeneous chemistry of atmospheric aerosols.^{2,6,7}

Knowledge of water structure at air/aqueous salt solution interfaces may shed light on reaction mechanisms and gas uptake at aqueous interfaces of environmental interest. For instance, it has been proposed that the presence of water, specifically in the

interfacial region, plays an important role in the heterogeneous hydrolysis of ions in the atmosphere.¹³⁹ This is particularly relevant to the uptake and the chemical transformation of atmospheric carbon dioxide by atmospheric aerosol and ocean surfaces^{52,140} since CO₂ readily undergoes hydration and chemical reaction when in the presence of water.⁴⁸⁻⁵¹ For ocean-air interactions, it is the surface aqueous layers that first encounter atmospheric CO₂ prior to and during its transformation to bicarbonate and carbonate.¹⁴¹

Currently, about 30% of the CO₂,⁵² $1.5 \pm 0.4 \times 10^{14}$ mol, emitted to the atmosphere by human activities is absorbed annually by the ocean. This serves as the largest sustained sink of excess atmospheric CO₂ resulting from fossil fuel burning and results in total inorganic carbon (T_{CO2}) content of the seawater of $\sim 2000 \mu\text{mol kg}^{-1}$.¹⁴² Considering the increasing concentration of CO₂ in the atmosphere (~ 385 ppm, IPCC 2007)⁵² and its potential impact on aqueous surface chemistry in the Earth's hydrological cycle via enhancing acidity of aqueous surfaces, the behavior of carbonate and bicarbonate ions in the interfacial region from reaction of CO₂ with water may be important.^{6,143}

While the flux of CO₂ between the ocean and the atmosphere is influenced by many factors inclusive of atmospheric concentration (partial pressure), temperature, salinity, and alkalinity, the knowledge of the surface preference and interfacial average distribution of carbonate and bicarbonate ions at the air/aqueous interface might facilitate a better understanding of the process of CO₂ absorption into the ocean. Moreover, due to decreasing pH of the ocean from increasing atmospheric CO₂ concentrations, the ratio of HCO₃⁻ to CO₃²⁻ is changing,⁵² which then may alter the water organization at the air-ocean interface and air-atmospheric aerosol interfaces, as is suggested from the results

presented here. These findings may also be relevant to thundercloud electrification. For example, in atmospheric lightning production, sulfate ions in the surface layer of ice particles are suggested to be responsible for charge transfer in thundercloud electrification¹⁶, and yet to our knowledge, carbonate and bicarbonate have not been implicated in any part of this process.

To understand the organization of relevant air/aqueous interfaces, we report the interfacial water transition dipole orientation in the presence of Na_2CO_3 and NaHCO_3 . The distribution of the solvated ions relative to their respective aqueous surfaces is inferred using heterodyne-detected vibrational sum frequency generation (HD-VSFG), a variant of vibrational sum frequency generation (VSFG). Additional insight is given on the perturbation of the interfacial water structure for each aqueous salt system.

The seminal publication of the water surface VSFG spectrum was reported in 1993,¹⁰⁰ just two years after the first published account of surface VSFG.¹⁴⁴ SFG is a second-order nonlinear optical process that demonstrates interface specificity and molecular sensitivity. The SFG response vanishes in centrosymmetric media,⁹⁸ and is sensitive to orientation and ordering of interfacial species.^{8,96,100-102,105,145} The in depth description of conventional VSFG spectroscopy has been given in Chapter 2. To date, VSFG has been applied extensively to characterize air/aqueous interfaces of acidic, basic, and aqueous salt solutions.^{96,136,145,146} However, our understanding of how various types of ions alter the interfacial hydrogen-bonding network at the air/water interface, namely the net water dipole orientation of water molecules at the air/aqueous salt solution, is still quite limited.

The conventional VSFG spectrum does not differentiate the net water dipole direction and suffers spectral distortion arising from cross terms that include contributions from the resonant real part of $\chi^{(2)}$ ($\text{Re } \chi^{(2)}$), the imaginary part of $\chi^{(2)}$ ($\text{Im } \chi^{(2)}$), and the nonresonant, $\chi_{NR}^{(2)}$. To deduce orientation information from the measured $|\chi^{(2)}|^2$ spectra (i.e. conventional VSFG spectra) in the O-H stretch region, discrete resonances have been assumed by different groups to fit the spectrum.^{32,147} However, the overall spectral shape arises from a continuous band of OH stretch resonances of interfacial water molecules that are hydrogen bonded to neighbors with a wide variety of geometries and strengths.^{29,93} Without knowledge of the resonant frequencies and their respective signs of their amplitudes, fitting these spectra becomes somewhat arbitrary. Additionally, coupling between water modes also plays a role in the spectral shape. As a result, despite the similarity of VSFG spectra obtained by different groups, detailed interpretation of the spectra often varies.^{111,112} This issue is mostly remedied by using a phase-resolved SFG method that enables absolute determination of the sign of $\chi^{(2)}$.

The phase-resolved VSFG technique has been pioneered by Shen and co-workers,^{29,93,109,118,119} named as phase-sensitive sum-frequency spectroscopy (PS-SFVG or PS-SFG). Benderskii and co-workers¹²⁰ and Tahara and co-workers^{91,121} developed this technique for broad bandwidth VSFG systems and named this technique as heterodyne-detected vibrational sum frequency spectroscopy (HD-VSFG). This phase-resolved VSFG method is based on interference of the sample response with an additional signal of phase reference, and hence provides the imaginary part of nonlinear susceptibility $\chi^{(2)}$, $\text{Im } \chi^{(2)}$, which directly reveals the net water dipole orientation of

surface species. In the current literature, HD-VSFG (also known as PS-SFG) has been utilized to elucidate the interfacial hydrogen-bonding network at air/neat water (including isotopic dilution by D₂O), air/acid/basic solutions, air/lipid and air/surfactant interfaces.^{29,91,93,109,118,119,121}

4.2 Experimental

Materials and preparation of salts solutions. Sodium carbonate (99.5~100.5%) was obtained from Mallinckrodt chemicals. Sodium bicarbonate (powder/certified ACS) was purchased from Fisher Scientific. The sodium carbonate salt was heated at 650 °C for 10 hrs before dissolving in Nanopure water. Nanopure water (not purged of CO₂) with a resistivity of 18.2 to 18.3 MΩ·cm and a measured pH of 5.5 was from a Barnstead Nanopure system (model D4741) with additional organic removing cartridges (D5026 Type I ORGANICfree Cartridge Kit; Pretreat Feed).

Stock solutions were prepared by dissolving salts in Nanopure and then were filtered using Whatman Carbon-Cap activate carbon filter, typically three times to eliminate organic impurities. Raman spectra were utilized to generate a calibration curve, and the concentrations of stock solutions were determined from the calibration curve. To facilitate comparison with previous conventional SFG studies and molecular dynamic (MD) simulations,^{70,84} 0.8 M and 1.1 M salt solutions were chosen in this study and then prepared by dilutions of desired amounts of stock solutions. The measured pH of 1.1 M Na₂CO₃ and 0.8 M NaHCO₃ solutions are 11.7 and 8.8, respectively. The resultant concentration of OH⁻ ions in the 1.1 M Na₂CO₃ is 0.01 M, relatively small compared to the salt ions. Owing to the sensitivity of SFG spectroscopy to organic contamination, all

of the water and salt solutions were proved to be free of organic impurities as revealed by the VSFG spectra obtained in the C-H region of 2800 to 3000 cm^{-1} . In addition, all solutions were conditioned at room temperature (23 ± 1 °C) over 24 hrs before use.

Methods: Heterodyne-Detected Vibrational Sum Frequency Generation (HD-VSFG). The broad bandwidth conventional VSFG and spectrometer setup has been described elsewhere¹³⁴⁻¹³⁷, with the HD-VSFG setup briefly described more recently.^{115,148} The HD-VSFG sample and detection setup used here is similar to the system reported by Tahara and co-workers.^{91,121} Both conventional VSFG and HD-VSFG systems have been detailed in Chapter 3.

4.3 Results and Discussion

Air/aqueous solution interfaces of Na_2CO_3 and NaHCO_3 salts have been previously investigated by conventional VSFG methods and MD simulation.^{70,84} Yet, no direct PS-SFG measurement has been conducted. Here we probe the net transition dipole orientation of the interfacial water molecules in the presence of these salts in the OH stretching region. The relative placement of the cations and anions, their average distribution, in the interfacial region is then inferred.

Neat water. Considering that we use the air/neat water interface as a reference for all spectra, to facilitate the discussion, the HD-VSFG spectrum of the air/neat water interface and its spectral interpretation is presented. To check the validity of the spectra, the deduced power $|\chi^{(2)}|^2$ spectrum of neat water from HD-VSFG with that measured directly from the conventional VSFG setup is compared. In this work, we focus on the hydrogen bonding region as discussed above; in the inset of Figure 4.1, the spectral range

is expanded for the conventional VSFG to include the dangling (free) OH region for reference. As determined by others and clearly accepted by researchers in this field, the dangling OH oscillator points into the air phase.^{29,91,93,100} In Figure 4.1 (top and middle panels), the conventional VSFG and the deduced $|\chi^{(2)}|^2$ spectra are shown, and are observed to be similar although the lowest and highest frequency edges of the deduced $|\chi^{(2)}|^2$ spectrum are lower in SFG intensity. This is due to low incident infrared energy (because of partitioning to the LO) of the spectral edges of the early HD-VSFG setup. Most obvious in the deduced $|\chi^{(2)}|^2$ spectrum is the relatively low SFG intensity from 3000 to 3100 cm^{-1} . In this case, the incident infrared energy is insufficient to adequately pump the transitions and normalization procedures do not remedy the problem.

As mentioned above, the $\text{Im } \chi^{(2)}$ spectra directly provide informative details, the sign and thus transition dipole orientation of each mode in addition to resonance information. The $\text{Im } \chi^{(2)}$ spectrum of neat water in the hydrogen bonded stretching region presented here (Figure 4.1 bottom panel) is similar to the results reported by Shen and co-workers and Tahara and co-workers.^{29,91,93} As revealed in Figure 4.1, the sign of $\text{Im } \chi^{(2)}$ is positive from 3000 cm^{-1} to 3200 cm^{-1} region and mostly represents the OH stretches in this subspectral region with a net orientation pointing up toward the vapor side of the interface. Recent theoretical investigations by Morita and coworkers^{149,150} bring into question the assignment of absolute orientation from the 3000 to 3200 cm^{-1} region. Yet, we can confidently assign the absolute transition dipole orientation of water molecules for those molecules that contribute to the more weakly hydrogen bonded spectral region, that is, from 3200 to 3500 cm^{-1} . This spectral region encompasses a large fraction of the

SFG intensity and bandwidth. The $\text{Im } \chi^{(2)}$ spectrum reveals a negative band above 3200 cm^{-1} indicating that water molecules have a net transition dipole orientation with their hydrogens pointing down toward the bulk although it is likely that the distribution of orientations is broad. It was also suggested by others that the top few layers of the water surface are largely responsible for the observed SF spectra while the subsequent layers make little contribution due to the rapid decay of interfacial molecular ordering when approaching isotropic bulk.^{29,91,93}

The salt solution SFG spectra are shown in Figure 4.2. For comparison, the conventional VSFG, deduced $|\chi^{(2)}|^2$, and the $\text{Im } \chi^{(2)}$ spectra are shown for the air/liquid interface of neat water (taken from Fig 4.1), 1.1 M Na_2CO_3 , and 0.8 M NaHCO_3 .

Na_2CO_3 . We first consider the aqueous Na_2CO_3 solution. In the left column the conventional VSFG, deduced $|\chi^{(2)}|^2$, and the $\text{Im } \chi^{(2)}$ spectra are shown. The Na_2CO_3 conventional VSFG spectra are in good agreement with conventional spectra obtained by Richmond et al.⁸⁴ The overall shape of the hydrogen bonded OH stretching region of the directly measured conventional VSFG spectrum and the deduced $|\chi^{(2)}|^2$ spectrum is similar, as expected. There is a slightly lower intensity in the low frequency region of the deduced $|\chi^{(2)}|^2$ spectrum due to the lower energies used in the HD-VSFG set up as was discussed above for the neat water spectra. In addition, the relatively large local oscillator (LO) signal enhances the noise in the low energy wings and this also cannot be normalized out. However, comparison between the water spectra in the same panel reveals interesting and valid differences.

When comparing the Na_2CO_3 solution spectra with that from neat water, the

conventional and deduced $|\chi^{(2)}|^2$ Na_2CO_3 spectrum (top and middle panels) shows an enhanced intensity below 3200 cm^{-1} and a weakened intensity at $\sim 3400\text{ cm}^{-1}$ relative to neat water. This suggests that there is a strengthening of the hydrogen bonds. However, it is evident from the $\text{Im } \chi^{(2)}$ spectrum of the air/ Na_2CO_3 solution interface that there are additionally significant changes at and above 3200 cm^{-1} compared to the neat water $\text{Im } \chi^{(2)}$ spectrum. The sign of the band below 3200 cm^{-1} flips from positive to negative in the presence of Na_2CO_3 salts, and a significantly stronger negative strength is observed in the $\text{Im } \chi^{(2)}$ spectrum from 3200 to 3450 cm^{-1} as compared to the neat water case. As aforementioned, the resultant concentration of OH^- ions in the 1.1 M Na_2CO_3 solution was 0.01 M , relatively small compared to the concentration of the salt ions. Additionally, according to Shen and co-workers, in the $\text{Im } \chi^{(2)}$ spectrum of the 1.2 M NaOH solution, the intensity of the negative 3400 cm^{-1} band was slightly weaker compared to neat water. We hence propose that the resultant OH^- ions in our Na_2CO_3 solution have a minor impact on the strengthening of the negative band in the $\text{Im } \chi^{(2)}$ spectrum. As stated above, the sign of the $\text{Im } \chi^{(2)}$ spectra reflects the net polar orientation of the corresponding OH stretches unambiguously for the spectral region above 3200 cm^{-1} . The negative sign from the spectrum reveals the net dipole orientation of interfacial water molecules with their hydrogen pointing down towards the bulk interior. The strong negative band in the $\text{Im } \chi^{(2)}$ spectrum suggests a relatively large fraction of interfacial water molecules have their dipole pointing toward the bulk solution in the presence of Na_2CO_3 salts. We interpret this finding arising from an electric field induced by the organization of near-surface sodium ions and near-interior carbonate ions in the aqueous interfacial region.

It has been pointed out that as small and relatively less polarizable ions, sodium cations are repelled from the surface.^{27,31,57,84,119} Hence, it is not likely that sodium ions exist at the very surface, but may exist in the sub surface region (termed near-surface above) to maintain their full hydration. However, based on our data, sodium ions appear to exist above the carbonate ions in order to provide the necessary field to align the water dipole with hydrogens pointing down (toward the carbonate). Therefore, the HD-VSFG result provides experimental evidence suggesting that the counter anions, that is, carbonate ions, are strongly repelled from the surface and reside on the bottom edge of the interfacial region (where lack of inversion symmetry ends), whereas sodium ions reside, on average, above the carbonate ions in the interface as illustrated in Figure 4.3a. This result is also supported by MD simulations by Miller and co-workers who proposed the repulsion of carbonate ions from the air/aqueous solution interface.⁷⁰

NaHCO₃. In addition to divalent carbonate anions, the interfacial water organization and structure at the air/aqueous interface in the presence of NaHCO₃ was investigated. As shown in the column on the right of Figure 4.2, the conventional, deduced $|\chi^{(2)}|^2$, and the $\text{Im } \chi^{(2)}$ SFG spectra from the 0.8 M NaHCO₃ solution closely resemble those from neat water. This was somewhat unexpected, although for the conventional VSFG spectrum the spectrum is consistent with previously published spectra from literature.^{70,84}

When comparing the 0.8 M NaHCO₃ conventional and deduced $|\chi^{(2)}|^2$ SFG spectra from Figure 4.2 (top and middle panel), the overall shape of the hydrogen bonding OH region is similar taking into account the slightly lower intensity in the low frequency

region as discussed above. When comparing the conventional and deduced $|\chi^{(2)}|^2$ NaHCO₃ spectra to those from neat water, there are no notable differences. This is also true for the comparison of the Im $\chi^{(2)}$ SFG spectra from the 0.8 M NaHCO₃ relative to neat water. The pH of the 0.8 M NaHCO₃ was 8.8; therefore, there is a relatively small concentration ($\sim 10^{-6}$ M) of OH⁻ ions in the solution. We assert that this relatively low OH⁻ concentration exerts little impact on the Im $\chi^{(2)}$ spectrum. Notably, contrary to the flip of sign of the band at 3200 cm⁻¹ observed in the Im $\chi^{(2)}$ spectrum in the presence of Na₂CO₃ salts, no appreciable changes are observed for the 0.8 M NaHCO₃ solution, which implies that the net polar orientation and structure of water molecules in the interface is mostly unchanged relative to the air/neat water interface. This also then implies that the bicarbonate and sodium ions are effectively dispersed in the hydrogen bonding network and do not have any appreciable preference for any specific region of the interface as illustrated in Figure 4.3(b). The sodium and bicarbonate ions in the 0.8 M NaHCO₃ solution do not perturb the interfacial water structure to any appreciable amount, and are accommodated in this region. An alternative explanation could be that the ions do not exist in the first several hundred nanometers below the surface; however, this is highly unlikely. (The SFG probe region, if not centrosymmetric, corresponds to \sim half of the shortest incident wavelength.)

On the other hand, it has been reported that NaHCO₃ has a negative adsorption as interpreted from an increase in surface tension relative to neat water, albeit a much more modest increase relative to that determined for sodium carbonate.¹⁵¹ The relatively smaller effect on surface tension is consistent with the smaller effect on the interfacial

water structure as observed here, yet the interpretation of negative adsorption clearly lacks the important details of preferential location of the ions in the interfacial region as suggested above.

Atmospheric aerosol and ocean surface chemistry implications

Aqueous phase aerosols and the ocean's surface absorb atmospheric gas phase CO_2 and given the solubility of CO_2 into water, carbonate concentrations of 1 to 10 micromolar and bicarbonate concentrations of 0.4 to 1.6 millimolar (calculated temperature range of 0 to 25° C) currently exist¹⁴² as calculated for the pH of sea water (7.75 to 8.2).⁵² Given the increasing concentration of CO_2 in the atmosphere, interfacial residence and chemistry of atmospheric aerosol and ocean surface water is important in considering the reactivity and uptake by these aqueous surfaces. Here we have shown that carbonate creates an increase in the interfacial thickness and creates a subsurface field by maintaining a charge separation between sodium and the less surface active carbonate. Whereas, bicarbonate and its counter cation sodium, intercalate in the dynamic matrix of the hydrogen bonding environment within the first few layers of the water surface. Although beyond the scope of this work, it is likely that the charge separation induced by carbonate will be maintained by sodium and carbonate ions even in the presence of bicarbonate. This suggests that the surface of aerosol and of the ocean will be impacted by changing ratios of carbonate to bicarbonate as atmospheric CO_2 concentrations continue to increase.

4.4 Conclusions

Here we have shown that CO_3^{2-} anions are buried well below the surface in a 1.1 M Na_2CO_3 aqueous solution, and that the sodium counter cations preferentially reside closer to the surface than the carbonate anions. This was inferred from directly determining that the water molecules in the interfacial region have their hydrogens on average pointing down toward the bulk aqueous solution. This preferred orientation arises from charge separation in the interfacial region, where on average the positively charged sodium cations are above the negatively charged divalent carbonate anions. Future work in our laboratory will focus on quantitatively assessing the anion – cation separation in the interfacial region by carrying out additional HD-VSFG studies of this salt at varying concentrations.

The bicarbonate ions organize very differently relative to the carbonate ions. It is inferred that the bicarbonate monovalent anions incorporate into the hydrogen bonding structure of the interfacial water molecules and the sodium cations reside on average near to the same depth as the bicarbonate anions. Thus, water structure is not significantly perturbed with the introduction of 0.8 M NaHCO_3 . Deciphering how close the bicarbonate approaches the surface is still somewhat unclear; however, if only the first few layers of water molecules give rise to the SFG signal intensity for the neat water surface, then bicarbonate and its counter cation sodium likely also reside in this region.

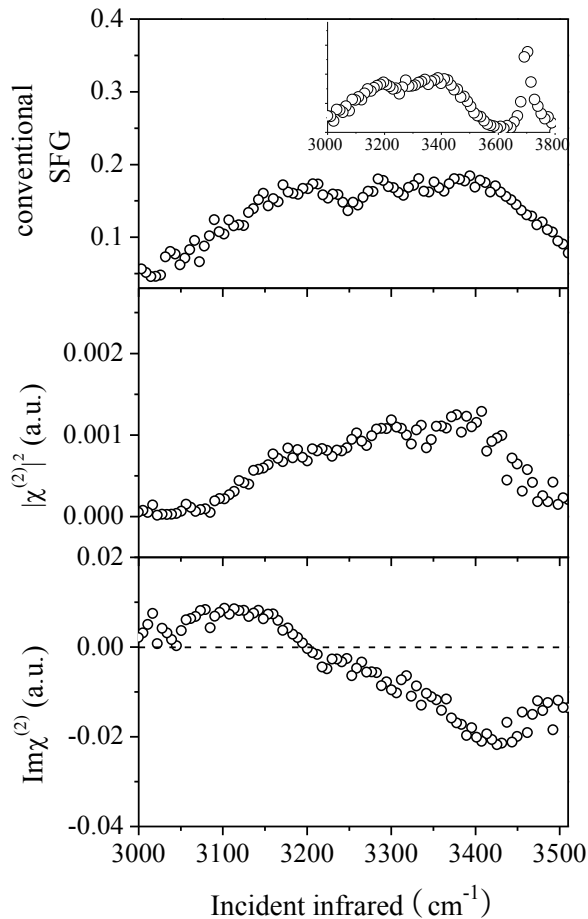


Figure 4.1 HD-VSFG and conventional VSFG spectra of neat water. $\text{Im } \chi^{(2)}$ VSFG spectra (bottom panel), deduced power spectrum (middle panel), conventional VSFG spectra (top panel). The inset in the top panel is full conventional VSFG spectrum from 3000 to 3800 cm^{-1} .

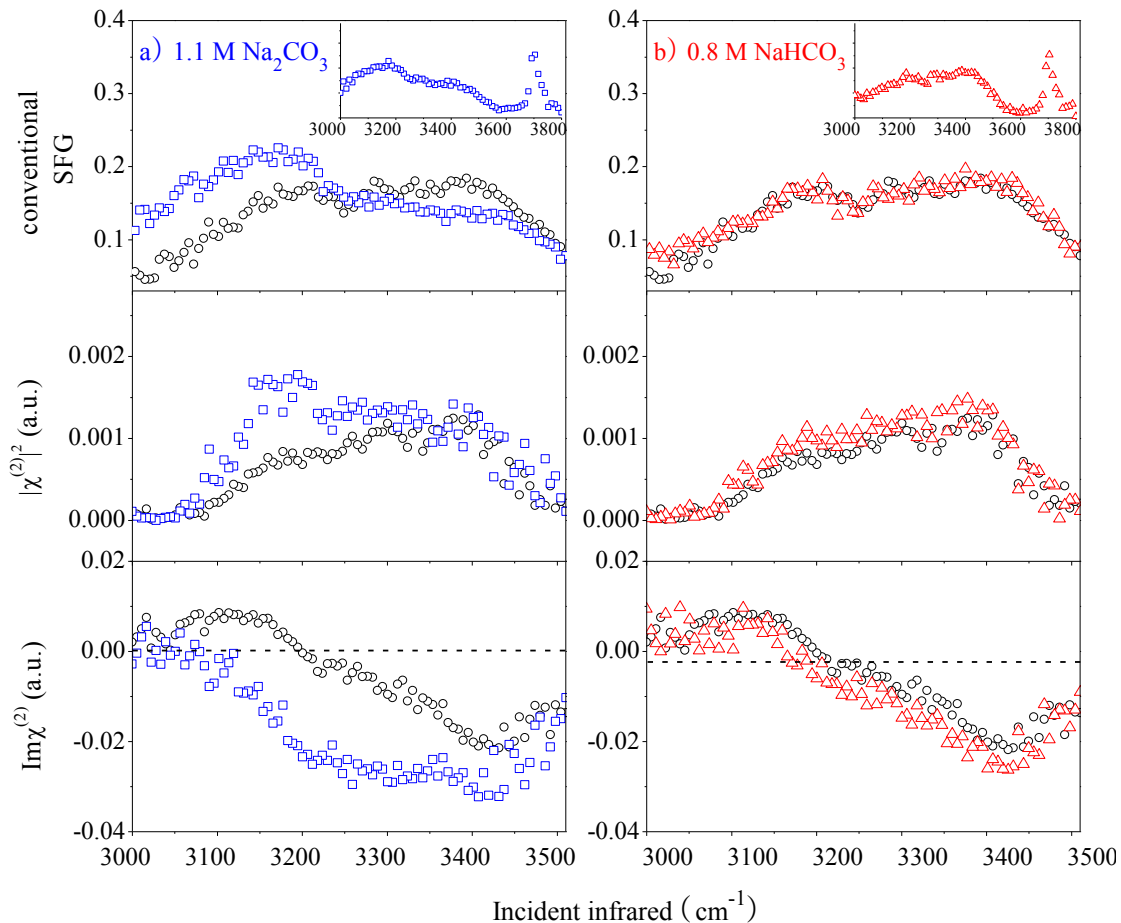


Figure 4.2 HD-VSFG and conventional VSFG spectra of water molecules at different vapor/aqueous salts solution interfaces: a) 1.1 M Na_2CO_3 , b) 0.8 M NaHCO_3 salt solution. $\text{Im} \chi^{(2)}$ SFG spectra (bottom panel), deduced power spectrum (middle panel), conventional VSFG spectra (top panel). Neat water spectra are shown as a reference (black circles). The insets in the top panels are conventional VSFG spectra showing the full 3000 to 3800 cm^{-1} region.

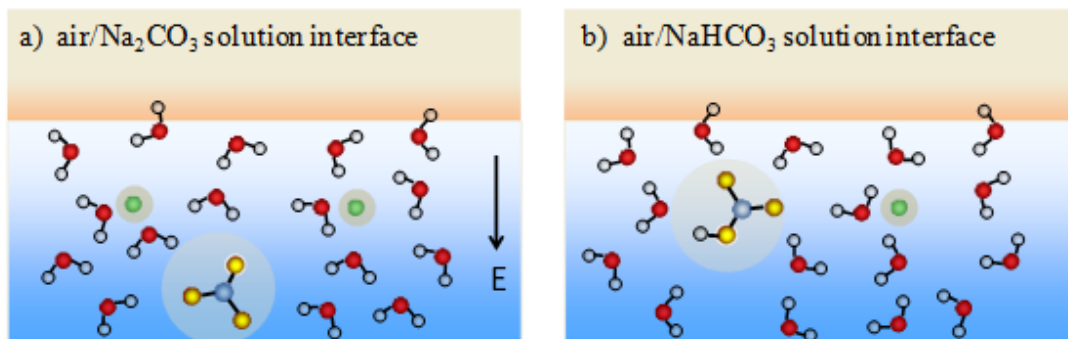


Figure 4.3 Illustration of water orientation at the air/aqueous salt solution interface of (a) 1.1 M Na_2CO_3 and (b) 0.8 M NaHCO_3 . Carbon and oxygen in carbonate and bicarbonate ions are bluish-gray and yellow spheres respectively, while sodium ions are green.

Chapter 5 Electric Field Reversal of Na₂SO₄, (NH₄)₂SO₄, and Na₂CO₃ relative to CaCl₂ and NaCl at the Air/Aqueous Interface revealed by Heterodyne-Detected Sum Frequency Spectroscopy

Reproduced in part with permission from Hua, W.; Jubb, A.M.; and Allen, H.C. “Electric Field Reversal of Na₂SO₄, (NH₄)₂SO₄, and Na₂CO₃ relative to CaCl₂ and NaCl at the Air/Aqueous Interface revealed by Phase-Sensitive Sum Frequency” *J. Phys. Chem. Lett.*, **2011**, 2, 2515-2520. Copyright 2011 American Chemical Society.

5.1 Introduction

Water organization at the air/aqueous salt solution interface is strongly influenced by ions, specifically, ion distributions that exist in the interfacial region. Revealing the organization of ions and their relative distributions within the air/aqueous interface is critically important for the understanding of processes occurring in every facet of life, from the environment to materials to biology. Interfacial organization of environmentally relevant ions such as those studied in this research has consequences for atmospheric aerosol chemistry,^{8,152} thundercloud electrification,¹⁶ geochemistry,^{17,153-156} and ocean surface processes.²² Particular emphasis in this research is on understanding atmospheric

aerosol aging of which existence of ions in the aerosol surface and subsurface regions, the interface, plays a critical role for reactivity and accessibility by gas phase oxidants.

To understand the distribution of ions in the interfacial region, we investigate water organization at air/aqueous salt solution interfaces in the presence of CaCl_2 , NaCl , Na_2SO_4 , $(\text{NH}_4)_2\text{SO}_4$, and Na_2CO_3 using heterodyne-detected vibrational sum frequency spectroscopy (HD-VSFG). Water organization is directly influenced by the direction and relative strength of the electric field generated in the interfacial region by the distribution of ions. The perturbation of the interfacial water organization by this electric field can involve both re-orientation and re-structuring of the water hydrogen-bond network as well as an increase in interfacial depth.

HD-VSFG is a variant of vibrational sum frequency generation (VSFG). In 1993, the seminal publication of the water surface VSFG spectrum was reported,¹⁰⁰ several years after the first published accounts of surface VSFG.^{144,157} In the recent past, VSFG has been used extensively to characterize air/aqueous interfaces of acidic, basic, and aqueous salt solutions.^{96,136,145,146} Yet the organization of ions at the air/aqueous interface is still not completely understood.

In the past it was accepted that ions were depleted from the aqueous surface revealing a negative surface excess based on surface tension measurement interpretation.^{9,25,26} This surface depletion is contrary to emerging thought for many ions, specifically halides.^{29,31,32,147,158} More recently however there is evidence for surface depletion of divalent anions and a proposed reversal of the interfacial electric field for sodium carbonate as shown in our recent HD-VSFG work,¹²⁴ for ammonium and sodium

sulfate salts as suggested by previous VSFG studies (conventional) and molecular dynamics (MD) simulations,⁵⁷ and by a recent phase-sensitive SFG study.¹³⁸ This is counter for the halide salts from previous studies^{32,147,158,159} including recent phase-sensitive SFG results as shown by Ji et al. and Tian et al..^{29,93,138} Results from HD-VSFG (also known as PS-SFG) studies have been critical to the understanding of the interfacial organization of these salt systems although conventional VSFG ($|\chi^{(2)}|^2$) studies have previously inferred this organization indirectly.^{57,147} The principle of conventional and heterodyne-detected VSFG spectroscopies have been introduced in Chapters 2 to 4.

5.2 Experimental

The broad bandwidth VSFG spectrometer and the HD-VSFG setup have been detailed in Chapter 3. The ssp polarization combination is used here. Only every fourth data point is shown in the SFG spectra to reduce spectral clutter. The phase accuracy with the current optical setup is $\sim 20^\circ \pm 5^\circ$.

For the solution preparation, sodium and ammonium sulfate (ACROS organics \geq 99% crystalline anhydrous, and Sigma-Aldrich \geq 99% ACS reagent grade), sodium carbonate (Fisher Scientific, ACS certified 99.5~100.5%), sodium and calcium chloride (Fisher Scientific ACS certified 99% purity, and USP/FCC 99%) were further purified. (We note that previous studies in our group found that higher purity salts (with higher trace metal purity) proved less pure with respect to organic contamination.) All the salts were heated at 650 °C for 10 hrs before dissolving in Nanopure water. Nanopure water

(not purged of CO₂) with a resistivity of 18.2 to 18.3 MΩ·cm and a measured pH of 5.5 was from a Barnstead Nanopure system (model D4741) with additional organic removing cartridges (D5026 Type I ORGANICfree Cartridge Kit; Pretreat Feed).

Stock solutions were prepared by dissolving salts in Nanopure water and then filtered using Whatman Carbon-Cap activate carbon filter usually two to four times to eliminate organic impurities. Raman spectra were used to generate a calibration curve which then was used for further determining the concentration of each carbonate and sulfate salt. The concentrations of the filtered chloride salt stock solutions were standardized on the basis of the Mohr titration technique,¹⁶⁰ in which silver nitrate (Fisher Scientific, reagent grade) and potassium chromate (E.M. Science, 99.5% purity) were applied as a titrate and an indicator, respectively. The measured concentrations of Na₂SO₄, (NH₄)₂SO₄, and Na₂CO₃ were 1.1 M and their respective pHs were 6.1, 5.4, and 11.7. Concentrations of CaCl₂ and NaCl were 1.8 M. All water and salt solutions were proved to be free of organic impurities as revealed by the VSFG spectra obtained in the C-H region of 2800 to 3000 cm⁻¹. All solutions were conditioned at room temperature (23 ± 1 °C) over 24 hrs before use.

5.3 Results and Discussion

Here we probe the net transition dipole orientation of the interfacial water molecules in the OH stretching region in the presence of calcium and sodium chloride, ammonium and sodium sulfate, and sodium carbonate salts. In the spectra presented here, positive $\text{Im } \chi^{(2)}$ refers to SFG active OH species with a net polar orientation pointing toward the surface. From the HD-VSFG data, the relative average distribution of the

cations and anions in the interfacial region is then inferred. To this end, both conventional VSFG $|\chi^{(2)}|^2$ spectra and the corresponding HD-VSFG $\text{Im } \chi^{(2)}$ spectra are presented, followed by further analysis using the $\text{Im } \chi^{(2)}$ difference spectra.

Conventional VSFG $|\chi^{(2)}|^2$ and HD-VSFG $\text{Im } \chi^{(2)}$ spectra of the air/aqueous solution interfaces of CaCl_2 , NaCl , Na_2SO_4 , $(\text{NH}_4)_2\text{SO}_4$, and Na_2CO_3 salts were obtained and are shown in Figures 5.1 and 5.2. The neat water $|\chi^{(2)}|^2$ and $\text{Im } \chi^{(2)}$ spectra are shown as a grey line in the same figures for reference. The neat water $|\chi^{(2)}|^2$ spectrum reveals the dangling OH bond of surface water at 3700 cm^{-1} and the broad continuum of hydrogen bond lengths in the lower frequency region from 3000 to 3600 cm^{-1} . In the lowest frequency region shown, it is accepted that these hydrogen bonds are relatively strong, and as one moves to higher frequency, the hydrogen bonding strength is significantly weaker. Additional assignments to this broad continuum continue to be controversial.^{109,110,150,161,162}

The $|\chi^{(2)}|^2$ spectra of all aqueous salt solutions shown in the first panel of Figures 5.1 and 5.2 are consistent with VSFG spectra obtained by others^{8,32,57,70,84,138,147,163} although the spectrum of CaCl_2 has not been previously published. Similar to our work on aqueous MgCl_2 , the $|\chi^{(2)}|^2$ spectrum in the hydrogen bonding OH stretch region shown by Fig. 5.1a narrows and the broad continuum OH stretch band is centered close to 3300 cm^{-1} .¹⁶⁴ This is very different relative to aqueous $\text{Ca}(\text{NO}_3)_2$ (and $\text{Mg}(\text{NO}_3)_2$) data that showed a dramatic drop in VSFG signal around 3200 cm^{-1} and large increases around

3400 cm^{-1} .⁸⁸ The 3300 cm^{-1} enhancement was interpreted as a weakening of the hydrogen bonding environment in the interfacial region for divalent cation-containing chloride solutions,¹⁶⁴ however the application of HD-VSFG to these systems, e.g. CaCl_2 as shown by Fig. 5.1b, necessitates a re-thinking of this previous interpretation.

Upon inspection of the $\text{Im } \chi^{(2)}$ spectrum of aqueous CaCl_2 in Figure 5.1b, a significant spectral change, larger positive enhancement from 3200 to 3400 cm^{-1} and a less negative intensity for 3400-3500 cm^{-1} , is observed relative to the NaCl and the neat water $\text{Im } \chi^{(2)}$ spectra. Only the more weakly hydrogen bonded water molecules have been perturbed by the interfacial electric field. The overall more positive enhancement may be indicative of Ca^{2+} ions being buried further toward the bulk solution so that there is an enhancement of the electric field perpendicular to the surface with Cl^- ions existing above the Ca^{2+} ions. This electric field within the interfacial region re-organizes the interfacial water molecules to have their net OH transition dipole orientation pointing toward the solution surface, along with a probable restructuring of the interfacial water as well as an increasing number of water molecules probed that then increases the interfacial depth. To a lesser extent, in the region around 3475 cm^{-1} , the water molecules are oriented opposite relative to the majority of the hydrogen bonded water molecules. Furthermore, distinguishable after evaluation of the HD-VSFG data, the observed decrease at 3200 cm^{-1} and enhancement at 3300 cm^{-1} in the conventional VSFG shown in Fig. 5.1a is the result of spectral convolution of the $\text{Im } \chi^{(2)}$ component with the $\text{Re } \chi^{(2)}$ component (Figure 5.3). The $\text{Re } \chi^{(2)}$ component of the calcium chloride salt solution features significant differences in intensity and the overall shape changes compared to the $\text{Re } \chi^{(2)}$ component

of neat water. Therefore, the 3300 cm^{-1} enhancement of the conventional VSFG spectrum is not a decrease in the overall hydrogen bonding environment as was previously suggested for MgCl_2 .¹⁶⁴ This is a powerful example of the necessity of HD-VSFG to study complex systems such as the hydrogen bonding continuum of interfacial water.

The $\text{NaCl Im } \chi^{(2)}$ spectrum is slightly more positive for the more weakly hydrogen bonded water molecules compared to neat water, consistent with the picture that Cl^- has a small surface propensity. The difference $\text{Im } \chi^{(2)}$ spectra for the various solutions with respect to the neat water spectrum are plotted in Figure 5.4, and are solely for ease of assessment and as a qualitative guides for the eyes. The difference spectra reveal that both NaCl and CaCl_2 spectra give rise to a greater degree of re-organization featuring more OH transition dipole moments pointing toward the surface of their respective solutions. Clearly, calcium chloride more strongly re-organizes the interfacial water molecules relative to sodium chloride for a similar cation concentration.

Figure 5.2 shows a comparison between the $|\chi^{(2)}|^2$ and $\text{Im } \chi^{(2)}$ spectra from aqueous Na_2CO_3 , $(\text{NH}_4)_2\text{SO}_4$, and Na_2SO_4 . As previously observed for conventional VSFG, significant enhancement of the hydrogen bonding region is present and was interpreted, for the most part, as an increase in the field perpendicular to the interface caused by the preference of SO_4^{2-} (and CO_3^{2-}) for increased solvation.⁵⁷ Recently both interpretations have been confirmed by phase-sensitive sum frequency (PS-SFVG) data by Tian et al.¹³⁸ for both sulfate salts and by Hua et al.¹²⁴ for sodium carbonate where all three salts produce a net orientation of the OH transition dipole moments pointing toward the bulk solution. However, after comparison of the three $\text{Im } \chi^{(2)}$ spectra, it is clear that

$(\text{NH}_4)_2\text{SO}_4$ re-organizes interfacial water hydrogen bonding to a greater degree which we attribute to the creation of a significantly larger electric field perpendicular to the interface relative to Na_2CO_3 and Na_2SO_4 . The order of largest to smallest electric fields is: $(\text{NH}_4)_2\text{SO}_4 > \text{Na}_2\text{SO}_4 > \text{Na}_2\text{CO}_3$, corresponding with the degree of water re-organization. There is a significant difference in the ammonium versus sodium sulfate data, which is clearly observed in the work presented here. The Tian et al.¹³⁸ PS-SFVG data does not resolve this difference.

As described above, Figure 5.4 shows a qualitative comparison of the five aqueous salt solutions after subtraction of neat water's $\text{Im } \chi^{(2)}$ spectrum from their respective $\text{Im } \chi^{(2)}$ spectra. The aqueous $(\text{NH}_4)_2\text{SO}_4$ causes the greatest disparity relative to neat water (the zero line). Further comparison between salt solution $\text{Im } \chi^{(2)}$ spectra reveals the competing preference for hydration of the ions, which culminates in their relative distributions within the interface. Figure 5.5 illustrates the reversal of the electric field relative to the surface as is suggested here for chloride and sulfate containing solutions.

Our results can be explained through understanding the hydration properties of each ion. Divalent anions, sulfate and carbonate, exhibit greater propensity for the bulk than the monovalent chloride anions, leading to a larger degree of charge separation between the relative ion distributions. This is consistent with cluster studies showing that divalent anions prefer to reside within the interior of the cluster while monovalent anions can exist on the cluster surface.^{9,56,77} In addition, the greater HD-VSFG $\text{Im } \chi^{(2)}$ intensity magnitude observed for $(\text{NH}_4)_2\text{SO}_4$ solutions versus the Na_2SO_4 is attributed to the surface preference of the ammonium ion.⁵⁷ Slight differences in $\text{Im } \chi^{(2)}$ signal intensity

between Na_2SO_4 and Na_2CO_3 solutions are consistent with the similar charge and hydration radius for these anions. The sulfate ion's slightly smaller hydration radius,¹⁶⁵ and thus greater charge density, may partially explain the slight HD-VSFG $\text{Im } \chi^{(2)}$ intensity magnitude increase for Na_2SO_4 solutions over Na_2CO_3 solutions as these factors will influence the respective ion's interfacial distribution. Differences observed for the chloride containing solutions can also be attributed to the surface charge densities of the two cations and thus the larger number of water molecules needed to fully solvate Ca^{2+} versus Na^+ due to the greater valency of calcium. This leads to Ca^{2+} ions on average residing deeper within the interface relative to Na^+ .^{9,166}

5.4 Conclusions

From the PS-SFG data, the $\text{Im } \chi^{(2)}$ spectra provide highly informative details, the sign and thus transition dipole orientation of each mode in addition to resonance information. Here we have shown that the sulfate and carbonate anion distributions are well below the surface and that the ammonium and sodium counter cation distributions on average preferentially reside closer to the surface. Moreover, ammonium sulfate creates the largest electric field perpendicular to the air/aqueous interface consistent with the picture of ammonium cations having a greater surface propensity relative to sodium cations.

Chloride ions, as discussed by others previously, are accommodated in the surface region, although these anions are less surface active relative to the larger and more polarizable bromide and iodide halides.^{9,138,147} Consistent with this, the calcium counter cation distributions are shown to exist predominantly below the chloride anion

distributions on average. This is opposite to the picture of the counter cations (sodium and ammonium) approaching the surface region for aqueous sulfate and carbonate solutions.

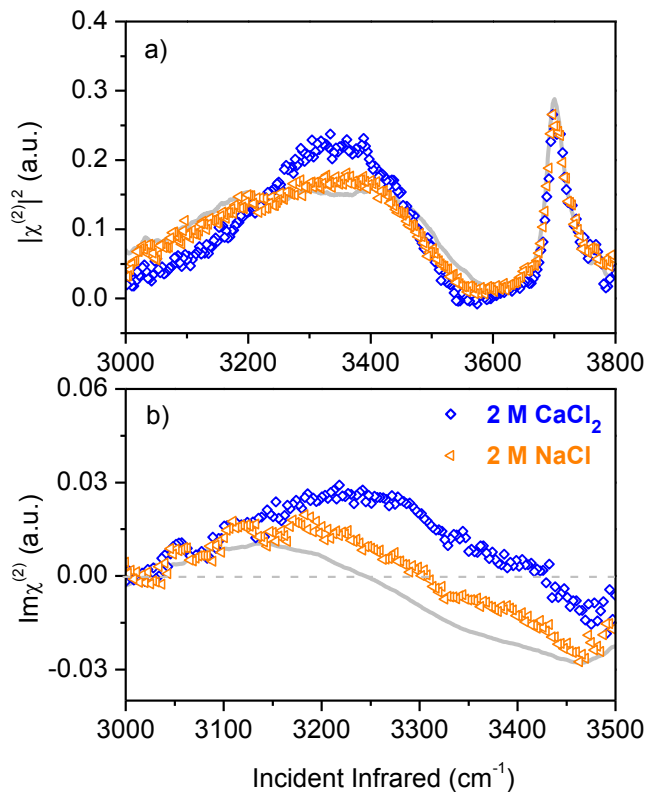


Figure 5.1 Conventional VSFG $|\chi^{(2)}|^2$ and HD-VSFG $\text{Im}\chi^{(2)}$ spectra of water molecules at vapor/aqueous solution interfaces of 1.8 M CaCl₂ and 1.8 M NaCl salt solutions. a) $|\chi^{(2)}|^2$ spectra of full 3000 to 3800 cm⁻¹ region (top panel), b) $\text{Im}\chi^{(2)}$ spectra (bottom panel). Neat water spectra are shown as a reference (light grey line).

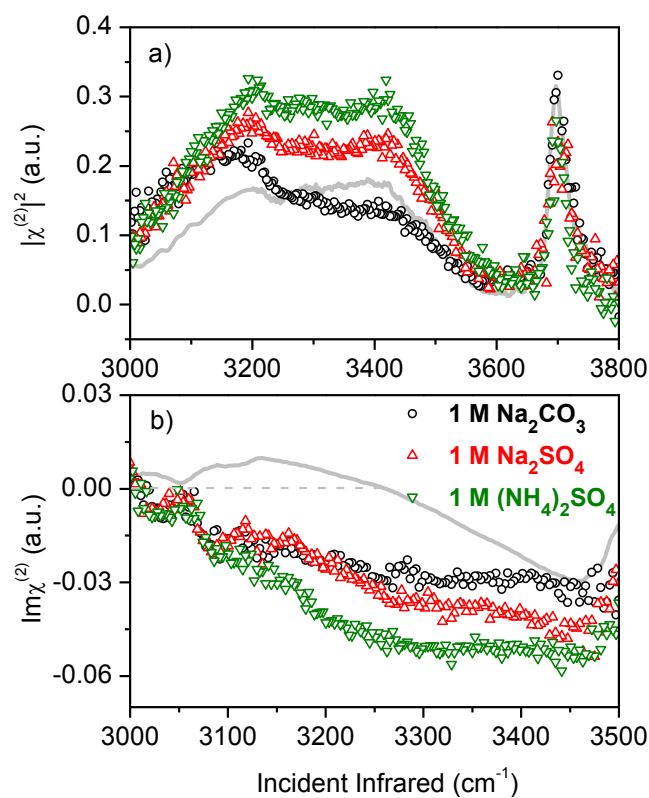


Figure 5.2 Conventional VSFG $|\chi^{(2)}|^2$ and HD-VSFG $\text{Im}\chi^{(2)}$ spectra of water molecules at vapor/aqueous solution interfaces of 1.1 M Na₂CO₃, 1.1 M Na₂SO₄, and 1.1 M (NH₄)₂SO₄ salt solutions. a) $|\chi^{(2)}|^2$ spectra of full 3000 to 3800 cm⁻¹ region (top panel), b) $\text{Im}\chi^{(2)}$ spectra (bottom panel) to 3500 cm⁻¹. Neat water spectra are shown as a reference (light grey line).

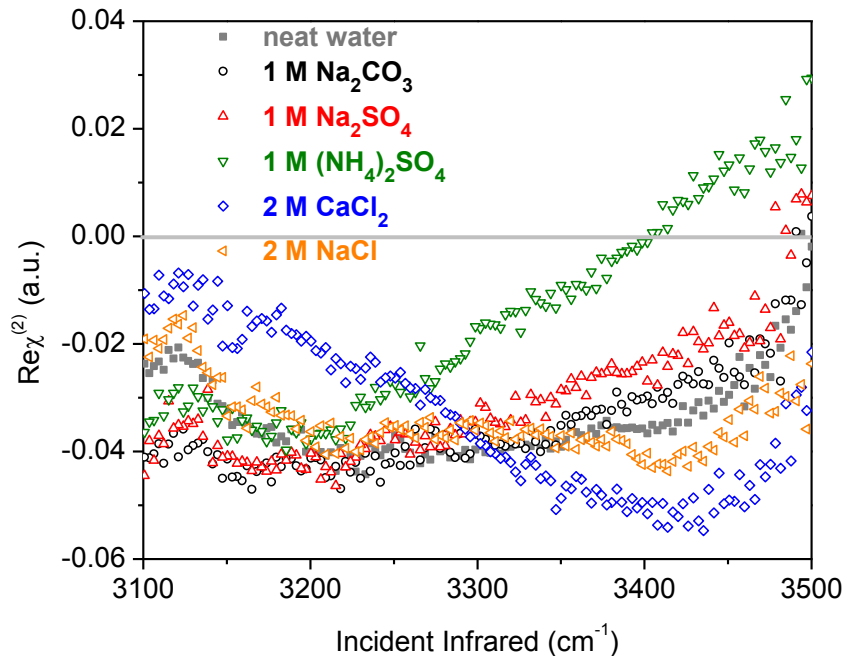


Figure 5.3 HD-VSFG $\text{Re } \chi^{(2)}$ spectra of water molecules at vapor/aqueous solution interfaces of neat water, 1.8 M CaCl_2 , 1.8 M NaCl , 1.1 M Na_2CO_3 , 1.1 M Na_2SO_4 , and 1.1 M $(\text{NH}_4)_2\text{SO}_4$ salt solutions.

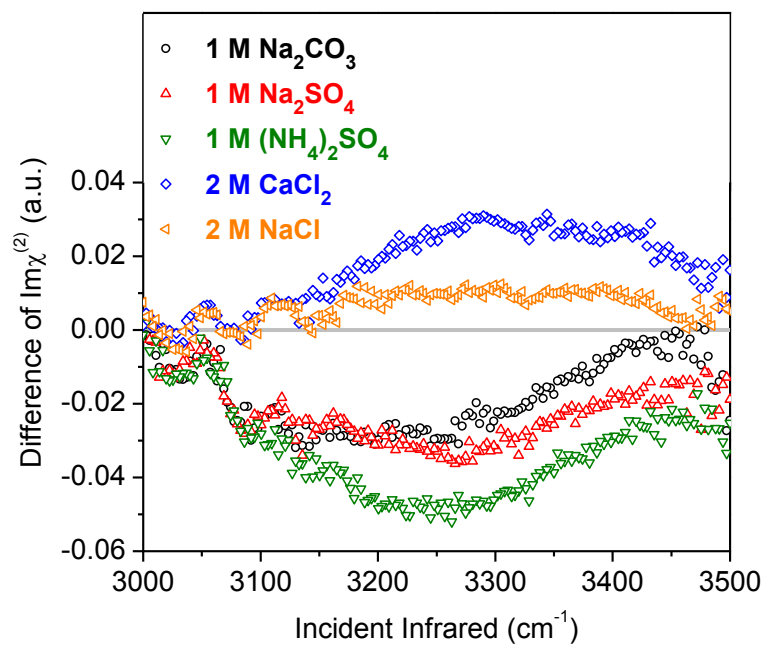


Figure 5.4 Difference HD-VSFG $\text{Im } \chi^{(2)}$ spectra ($\text{Im } \chi^{(2)}$ salt spectrum minus $\text{Im } \chi^{(2)}$ water spectrum) for the indicated salts. These spectra represent qualitative differences between the $\text{Im } \chi^{(2)}$ solution spectra and neat water's $\text{Im } \chi^{(2)}$ response.

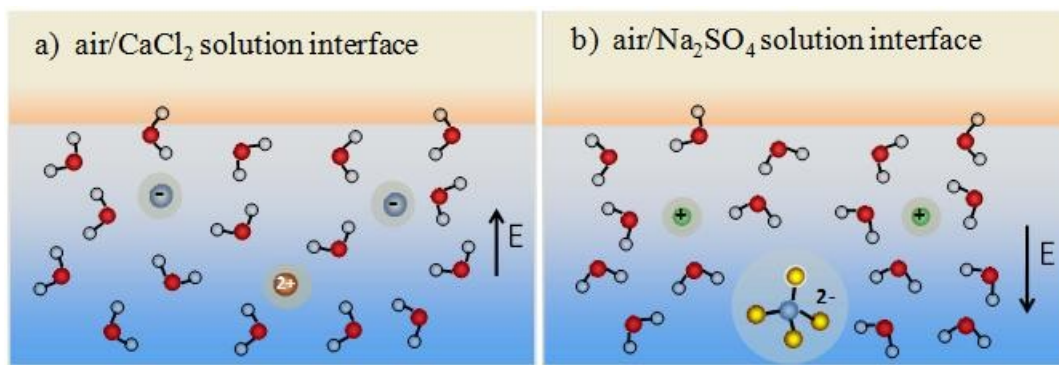


Figure 5.5 Illustration of water orientation at the air/aqueous salt solution interface of (a) 1.8 M CaCl₂ and (b) 1.1 M Na₂SO₄ solutions.

**Chapter 6 Impact of Salt Purity on Water Organization at Bare Air/Aqueous
Solution Interfaces and Influence of Salt Purity on the Interactions between Na⁺
Ions and Carboxylate Headgroup of Palmitic Acid Monolayers**

**6.1 Impact of Salt Purity on Interfacial Water Organization at Bare Air/Aqueous
Solution Interfaces**

Reproduced in part with permission from Hua, W.; Verreault, D; Adams, E.M.; Huang, Z.S.; and Allen, H.C. “Impact of Salt Purity on Interfacial Water Organization Revealed by Conventional and Heterodyne-Detected Vibrational Sum Frequency Generation Spectroscopy” *J. Phys. Chem. C*, **2013**, 117, 19577-19585. Copyright 2013 American Chemical Society.

6.1.1 Introduction

The impact of inorganic ions on interfacial water organization at air/aqueous interfaces has been a topic of sustained interest, particularly because of its relevance in atmospheric aerosol chemistry,^{6,7,167,168} geochemistry,¹⁹⁻²¹ and oceanic chemistry,²² among others. In recent years, intensive efforts have been invested through both computational and experimental methods in the understanding of the surface of aqueous salt solutions.^{8-10,128,169-171} For instance, the combination of molecular dynamics (MD) simulations and

surface-specific nonlinear optical techniques, such as second harmonic generation (SHG),^{28,79} conventional^{32,87,96,136} and, more recently, heterodyne-detected vibrational sum frequency generation (HD-VSFG) spectroscopy^{29,91-93,121} as well as two-dimensional (2D)-SFG spectroscopy,¹⁷²⁻¹⁷⁴ have allowed unprecedented access to the molecular-level picture of water organization and ion distributions at air/aqueous interfaces.

In the last decade, numerous conventional VSFG and HD-VSFG spectroscopic studies have systematically investigated the surface propensity and influence of common inorganic salts such as chlorides and other halides,^{32,57,94,125,138,147,163,164,175} carbonates,^{70,124,125} nitrates,^{68,88,89,138} and sulfates,^{57,84,125,138} on the interfacial water organization. Although there is some relative agreement on the effects of inorganic ions on the interfacial water spectrum and on their relative location within the interface, a lack of reproducibility between conventional VSFG and HD-VSFG spectra from different research groups as well as with other surface-sensitive techniques^{159,176} still exists in the literature. Aside from instrumental and methodological factors, a possible explanation for this discrepancy could come from the use of commercial salts of different grades and/or from salts and salt solutions that have undergone different processing (e.g., being used as-received, baking, filtering, baking and then filtering, etc.; see Table 6.1).^{28,32,57,68,70,84,87-89,124,125,138,164} However, aside from sporadic reports regarding halide salts,^{28,94} to the author's knowledge, no study using conventional VSFG and HD-VSFG spectroscopy has so far systematically compared the influence of salt purity and/or different prior treatments of salts and their solutions on the spectrum in the water OH stretching region for a variety of salts, particularly molecular ion-based ones.

To assess the impact of salt purity on the interfacial water organization and to establish a standardized pretreatment procedure, conventional VSFG spectra were measured in the water OH stretching ($3000\text{--}3800\text{ cm}^{-1}$) and in the CH stretching ($2800\text{--}3000\text{ cm}^{-1}$) regions and HD-VSFG spectra in the OH stretching region from the aqueous interfaces of solutions made with ACS and ultrapure (UP) grade commercial salts, with and without prior treatment. In the case of salts with high melting points (NaCl), VSFG spectra were also obtained for solutions made from baked-only ACS and UP grade salts. The results regarding carbonate, sulfate, and chloride salts reveal that for the same chemical species UP grade salts ($>99.99\%$) versus ACS grade ones ($\geq 99\%$) display highly similar conventional VSFG and HD-VSFG spectra in the OH stretching region, provided that the solutions be treated beforehand. However, untreated solutions from UP grade salts show a greater amount of organic impurities in comparison to ACS grade salts and greatly distort the spectrum in the water OH stretching region such that they should be used with caution in any study of interfacial water organization on aqueous solutions.

6.1.2 Experimental

Materials. ACS grade (purity $\geq 99\%$) and UP grade salts (purity ranging from 99.99% to 99.999%) were purchased from several suppliers: NaCl (ACS certified, $\geq 99\%$, Fisher Scientific; trace metals basis, 99.999% , Acros Organics), Na_2CO_3 (ACS certified, Primary Standard, Mallinckrodt Chemicals; trace metals basis, 99.999% , Acros Organics), Na_2SO_4 (ACS certified, $\geq 99\%$; trace metals basis, $\geq 99.99\%$, Sigma-Aldrich), $(\text{NH}_4)_2\text{SO}_4$ (ACS reagent, $\geq 99\%$, Acros Organics; trace metals basis, 99.9999% , Acros Organics), and LiNO_3 (ACS certified powder, Fisher Scientific). Nanopure water (not

purged of CO₂) with a resistivity of 18.2–18.3 MΩ·cm and a measured pH of 5.6 was obtained from a Barnstead Nanopure system (model D4741, Thermolyne Corporation) equipped with additional organic removing cartridges (D5026 Type I ORGANICfree Cartridge Kit; Pretreat Feed). All containers and glassware were carefully cleaned using concentrated sulfuric acid with addition of a strong oxidizer, ammonium peroxydisulfate, and then thoroughly rinsed with copious ultrapure water.

Preparation of Salt Solutions. Stock salt solutions for VSFG measurements were prepared by dissolving ACS and UP grade salts in Nanopure water. Owing to its ultrahigh sensitivity, VSFG spectra obtained in the CH stretching region (2800–3000 cm⁻¹) were utilized as a probe to verify the presence of trace amount organic residues. As revealed in these spectra, organic contamination was found in all stock salt solutions prior to any pretreatment. To completely eliminate organic impurities, as-received salts and their stock solutions underwent either one of the following pretreatments: (1) salt baking first followed by solution filtration or (2) filtration only (see Table 6.2). Baking was only applied for salts with a high melting point (e.g. $T_m \geq 650$ °C for carbonate, sulfate, and chloride salts) and the temperature chosen was at least 50 °C lower than the melting point. Most salts (except (NH₄)₂SO₄ and LiNO₃) were baked at ~600 °C for 10 h in a muffle furnace (Isotemp model 550-14, Fisher Scientific). Stock salt solutions were then filtered using activated carbon filters (Whatman Carbon Cap 75, Fisher Scientific). Depending on the abundance of organics in each salt, two or more filtration steps were performed: chloride solutions (2 times), carbonate and sulfate solutions (2–4 times), and nitrate solutions (4–6 times). For salts with a low melting point (< 500 °C), pretreatment

only refers to filtration. Salts from several different batches were tested and compared in this work, and no appreciable disparities were observed. Raman calibration curves were obtained to determine the concentration of carbonate, sulfate, and nitrate after filtration based on their vibrational symmetric stretch ion mode (see Figure 6.1), while chloride solutions were standardized by Mohr titration.¹⁶⁰ The measured pH of most solutions was found to fall in the range 5–7 (except Na₂CO₃ which had a pH~12). All pretreated salt solutions were shown to be free of organic impurities as revealed by the conventional VSFG spectra obtained in the CH stretching region (see Figure 6.2). All solutions were thermally equilibrated to room temperature (23 ± 1 °C) over 24 h before use. No degassing or N₂-purging has been applied on them.

The instrumental details of conventional VSFG and HD-VSFG spectroscopies have been given in Chapter 3. Conventional VSFG and HD-VSFG spectra of neat water in the OH stretching region obtained during the entire experimental period is presented to demonstrate system and phase stability (see Figure 6.3). To check the validity in the general trend of these spectra, the deduced power $|\chi^{(2)}|^2$ spectra of each salt solution reconstructed from the HD-VSFG results are compared to those measured directly by conventional VSFG spectroscopy (see Figure 6.4).

6.1.3 Results and Discussion

Conventional and Heterodyne-Detected VSFG Spectra of Pretreated Salt Solutions for Different Purity Grade Salts. Figure 6.5 shows the comparison between conventional VSFG spectra in the OH stretching region of pretreated 1 M Na₂CO₃, Na₂SO₄, (NH₄)₂SO₄, and NaCl salt solutions made from ACS and UP grade salts. A

typical VSFG spectrum of the neat air/water interface is also shown as reference for all salt solution spectra. This spectrum spans a large spectral region from 3000 to 3800 cm^{-1} and consists of a very broad band ranging from 3000 to $\sim 3600 \text{ cm}^{-1}$ and a narrow band centered at around 3700 cm^{-1} . The broad spectral band reflects the collective OH stretching modes of hydrogen-bonded surface and subsurface (i.e., a few Å away from the surface) water molecules with a broad continuum of geometries and strengths;^{8,93,164} the hydrogen bonding strength weakens as one goes from low to high frequencies. The narrow band at 3700 cm^{-1} is assigned to the dangling OH stretching of topmost surface water molecules with their OH bonds protruding into the vapor phase.¹⁰⁰

The conventional VSFG spectra of pretreated Na_2SO_4 and $(\text{NH}_4)_2\text{SO}_4$ salt solutions show greater SFG signal intensity over the entire broad region relative to that of neat water, while that of the Na_2CO_3 solution displays signal enhancement only below 3200 cm^{-1} with a weakened intensity for the higher frequency region ($\sim 3200\text{--}3450 \text{ cm}^{-1}$). In contrast, the conventional VSFG spectrum of NaCl remains practically unchanged compared to that of neat water. No appreciable differences are observed for the VSFG signal of the dangling OH peak for all salts studied. The observed changes in the broad region for carbonate and sulfate solutions have been interpreted as an increase in the electric field magnitude normal to the interface caused by the preferential distribution of CO_3^{2-} and SO_4^{2-} ions within the interface.⁵⁷

Moreover, it can be seen from Figure 6.5 that there is no significant intensity and shape differences between corresponding conventional VSFG spectra of pretreated ACS and UP grade salt solutions studied (LiNO_3 spectrum in Figure 6.6). The relative trend

observed here between the conventional VSFG spectra from sulfate salts and water is in good agreement with those previously reported on solutions made from as-received UP grade salts,⁸⁴ and with pretreated solutions from ACS^{57,125} and UP grade salts.¹³⁸ Noteworthy is the fact that despite using as-received UP grade salts (e.g. Na₂CO₃, 99.95%; Na₂SO₄, 99.99%), Tarbuck and Richmond observed no CH signal in their conventional VSFG spectra that would indicate the presence of organic contamination.⁸⁴ However, a similar situation was not found by Koelsch et al. in their comparison of VSFG spectra of as-received and purified 1 M NaI solution (in this case “surface chemical purity” was assessed using a surface tension-based purification method)¹⁷⁷ made from as-purchased UP grade salt (99.999%) nor for the case of untreated UP grade salts shown here (see discussion below).⁹⁴ This apparent discrepancy is not surprising as it may well reflect the variations in organic impurity over time between salt batches, between suppliers, and even from the same supplier. Also notable is the reversal of signal intensity in the conventional VSFG spectra of Na₂SO₄ and (NH₄)₂SO₄ pretreated solutions (see Figure 6.5a,c) from Allen and co-workers⁵⁷ relative to those reported by Tian et al.¹³⁸ An explanation for this discrepancy could come from the difference in the applied solution filtration methods. It is possible that the method privileged by Tian et al., primarily used for the removal of insoluble microparticles,²⁸ could have been less effective in the thorough elimination of organic contaminants.

The change in the overall shape of the hydrogen-bonded region with salt addition suggests that the presence and distribution of the ions within the interfacial region perturb water organization to different extents and force a rearrangement of the hydrogen-

bonding network. However, little information concerning the relative distributions of cations and anions in the interface can be inferred from conventional VSFG spectra because of the loss of phase information (i.e., OH transition dipole moment orientation) inherent to conventional VSFG spectroscopy. In order to gain further insight into the effects of ions on the orientation of water molecules and, in turn, on the relative ion distribution, HD-VSFG spectroscopy is utilized. In contrast to conventional VSFG spectroscopy, this technique provides directly the sign (i.e., orientation) and magnitude of the net water transition dipole moment for each vibrational mode.

HD-VSFG spectra in the hydrogen-bonded stretching region (3000–3600 cm^{-1}) from the pretreated solutions of each salt are shown in Figure 6.7. Again, the $\text{Im} |\chi^{(2)}|$ spectrum of neat water serves here as reference and is similar to the ones reported previously.^{29,91,121} This spectrum displays positive and negative bands located below and above a zero crossing point at $\sim 3200 \text{ cm}^{-1}$, which represent water molecules with a net OH transition dipole moment oriented towards and away from the vapor phase, respectively. In contrast to the higher frequency region, the assignment of absolute orientation in the lower frequency still remains debated due to recent computational analysis.^{149,150,178}

As can be seen in Figure 6.7, similar to conventional VSFG spectra, no significant difference can be observed in the intensity and the shape of the HD-VSFG spectra between ACS and UP grade salt solutions after pretreatment (e.g. filtration). These serve as evidence that pretreated UP grade salts have a negligible effect in the study of water structure for bare aqueous salt solutions. (This is not necessarily true for studies of lipids

on salt subphase.¹⁷⁹⁻¹⁸¹) HD-VSFG spectra of Na₂CO₃, Na₂SO₄, and (NH₄)₂SO₄ pretreated salt solutions all show greater negative intensity in the ~3050–3500 cm⁻¹ spectral region comparatively to neat water. This negative enhancement can be attributed to the presence of an ion-induced electric field in the interfacial region (e.g. carbonate and sulfate anions residing closer to the isotropic aqueous bulk with their cations located above them), which then causes water molecules to reorganize and to have a net orientation towards the bulk solution. A comparison of the Im $|\chi^{(2)}|$ spectra for the pretreated solutions made with ACS grade salts indicates clearly that the magnitude of this electric field from largest to smallest and, therefore, the extent of water reorganization, follows the series (NH₄)₂SO₄ > Na₂SO₄ > Na₂CO₃ (Figure 6.7d). This trend is also consistent with the one observed previously with pretreated solutions from ACS grade salts.¹²⁵

Conventional VSFG Spectra of Pretreated and Untreated Salts of Different Purity Grades. In order to emphasize the importance and to assess the effectiveness of solution pretreatment, a direct comparison was made between conventional VSFG spectra in the OH stretching region of 1 M (NH₄)₂SO₄ solutions made from ACS and UP grade salts, *before* and *after* pretreatment (Figure 6.8a). Conventional VSFG spectroscopy has been preferred here over its more involved heterodyne-detected variant because the focus here is not about the change of water transition moment orientation caused by the presence of specific salts, but instead the spectral perturbations introduced by their impurities. As shown previously, there is no observable spectral difference between the VSFG spectra of pretreated ACS and UP grade (NH₄)₂SO₄ solutions.

Interestingly, the VSFG spectrum for the untreated ACS grade $(\text{NH}_4)_2\text{SO}_4$ solution overlaps very well with the pretreated ones, indicating that the low amount of organic impurities present in the ACS grade salt do not affect the interfacial water organization. In contrast, the untreated UP grade $(\text{NH}_4)_2\text{SO}_4$ solution exhibits remarkable differences in its VSFG spectrum with a marked intensity increase in the lower frequency region, a small decrease in the higher frequency region, and a complete disappearance of the dangling OH peak at 3700 cm^{-1} . The suppression of the water dangling OH peak has been observed previously for surfactant systems such as insoluble alcohols, fatty acids, and phospholipids monolayers and has been attributed to the presence of adsorbed surfactants replacing surface water molecules at the interface.^{100,182}

To verify the presence of possible surfactant species, conventional VSFG spectra partially encompassing the CH stretching region ($\sim 2850\text{--}3000\text{ cm}^{-1}$) have been obtained for untreated 1 M $(\text{NH}_4)_2\text{SO}_4$ solutions made from ACS and UP grade salts (Figure 6.8b). Despite the lower signal-to-noise ratio at the edge of this broad spectral window, two distinctive peaks associated with CH_3 and terminal CH_2 symmetric ($\sim 2865\text{ cm}^{-1}$), and CH_2 asymmetric ($\sim 2913\text{ cm}^{-1}$) stretching modes can be distinguished in the VSFG spectrum of untreated UP grade $(\text{NH}_4)_2\text{SO}_4$ solution, thus confirming the presence of surfactants. In comparison, untreated ACS grade $(\text{NH}_4)_2\text{SO}_4$ solution show very little to no organic contamination in the same spectral region. This result clearly demonstrates that prior to pretreatment the UP grade $(\text{NH}_4)_2\text{SO}_4$ contains much more organic impurities than its ACS grade equivalent. This could possibly be due to the different industrial processes employed in the purification of UP (trace metals basis) and ACS

grade salts, the former presumably using chelating surfactant compounds for the precipitation or retention of unwanted inorganic ions.¹⁸³⁻¹⁸⁵

In the case of high melting point halide salts, one could also resort to salt baking as a suitable and easy to use alternative to solution filtration in the removal of organic impurities. Baking also limits the salt loss due to filtration and the need for subsequent concentration calibration. Figure 6.9a shows, for instance, a comparison between conventional VSFG spectra in the OH stretching region of 1.5 M NaCl solutions made from ACS and UP grade salts that underwent either baking or filtration steps. It can be seen that both treatment on ACS and UP grade NaCl solutions give nearly identical spectra in the OH region. In other words, salt baking and solution filtration appear to be comparable methods when it comes to organics removal. This is also the case for 2 M NaBr solution (data not shown). A complete removal of organic contaminants has also been demonstrated previously by Bian et al. by comparing the VSFG spectrum in the CH stretching region of concentrated NaBr solutions made from unbaked and baked salt.²⁸ However, in the case of Na₂CO₃ and Na₂SO₄, two high melting point molecular ion-based salts, similar VSFG measurements performed on baked and filtered solutions indicate that baking, even over an extended time period, proved to be less effective (data not shown). Solutions made from baked ACS grade Na₂CO₃ and Na₂SO₄ salts still showed the presence of organic impurities in the CH region and were often slightly cloudy which resulted in poorly reproducible VSFG spectra in the OH region. This could be due to the presence of floating microparticles (submicron-sized) in these solutions, which could only be removed through filtration.²⁸ It has been reported that such

microparticles act as a secondary source of contamination and exist at the surface of sodium halide solutions, whether the salt has been baked or not. It was hypothesized that these particles could possibly originate from carbonized organic contaminants that cannot be detected in the CH stretching region by conventional VSFG spectroscopy but instead with non-resonant SHG fluctuation measurements on the solution surface. However, the conventional VSFG results obtained here in the CH region on ACS grade Na_2CO_3 and Na_2SO_4 salt solutions could be due in fact to insoluble microparticles or aggregates containing organic contaminants that survived the baking process and which would be detectable.

Similar to the case of $(\text{NH}_4)_2\text{SO}_4$ (Figure 6.8b), the untreated 1.5 M NaCl solution made from ACS grade salts display a nearly identical VSFG spectrum to those of pretreated solutions (Figure 6.9b). The untreated UP grade NaCl, on the other hand, shows a significantly different spectrum over the entire OH stretching region, although with less dramatic changes than those observed for unfiltered $(\text{NH}_4)_2\text{SO}_4$ solution. For instance, the intensity of the dangling OH peak is still reduced but to a lesser extent, mostly due to the smaller amount of surfactants contained in untreated NaCl salt. These results somewhat differ with those of Tarbuck and Richmond who used UP salts as-received and showed no evidence of organic contamination in the CH stretching region.⁸⁴ As mentioned above, this could be an indication of the variability in organic impurities between suppliers. Hence, in order to avoid such potential contamination, solutions made from UP grade salts *must* be treated by filtration or preferably by salt baking (depending

on the melting point) followed by solution filtration, before being used in surface-sensitive spectroscopic studies of aqueous interfaces.

6.1.4 Conclusions

It is shown in this work that no apparent difference is observed in the OH stretching region of conventional VSFG and HD-VSFG spectra between ACS and UP grade salts after pretreatment (either salt baking followed by solution filtration or simply filtration for low melting point salts). It is demonstrated that UP grade salts contain much more organic impurities than the corresponding ACS grade salts, and these impurities largely affect the salt solution spectra in the water OH stretching region. This presumably results from the industrial use of chelating surfactants for the removal of trace metals.

For halide salts such as chlorides, baking serves as a suitable alternative to solution filtration in the removal of organic impurities. In contrast, the similarity in conventional VSFG and HD-VSFG spectra between pretreated ACS and UP grade salt solutions suggests that the ACS grade salts are adequate for the spectroscopic investigation of water organization at bare air/aqueous salt solution interfaces. This result is of significance as it should ensure greater reproducibility and better comparison of VSFG measurements at the bare air/solution interface between different research groups and provide a more defined benchmark for computational models.

Although it was not shown in the current work, it is likely that organic contamination is predominant at higher salt concentrations. The question on the minimal level at which organic impurities begin to have an effect on interfacial water spectral features still needs to be carefully examined by further concentration studies.

Furthermore, for studies that investigate binding effects of ions to surfactants (e.g. fatty acids and phospholipids monolayers) on aqueous salt solution subphases, the impact of salt purity is currently not well established. However, recent results suggest that for surfactant surface studies, organic contaminants are not as critical as trace metal impurities.

Considering the variation in the production methods from any given supplier, or between several suppliers or between product batches, there is no guarantee that a given salt will have the same level of organic impurities over time. Since organic impurities are not usually specifically tested, one cannot rely on the specifications as an infallible guide for surface-chemical purity. Hence, regardless of the salt source, unless the specific batch has been tested and shown to be free of surface-active impurities, it is strongly recommended to filter salt solutions but preferably bake the salts (depending on the salt melting point) and then filter the solutions before studying interfacial water organization of aqueous salt solutions. Also the use of complementary techniques (as already shown by few research groups) such as second harmonic generation for floating microparticle detection and surface tension can serve as valuable indicators of surface chemical cleanliness. Even though these recommendations could be simply viewed as “common good standard analytical practice”, it is still not widely recognized and adopted throughout the nonlinear surface spectroscopy community. The current work should hopefully serve as a cautionary warning for future studies on aqueous surfaces.

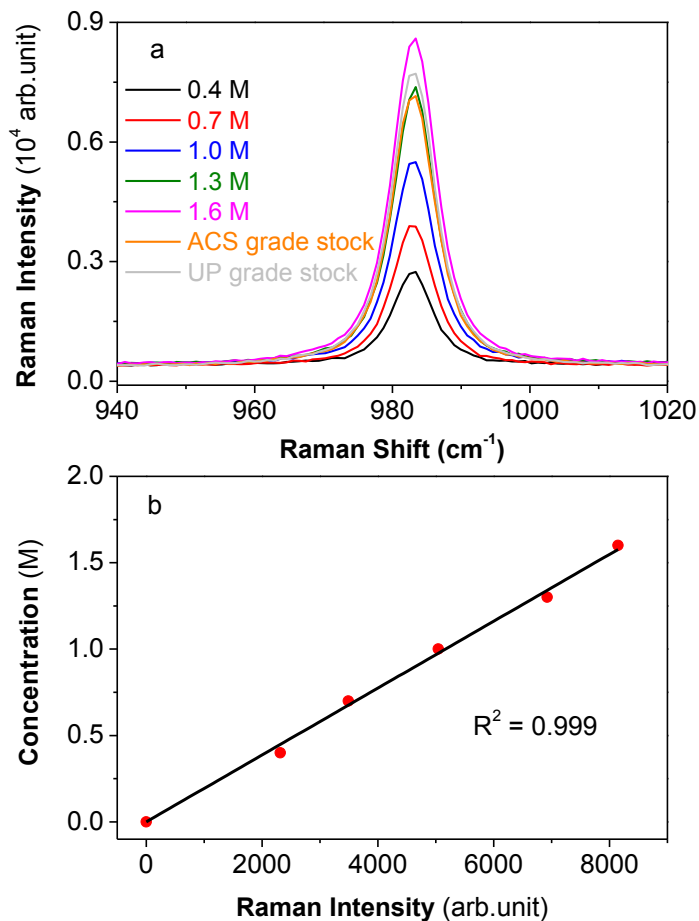


Figure 6.1 (a) Raman spectra of 0.4 M, 0.7 M, 1.0 M, 1.3 M, 1.6 M Na_2SO_4 , as well as ACS and UP grade pretreated Na_2SO_4 stock solutions, (b) Calibration curve of Na_2SO_4 solutions using the height of the vibrational symmetric stretch ion mode of each individual Raman spectrum. The concentrations of other sulfate, carbonate, and nitrate stock solutions were determined in the same manner.

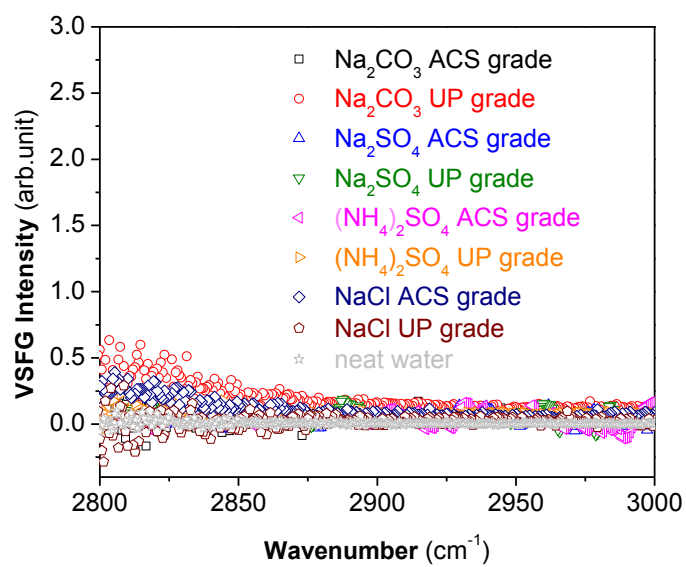


Figure 6.2 Conventional VSG spectra in the CH stretching region (2800–3000 cm⁻¹) of neat water and all stock salt solutions studied after filtering 2 to 4 times.

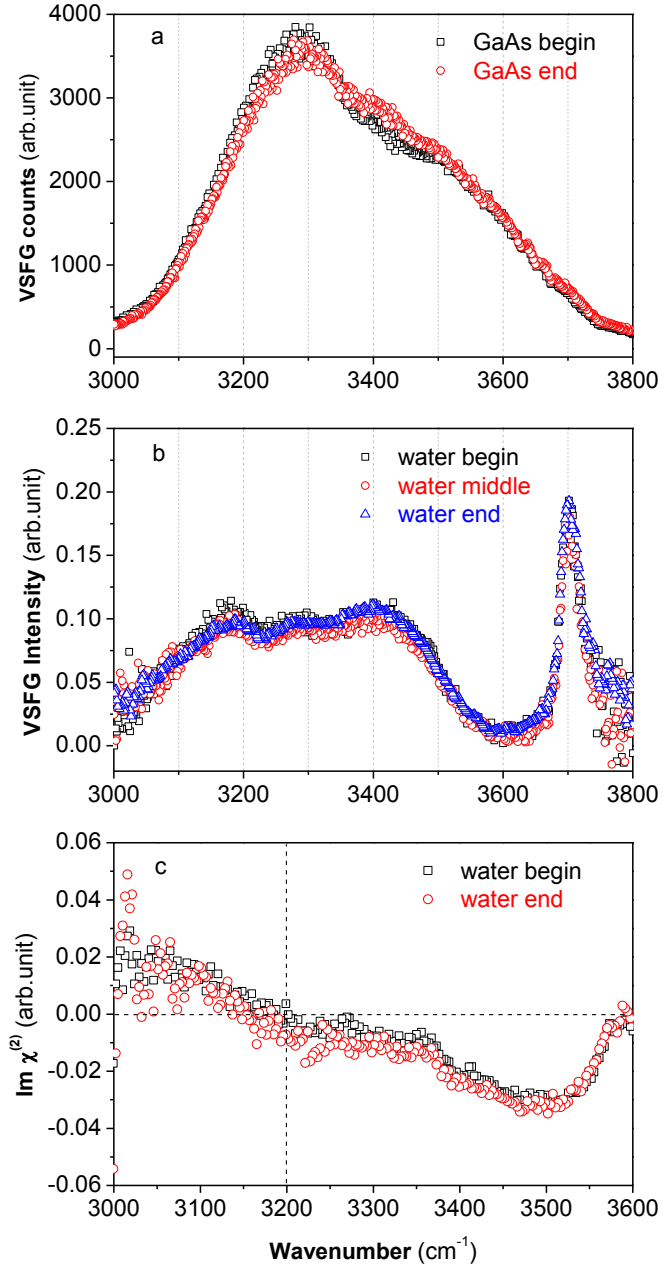


Figure 6.3 Stability of SFG system shown by the GaAs profile, conventional VSFG and HD-VSFG $\text{Im } \chi^{(2)}$ spectra of neat water in the OH stretching region (3000–3800 cm^{-1}). (a) GaAs profile and (b) conventional VSFG spectra in the OH stretching region, and (c) $\text{Im } \chi^{(2)}$ spectra in the OH stretching region from 3000 to 3600 cm^{-1} .

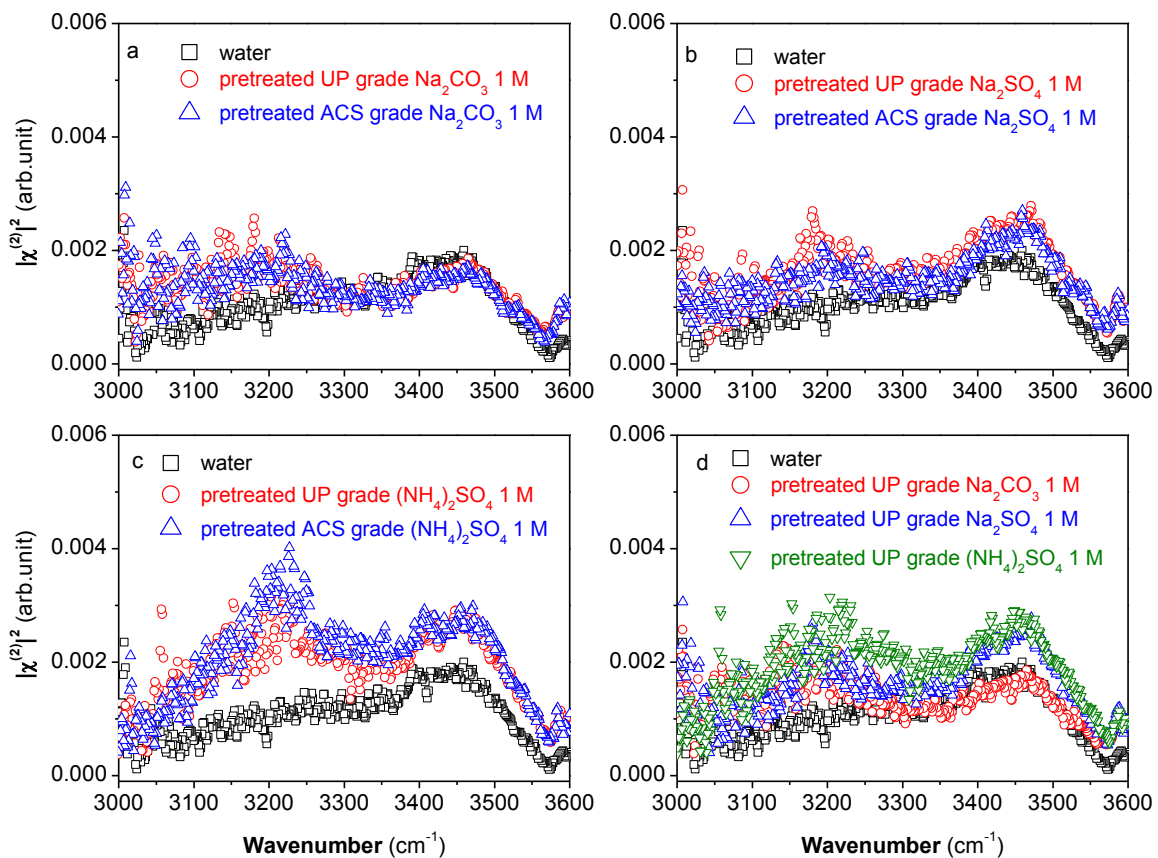


Figure 6.4 Deduced power spectra $|\chi^{(2)}|^2$ from HD-VSFG results of ACS and UP grade salt solutions in the OH stretching region (3000–3600 cm^{-1}). (a) 1 M Na_2CO_3 , (b) 1 M Na_2SO_4 , (c) 1 M $(\text{NH}_4)_2\text{SO}_4$, and (d) comparison of all 1 M salt solutions. Neat water spectra are shown as reference.

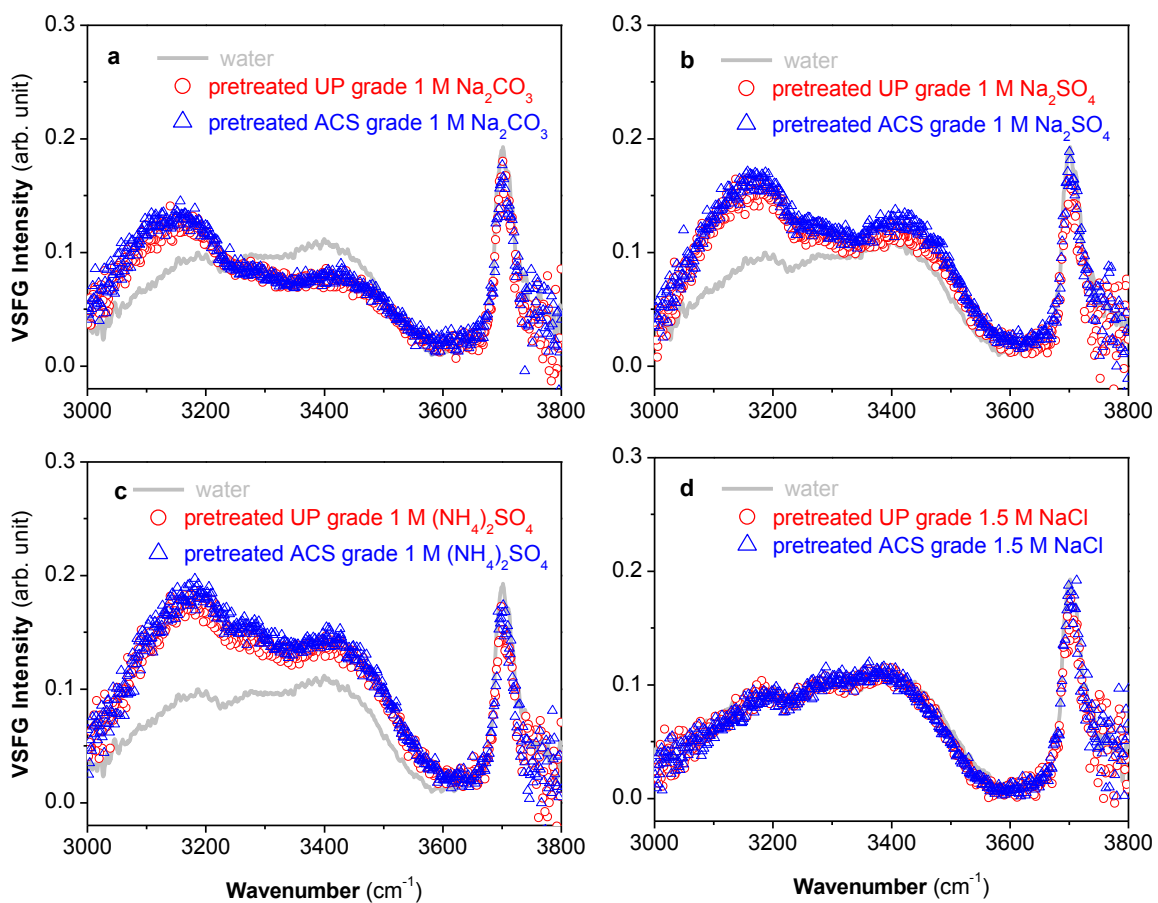


Figure 6.5 Comparison between conventional VSGF spectra from ACS and UP grade salt solutions in the OH stretching region ($3000\text{--}3800\text{ cm}^{-1}$) after pretreatment. (a) $1\text{ M Na}_2\text{CO}_3$, (b) $1\text{ M Na}_2\text{SO}_4$, (c) $1\text{ M (NH}_4)_2\text{SO}_4$, and (d) 1.5 M NaCl . The VSGF spectrum of neat water is also shown as reference by a grey line.

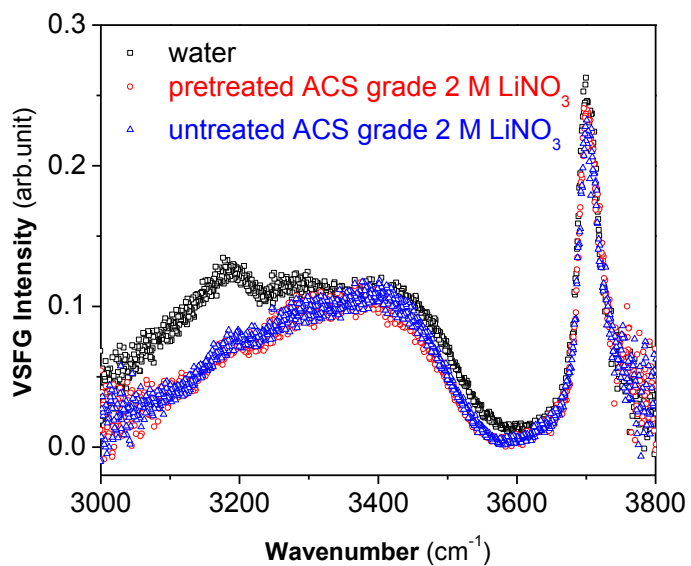


Figure 6.6 Conventional VSFG spectra of neat water and ACS grade 2 M LiNO₃ solution in the OH stretching region (3000–3800 cm⁻¹) before and after filtration.

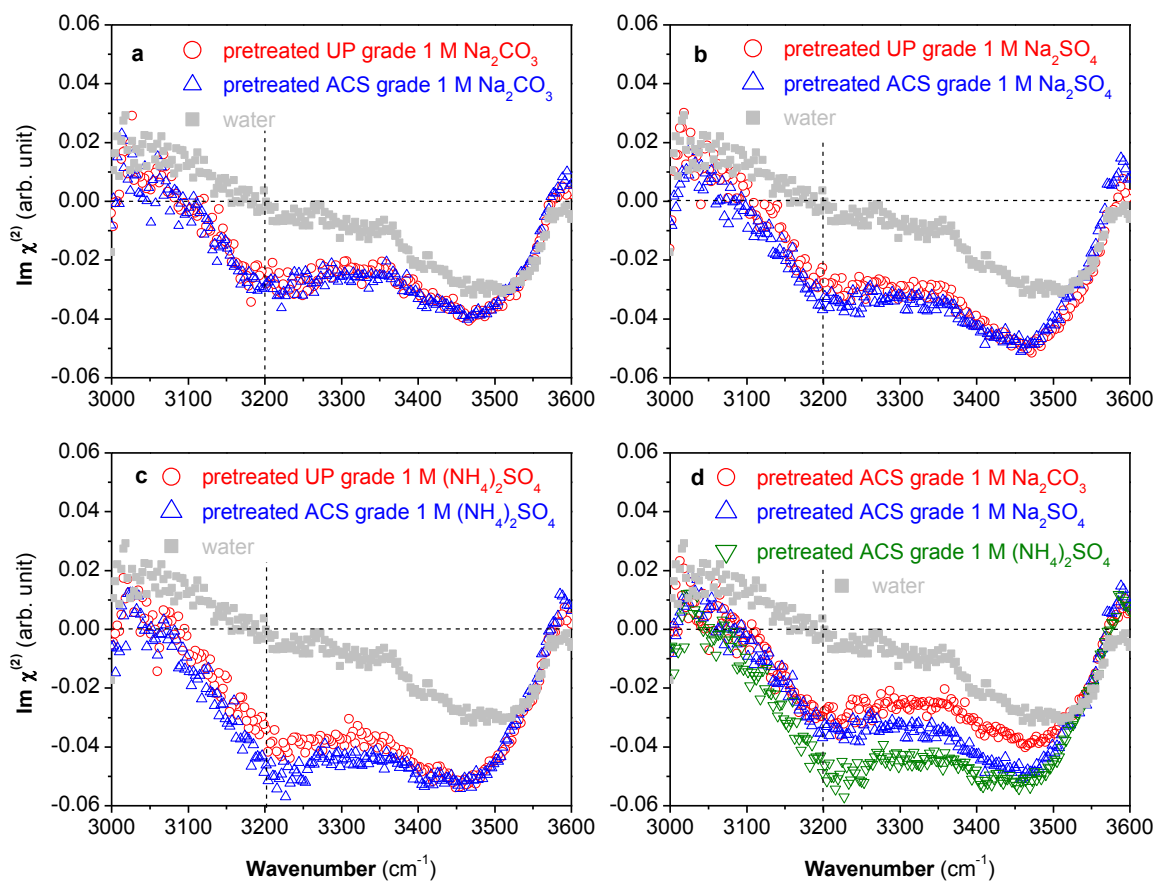


Figure 6.7 Comparison between HD-VSFG spectra from ACS and UP grade salt solutions after pretreatment. (a) 1 M Na_2CO_3 , (b) 1 M Na_2SO_4 , (c) 1 M $(\text{NH}_4)_2\text{SO}_4$, and (d) comparison of all 1 M salt solutions. The VSFG spectrum of neat water is also shown as reference.

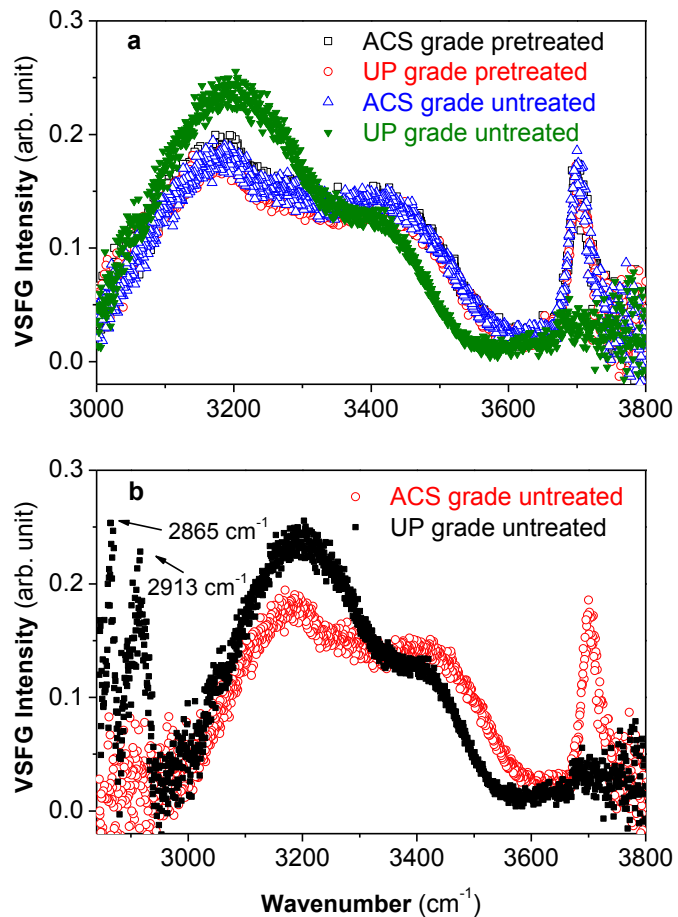


Figure 6.8 (a) Comparison between conventional VSGF spectra of untreated and pretreated 1 M (NH₄)₂SO₄ solutions made from ACS and UP grade salts. (b) Comparison between conventional VSGF spectra of untreated 1 M (NH₄)₂SO₄ solutions made from ACS and UP grade salts.

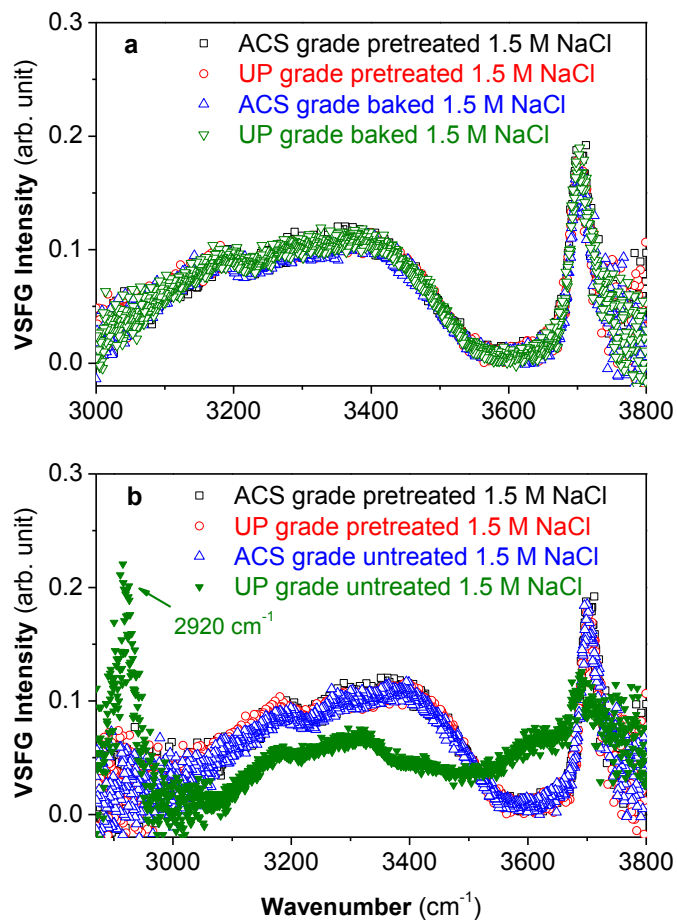


Figure 6.9 (a) Comparison between conventional VSGF spectra of baked or filtered 1.5 M NaCl solutions made from ACS and UP grade salts. (b) Comparison between conventional VSGF spectra of pretreated and untreated 1.5 M NaCl solutions made from ACS and UP grade salts.

Table 6.1 Comparative list of purity of salts used in previously published SHG, conventional VSG and HD-VSG studies at the air/solution interface.

Salt	Supplier	Grade and Purity	Salt Baking	Solution	Ref.
<i>Halides</i>					
NaCl	GFS Chemicals	n/a	no	yes ^{a,d}	87
NaF, NaCl, NaBr, NaI	Sigma-Aldrich	ACS reagent, 99%+	no	no	32
NaF, NaCl, NaBr, NaI	Fisher Scientific	ACS certified	no	yes ^{d,e}	30
NH ₄ Cl	n/a	n/a	no	yes ^d	57
NaCl, NaBr, NaI	Acros Organics	ACS reagent, 99%+	yes (500 °C, >6 h)	no ^d	28
MgCl ₂ ·6H ₂ O	Fisher Scientific	ACS certified	no	yes	164
NaCl, KCl, NH ₄ Cl	Sigma-Aldrich	TMB, 99.999% (NaCl, KCl), 99.998% (NH ₄ Cl)	yes (NaCl, KCl, 500 °C)	yes ^a	138
NaCl, CaCl ₂	Fisher Scientific	ACS certified, 99%	yes (650 °C, >10 h)	yes ^d	125
NaI	Sigma-Aldrich	99.999%	yes	yes ^e	94
<i>Carbonates</i>					
Na ₂ CO ₃ , NaHCO ₃	Aldrich	99.995% (Na ₂ CO ₃), ≥99.5% (NaHCO ₃)	no	no	84
Na ₂ CO ₃	Spectrum Chemical	99%	no	no	70
NaHCO ₃	Mallinckrodt Chemicals	99.7–100.3%	no	no	
Na ₂ CO ₃	Fisher Scientific	ACS certified, 99.5–100.5%	yes (650 °C, >10 h)	yes ^d	124

Continued

Table 6.1 continued

Salt	Supplier	Grade and Purity	Salt Baking	Solution	Ref.
<i>Nitrates</i>					
NaNO ₃ (HNO ₃ + NaOH)	GFS Chemicals	n/a	n/a	yes ^{a,d}	87
Mg(NO ₃) ₂ , Ca(NO ₃) ₂ , Sr(NO ₃) ₂	Fisher Scientific	n/a	no	yes ^d	89
Mg(NO ₃) ₂ ·H ₂ O, Ca(NO ₃) ₂ ·4H ₂ O, Sr(NO ₃) ₂	Fisher Scientific	ACS certified, 98.0–102.0%, 99.0–103.0%, 99.0%	no	yes ^d	88
NaNO ₃	Sigma-Aldrich	TMB, 99.995%	no	yes ^a	138
LiNO ₃ , NaNO ₃ , Mg(NO ₃) ₂ ·6H ₂ O	Fisher Scientific	Fisher Bioreagents, ≥99.0%, ACS grade, 98–102%	no	yes ^d	68
NH ₄ NO ₃	MP Biomedicals	UP grade, >99%			
<i>Sulfates</i>					
KHSO ₄	GFS Chemicals	n/a	no	yes ^{a,d}	87
Na ₂ SO ₄ , (NH ₄) ₂ SO ₄	n/a	n/a	no	yes ^d	57
Na ₂ SO ₄ , NaHSO ₄ ·H ₂ O	Aldrich	99.99% (Na ₂ SO ₄), 99% (NaHSO ₄)	no	no	84
Na ₂ SO ₄ , (NH ₄) ₂ SO ₄	Sigma-Aldrich	TMB, 99.99% (Na ₂ SO ₄) 99.999% ((NH ₄) ₂ SO ₄)	yes (Na ₂ SO ₄ , 500 °C)	yes ^a	138
Na ₂ SO ₄	Acros Organics	≥99%	yes (650 °C, >10 h)	yes ^d	125
(NH ₄) ₂ SO ₄	Sigma-Aldrich	ACS reagent, ≥99%			

Legend: ^a Purification using syringe filters; ^b Purification using activated carbon filters; ^c Purification using Lunkenheimer method;¹⁷⁷ ^d Salt solutions were checked for organic contamination with VSFG spectra in the CH stretching region (2800–3000 cm⁻¹); ^e NaF was purified only by recrystallization. n/a, not available; TMB, trace metals basis.

Table 6.2 Standardized pretreatment procedure for inorganic salts purification.

Pretreatment	Salt		
	<i>Metal halides</i>	<i>Molecular ion-based</i>	
	High T_m (e.g. NaCl)	High T_m (e.g. Na ₂ CO ₃ , Na ₂ SO ₄)	Low T_m (e.g. (NH ₄) ₂ SO ₄ , LiNO ₃)
Salt baking + Solution filtration	✓	✓	✗
Solution filtration only	✓	✓	✓
Salt baking only	✓	✗	✗

6.2 Influence of Salt Purity on the Interactions between Na⁺ Ions and Carboxylate Headgroup of Palmitic Acid Monolayers

Reproduced in part with permission from Huang, Z.S.; Hua, W.; Verreault, D; and Allen, H.C. “Influence of Salt Purity on Na⁺ and Palmitic Acid Interactions” *J. Phys. Chem. A*, Accepted – In Press. Copyright 2013 American Chemical Society.

6.2.1 Introduction

The effects of salt purity on the interfacial water organization of various bare aqueous salt solutions have been investigated in Section 6.1. Incidentally, much less work has been done to address the impact of the trace amount of polyvalent cations at air/surfactant interfaces.¹⁸⁶

Cation-specific effects in aqueous solutions are essential to many chemical, biochemical, and atmospheric processes.¹⁸⁷⁻¹⁹⁵ Particularly, Na⁺ and K⁺, as the two most abundant alkali cations in intra- and extracellular fluids, play a critical role in cell signaling.^{196,197} Most of the results obtained so far with Na⁺ and K⁺ ions have suggested that Na⁺ has a stronger binding affinity to COO⁻ relative to K⁺.^{189,194,198,199} However, a VSFG spectroscopy study by Tang and Allen pointed out a greater affinity of K⁺ than Na⁺ for the COO⁻ group of palmitic acid monolayers, in contradiction with the “law of water matching affinities”.¹⁹¹ This controversial finding initiated further experiments to assess the effect of salt purity and pretreatments on such studies. Aside from instrumental and methodological factors, the purity of the salts utilized in the current experimental work was evaluated for their spectroscopic impact. Salts with different purities and

pretreatments have been used among research groups, as shown in Table 6.3. Note that there is typically a 1-2% contamination level in the ACS grade salts, part of which are polyvalent cations such as Mg^{2+} , Ca^{2+} , Fe^{3+} , Pb^{2+} , and Ba^{2+} . The presence of such polyvalent cations, even in trace amounts, could significantly alter the binding affinities of monovalent cations and perturb the interfacial water organization through binding to the carboxylate group.¹⁸⁶

In this work, we clarify the impact of salt purity on the study of binding between one alkali cation (Na^+) and the carboxylate group of palmitic acid (PA) monolayers at air/aqueous interfaces by means of VSFG spectroscopy. Our results reveal significantly different binding affinity of Na^+ cations with the headgroup of PA by using filtered UP versus ACS grade salt solutions as subphase. During the spectral monitoring, for the whole OH stretching region, the intensity remains low and constant for the UP salt solutions but undergoes a gradual decrease over time for ACS grade salt solutions. The different spectral behavior is likely due to the stronger affinity of polyvalent metal ions present in the ACS grade salt.

6.2.2 Experimental

Materials. PA ($\text{CH}_3(\text{CH}_2)_{14}\text{COOH}$, $\geq 99\%$) and acyl chain deuterated d_{31} -PA ($\text{CD}_3(\text{CD}_2)_{14}\text{COOH}$, 98%) were purchased from Sigma-Aldrich and Cambridge Isotopes, respectively. ACS grade ($\geq 99\%$) and UP grade (trace metals basis, 99.999%) NaCl salts were purchased from Fisher Scientific and Acros Organics, respectively.

Preparation of Lipid and Aqueous Salt Solutions. PA and d_{31} -PA solutions were prepared at a 1.5 mM concentration by dissolution in spectroscopic grade

chloroform (Sigma-Aldrich). Both UP and ACS grade NaCl salts were baked at ~ 600 °C for 10 h in a muffle furnace (Isotemp model 550-14, Fisher Scientific). The preparation of stock salt solutions has been described in Section 6.1.2.

Equilibrium Spreading of PA Monolayers. PA monolayers were overspread (~ 10 μL) on water and salt solutions in Petri dishes (5 cm diameter). The quantity of spread PA was equivalent to a mean molecular area of ~ 21 $\text{\AA}^2/\text{molecule}$,²⁰⁰ which corresponds to a 2D-ordered (tilted liquid-condensed) phase.²⁰¹ Following spreading, 10 min was allowed for solvent evaporation, after which VSFG spectra were collected for ~ 1 h. The acquisition time for each spectrum was 5 min.

6.2.3 Results and Discussion

In the following discussion, VSFG spectra of PA monolayers in the OH stretching regions are presented. It is also known that the intensity of the spectra may change with time due to monolayer relaxation²⁰² that can affect the comparison of the binding affinity of cations to carboxylate groups. Therefore a time study was performed to see how the spectra change for aqueous solutions made from UP and ACS grade salts.

Indirect Evidence of Na^+ Interactions with Carboxylate Group from the OH Stretching Region. As mentioned previously, the organization of water molecules in the OH stretching region is highly sensitive to its environment. For instance, the influence of trace amounts of organics on the interfacial water structure has been extensively studied.^{114,131,186,203-205} Since all the salts used here are free of organics after pretreatment,

the spectral change observed here can only be attributed to the cation-carboxylate binding.

Figure 6.10a presents the VSFG spectrum in the OH stretching region of a PA monolayer on neat water. There are four bands located at $\sim 2940\text{ cm}^{-1}$, $\sim 3200\text{ cm}^{-1}$, $\sim 3450\text{ cm}^{-1}$, and $\sim 3600\text{ cm}^{-1}$. The 2940 cm^{-1} peak is assigned to the Fermi resonance of the CH_3 symmetric stretch with the overtone of the bending mode.^{191,206} The broad band from 3200 cm^{-1} to 3450 cm^{-1} is a signature of collective OH stretching modes of hydrogen-bonded water molecules that display complex coordination and cooperativity in the interfacial region.^{121,129,130} The 3600 cm^{-1} peak results from weakly hydrogen-bonded OH groups of both fatty acid and water. These features are consistent with the VSFG spectra reported by Miranda et al.²⁰⁶ and Tang and Allen.^{191,205} Although as mentioned earlier, most of PA molecules are intact at the water surface, a small amount of deprotonated carboxylic groups still exists, and, in turn, the presence of an electric field induced by this deprotonation can change the interfacial water structure,²⁰⁵ as shown by the higher intensity relative to neat water in Figure 6.10a. Note that the spectra in Figure 6.10a are slightly different from previously reported ones, especially in the region from ~ 3600 to 3700 cm^{-1} .²⁰⁵ This was probably caused by the lower energy on the high frequency side of our previous incident IR profile that was not easily normalized out.

In the presence of NaCl in the subphase, the VSFG spectra of the PA monolayers have significantly changed (Figure 6.10b, c). The intensity of OH stretching bands on UP grade NaCl solution (Figure 6.10b) changes dramatically relative to PA on neat water. The lower intensity in the high frequency region in Figure 6.10b relative to Figure 6.10a

indicates a loss of local ordering between water molecules just below the PA monolayer due to charge screening. In other words, the interaction of Na^+ with the COO^- headgroups gives rise to a less charged interface that weakly aligns the water molecules. This explanation for the spectral intensity attenuation relative to PA on neat water is in accordance with previous VSFG studies of surfactant monolayers on salt solutions.^{121,186,204,205} In addition, the intensity remains constant even 30 min after spreading the PA monolayer on the UP grade NaCl solution, suggesting that a stable monolayer is formed. It could serve as evidence that the trace amounts of polyvalent metal ions in the UP grade NaCl salt did not result in a significant perturbation of the interfacial water organization.

In contrast, the VSFG spectra of a PA monolayer on ACS grade NaCl solution resemble that on neat water (compare Figure 6.10a and c). The three broad bands in the region from 3000 to 3800 cm^{-1} are easily discernible and the peak assignment is similar to that on the neat water subphase, although the peak intensity decreases, especially at $\sim 3200 \text{ cm}^{-1}$. The spectral intensity decrease provides evidence of cations binding to COO^- , as the water molecules become less aligned by the weaker interfacial electric field and the headgroup becomes less ordered with respect to orientation.^{121,186,203-205} Despite the overall lower intensity relative to PA on neat water, the spectral intensity on ACS grade subphase is much higher at 3500 cm^{-1} than for PA on UP grade NaCl solution. As shown in Table 6.3, the concentrations of polyvalent cations in UP and ACS grade NaCl salts are ≤ 10 ppm and ~ 40 ppm, respectively. Gurau et al. has reported the marked effect of trace amounts of divalent cations (1 and 10 μM) on a arachidic acid ($\text{CH}_3(\text{CH}_2)_{18}\text{COOH}$)

monolayer in the OH stretching region relative to neat water.¹⁸⁶ It is expected that the impurity level of polyvalent cations between the UP and ACS grade salts in our experiment is sufficient and leads to the significant difference observed between Figure 6.10b and 6.10c.

The most significant difference between the UP and ACS grade salt solutions is the intensity changes with elapsed time. Unlike the VSFG spectra given in Figure 6.10b, those in Figure 6.10c decreased in intensity and then became unchanged after about 1 h. As more polyvalent metal cations present in the ACS grade salt, which have stronger binding affinity, bind to COO^- groups, the water hydrogen bonding structure changes. Accordingly, the ionic complex between cation and COO^- becomes predominant and leads to an increasing peak intensity of P-O vibrational mode ($\sim 1470 \text{ cm}^{-1}$, data not shown). The two complementary views of the binding mechanism revealed by the VSFG spectra from the COO^- and OH stretching region are consistent with each other.

Based on the spectral changes of PA monolayers on UP and ACS grade NaCl solutions in both the COO^- (data not shown) and OH stretching regions, the purity of alkali salts is found to have a great impact on the resulting VSFG spectra of fatty acids spread on their solutions (even after pretreatment). This may further cause difficulty in determining the relative binding affinity of cations, for example Na^+ vs. K^+ . Therefore, UP alkali salts are highly recommended for studies of cation-carboxylate binding. Note that the impact of organic contaminants with the UP grade salt on the cation-carboxylate binding has not yet been studied.^{189,190} Furthermore, to gain a better understanding of the

cation-surfactant interaction, a complete study of other salts and surfactants (e.g. phospholipids) as well as of pretreatment effects is needed.

6.2.4 Conclusions

PA monolayers at the air/NaCl solution interface were monitored over time by VSG spectroscopy in the OH stretching regions after spreading on the pretreated solutions prepared from UP and ACS grade NaCl salts. Significant differences were observed between the UP and ACS grade salt solutions spectra. In the OH stretching region, the intensity of the broad band from 3000 to 3800 cm^{-1} remains unchanged for the UP salt solution but gradually decreases for the ACS one.

These results demonstrate the impact of trace metal contaminants on the cation-carboxylate binding, and these impurities largely affect the spectra of PA in both spectral regions. The changes in the spectra for UP salt solution are related to monolayer relaxation, but for ACS salt subphase, the changes are likely due to the trace metal impurities that strengthen the cation-carboxylate binding. The information conveyed by the VSG spectra of PA monolayers in the COO^- (data not shown) and OH stretching regions are consistent with each other. The grade of alkali salts therefore proves to be critical in exploring the cation-carboxylate binding and comparing relative binding affinity of different cations. The use of UP grade salt is strongly recommended especially in the studies related to alkali-carboxylate interactions. However, whether the salt purity effect applies to the interactions between other monovalent cations and negatively

charged moieties such as the phosphate group in phospholipids is still unknown. More generally, special care should be taken in the selection of chemicals when investigating air/aqueous surfactant interfaces with surface-sensitive techniques.

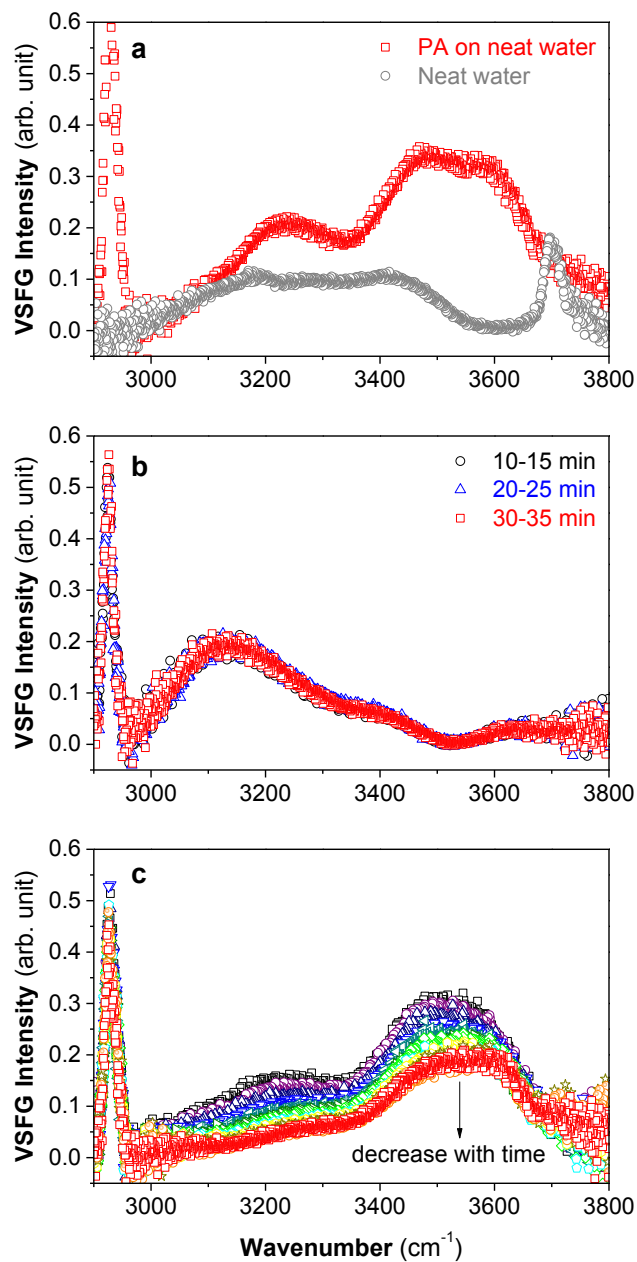


Figure 6.10 VSFG spectra of PA monolayers on neat water and NaCl salt solutions in the OH stretching region (3000-3800 cm^{-1}) up to about 1 h after spreading. (a) PA on neat water, (b) UP grade 0.6 M NaCl solution, and (c) ACS grade 0.6 M NaCl solution. Spectra were taken every 7 min on average approximate 10 min after spreading.

Table 6.3 Salts with different purities and pretreatment used among research groups in studies of alkali cation-carboxylate interactions.

salt/carboxylate source	supplier	grade and purity	salt baking	solution filtration	ref
NaCl, KCl/polypeptide	Sigma-Aldrich	NaCl: 99.999%, KCl: 99.999%	no	no	180
NaCl, KCl/palmitic acid	Fisher Scientific	NaCl: ACS certified, 99% KCl: EP/BP/USP/FCC, 99%	no	yes	191
NaCl, KCl/protein	Lachema	p. a. grade	not specified	not specified	195
NaCl, KCl/amino acid	Sigma-Aldrich	highest purity commercially available	no	no	193
NaOH, KOH/dicarboxylate acid	n/a	n/a	not specified	not specified	192
HCOONa, HCOOK, CH ₃ COONa, CH ₃ COOK	Sigma-Aldrich	98% or higher	no	no	194
NaCl/palmitic acid (UP grade)	Acros Organics	trace metals basis, 99.999% polyvalent cations: ≤10 ppm	yes	yes	this work
NaCl/palmitic acid (ACS grade)	Fisher Scientific	ACS certified ACS, 99% polyvalent cations: ~40 ppm	yes	yes	this work

Chapter 7 Surface Prevalence of Perchlorate Anions at the Air/Aqueous Interface

Reproduced in part with permission from Hua, W.; Verreault, D.; and Allen, H.C. “Surface Prevalence of Perchlorate Anions at the Air/Aqueous Interface” *J. Phys. Chem. Lett.*, Accepted. Copyright 2013 American Chemical Society.

7.1 Introduction

The surface propensity and distribution of inorganic ions at the air/aqueous interface, and their impact on interfacial water organization has been a topic of long-standing interest due to their importance in a wide range of natural and technological processes. For example, various ions play critical roles in the kinetics and mechanisms of heterogeneous chemical reactions at the air/aqueous interface of atmospheric aerosols.^{2,6,167} The currently adopted molecular view of ion adsorption proposed by molecular dynamics (MD) simulation results suggests that small, non-polarizable ions like F^- and/or multiply charged ions (e.g. SO_4^{2-}) are excluded from the air/aqueous interface, while large polarizable halide ions (e.g. Br^- and I^-) have a strong surface propensity.^{9,11,27,56,207} This prediction has since been supported by numerous experimental studies using various surface-sensitive techniques such as ambient pressure X-ray photoelectron spectroscopy (AP-XPS), second harmonic generation (SHG), and vibrational sum frequency generation (VSFG) spectroscopy.^{28,30-32,208,209} Even though the

factors and/or driving forces behind ion adsorption are debated, further computational and experimental work on other anions (e.g. SO_4^{2-} , NO_3^- , I^-) has suggested that surface propensity of anions correlates inversely with the order of the anion Hofmeister series: $\text{CO}_3^{2-} > \text{SO}_4^{2-} > \text{F}^- > \text{Cl}^- > \text{Br}^- \sim \text{NO}_3^- > \text{I}^- > \text{ClO}_4^- > \text{SCN}^-$.^{9,25,210,211}

Considering that chaotropic ions such as Br^- , I^- , and SCN^- are known to be enriched at the air/aqueous interface, the surface propensity of perchlorate (ClO_4^-) ions seems somewhat predictable. In fact, the surface enhancement of ClO_4^- ions has been postulated as early as 1957 based on the negative surface potential values measured from aqueous NaClO_4 solutions.²¹² Despite the fact that ClO_4^- ion-induced changes in the conformation of surfactant monolayers and their influence on the vicinal water organization were well established,²¹³ molecular-level information about ClO_4^- ion surface propensity and its impact on water hydrogen-bonding network at the bare air/salt solution interface was still lacking. It is only recently that the surface enhancement of ClO_4^- ions has been predicted by MD simulations⁷¹ and a surface-bulk partitioning model,⁶² as well as demonstrated experimentally using electrospray/mass spectrometry⁷² and AP-XPS.⁷¹ Moreover, it was shown that the presence of ClO_4^- ions affects the evaporation mechanism and kinetics at the air/aqueous interface of concentrated NaClO_4 solutions.⁵⁵

Aside from its fundamental interest in physical chemistry, ClO_4^- has also drawn much attention as an emerging environmental pollutant of drinking water and food.^{54,214-216} Because of its low surface charge density, it has a reduced affinity for metal cations, a characteristic that makes it highly soluble. As such ClO_4^- ions tend not to sorb appreciably

to minerals and remain exceedingly mobile, thus leading to widespread contamination of natural aqueous systems.⁵³ The environmental occurrence of ClO_4^- ions can be related to either anthropogenic or natural sources such as nitrate mineral deposits and aerosols. It has been suggested that natural perchlorate species could be formed by heterogeneous reactions on chloride-containing aerosols by electric discharge or by exposition to high ozone concentrations.^{217,218} In order to understand these phenomena, it would therefore be helpful to have molecular insight into the interfacial behavior of ClO_4^- ions at the air/aqueous interface.

Despite the fact that the surface propensity of ClO_4^- ions has been explored, their interfacial distribution and that of their counter cations, as well as their influence on the interfacial water hydrogen-bonding network, in particular the net dipole orientation of water molecules, still remain largely unknown. In this Letter, we employed both conventional and heterodyne-detected vibrational sum frequency generation (HD-VSFG) spectroscopy to gain some further insight into these questions. In contrast to conventional VSFG spectroscopy that measures the squared absolute value of the second-order nonlinear susceptibility ($\chi^{(2)}$), HD-VSFG spectroscopy, by being based on the interference of the sample SFG response with that of a phase reference, can provide both the real (Re) and imaginary (Im) parts of $\chi^{(2)}$. The sign of $\text{Im } \chi^{(2)}$ relates directly, not to the orientation of interfacial water molecules, but rather to that of the average OH transition dipole moment;^{92,107,123,131,208} even though these two parameters are related, the exact molecular detail of their connection are currently not well established. The experimental setup for conventional VSFG and HD-VSFG spectroscopy has been

described elsewhere.^{124-126,203}

7.2 Experimental

Materials. $\text{NaClO}_4 \cdot \text{H}_2\text{O}$ (Fisher Scientific, Crystalline/Laboratory) were used as-received. Nanopure water (not purged of CO_2) with a resistivity of 18.2–18.3 $\text{M}\Omega\text{-cm}$ and a measured pH of 5.6 was obtained from a Barnstead Nanopure system (model D4741, Thermolyne Corporation) equipped with additional organic removing cartridges (D5026 Type I ORGANICfree Cartridge Kit; Pretreat Feed).

Preparation of Salt Solutions. NaClO_4 stock salt solution for VSFG measurements was prepared by dissolving salt in Nanopure water. Owing to its ultrahigh sensitivity, VSFG spectra obtained in the CH stretching region ($2800\text{--}3000\text{ cm}^{-1}$) were utilized as a probe to verify the presence of trace amount organic contaminants. As revealed in these spectra, organic contamination was found in NaClO_4 stock salt solution prior to any pretreatment (data not shown). To completely eliminate organic impurities, NaClO_4 stock solution was filtered four times using activated carbon filters (Whatman Carbon Cap 75, Fisher Scientific). After thorough removal of organic contaminations, for the same inorganic salt, solutions made from ACS and ultrapure grade salts (trace metal basis, purities ranging from 99.99% to 99.9999%) perturb the conventional and HD-VSFG spectra in the OH stretching region mostly to the same extent.¹²⁶ Raman calibration curves were obtained to determine the concentration of perchlorate after filtration based on vibrational symmetric stretch mode of ClO_4^- ion ($\sim 935\text{ cm}^{-1}$). The measured pH of 1.7 M NaClO_4 was ~ 5.9 . The pretreated (filtered) NaClO_4 stock salt solution was shown to

be free of organic impurities as revealed by the conventional VSFG spectra obtained in the CH stretching region (Figure 7.1). All solutions were thermally equilibrated to room temperature (23 ± 1 °C) over 24 h before use. No degassing or N₂-purging has been applied on them.

Conventional and Heterodyne-Detected Vibrational Sum Frequency Generation Spectroscopy. Conventional VSFG and HD-VSFG spectroscopy measurements were performed on a broad-bandwidth VSFG spectrometer setup which has been described in detail in Chapter 3. Neat water spectra were used as a reference for salt comparison to assess reproducibility during the whole experimental period. The reproducibility for both conventional and HD-VSFG ($\text{Im } \chi^{(2)}$) spectra of neat water is demonstrated in the Figure 7.2. To check the validity in the general trend of these spectra, the deduced $|\chi^{(2)}|^2$ power spectra of each salt solution (Figure 7.3a) reconstructed from the HD-VSFG results are compared to those measured directly by conventional VSFG spectroscopy. Only every fourth data points are plotted in the HD-VSFG spectra to avoid spectral clutter.

Infrared and Raman Spectroscopy. Attenuated total reflection Fourier transform infrared (ATR-FTIR) spectroscopy and Raman spectroscopy for bulk solution measurements were also performed. The setups for both measurements have been described in detail in Chapter 3 and elsewhere.²¹⁹ The Raman and IR spectra of 1.0 and 1.7 M NaClO₄ salt solutions are shown in Figure 7.4.

7.3 Results and Discussion

Figure 7.5a shows conventional VSFG spectra of the interfacial region of neat

water and NaClO₄ aqueous salt solution measured in the OH stretching region (3000–3800 cm⁻¹) under the *ssp* (for sum frequency (*s*), visible (*s*), and IR (*p*) beams, respectively) polarization combination. The interfacial region refers hereafter to the region which lacks inversion symmetry, hence SFG-active. In the case of neat water, only the topmost layers (~1–3) are believed to be responsible for the observed SFG signal, while the adjacent sublayers make little contribution;^{208,220} however, the presence of ions generates an interfacial electric field by forming an ionic double layer which extends the region of noncentrosymmetry. Water organization is directly influenced by the direction and relative strength of the ion-induced electric field in the interfacial region. The perturbation of the interfacial water organization involves both reorientation and restructuring of the water hydrogen-bond network which, in turn, leads to an increase in the interfacial depth, i.e. to a greater number of water molecules probed due to their SFG activity. The neat water VSFG ($|\chi_{\text{eff}}^{(2)}|^2$) spectrum reveals a broad region spanning from 3000 to 3600 cm⁻¹ representing water molecules with a broad continuum of hydrogen bond lengths, and a narrow band at 3700 cm⁻¹ assigned to the distinct dangling OH bond of water molecules located in the topmost layer. In the lower frequency part of the broad region, it is accepted that hydrogen bonds are relatively strong, and as one moves to higher frequency, the hydrogen bonding strength weakens significantly. Additional assignments to this broad continuum remain controversial.^{109,110,150,161,178}

The conventional VSFG spectrum of a 1.0 M NaClO₄ aqueous salt solution shows an uneven decrease in SFG signal intensity relative to that of neat water across the entire broad OH stretching region from 3000 to 3600 cm⁻¹, particularly below ~3300 cm⁻¹

(Figure 7.5a). However, no appreciable difference is observed for the dangling OH peak. To the authors' knowledge, no conventional VSFG spectrum of NaClO₄ or any other perchlorate salt solution has been previously reported. The intensity decrease of the broad OH stretching region suggests that the overall population of hydrogen-bonded water species that contribute to the SFG signal may be diminished. Additionally, it provides some evidence that the presence of the ClO₄⁻ anions in the interfacial region causes a definite perturbation of the water hydrogen-bonding network. In fact, these changes observed in the conventional VSFG spectrum of the NaClO₄ salt solution surface seem to correlate well with those from the corresponding bulk IR and Raman spectra (see Supporting Information). Previous ATR-IR and Raman studies have shown that the addition of ClO₄⁻ anions to water leads to: (1) a decrease in the absorbance and Raman intensity of lower frequency bands (~3230 and ~3370 cm⁻¹) and, concomitantly, (2) the emergence of a new band at higher frequency (~3600 cm⁻¹).²²¹⁻²²⁶ The former bands have been assigned to water molecules fully hydrogen-bonded to their nearest neighbors, whereas the latter has been associated with water molecules weakly hydrogen-bonded to the ClO₄⁻ anions.²²¹⁻²²⁶ The changes in these spectral features with salt concentration are believed to be due to the fact that the tetrahedral ClO₄⁻ anion acts as one of the most effective chaotropic ions by forming weak hydrogen bonds with adjacent water molecules, thereby perturbing the water hydrogen bonding network. As in the bulk, it is conceivable that ClO₄⁻ anions affect the network between hydrogen-bonded interfacial water molecules (whether weakly or strongly coordinated) in a similar manner. Moreover, as with the IR and Raman spectra, a weak band (shoulder) appears upon closer

inspection of our VSFG spectrum at $\sim 3620\text{ cm}^{-1}$, suggesting that some of the water molecules weakly bonded to ClO_4^- anions are SFG-active.

Despite a correlation between the spectral changes observed in the broad OH stretching region of the conventional VSFG spectrum and that from the IR and Raman spectra, the contribution of possible interference effects (e.g. interference with the non-resonant background, convolution effects between the real and imaginary part of the nonlinear susceptibility, etc.) to these changes cannot be completely excluded.⁹³ For example, the signal enhancement observed at $\sim 3300\text{ cm}^{-1}$ in the conventional VSFG spectrum of CaCl_2 salt solutions,¹²⁵ has been shown to come from convolution effects between the $\text{Re } \chi^{(2)}$ and $\text{Im } \chi^{(2)}$ parts. Hence, to rule out the presence of such effects in the case of NaClO_4 salt solutions, it is advantageous to utilize HD-VSFG spectroscopy.

As mentioned above, the HD-VSFG ($\text{Im } \chi^{(2)}$) spectrum directly provides the sign and thus the net transition dipole moment orientation of SFG-active OH vibrational stretching modes, and the magnitude of the positive or negative intensities reveal the extent of the O \rightarrow H dipole orientation, i.e. directed either towards or away from the surface, respectively. Note that the interpretation of $\text{Im } \chi^{(2)}$ spectra given herein is based on the *relative* spectral difference between neat water and the aqueous salt solutions. The $\text{Im } \chi^{(2)}$ spectrum of neat water in the OH stretching region shown in Figure 7.5b is similar to those reported previously by others.^{131,208} The positive sign of the $\text{Im } \chi^{(2)}$ spectrum of neat water in the $3000\text{--}3200\text{ cm}^{-1}$ region suggests that the OH stretching net transition dipole moment is oriented towards the surface; however, the assignments for this region continue to be discussed.^{110,150,178,208} In contrast, the interpretation of the negative band in

the $\text{Im } \chi^{(2)}$ spectrum from 3200 to 3600 cm^{-1} is not contested. Although the orientational distribution is likely to be broad, the OH stretches in this frequency range have a net transition dipole moment directed on average toward the isotropic bulk solution.

The $\text{Im } \chi^{(2)}$ spectra of the air/aqueous interface of NaClO_4 salt solutions at different concentrations are shown in Figure 7.5b. To date, there has been no published accounts of $\text{Im } \chi^{(2)}$ spectrum from the bare air/aqueous interface of perchlorate salt solutions. Relative to neat water, significant spectral changes, in the form of an enhanced positive signal intensity in the lower frequency region and a reduced negative intensity for the higher frequency region, can be seen for both NaClO_4 solutions. Furthermore, at the higher salt concentration, the intensity of the $\text{Im } \chi^{(2)}$ spectrum undergoes a sign reversal in the spectral region from 3200 to 3600 cm^{-1} . The presence of hydronium (H_3O^+) in the NaClO_4 solutions should only play a minor role in the overall change observed in their $\text{Im } \chi^{(2)}$ spectra because of the negligible pH variation relative to neat water (neat water: 5.6; 1.7 M NaClO_4 : 5.9). The change of the $\text{Im } \chi^{(2)}$ spectra of NaClO_4 solution can be more clearly seen by taking the $\text{Im } \chi^{(2)}$ difference spectra with respect to neat water (inset of Figure 7.5b). The positive increase in the spectra of NaClO_4 salt solutions observed here can be physically rationalized by having a positive electric field generated between ClO_4^- anions residing on average predominantly above Na^+ cations, closer to the surface. In other words, ClO_4^- ions exhibit a stronger surface preference than Na^+ ions. This molecular picture is consistent with recent MD simulations using a polarizable force field that predicted the formation of an ionic double layer with a maximal ClO_4^- ion density near the air/aqueous interface.⁷¹ A decrease in $\text{ClO}_4^-/\text{Na}^+$ and

ClO_4^-/O ratios with increasing depth as obtained by AP-XPS on 1 M NaClO_4 solution further supported the surface enhancement of ClO_4^- ions; however, the presence of a double layer structure could not be decisively confirmed.⁷¹

To explain these results of Figure 7.5b, various physical scenarios can be invoked. One possible explanation would be that because different water species contribute either negatively or positively to this region of the $\text{Im } \chi^{(2)}$ spectrum, it is quite likely that NaClO_4 addition to water reduces the population of water species contributing negatively, or vice versa, thus allowing the spectrum to become more positive. For instance, the observed net change in the water OH transition dipole moment with increasing salt concentration may result from the increasing population of water molecules weakly bonded to interfacial ClO_4^- anions. These water molecules could have their O–H groups directed on average towards the vapor phase for more surface-active ClO_4^- ions. The OH group contribution then could determine the sign of the $\text{Im } \chi^{(2)}$ spectrum. Yet, because of the symmetry of the ClO_4^- ion, the SFG selection rules would dictate that such water molecules would only make a minor contribution to the overall SFG signal. This seems to be supported by the weak band detected at $\sim 3620 \text{ cm}^{-1}$ in the conventional VSFG spectrum. Obviously, as shown by the conventional VSFG spectrum, it is likely that many other water species could be affected by the presence of ClO_4^- anions.⁷¹ Unfortunately, current spectroscopic methods do not provide such information.

Another physical scenario that could be put forward to explain the $\text{Im } \chi^{(2)}$ sign reversal involves the generation of a net positive electric field induced by the distribution of ClO_4^- ions and their Na^+ counterions in the interfacial region, i.e. by the formation of

an ionic double layer within the interface. The ion-induced interfacial electric field, in turn, would cause the reorganization of the interfacial water molecules which now have their net transition dipole moment more oriented towards the surface. As shown in Figure 7.5b, the direction and magnitude of the ion-induced electric field at the air/aqueous interface of NaClO₄ salt solutions display a marked concentration dependency. This effect has an impact on the net dipole orientation of interfacial water molecules, mainly those that are weakly hydrogen-bonded (3200–3550 cm⁻¹ spectral region). The net influence of concentration on the direction and magnitude of the induced electric field is illustrated schematically in Figure 7.6. At the neat water surface, the electric field is slightly negative due to the net, but weak, orientation of water dipoles pointing towards the aqueous isotropic bulk (seen in the Im $\chi^{(2)}$ spectrum from 3200 to 3600 cm⁻¹).^{131,208} At low salt concentrations, the distribution of ClO₄⁻ ions and their Na⁺ counterions may generate an additional electric field that counteracts and slightly reduces the magnitude of the overall electric field exerted on water molecules. The net orientation of this field remains however unchanged as the Im $\chi^{(2)}$ spectra of NaClO₄ salts in the 3200–3550 cm⁻¹ region are still showing a negative intensity. In a slightly more concentrated regime, the magnitude of the ClO₄⁻-induced electric field eventually give rise to a strong enough electrical field capable of completely inverting the net dipole orientation of interfacial water molecules, thus resulting in purely positive Im $\chi^{(2)}$ spectra. The presence of a net positive electric field at the surface of NaClO₄ and other perchlorate salt solutions is supported by experimentally measured negative surface potentials (recalling that $\mathbf{E} = -\nabla V$).^{212,227,228}

Such a complete reversal of the average orientation of the net transition dipole moment of weakly hydrogen-bonded interfacial water molecules observed here for ClO_4^- has so far not been reported for other chaotropic ions including the surface-enhanced Γ ions.^{124,125,138,208} It is noteworthy that although SCN^- , ClO_4^- , and Γ ions are all monovalent anions, the overall lineshape of their conventional VSG spectra and their variation with concentration increase differ significantly.^{30,229} In comparison to ClO_4^- which displays a decreasing intensity across the entire OH stretching region, SCN^- and Γ ions show concurrent decrease and increase at $\sim 3200\text{ cm}^{-1}$ and $\sim 3450\text{ cm}^{-1}$, respectively, indicative of a very different disordering effect on the interfacial water network. A shape anisotropy effect between these anions (i.e. tetrahedral (ClO_4^-) vs. spherical (Γ) vs. linear (SCN^-)) may be largely responsible for this difference. Interestingly, an enhanced negative interfacial electric field inferred from the $\text{Im } \chi^{(2)}$ spectrum of the large polarizable sulfate (SO_4^{2-}) has also been previously reported.^{125,138} However, the direction of the induced electric field for SO_4^{2-} and ClO_4^- (Figure 7.6) and the surface propensity of these two tetrahedral-structured oxyanions in the interfacial region are very different. This suggests that, in addition to shape/geometry effect, charge effect of the ions plays a key role in determining the ion distribution and water organization at air/aqueous salt solution interfaces.

7.4 Conclusions

In summary, from the HD-VSG results obtained here, it is clear that ClO_4^- ions are present at the air/aqueous interface of NaClO_4 salt solutions and that, as a result,

interfacial water structure is significantly reorganized. ClO_4^- ions reside preferentially on average above their Na^+ counterions. This was inferred from the positive direction of the net OH transition dipole moment of interfacial water molecules on average more towards the surface. Increase in salt concentration leads to the complete sign reversal of the $\text{Im } \chi^{(2)}$ spectrum. Possible scenarios explaining this effect includes the increase in population of water species contributing positively to the $\text{Im } \chi^{(2)}$ spectrum or the generation of a net positive electric field induced by the creation of an ionic double layer in the interfacial region. Although the true molecular origins of this concentration dependency remain at present somewhat speculative, previous surface potential and XPS measurements tend to support the latter interpretation. To our knowledge, this is the first investigation of water organization at the air/aqueous interface of NaClO_4 salt solution using conventional VSFG and HD-VSFG spectroscopy. Nevertheless, further theoretical and experimental efforts are needed to fully decipher the effects of concentration and cation identity on the distribution of ClO_4^- ions and its accompanying counter cations.

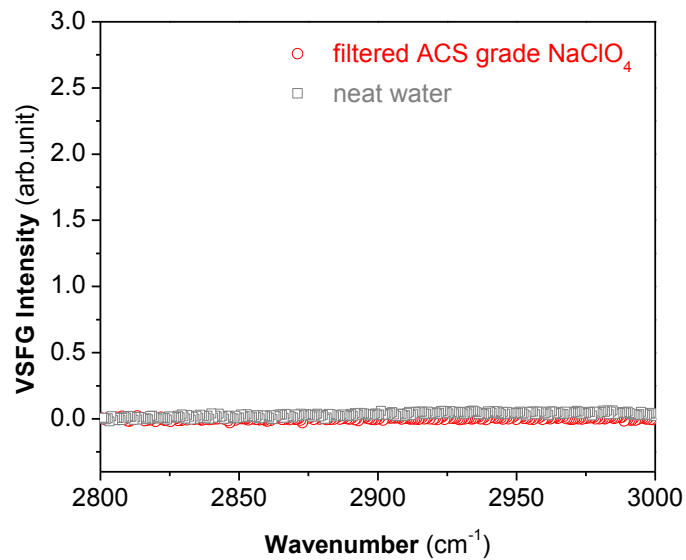


Figure 7.1 Conventional VSFG spectra in the CH stretching region (2800–3000 cm⁻¹) of the air/aqueous interface of neat water and filtered NaClO₄ stock salt solution.

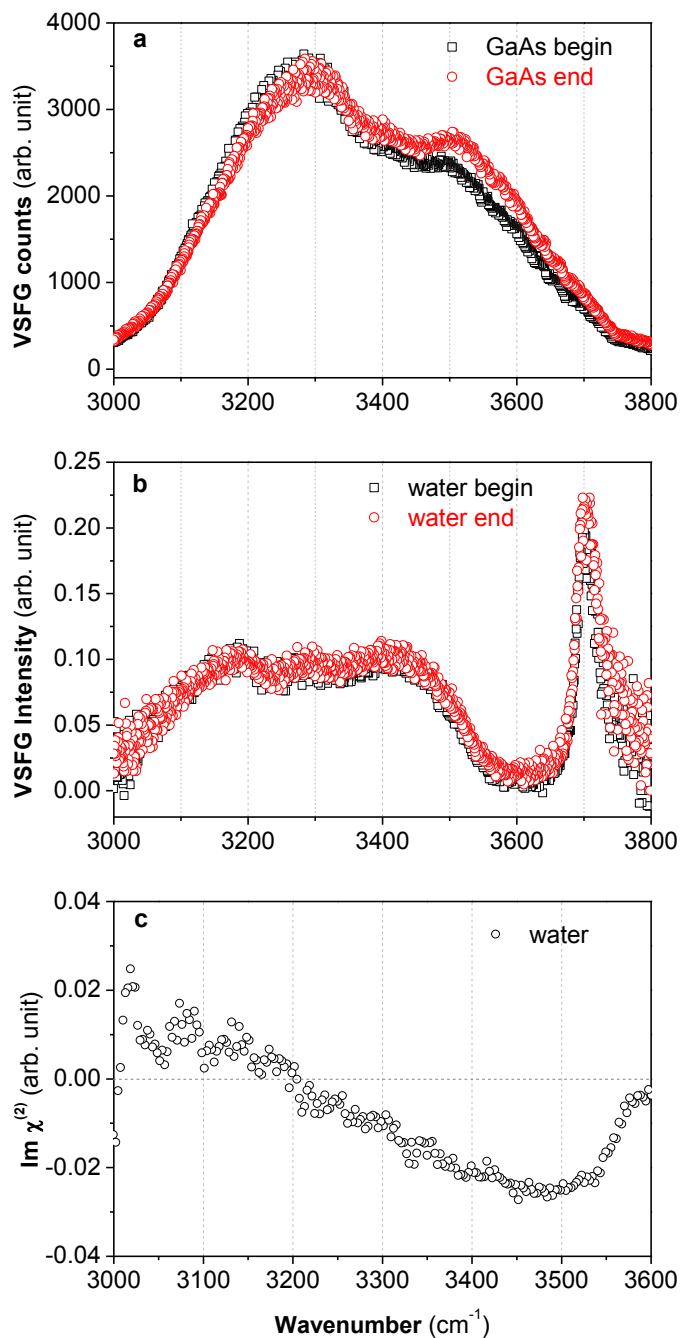


Figure 7.2 Stability of SFG system shown by the GaAs profile, conventional VSG and HD-VSFG $\text{Im } \chi^{(2)}$ spectra of neat water in the OH stretching region (3000–3800 cm^{-1}). (a) GaAs profile and (b) conventional VSG spectra, and (c) $\text{Im } \chi^{(2)}$ spectra in the OH stretching region from 3000 to 3600 cm^{-1} .

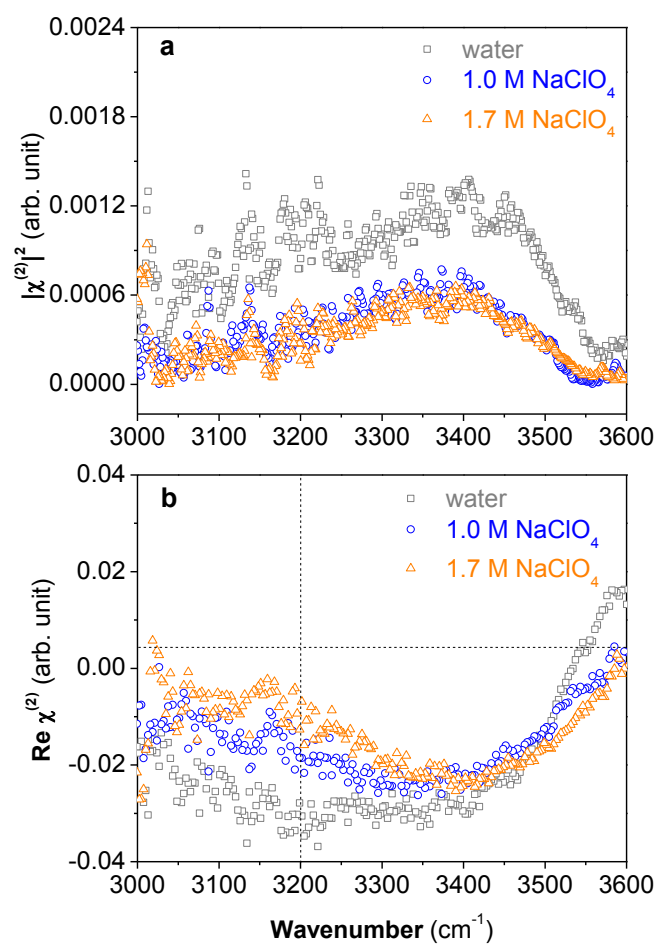


Figure 7.3 (a) Deduced power spectra $|\chi^{(2)}|^2$ and (b) $\text{Re } \chi^{(2)}$ spectra from HD-VSFG results of 1 M and 1.7 M NaClO_4 salt solutions in the OH stretching region (3000–3600 cm^{-1}). Neat water spectra are shown as reference.

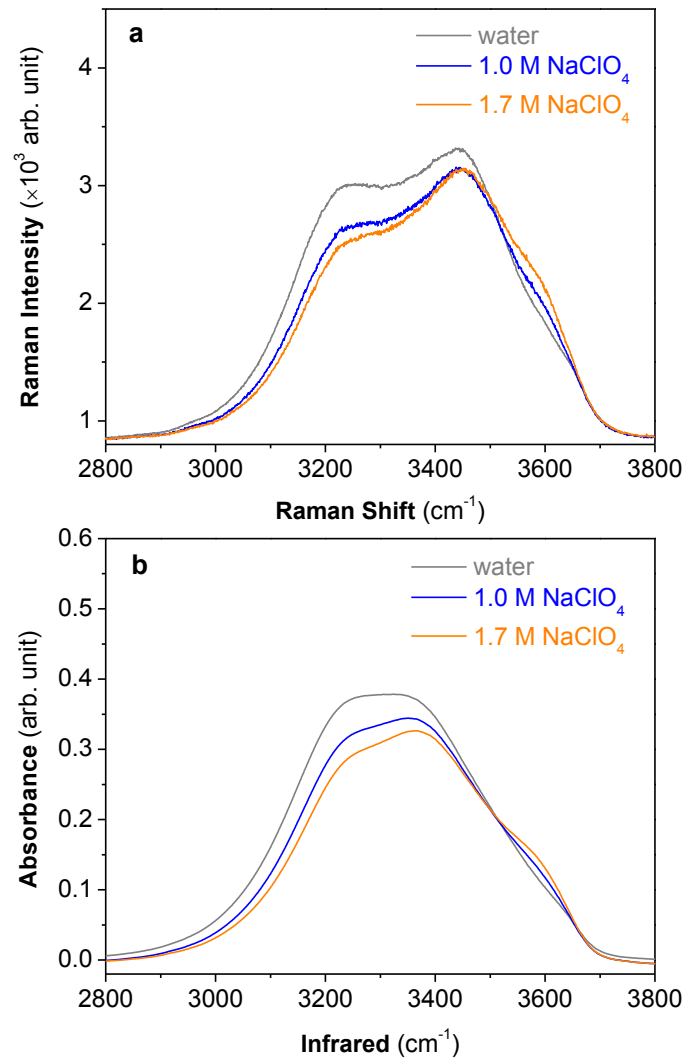


Figure 7.4 (a) Raman spectra and (b) IR spectra of 1.0 M and 1.7 M NaClO_4 salt solutions. Neat water spectrum is shown as a reference.

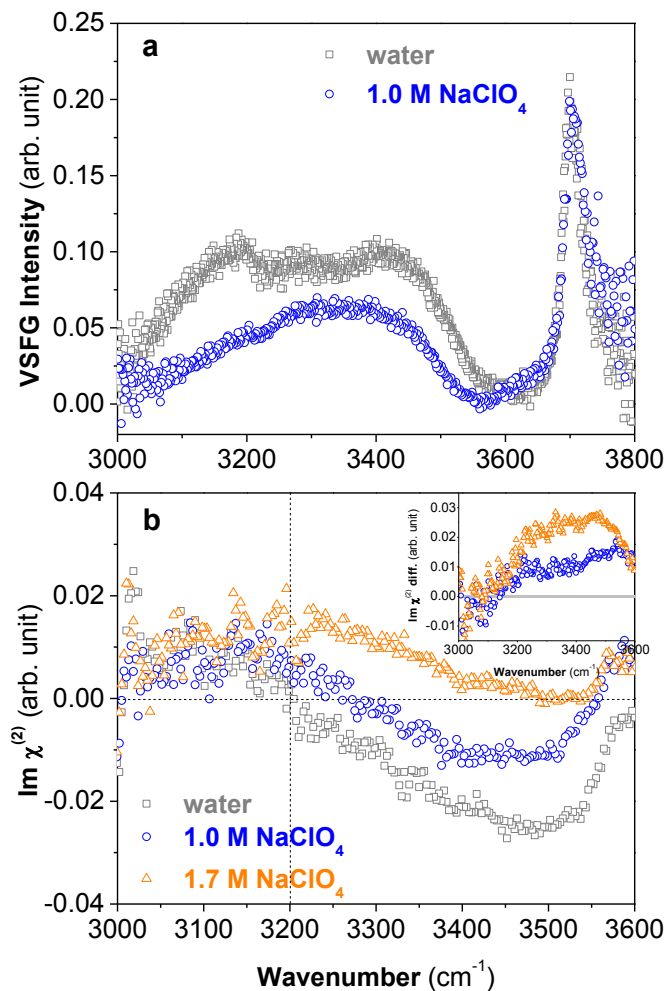


Figure 7.5 (a) Conventional VSGF $|\chi_{\text{eff}}^{(2)}|^2$ spectra of the air/aqueous interfaces of neat water and 1.0 M NaClO₄ salt solutions across the entire OH stretching region (3000–3800 cm⁻¹). (b) HD-VSGF Im $\chi^{(2)}$ spectra of air/aqueous interfaces of 1.0 and 1.7 M NaClO₄ salt solutions. Neat water spectrum is shown as a reference. Inset: Im $\chi^{(2)}$ difference spectra (Im $\chi^{(2)}$ salt spectrum minus Im $\chi^{(2)}$ neat water spectrum) of the same salt solutions found in (b).

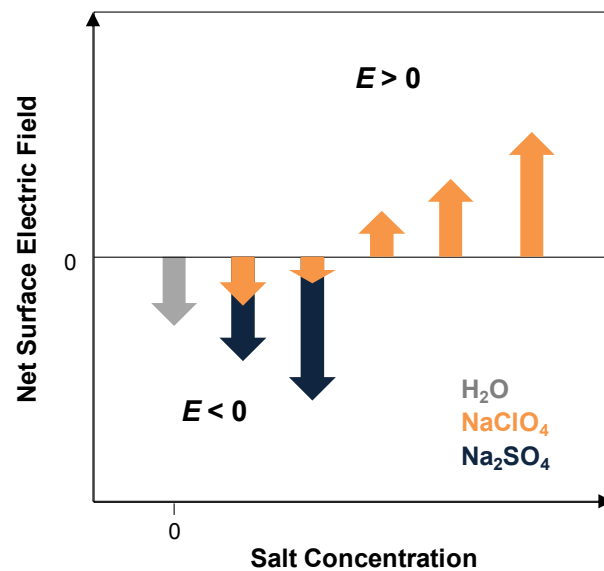


Figure 7.6 Diagram qualitatively demonstrating the salt concentration dependence of the magnitude and direction of the overall electric field as exemplified by $NaClO_4$ and Na_2SO_4 salt solutions.

Chapter 8 Cation Effects on Water Organization at the Air/Aqueous Nitrate Solution Interfaces

8.1 Introduction

Water organization at air/aqueous interfaces is strongly influenced by inorganic ions, specifically ion distributions that exist in the interfacial region where the molecular environment changes from the bulk to the surface. It has been shown, in many cases, that the molecules residing in the interfacial region are responsible for driving the heterogeneous chemistry of atmospheric aerosols.^{2,6,7} Knowledge of interfacial water organization and ion distributions is thus highly relevant to atmospheric aerosol chemistry,⁶⁻⁹ in addition to ice/snowpack chemistry,¹²⁻¹⁵ thundercloud electrification,¹⁶ geochemistry,¹⁷⁻²¹ and ocean surface processes,²² among others. With perspective toward atmospheric chemistry, understanding aerosols is critical as their roles in air pollution and climate change are still not completely understood.

Nitrate (NO_3^-) ions along with chloride, bromide, sulfate, and bisulfate ions are among the most abundant anions in atmospheric aerosols and terrestrial water sources.^{7,45,230} For example, gaseous ammonia reacts with nitric acid (HNO_3) in the atmosphere, a product of the heterogeneous hydrolysis of NO_2 , and forms NH_4NO_3 , an important semi-volatile component in aerosols. In marine regions, NO_3^- ions are

generated by heterogeneous reactions of sea salt aerosols. For example, NaCl and MgCl₂ react with HNO₃, NO₃ radicals, N₂O₅, and ClONO₂,^{45,46} resulting in the generation of NaNO₃ and Mg(NO₃)₂ in/on aerosols and the significant depletion of chloride ions in sea salt aerosols, as well as yielding photochemically active gaseous halogen products. These reactions are strongly associated with tropospheric ozone formation through reactions with volatile organic compounds (VOCs).^{7,45} In addition, nitrate salt aerosols can be formed via reactions of mineral dust aerosols with nitrogen oxides (NO_x).⁴⁶ Nitrate ions also play a crucial role in ice and snowpack chemistry by acting as a source of NO_x and OH radicals via photolysis.²³¹⁻²³⁴ The resultant fluxes of NO_x and OH radicals from ice and snow may exert a significant impact on the chemistry of the atmospheric boundary layer. Considering the critical roles that NO₃⁻ ions play in various aspects of atmospheric chemistry, knowledge about their distribution and that of their counter cations as well as their influence on the water organization at the air/aqueous interface is required. It is well known that Na⁺, NH₄⁺ and Mg²⁺ are pervasive cations in atmospheric aerosols,^{235,236} while Na⁺ and Mg²⁺ are the most common cations in seawater.²³⁰ Hence, the distribution of these cations in the interfacial region has also drawn significant attention.^{9,27,30,57,88,237,238}

Traditionally, it was accepted that ions are depleted from the aqueous surface and exhibit a negative surface excess on the basis of surface tension measurement interpretation.^{9,23-26} However, work in the last decade regarding halides' surface propensity gave rise to a rethinking of ion surface depletion.^{27,30-32,208} Large halide ions, such as iodide, are now believed to have a strong surface propensity,^{27,28,208} although the

integrated ionic distribution in the interfacial region still maintains a negative surface excess. In the same manner for NO_3^- ions, computational studies have been implemented to explore their partitioning at the air/aqueous interface. Salvador et al. predicted that NO_3^- anions prefer interfacial over bulk solvation,⁶⁴ while Dang et al. found that the probability of finding NO_3^- anions at the aqueous interface is low.⁶⁵ This apparent contradiction has since been attributed to the different treatment of NO_3^- ion polarizability in the polarizable molecular dynamics (MD) simulations. Moreover, these simulations were done without including counter cations. More recently, refined MD simulations have taken into account the effect of counter cations on the interfacial NO_3^- ion distribution. Thomas et al. predicted that NO_3^- anions reside primarily in the bulk and only a small concentration exists at the air/aqueous interface of NaNO_3 solution.⁶⁶ Similarly, Minofar et al. also reported for $\text{Mg}(\text{NO}_3)_2$ solution a very weak surface propensity for NO_3^- ions.⁶⁷ These somewhat conflicting results regarding the surface propensity of NO_3^- ions in simulations with or without counter cations call for further theoretical and experimental efforts. However, it remains unclear how the introduction of a counter cation affects the outcome of such simulations.

Various experimental techniques among which, mass spectrometry/electrospray,⁷² glancing-angle Raman spectroscopy,⁷³ IR spectroscopy,⁷⁴ and X-ray photoemission spectroscopy (XPS),⁷⁸ have been applied to unravel the partitioning of NO_3^- ions at air/aqueous interfaces. Several other experiments have investigated the distribution of NO_3^- and its impact on interfacial water structure by utilizing surface-sensitive nonlinear optical techniques such as second harmonic generation (SHG)^{28,79} and vibrational sum

frequency generation (VSFG) spectroscopy.^{103,104,146,239} For instance, with the help of resonant SHG spectroscopy, Otten et al. showed the existence of NO_3^- ions in the interfacial region of aqueous solution but no strong enhancement in its concentration.⁷⁹ Schnitzer et al. looked at changes to the hydrogen-bonding network and to the free OH at the air/aqueous nitrate solution interface in the presence of Na^+ cations.⁸⁷ The perturbation of NO_3^- ions on the interfacial water hydrogen-bonding network in the presence of divalent cations was determined as well by Xu et al.⁸⁸ They further demonstrated the presence of NO_3^- ions in the interfacial region by directly probing their vibrational symmetric stretching mode, and found unique behavior for aqueous $\text{Mg}(\text{NO}_3)_2$ compared to $\text{Sr}(\text{NO}_3)_2$ and $\text{Ca}(\text{NO}_3)_2$.⁸⁹ The NO_2 group of nitric acid has also been studied in different spectral regions using VSFG spectroscopy by Soule et al.⁹⁰ However, a more detailed picture of the distribution of NO_3^- ions and their counter cations, and how they alter the interfacial hydrogen-bonding network still remains elusive. Recently, the emergence of phase-sensitive heterodyne-detected sum frequency generation (HD-VSFG, also known as PS-SFG) spectroscopy, a variant of conventional VSFG spectroscopy based on interference of the sample SFG response with a phase reference, provides additional information.^{92,93,131,208} The main advantage of HD-VSFG spectroscopy is that it provides the imaginary part of the nonlinear susceptibility $\chi^{(2)}$ ($\text{Im } \chi^{(2)}$), a parameter which relates directly to the net dipole orientation of interfacial water molecules.

To understand the distribution of NO_3^- ions and their counter cations, the water organization at air/aqueous salt solution interfaces in the presence of NaNO_3 , $\text{Mg}(\text{NO}_3)_2$,

NH_4NO_3 , and LiNO_3 salts is investigated using conventional VSFG and HD-VSFG spectroscopy. (The smallest alkali metal cation, Li^+ , was also included here to investigate fundamental questions regarding the driving force behind surface propensity, or lack thereof, in relation to NO_3^- anions.) Additional insight is given on the interfacial electric field arising from the net interfacial water orientation caused by charge separation of the distribution of nitrate and its counter cation in each aqueous salt system.

8.2 Experimental

Materials and Preparation of Salt Solutions. NaNO_3 (Fisher Scientific, $\geq 99\%$ colorless crystals, Fisher BioReagents), NH_4NO_3 (MP Biomedicals, ultrapure grade, $>99\%$), $\text{Mg}(\text{NO}_3)_2 \cdot 6\text{H}_2\text{O}$ (Fisher Scientific, ACS grade, $>98\%$), LiNO_3 (Fisher Scientific, ACS certified powder) were used as-received. Nanopure water (not purged of CO_2) with a resistivity of 18.2 to 18.3 $\text{M}\Omega\cdot\text{cm}$ and a measured pH of 5.6 was obtained from a Barnstead Nanopure system (model D4741, Thermolyne Corporation) with additional organic removing cartridges (D5026 Type I ORGANICfree Cartridge Kit; Pretreat Feed).

Stock solutions for SFG measurements were prepared by dissolving salts in Nanopure water and then filtered using carbon-activated filter (Whatman Carbon Cap 75, Fisher Scientific) usually four to six times to completely eliminate organic impurities. Raman calibration curves were generated for each nitrate salt solution in order to determine the concentration following filtration (Figure 8.1). The measured pH of 1.7 M NaNO_3 , 1.6 M NH_4NO_3 , 1.0 M $\text{Mg}(\text{NO}_3)_2$, and 2.0 M LiNO_3 was between 5 and 7. All salt solutions were shown to be free of organic impurities as revealed by VSFG spectra

obtained in the CH stretching region from 2800 to 3000 cm^{-1} (Figure 8.2). All solutions were conditioned at room temperature (23 ± 1 °C) over 24 h before use.

Most of the nitrate salts used here were of ACS reagent grade (>98%). Ultrahigh purity salts (on the basis of higher trace metal purity) typically reveal greater organic contamination and its effect on the VSFG water spectra in the OH-bonded region can vary depending on the amount present. In addition, previous results regarding carbonate, sulfate, and chloride salts reveal that for the same chemical species ultrapure grade salts (>99.99%) versus high purity salts (~99%) display highly similar conventional VSFG and PS-SFG spectra in the OH region after pretreatment of salts and salt solutions.¹²⁶

Methods. VSFG and HD-VSFG Spectroscopy. Conventional VSFG and HD-VSFG spectroscopy measurements were performed on a broad-bandwidth VSFG spectrometer setup which has been described in detail in Chapter 3. Neat water spectra were used as a reference for salt comparison to assess reproducibility during the entire experimental period. The reproducibility for both conventional VSFG and HD-VSFG spectra of neat water is demonstrated in the Figure 8.3. Note that the zero crossing point of $\text{Im } \chi^{(2)}$ spectra shown in this study was adjusted to match that published by Shen and co-workers,^{93,208} although critical here is that all $\text{Im } \chi^{(2)}$ spectra of salt solutions are compared to the neat water $\text{Im } \chi^{(2)}$ spectrum. Thus our interpretation is based on the *relative* spectral difference between neat water and the salt solutions. To check the validity of the $\text{Im } \chi^{(2)}$ spectra, the $|\chi^{(2)}|^2$ power spectra of nitrate salt solutions deduced from HD-VSFG (Figure 8.4) were compared to that measured directly by conventional VSFG spectroscopy. A high similarity of their spectral shape is a necessary but

insufficient criterion to prove the validity of the $\text{Im } \chi^{(2)}$ spectra. To avoid spectral clutter, only every fourth data point is plotted in the HD-VSFG spectra. $\text{Re } \chi^{(2)}$ spectra deduced from HD-VSFG of water molecules at air/aqueous nitrate salt solution interfaces is presented in Figure 8.5.

Infrared and Raman Spectroscopy. Attenuated total reflection Fourier transform infrared (ATR-FTIR) spectroscopy and Raman spectroscopy for bulk solution measurements were also performed. The setups for both measurements have been described in detail in Chapter 3 and elsewhere.²¹⁹ The Raman and IR spectra of nitrate salt solutions are shown in Figure 8.6 and Figure 8.7, respectively.

8.3 Results and Discussion

Conventional VSFG Spectra of Air/Nitrate Solution Interfaces. VSFG spectra of the interfacial region of NaNO_3 , $\text{Mg}(\text{NO}_3)_2$, NH_4NO_3 , and LiNO_3 salt solutions are shown in Figure 8.8. The interfacial region refers hereafter to the region where concentration gradients exist, and which has no inversion symmetry, hence SFG active. The neat water $|\chi_{\text{eff}}^{(2)}|^2$ is also given as reference for all salt solution spectra. The neat water $|\chi_{\text{eff}}^{(2)}|^2$ spectrum reveals a broad region spanning from 3000 to 3600 cm^{-1} representing water molecules with a broad continuum of hydrogen bond lengths, and a narrow band at 3700 cm^{-1} assigned to the distinct dangling OH bond of water molecules located in the topmost layer. In the lower frequency part of the broad region, it is accepted that hydrogen bonds are relatively strong, and as one moves to higher frequency, the hydrogen bonding strength weakens significantly. Additional assignments to this broad continuum continue to be discussed.^{109,110,150,161}

The VSFG spectra of NaNO_3 , NH_4NO_3 , and LiNO_3 solutions show weakened intensity from 3000 to 3600 cm^{-1} relative to that of neat water, particularly below 3200 cm^{-1} , while no appreciable differences are observed for the dangling OH peak (Figure 8.8a, c, d). In contrast, the spectrum of $\text{Mg}(\text{NO}_3)_2$ shown in Figure 8.1b narrows and the broad continuum OH stretch band is enhanced around 3300 to 3400 cm^{-1} . The intensity of the dangling OH peak drops significantly relative to neat water in the presence of $\text{Mg}(\text{NO}_3)_2$. The $|\chi_{\text{eff}}^{(2)}|^2$ spectra of NaNO_3 and $\text{Mg}(\text{NO}_3)_2$ solutions are consistent with those published previously,^{87,88} however, no VSFG spectra of NH_4NO_3 and LiNO_3 have so far been reported for comparison. Schnitzer et al. observed a decrease in intensity of the dangling OH peak for NaNO_3 solution which becomes more significant as the solution concentration was increased, as might be expected.⁸⁷ It was suggested that perturbation of dangling OH groups on NaNO_3 salt solutions is a function of ionic strength, ion association, and anion charge density,⁸⁷ while the decrease of the 3700 cm^{-1} peak in the presence of $\text{Mg}(\text{NO}_3)_2$ was shown to be at least partly due to a reorientation of the dangling OH moiety.⁸⁸ Similar observations were also reported in later studies by Allen and co-workers with concentrated (~ 5 M) NaCl and MgCl_2 solutions.^{164,239}

The intensity decrease of the OH stretching continuum region in the NaNO_3 , NH_4NO_3 , LiNO_3 spectra and the intensity enhancement in the $\text{Mg}(\text{NO}_3)_2$ spectra at 3300 cm^{-1} suggest that there is a weakening of the overall hydrogen bonding network in the nitrate salt solution interface. However, this simple explanation needs to be revisited as our previous HD-VSFG results obtained with CaCl_2 solutions revealed that the 3300 cm^{-1} enhancement of the conventional VSFG spectrum was not due to a decrease in the overall

hydrogen bonding strength but rather attributed to spectral convolution effects between the real and imaginary components of the VSFG spectra.^{107,125} In order to delineate these effects and to better understand the complex OH stretching continuum of interfacial water in the presence of NO₃⁻ ions, it becomes advantageous to utilize HD-VSFG spectroscopy.

HD-VSFG Spectra of Air/Nitrate Solution Interfaces. As described above, in addition to resonance information, the Im $\chi^{(2)}$ spectra directly provide the sign and thus the net transition dipole moment orientation of SFG-active OH vibrational stretching modes, and the magnitude of the positive or negative intensities reveal the extent of the O→H dipole orientation, i.e. directed either towards or away from the surface, respectively. To facilitate the following discussion, the Im $\chi^{(2)}$ spectrum of the neat water interface and its spectral interpretation are also given. The Im $\chi^{(2)}$ spectrum of neat water in the OH stretching region shown in Figure 8.9 is similar to the results reported by Shen and co-workers and Tahara and co-workers.^{93,131,208} The sign of the Im $\chi^{(2)}$ spectrum of neat water in the 3000—3200 cm⁻¹ region is positive suggesting that the OH stretch net transition dipole moment is oriented towards the surface; however, the assignment of absolute orientation for this region has not been fully explained by recent theoretical predictions.^{149,150,240} In contrast, the Im $\chi^{(2)}$ spectrum from 3200 to 3600 cm⁻¹ reveals a negative band, and this spectral region interpretation is not contested. Although the orientational distribution is likely to be broad, the OH stretches in this frequency range have a net transition dipole moment directed on average toward the isotropic bulk solution.

In the case of neat water, only the topmost layers (~1-3) of the water surface are

believed to be responsible for the observed SFG signal while the subsequent layers make little contribution,^{92,93,131,208} however, the presence of ions may induce an electric field in the interface by forming an ionic double layer. This has the effect to extend the region of noncentrosymmetry, a requirement for SFG activity. Water organization is directly influenced by the direction and relative strength of the electric field generated in the interfacial region by the ion distributions. The perturbation of the interfacial water organization by this electric field can involve both reorientation and restructuring of the water hydrogen-bond network which, in turn, leads to an increase in interfacial depth, i.e. to a greater number of water molecules probed due to their SFG activity.

The HD-VSFG $\text{Im } \chi^{(2)}$ spectra of the air/aqueous interfaces of NaNO_3 , $\text{Mg}(\text{NO}_3)_2$, NH_4NO_3 , and LiNO_3 salt solutions are shown in Figure 8.9. Significant spectral changes, seen in the form of an enhanced positive signal intensity in the lower frequency region and a reduced negative intensity for the higher frequency region relative to the neat water $\text{Im } \chi^{(2)}$ spectrum, can be observed for all nitrate solutions. The $\text{Im } \chi^{(2)}$ spectrum of NaNO_3 solution presented here is in good agreement with that previously reported by Tian et al.,¹³⁸ however, up until now, there has been no published accounts of $\text{Im } \chi^{(2)}$ spectra from other nitrate solutions. The overall enhancement from 3200 to 3500 cm^{-1} can be attributed to the generation of an electric field induced by the distribution of NO_3^- anions and their counter cations in the interfacial region, i.e. by the different ion density profiles within the interface. It has been demonstrated by XPS that NO_3^- ions prefer bulk solvation but still can be partially found in the top surface layers.⁷⁸ These results are consistent with the predictions from MD simulations that NO_3^- ions display a weak

surface propensity.^{66,67,69} The presence of the induced interfacial electric field, in turn, causes a reorganization of the interfacial water molecules which now have their net transition dipole moment more oriented towards the surface.

More importantly, Figure 8.9 also reveals that the direction and magnitude of this electric field appears to be both cation- and concentration-dependent. Together, these two effects have an impact on the orientation of interfacial water molecules which translates into a less negative intensity of the $\text{Im } \chi^{(2)}$ spectra, mainly in the weakly hydrogen bonding 3200—3500 cm^{-1} spectral region. Here, any pH effect can be ruled out since the pHs of all nitrate solutions fall in the range of 5—7, such that the concentration of hydronium (H_3O^+) ions, which are known to be disruptive to the hydrogen-bonding network,⁹³ remains quite low. Therefore, the pHs of nitrate solutions should only play a minor role in the overall change observed in their $\text{Im } \chi^{(2)}$ spectra. Taken together, all these observations from the HD-VSFG spectra indirectly confirm the presence/existence of NO_3^- ions at the air/aqueous interface.⁷⁹

As shown in Figure 8.9, it is evident that interfacial water molecules in nitrate solutions are preferentially oriented towards the vapor phase, but to a different extent depending on the cation identity, assuming a constant OH transition moment strengths for different salts. The Raman and IR spectra of nitrate salt solutions in the OH-bonded region are shown in Figures 8.6 and 8.7. When the NO_3^- ion concentration is high (~2 M) and kept almost constant, nitrate salts exhibit different $\text{Im } \chi^{(2)}$ spectra relative to that of neat water. For instance, the presence of NH_4^+ ions has only a minor effect on water molecules organization, whereas Mg^{2+} ions have the largest one (Figure 8.9b,c). To see

more clearly the effect of the induced interfacial electric field change on the $\text{Im } \chi^{(2)}$ spectra caused by the different NO_3^- /cation distributions, the $\text{Im } \chi^{(2)}$ difference spectra for various nitrate solutions with respect to neat water are plotted in Figure 8.10. The difference spectra reveal that $\text{Mg}(\text{NO}_3)_2$ more strongly reorganizes and orients interfacial water molecules and gives rise to a larger electric field relative to other nitrate salts. Based on the magnitude of their respective induced electric field and, subsequently, on their impact on the reorganization of the interfacial water network, cations can be ranked as $\text{Mg}^{2+} > \text{Na}^+ \approx \text{Li}^+ > \text{NH}_4^+$. The larger enhancement in the $\text{Im } \chi^{(2)}$ spectra of $\text{Mg}(\text{NO}_3)_2$ solution compared to other nitrate solutions (at similar nitrate concentrations) suggests that the induced net electric field may originate either from a greater charge separation or a greater number of separated ionic charges, or a combination of both. However, at this point, HD-VSFG spectroscopy cannot differentiate between these scenarios; to clarify this issue further theoretical examination is clearly needed.

The simplest picture of the ion distributions of nitrate salts emerging from the $\text{Im } \chi^{(2)}$ spectra has the cations located on average predominantly below NO_3^- anions. It is also possible that the density profile of some cations (e.g. Mg^{2+}) exhibits a multilayer-like structure,^{67,241} and that NO_3^- ions adopt a similar broad distribution gradient in the interface due to the electroneutrality requirement, although it is hard to distinguish between these scenarios directly from our HD-VSFG results. In addition, the $\text{Mg}(\text{NO}_3)_2$ $\text{Im } \chi^{(2)}$ result is consistent with the prediction from MD simulations.⁶⁷

Unfortunately, concerning the relative location between cations, the picture becomes somewhat more complicated. However, some tentative interpretations regarding

the interfacial electric field and ion surface propensity have been put forward by combining HD-VSFG spectroscopy results with the ion distribution profiles from MD simulations. One of these interpretations has been developed by Tian et al. to explain the difference in their phase-sensitive SFG spectra between HCl and HI acidic solution.⁹³ In this treatment, it was argued that the stronger overall surface field effect displayed by the $\text{Im } \chi^{(2)}$ spectra of HCl was a result of the greater charge separation between H_3O^+ and Cl^- ions, even though the surface concentration of H_3O^+ was higher in HI as shown in MD simulations by Ishiyama and Morita.²⁴² Similarly, a ranking of ion surface propensity was proposed for a series of selected salts based on the magnitude and direction of the interfacial electric field deduced from their respective $\text{Im } \chi^{(2)}$ spectra.¹³⁸ Following Tian's argument, the enhancement in the $\text{Im } \chi^{(2)}$ spectra of $\text{Mg}(\text{NO}_3)_2$ observed here can be physically rationalized by having Mg^{2+} ions residing, on average, deeper in the interfacial region, closer to the isotropic aqueous bulk compared to Na^+ ions. In other words, Na^+ ions have a greater surface propensity than Mg^{2+} in nitrate solutions. In the same manner, the surface propensity of cations in the nitrate salt solution interface could thus be inferred from the magnitude of their respective induced electric field, following the order of $\text{NH}_4^+ > \text{Li}^+ \approx \text{Na}^+ > \text{Mg}^{2+}$. The relative location of NH_4^+ and Mg^{2+} ions is illustrated schematically in Figure 8.11a.

Despite its simplicity, this picture may not reflect the true ion distribution in the interfacial region. For example, recent MD simulations of the ion density profiles of a series of nitrate solutions by Callahan et al. predicted no significant difference in the surface propensity of Mg^{2+} and Na^+ .⁶⁹ In contrast, for $\text{Mg}(\text{NO}_3)_2$ solution, the surface

concentration of NO_3^- ions was much higher than for NaNO_3 solution, which may account for the enhanced interfacial electric field. In addition, it was shown that the water number density varied significantly from salt to salt.⁶⁹ More generally, these results may be symptomatic and reveal that there could be no simple universal interpretation of the ion surface propensity that is applicable to all inorganic ions. Instead, many factors are thought to be responsible for cation surface propensity.⁹

The surface charge density of cations could play a critical role in determining the magnitude of the induced electric field in nitrate solutions and, in turn, could also have an impact on their surface propensity. Considering the bare (unhydrated) ionic radii of Li^+ (0.60 Å), Mg^{2+} (0.65 Å), Na^+ (0.95 Å), and NH_4^+ (1.5 Å) and their corresponding ionic charge,^{187,243} the trend of the induced electric field for the aqueous nitrate solutions follows that of decreasing surface charge density except for Na^+ and Li^+ . Although ionic radii values given in the literature vary to some extent, the overall trend with surface charge density remains the same.^{244,245} Recently, it was argued by Levin that ion surface propensity could be the result of the competition between attractive cavitation and repulsive electrostatic energies.²⁴⁶ Hence, for small and strongly hydrated (i.e. weakly polarizable) ions, the electrostatic penalty of approaching the interface is larger than the cavitation energy, thus favoring bulk solvation. In contrast, for large and weakly hydrated (i.e. polarizable) ions, the small electrostatic penalty of exposing ionic charge to the low dielectric environment is largely compensated by the cavitation energy, hence favoring surface solvation. Following this model, small weakly polarizable cations like Mg^{2+} , Li^+ and Na^+ should be repelled from the interface; ions with higher charge

densities should be located deeper in the interfacial region, while the polarizable NH_4^+ should have a higher surface propensity. The situation of NO_3^- ion is less obvious. It was reported in another PS-SFG study that NO_3^- ions should have a large surface propensity, surpassed only by I^- ions, although it is not yet clear whether it has negative or positive surface excess.¹³⁸ Based on the surface charge density argument and Levin's model, the order of surface propensity should be $\text{NO}_3^- > \text{NH}_4^+ > \text{Na}^+ > \text{Li}^+ > \text{Mg}^{2+}$, consistent with the one deduced using Tian's interpretation. However, electrostatic repulsion fails to account for the unexpected similar cation effect found in LiNO_3 and NaNO_3 solutions (Figure 8.10).

The surface propensity of Li^+ vs Na^+ may originate from possible differences in ion pairing of the cations with nitrate. For example, it was shown that ion pairing with nitrate affects differently the surface propensity of divalent cations like Mg^{2+} and Ca^{2+} .⁸⁸ In the same manner, one could assert that Na^+ ions have a greater tendency to interact with NO_3^- and reside closer to them than Li^+ ions, although such ion pairing effects, at most solvent-shared, are weaker than with divalent ions. This would also go along with the prediction of the law of water matching affinities which would favor interactions between the weakly hydrated NO_3^- anion and Na^+ ,¹⁹⁸ the less strongly hydrated cation. In addition, it has been shown previously from VSFG studies of NaNO_3 solutions that ion pairing can effectively disrupt the water hydrogen-bonding network.⁸⁷

The peculiar behavior of Li^+ ions has also been observed elsewhere in the theoretical description of the surface tension of concentrated solutions.²⁴⁷ Again, the presence of potential ion pairs was mentioned as a possible source of deviation; however

no definite correlation is established here. Another possibility might come from the presence of two hydration shells in the case of Li^+ ions compared to Na^+ ions,²⁴⁸ which could more effectively screen the Li^+ ion surface charge. This is supported by infrared results from Lisy and co-workers on alkali ion water clusters ($n = 4, 5$) showing that ion-water electrostatic interactions and, in turn, the shift of the OH stretching mode frequency, are greater for Na^+ ions.²⁴⁹ More experimental and computational work is obviously needed to understand this anomaly.

Although the $\text{Im } \chi^{(2)}$ spectra of LiNO_3 and NaNO_3 solutions cannot be solely rationalized by the surface charge density effect, results here are in good agreement with the surface-bulk partitioning model of Pegram and Record.^{62,63} According to this model, the individual cation partition coefficients, defined as the ratios of molal concentrations of the ions in the surface and bulk regions, are predicted to follow the series $\text{NH}_4^+ > \text{Li}^+ \approx \text{Na}^+$. The value for the partition coefficient of Li^+ is almost identical to that of Na^+ , even though it comes with a large uncertainty.^{62,63}

Among all the cations studied in this work, Mg^{2+} has the largest surface charge density. Hence, the large increase observed in the $\text{Im } \chi^{(2)}$ spectrum of $\text{Mg}(\text{NO}_3)_2$ solution versus other nitrate solutions (Figure 8.10) could be partially attributed to Mg^{2+} surface charge density and its hydration compared to monovalent cations. An inner hydration shell for Mg^{2+} containing six water molecules has been proposed by various computational studies,^{243,250,251} while Li^+ and Na^+ cations are suggested to have four to six and five to six water molecules in their first solvation shell, respectively.^{243,252-255} Additionally, the majority of surface water molecules in large-size Mg clusters ($n = 32$)

are found to be optimally hydrogen-bonded, with a fraction of these only accepting one hydrogen bond and donating another.²³⁷ As such, Mg^{2+} ions affect hydration layers over a longer range than monovalent and other larger-size divalent cations.

One may assume that the water molecules in the ion solvation shell make considerable contribution to the reorganization of the interfacial hydrogen-bonding network. However, it was suggested by different research groups that even di- and trivalent ions do not significantly alter the density or orientation of water more than two water molecules away.^{198,256,257} In addition, the orientation of those water molecules that are tightly bound in the hydration shell of the individual ion may only be partially SFG-active, particularly in the case of small spherical cations, due to the vanishing of the SFG signal in centrosymmetric environments. Hence, the ion-water interactions may have a minor impact on the $\text{Im } \chi^{(2)}$ spectra of salt solutions; instead, the electric field induced by ion distributions in the interfacial region, which could be viewed as an ionic double layer, may primarily drive the reorganization of water molecules.

As stated previously, the sign and the magnitude of the $\text{Im } \chi^{(2)}$ spectra, that is, the net orientation of interfacial water molecules, is also concentration-dependent. The net influence of concentration as well as cation identity on the direction and magnitude of the induced electric field are illustrated schematically by a model in Figure 8.11b. At the neat water surface, the electric field (seen from 3200 to 3500 cm^{-1}) is slightly negative due to the net, but weak, orientation of water molecules pointing towards the aqueous isotropic bulk.^{93,131,208} As mentioned above, the addition of nitrate salts affects the organization of interfacial water molecules. At low concentrations, the distribution of NO_3^- ions and their

counter cations generates an additional electric field that counteracts and slightly reduces the magnitude of the overall electric field acting on water molecules in neat water. The net orientation of this field remains however unchanged as the HD-VSFG $\text{Im } \chi^{(2)}$ spectra of monovalent nitrate salts in the 3200—3500 cm^{-1} region are still showing a negative intensity. In a more concentrated regime, the magnitude of the ion-induced electric field is sufficient to force a reversal of water orientation. It is expected that, at even higher concentrations, all of these cations in the nitrate solutions, particularly the divalent ones, would eventually give rise to a strong enough electrical field capable of completely inverting the net orientation of interfacial water molecules, thus resulting in purely positive $\text{Im } \chi^{(2)}$ spectra, as shown in Figure 8.11b.

Implications for Atmospheric Chemistry and Thundercloud Electrification.

Nitrate ions are commonly found in atmospheric aerosols, sea ice, and snowpacks through heterogeneous reactions and direct deposition.^{6,41-44} It is evident that both the kinetics and mechanisms of interfacial reactions are different from those in the isotropic bulk phase.²⁻⁵ Hence, the indirect experimental evidence of the presence of NO_3^- ions within the air/aqueous solution interfaces inferred from our HD-VSFG results may provide more insight for atmospheric chemistry. For instance, it may help to understand the currently underestimated photolysis rates of NO_3^- ions in the polar snowpack in the absence of bromide and chloride ions.¹³ This enhanced photochemistry, the production of NO_x and OH radicals through photolysis, may influence the oxidizing capacity of the atmosphere.

The surface propensity of NO_3^- ion and its counter cations may also shed some

light on charge transfer in thundercloud electrification processes. It is found in a large range of observations that the enhanced positive lightning is associated with smoke, rich in nitrates and chlorides, yet the origin of this phenomenon is not fully understood.¹⁶ The findings presented here on the ion distributions and the presence of NO_3^- ions in the interface may help provide a physical explanation for the enhanced positive lightning, the net transfer of positive charge from the cloud to the ground. For instance, NO_3^- ions residing closer to the surface of the larger falling ice particles in thunderclouds (graupels) could be preferentially transferred to the quasi-liquid interfacial layer of the small rising ice crystals during collisions between ice crystals and graupels, resulting in the positive charging of the falling graupels.

8.4 Conclusions

From the HD-VSFG data, it is shown that NO_3^- ions are present at the air/aqueous interface of all nitrate salt solutions studied here. As a result, interfacial water structure is significantly reorganized. Nitrates ions reside preferentially above their counter cations. This was inferred from the directly determined net transition dipole orientation of interfacial water molecules with their hydrogen atoms pointing on average more towards the surface relative to neat water. Moreover, nitrate salts perturb the interfacial water network to different extents due to the identity of the counter cation. $\text{Mg}(\text{NO}_3)_2$ creates the largest electric field while NH_4NO_3 generates the smallest. Chemical identity and concentration lead to a change of the sign of the $\text{Im } \chi^{(2)}$ spectra, that is, the reversal of the direction of the net interfacial electric field. The magnitudes of the induced electric field are ranked, for higher concentration solutions, in the order $\text{Mg}^{2+} > \text{Na}^+ \approx \text{Li}^+ > \text{NH}_4^+$,

generally consistent with the order of their respective surface charge density with the exception of Na^+ and Li^+ ions. Obviously, other factors come into play in addition to surface charge density of cations. Future work in our laboratory will focus on further assessing the influence of ion pairing interactions in ion distributions in the interfacial region by carrying out additional HD-VSFG studies of alkaline earth and transition divalent cation nitrate salts.

It is evident that the counter cations play a crucial role for the ion distributions in the air/nitrate solution interfacial region, and in the perturbation of the interfacial water network. To our knowledge, this is the first systematic demonstration of the counter cation effect employing HD-VSFG spectroscopy. Whether or not this effect can be interpreted on the basis of larger charge separation or greater number of separated charges or the net effect of them cannot yet be resolved. To this end, further, theoretical exploration would be helpful to decipher the microscopic picture of how NO_3^- ions and its accompanying counter cations are distributed in the interface and to determine what other factors drive interfacial solvation of ions, particularly in the competition between Li^+ and Na^+ ions. By examining all the currently available experimental and computation work, it is difficult to foresee whether there is a universal interpretation that could elucidate ion surface propensity for all inorganic ions. Also shown here, the existence of these ions in the interface may have potentially important implications for atmospheric chemistry and thundercloud electrification.

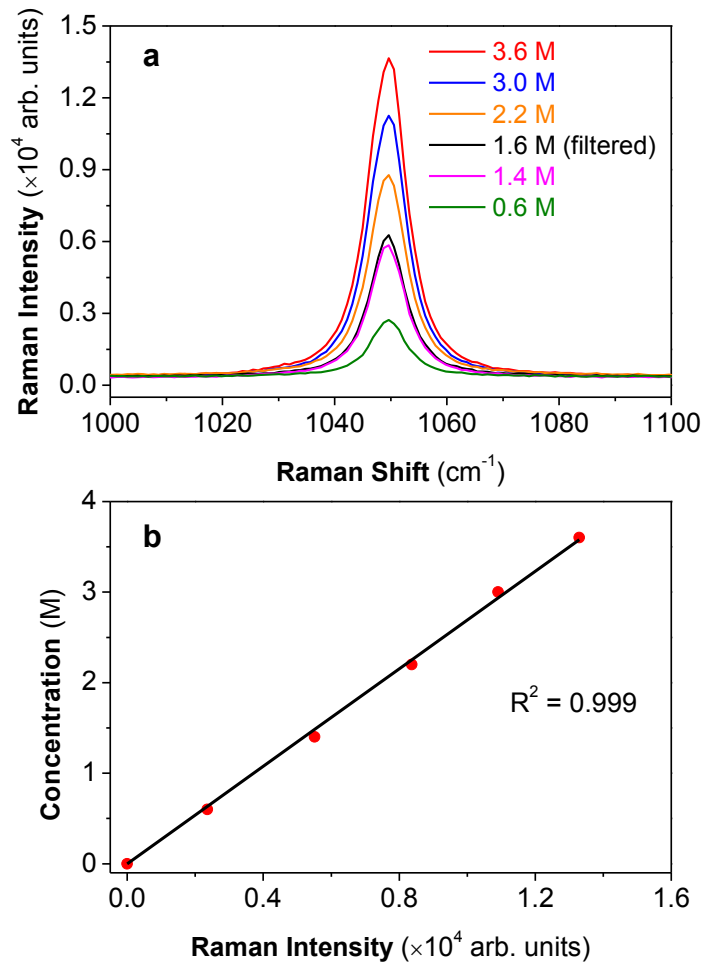


Figure 8.1 (a) Raman spectra of 0.6, 1.4, 2.2, 3.0, and 3.6 M unfiltered NH_4NO_3 , as well as filtered SFG stock solution (1.6 M), (b) Calibration curve of NH_4NO_3 solutions using the height of each individual Raman spectra. The concentrations of other nitrate SFG stock solutions were determined in the same manner.

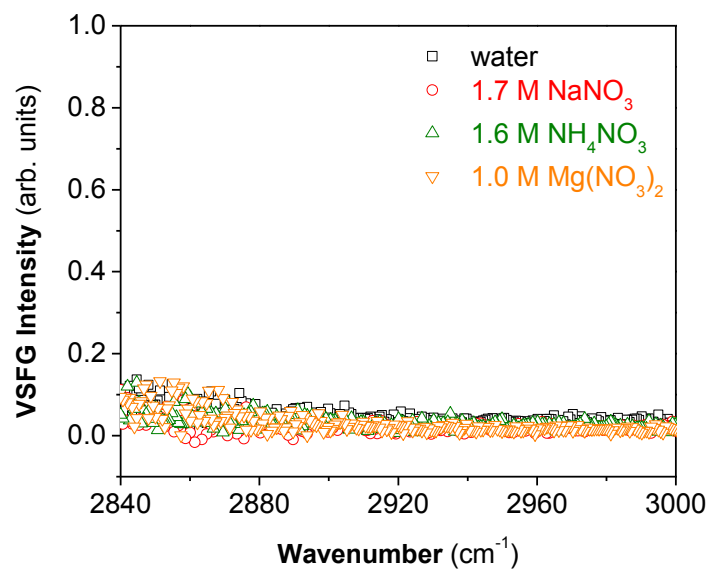


Figure 8.2 Conventional VSFG spectra of neat water, 1.7 M NaNO₃, 1.6 M NH₄NO₃, and 1.0 M Mg(NO₃)₂ salt solutions in the CH stretching region (2800–3000 cm⁻¹).

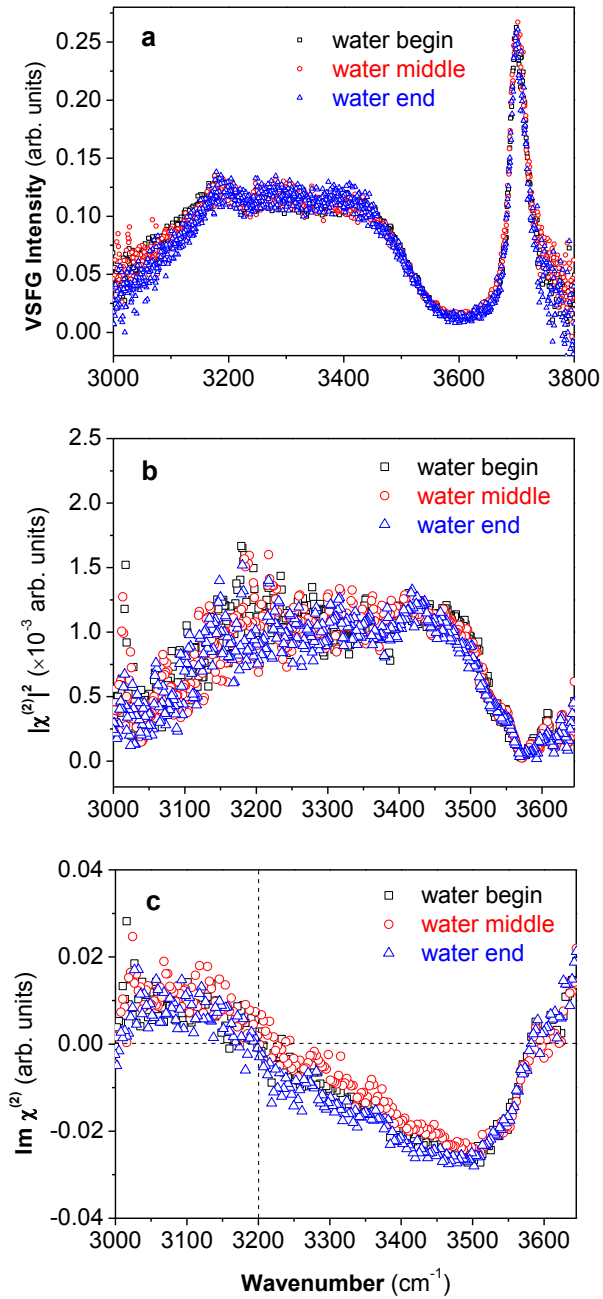


Figure 8.3 SFG spectra at the air/water interface in the OH stretching region (3100–3800 cm⁻¹). (a) $|\chi_{\text{eff}}^{(2)}|^2$ spectra, (b) deduced $|\chi^{(2)}|^2$ power spectra from HD-VSFG, and (c) Im $\chi^{(2)}$ spectra.

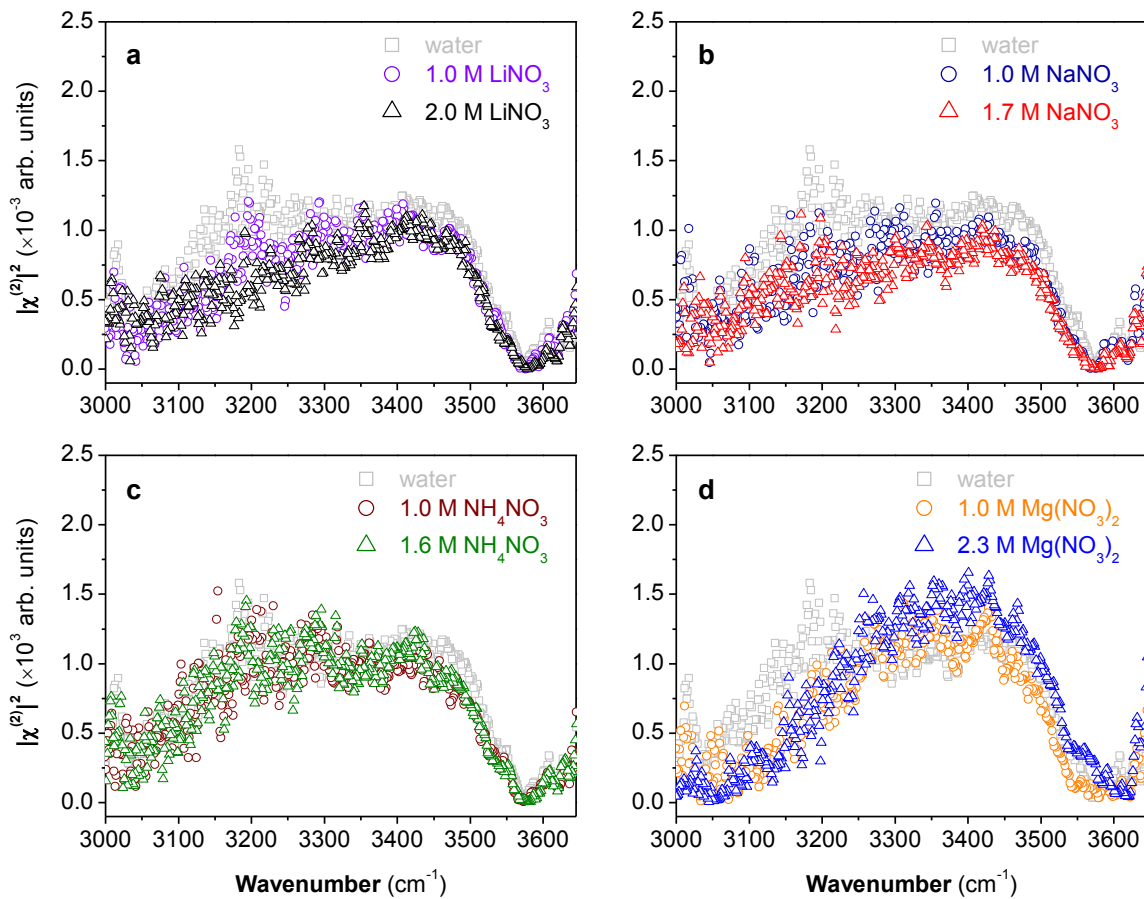


Figure 8.4 Deduced $|\chi^{(2)}|^2$ power spectra from HD-VSFG at air/aqueous solution interfaces of (a) 1.0 M and 2 M LiNO_3 , (b) 1.0 M and 1.7 M NaNO_3 , (c) 1.0 M and 1.6 M NH_4NO_3 , and (d) 1.0 M and 2.3 M $\text{Mg}(\text{NO}_3)_2$ salt solutions. Neat water spectrum is shown as a reference.

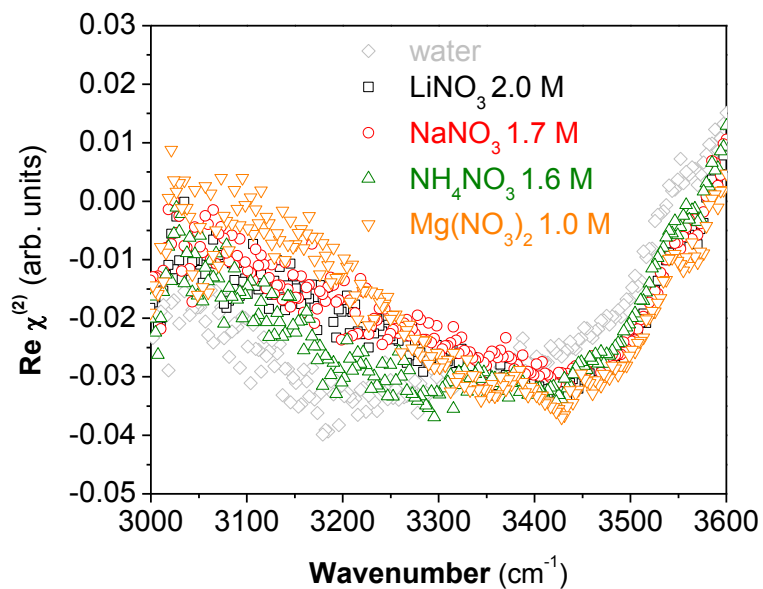


Figure 8.5 HD-VSFG $\text{Re } \chi^{(2)}$ spectra at air/aqueous solution interfaces of neat water, 2.0 M LiNO_3 , 1.7 M NaNO_3 , 1.6 M NH_4NO_3 , and 1.0 M $\text{Mg}(\text{NO}_3)_2$ salt solutions. Neat water spectrum is shown as a reference.

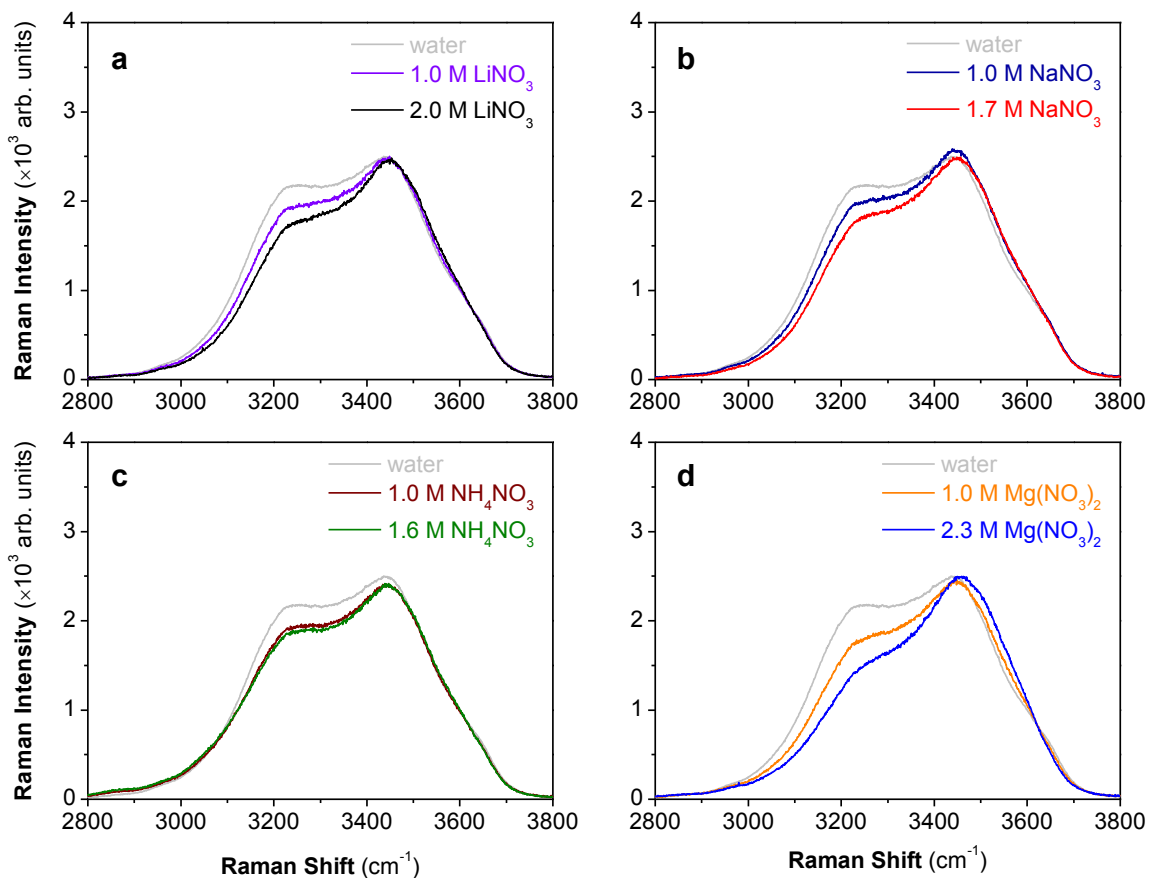


Figure 8.6 Raman spectra of (a) 1.0 M and 2 M LiNO_3 , (b) 1.0 M and 1.7 M NaNO_3 , (c) 1 M and 1.6 M NH_4NO_3 , and (d) 1.0 M and 2.3 M $\text{Mg}(\text{NO}_3)_2$ salt solutions. Neat water spectrum is shown as a reference. The ~ 2 M NO_3^- spectra reveal a relatively constant Raman transition moment strength.

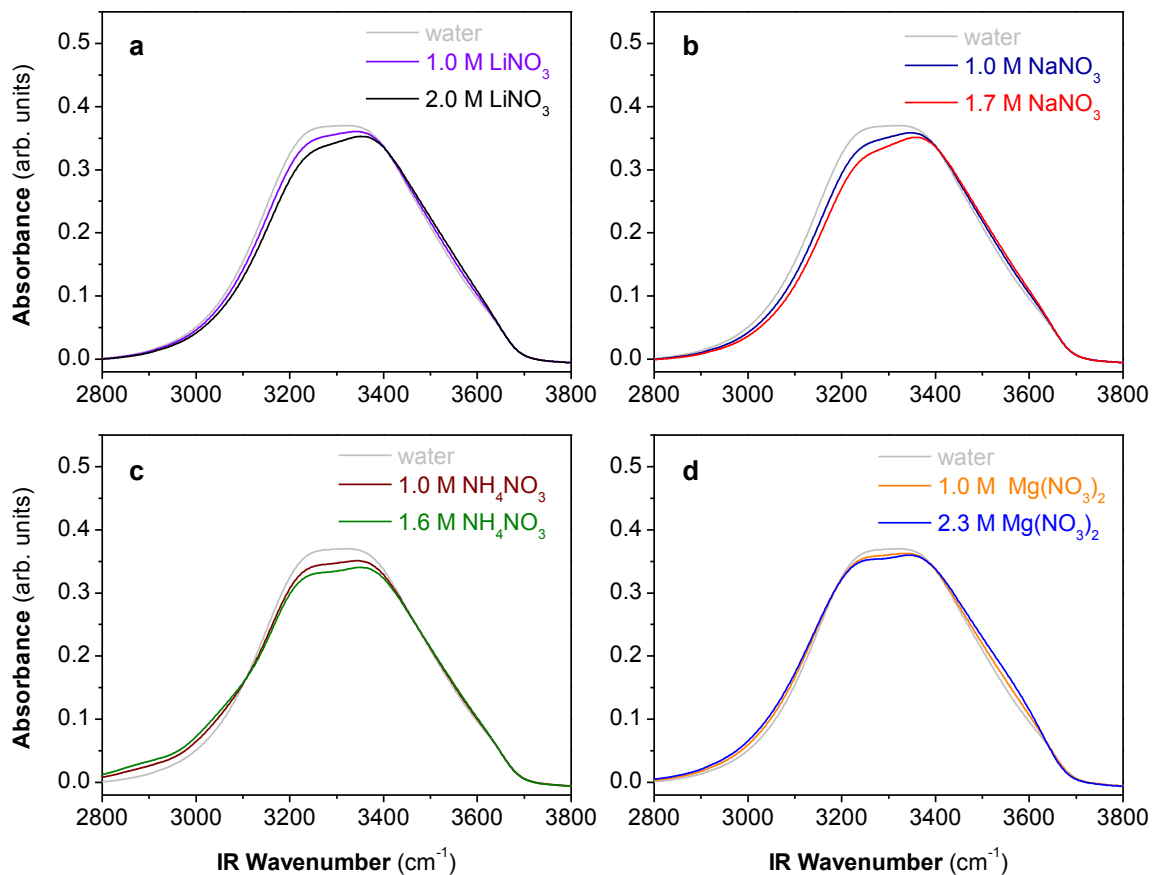


Figure 8.7 IR spectra of (a) 1.0 M and 2.0 M LiNO_3 , (b) 1.0 M and 1.7 M NaNO_3 , (c) 1.0 M and 1.6 M NH_4NO_3 , and (d) 1.0 M and 2.3 M $\text{Mg}(\text{NO}_3)_2$ salt solutions. Neat water spectrum is shown as a reference. The ~ 2 M NO_3^- spectra reveal a relatively constant IR dipole moment strength.

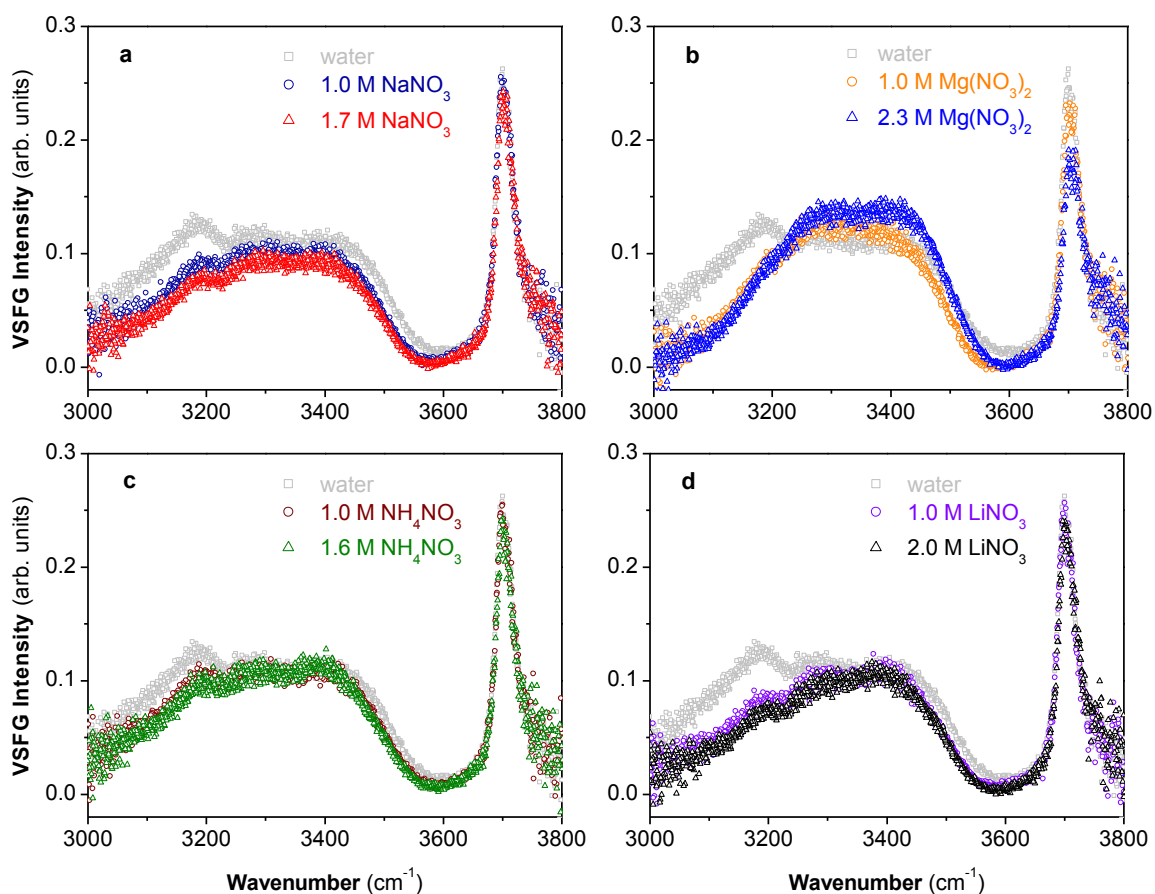


Figure 8.8 Conventional VSFG $|\chi_{\text{eff}}^{(2)}|^2$ spectra of air/aqueous interfaces of (a) 1.0 M and 1.7 M NaNO_3 , (b) 1.0 M and 2.3 M $\text{Mg}(\text{NO}_3)_2$, (c) 1.0 M and 1.6 M NH_4NO_3 , and (d) 1.0 M and 2.0 M LiNO_3 salts solutions over the entire OH stretching region (3000–3800 cm^{-1}). Neat water spectrum is shown as a reference. Legend colors in this figure will be followed in all subsequent figures.

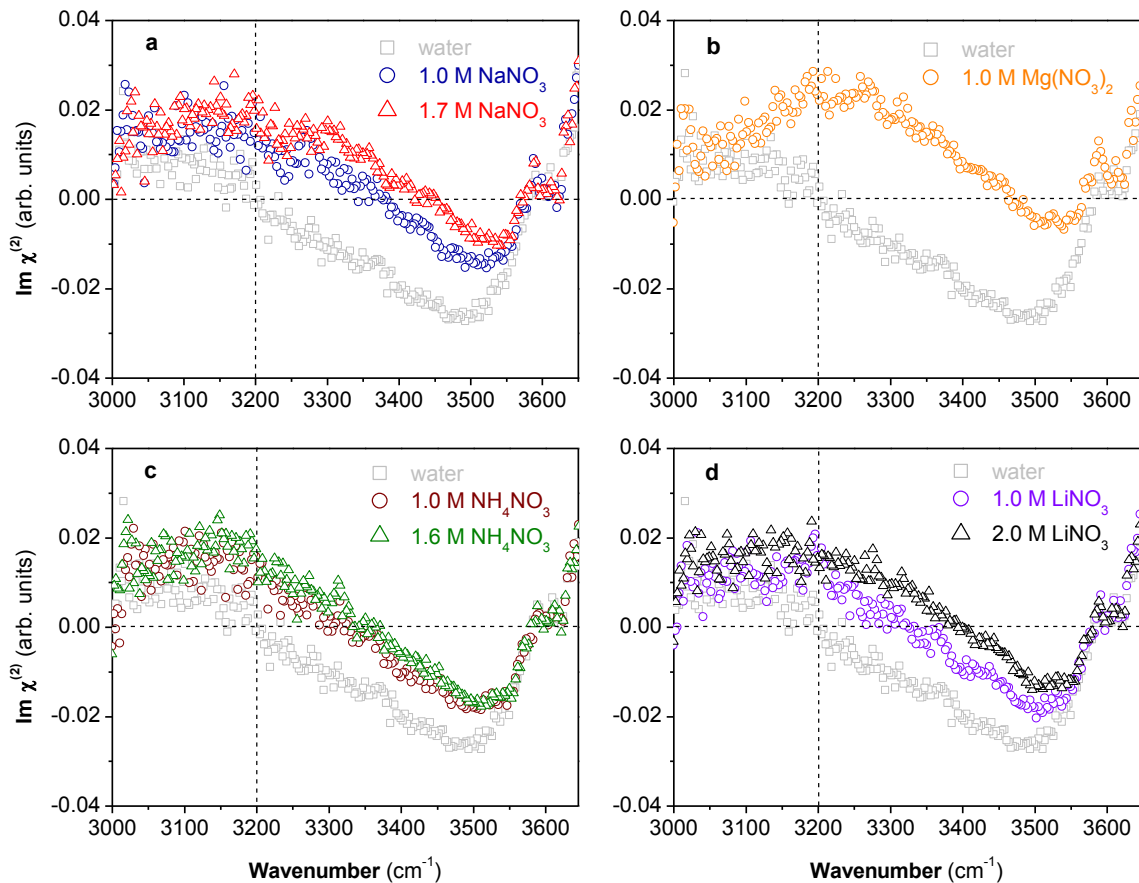


Figure 8.9 HD-VSFG $\text{Im } \chi^{(2)}$ spectra of air/aqueous interfaces of (a) 1.0 M and 1.7 M NaNO_3 , (b) 1.0 M $\text{Mg}(\text{NO}_3)_2$, (c) 1.0 M and 1.6 M NH_4NO_3 , and (d) 1.0 M and 2.0 M LiNO_3 salt solutions. Neat water spectrum is shown as a reference.

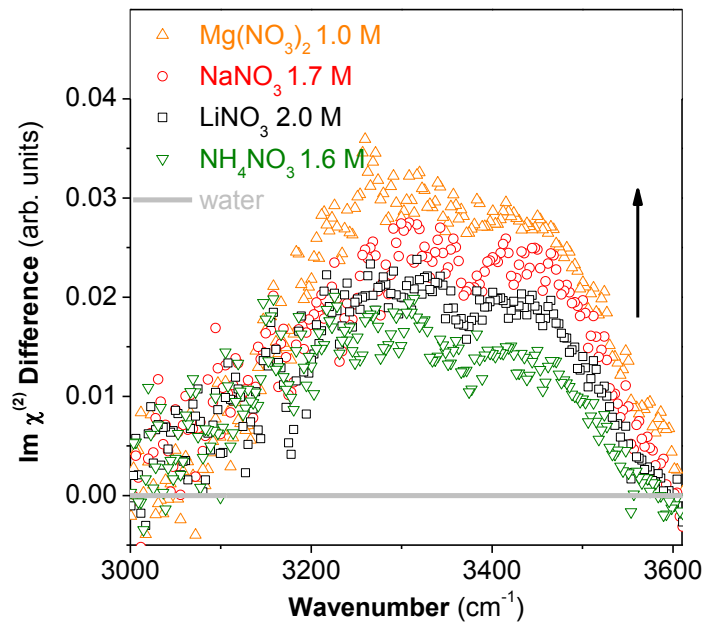


Figure 8.10 HD-VSFG $\text{Im } \chi^{(2)}$ difference spectra ($\text{Im } \chi^{(2)}$ salt spectrum minus $\text{Im } \chi^{(2)}$ water spectrum) for the indicated salts.

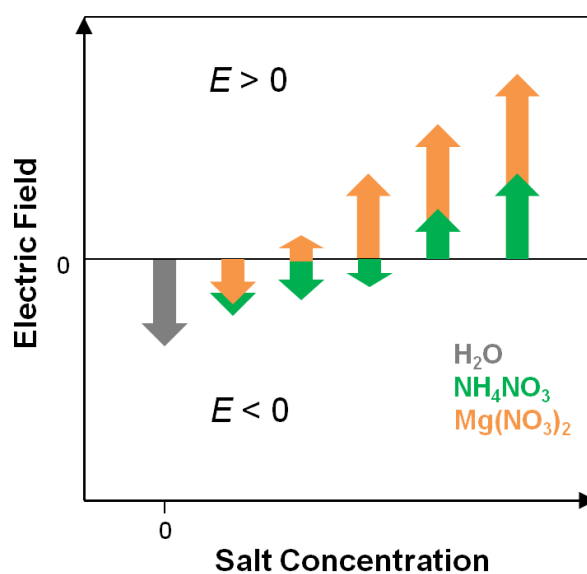
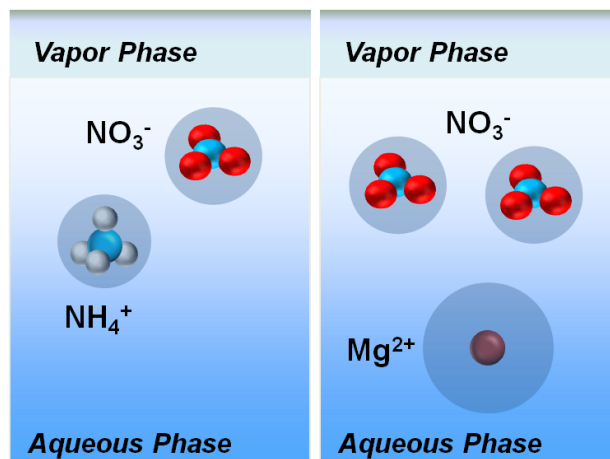


Figure 8.11 (a) Illustration of the relative location for NO_3^- and its counter cations at the air/aqueous interface of NH_4NO_3 and $\text{Mg}(\text{NO}_3)_2$ salt solutions. (b) Diagram qualitatively demonstrating the salt concentration dependence of the magnitude and direction of the overall electric field.

Chapter 9 Conclusions, and Specific Ion Properties and Potential Driving Forces Dictating Interfacial Distributions of Oxyanions (ClO_4^- , NO_3^- , SO_4^{2-} , and CO_3^{2-})

9.1 Introduction

Aside from its interest in environmental, atmospheric and oceanic chemistry, the study of polyatomic ions can facilitate a better understanding of fundamental questions in physical chemistry. Over the last century, ion-specific effects have been encountered in a variety of biological and physico-chemical processes.²⁵⁸ These effects have been often organized in the form of a ranking of the influence of ions on a given process or phenomenon known as the Hofmeister series. It was originally discovered by Franz Hofmeister who first provided a qualitative ranking of inorganic anions and cations originally based on their effectiveness as agents in protein precipitation.²⁵⁹ Such effects which are generally more pronounced for anions than for cations have been extensively studied due to their critical roles in a broad range of fields from colloidal assembly to biochemistry and physiology.^{210,260} The typical ranking order for the anion series is as follows: $\text{CO}_3^{2-} > \text{SO}_4^{2-} > \text{S}_2\text{O}_3^{2-} > \text{H}_2\text{PO}_4^- > \text{F}^- > \text{Cl}^- > \text{Br}^- \sim \text{NO}_3^- > \text{I}^- > \text{ClO}_4^- > \text{SCN}^-$. The species to the left of series are referred to as kosmotropes (strongly hydrated), while those on the right are known as chaotropes (weakly hydrated). These terms arise from the ion's ability to alter the hydrogen bonding network of water.²⁵⁸ However, the chemistry of

anions at bare air/aqueous interfaces, that is, in the absence of macromolecules, is not yet well understood particularly for polyatomic ones.

Traditionally, it was accepted that aqueous surface are devoid of ions on the basis of surface tension measurement interpretation.^{9,23-26} However, molecular dynamics (MD) simulation results from Jungwirth and Tobias gave rise to a rethinking of ion surface depletion.²⁷ They proposed that large halide ions, such as bromide and iodide, have a strong propensity for the surface, although the integrated ionic distribution in the interfacial region still maintains a negative surface excess. This prediction was subsequently confirmed by numerous experiments using various techniques.²⁸⁻³²

A series of ion and solvent properties, including ion size,^{9,84,170,207,246,261-263} geometry,⁸⁴ charge/surface charge density,^{84,262} polarizability of ions^{27,31,207,264} and solvent molecules^{58,265,266}, and various energy and driving forces, such as hydration free energy,²⁶⁷⁻²⁷⁰ dispersion forces,²⁷⁰⁻²⁷³ cavitation energy,^{246,261,274} hydrophobic solvation,^{269,275,276} and ion-specific chemical interactions,²⁷⁷ and some other factors, such as capillary waves,²⁶⁸ interfacial roughness/surface curvature,^{262,278} among others, have been utilized to explain the surface propensity of ions, particularly halide anions.^{27,31} Comparatively, molecular-level information regarding the interfacial behavior of more complicated polyatomic anions and their driving forces is still quite limited. Although Shultz and co-workers and Tarbuck and Richmond have pointed out that size, geometry (electronic distribution) and charge are critical for the distribution of oxyanions,^{84,146} only a few anion species have so far been examined. To date, no systematic experimental and/or theoretical comparison of oxyanions is yet available.

The interfacial distribution of ClO_4^- , NO_3^- , SO_4^{2-} , and CO_3^{2-} ions and their Na^+ counterions, and their impact on the water organization at the air/aqueous salt solution interfaces have been investigated using conventional VSFG and HD-VSFG spectroscopy in previous chapters. Additional insight is also given on the interfacial electric field arising from the charge separation of the oxyanion and its counter cation in each aqueous salt system. Here, to facilitate a better understanding of interfacial distribution of polyatomic ions and to prompt future development of more realistic model, the relationship between interfacial distributions of a series of oxyanions and their specific properties such size, geometry, charge, and polarizability are analyzed. In addition, various potential driving forces dominating ion's surface propensity are preliminarily discussed.

9.2 Results and Discussion

9.2.1 Surface Propensity of Oxyanions Inferred from HD-VSFG spectra

Conventional VSFG and HD-VSFG spectra of the interfacial region of Na_2SO_4 , NaNO_3 , Na_2CO_3 , and NaClO_4 salt solutions are shown in Figure 9.1. The interpretation of each spectrum can be found in previous chapters. As shown in Figure 9.1c and d, it is evident that interfacial water molecules in the oxyanion-containing solutions are preferentially oriented with respect to neat water, but to a different extent depending on the anion identity. When the Na^+ ion concentration is high (~ 2 M) and kept almost constant, oxyanion salts exhibit different $\text{Im } \chi^{(2)}$ spectra relative to that of neat water. To see more clearly the effect of the interfacial electric field on the $\text{Im } \chi^{(2)}$ spectra caused by the different Na^+ /oxyanion distributions, the $\text{Im } \chi^{(2)}$ difference spectra for various

oxyanion solutions with respect to neat water are plotted in Figure 9.2. The difference spectra reveal that at a constant cation concentration (~ 2 M) SO_4^{2-} and ClO_4^- reorient interfacial water molecules to a greater extent. The larger enhancement in the $\text{Im } \chi^{(2)}$ spectra of NaClO_4 and Na_2SO_4 compared to other oxyanion-containing salts (at similar cation concentrations) suggests that the enhanced net electric field may originate either from a greater charge separation or a greater number of separated ionic charges, or a combination of both. However, at this point, HD-VSFG spectroscopy cannot differentiate between these scenarios; to clarify this issue further theoretical examination is clearly needed.

While it is difficult for HD-VSFG spectroscopy alone to fully resolved the above-mentioned issues, a simple molecular picture of the ion distributions and a tentative ranking of ion surface propensity could be proposed here for a series of selected oxyanion salts based on the direction and magnitude of the interfacial electric field deduced from their respective $\text{Im } \chi^{(2)}$ spectra. The correlation between interfacial electric field and ion surface propensity was first developed by Tian et al. to explain the differences between $\text{Im } \chi^{(2)}$ spectra, which can be generally understood as a weaker (stronger) electric field effect should be the result of the thinner (or thicker) ionic double layer formed by ion/counterion distributions with comparable (or dissimilar) surface propensity.^{93,138} Following Tian's argument, the enhancement in the $\text{Im } \chi^{(2)}$ spectra of NaClO_4 and NaNO_3 observed here can be physically rationalized by having Na^+ ions located on average predominantly below ClO_4^- and NO_3^- anions, while ClO_4^- ions reside, above the NO_3^- ions, closer to the water surface. In other words, ClO_4^- ions have a greater surface

propensity than NO_3^- . In the same manner, the Na_2SO_4 and Na_2CO_3 $\text{Im } \chi^{(2)}$ spectra can be rationalized by having both divalent anions residing deeper in the interfacial region relative to their Na^+ counter cation, having SO_4^{2-} ions penetrating closer to the isotropic bulk than CO_3^{2-} ions. The overall surface propensity of ions studied herein could thus be inferred, following the order of $\text{ClO}_4^- > \text{NO}_3^- > \text{Na}^+ > \text{CO}_3^{2-} > \text{SO}_4^{2-}$. The relative location of oxyanions and Na^+ ions is illustrated schematically in Figure 9.3a. The inferred ion distributions are consistent with the predictions from MD simulations that ClO_4^- exhibits a stronger surface preference⁷¹ and NO_3^- ions display a weaker surface propensity,^{66,67} while SO_4^{2-} and CO_3^{2-} are buried well within the interfacial region.^{124,125,138} Additionally, the surface propensity of oxyanions inferred from our HD-VSFG results are in accordance with the predictions from the surface-bulk partitioning model.⁶² As discussed above, the net orientation of interfacial water molecules that is revealed by the sign and the magnitude of the $\text{Im } \chi^{(2)}$ spectra is also concentration-dependent. The net influence of concentration as well as anion identity on the direction and magnitude of the induced electric field are illustrated schematically by a model in Figure 9.3b.

9.2.2 Hofmeister Series and Driving Forces for Oxyanions

As discussed above, the surface propensity of oxyanions at the air/aqueous solution interfaces follows the order of $\text{ClO}_4^- > \text{NO}_3^- > \text{CO}_3^{2-} > \text{SO}_4^{2-}$. Note that this ranking follows an inverse Hofmeister series with the exception of CO_3^{2-} and SO_4^{2-} ions. A reversal of the Hofmeister series ($\text{SO}_4^{2-} < \text{NO}_3^- < \text{I}^-$) regarding anion affinity for the air/water interfaces has been predicted by MD simulations.^{9,25} This indicates that the mechanism that drives ion distributions is unique at the bare air/salt solution interfaces in

comparison to other interfaces involving the presence of macromolecules such as lipids, proteins, or colloids. For instance, the ordering of anions at the air/lipid interface is interpreted as an individual anion's ability to penetrate the headgroup region of the monolayer, thereby disrupting the hydrocarbon packing.²⁷⁹ The interactions of anions and macromolecules in many aqueous interfaces are well explained by the "Law of Matching Water Affinities" proposed by Collins et al.,¹⁹⁸ which suggests that oppositely charged ions exhibit stronger interactions and tend to form contact ion pairs when they are of the same type (chaotropic or kosmotropic). However, this empirical law cannot satisfactorily account and explain all the phenomena at bare air/aqueous interfaces. For example, although Mg^{2+} and SO_4^{2-} ions are both strongly hydrated,^{9,170,280} the amount of ion pairing is generally small (less than 10%) for MgSO_4 , even at high salt concentrations.²⁸⁰ One will then encounter an open question: what is the physical origin of the reversed anion Hofmeister series observed at bare air/aqueous interfaces? A series of potential driving forces and their controlling factors are further discussed below.

As mentioned above, the surface propensity of inorganic ions is believed to be correlated with specific ion properties (or features) such as their size, geometry, polarizability, and charge. Caution is however required when it comes to the interpretation of these results. For instance, by incorporating polarizability into the MD calculations, the finding that the simulated surface propensity of anion could be in accord with experimental evidence only indicates that deficiencies of previous models have been corrected and does not mean that anion enrichment should be primarily determined by their polarizability. Moreover, these ion properties may be related to several different,

even competing forces of solvation, therefore it would be more reasonable to interpret the ion partitioning at bare air/aqueous interfaces on the basis of energy balance between opposing effects rather than simply correlating propensity with specific ion properties. Various forces/energy including dehydration energy, electrostatic energy, cavitation energy, anisotropic solvation, and dispersion forces, among others, have been suggested to be responsible for driving surface propensity of ions, although an estimation of their contribution vary significantly among studies. In the following section, several selected energy/forces are further discussed and then the significance of each specific ion property is compared.

The dominant role of dehydration free energy in deciding anion surface propensity has been postulated.^{72,268,269,281} It has been argued by Cheng et al. that the surface propensity of anions is determined by the competition between ion dehydration energy and nonlocal stabilization energy resulting from the depression of interfacial water permittivity by local ion excesses.⁷² Considering that the concentration dependences of the static permittivities and relaxation time of water in salt solutions are mostly independent of the nature of anions,²⁸² dehydration free energies largely accounts for surface propensity of anions.⁷² This assumption is validated by the oxyanion species studies in the present work. The value of dehydration free energy decreases in the order of ClO_4^- (-214 kJ/mol) > NO_3^- (-306 kJ/mol) > CO_3^{2-} (-479 kJ/mol) > SO_4^{2-} (-1090 kJ/mol),²⁸³ demonstrating the same trend as the surface propensity proposed above. Interestingly, the dehydration free energy of Cl^- and HCO_3^- ions are -347 kJ/mol and -368 kJ/mol, respectively. These value falls between those of NO_3^- and CO_3^{2-} ions, indicating a

weak or even neutral surface propensity for these two ions, respectively, in agreement with previous results.^{9,124,125,138} Archontis and Leontidis found that the solvation free energy of Γ at interface is associated with the ionic polarizability and the reduced cavity accommodating the solute.²⁸¹ Very recently, Arslanargin and Beck further partitioned the absolute hydration free energy at the vapor /water interface into cavity formation, attractive van der Waals, local electrostatic and far-field electrostatic contributions;²⁶⁹ however, a quantitative analysis is not yet available for oxyanions. Similarly, a good correlation of solvation energy with the surface tension of salt solutions was found by Boström et al.²⁷⁰

The key role of electrostatic energy in determining ion's surface propensity has long been recognized even though it does not provide a complete picture. Electrostatic forces (image charge repulsion) are described within the model of a charged sphere in a dielectric continuum. Note that several critical effects such as difference between anion versus cation solvation, polarization and dispersion effects, and solvation entropy effects are not well characterized in such a model.⁹ Electrostatic forces are intimately related to the image charge which is proportional to the charge of ion; therefore, charge could be used as a simplified factor to estimate electrostatic forces. In other words, electrostatic interactions of divalent ions i.e. SO_4^{2-} ions, favor bulk solvation and are generally stronger than monovalent ions (the small F^- ion may be an exception).^{9,56,77}

Recently, it was argued by Levin that ion surface propensity could be a consequence of the competition between attractive cavitation and repulsive electrostatic energies.²⁴⁶ Hence, for small and strongly hydrated (i.e. weakly polarizable) ions, the

electrostatic penalty of approaching the interface is larger than the cavitation energy, thus favoring bulk solvation. In contrast, for large and weakly hydrated (i.e. polarizable) ions, the small electrostatic penalty of exposing ionic charge to the low dielectric environment is largely compensated by the cavitation energy, hence favoring surface solvation. The cavitation energy which drives ions towards the interface is germane to the size of ions. For small cavities with radius less than 4 Å, the energy cost increases proportionately to their volume, while for larger cavities the energy cost scales with cavity surface area. Although the values given in the literature vary to some extent,^{165,284} the ionic radii of the oxyanions studied herein are all less than 4 Å, indicating that their cavitation energy could be compared based on their respective volume.

Anisotropic (asymmetric) solvation has also been suggested to be a one of the major driving force for the interfacial activity of polarizable anions.⁹ For instance, asymmetric solvation in water clusters was predicted for soft inorganic ions such as chloride,^{285,286} nitrate^{64,74} and azide.²⁸⁷ Recently, Wick and Xantheas investigated the anisotropic solvation of Cl⁻ and I⁻ ions at the interface and in the bulk using MD simulations.²⁷⁶ They observed a qualitatively similar first solvation shell structure at the interface and in the bulk. The solvation structure of the more polarizable I⁻ anion was found to be more anisotropic than Cl⁻ at both the interface and in the bulk. It was found that the anisotropy of solvation structure is correlated with polarizability, but shows an inverse correlation with anion size. They further proposed that the extinction of somewhat hydrophobic cavity in the bulk is a driving force for anion interfacial activity. To the author's best knowledge, no similar work has been carried out to investigate the

anisotropic solvation structure of the oxyanions at the air/aqueous interface. In addition to anisotropic solvation, the importance of a closely related driving force, hydrophobic solvation, in the ion adsorption to the air/water interface has been proposed by Horinek et al.²⁷⁵ They argued that hydrophobic solvation could largely account for the interfacial ion behavior (as exemplified by the enhancement of I⁻ ions), and found that ion repulsion from the interface decreases with increasing ion size. Indeed, this argument may overestimate the contribution of this force; however, the overall role of anisotropic (hydrophobic) solvation needs to be taken into account in future theoretical predictions.

Dispersion forces are believed to be critical in determining ion specificity at air/aqueous interface. Ninham and co-workers pointed out that the inclusion of dispersion forces is of key importance to systems with high salt concentrations where these forces can be expected to govern the specific ion effects, while electrostatics become dominant at low salt concentrations.^{272,288} Ionic dispersion forces could be generally decomposed into ion-solvent, ion-ion and ion-interface interactions, and largely depend on ion polarizabilities and size.^{211,289} Inclusion of dispersion forces explained well the Hofmeister effects of spherical halide ions; however, agreement between theory and experiment seems to break down when the theory is applied to polyatomic ions such as nitrates and perchlorates.^{211,273} As suggested already, this is an indication that a consideration of geometry (shape) effect is indispensable for the advancement of theoretical calculations. Noticeably, an opposing suggestion also emerged recently, arguing that dispersion forces do not play a significant role in determining the surface tension or the Hofmeister series of electrolyte solutions.¹⁶⁵ These contradictory

calculations results obviously call for further validation.

Interfacial flexibility of aqueous interfaces, despite its intrinsic importance, has drawn limited attention in early theoretical approaches regarding their role in shaping ion's interfacial distributions.²⁷⁸ Until recently, Noah-Vanhouche and Geissler incorporated this neglected factor into their MD study and predicted that ion distribution in the interfaces may originate from a competition between strong opposing forces, primarily due to hydrophobic forces (volume exclusion) and dielectric polarization. At vapor/aqueous interface, the fluctuations of the electric field and electrostatic potential that ion experiences attenuate much more gradually than for a quiescent planar interface. Meanwhile, interfacial flexibility also affects the entropic benefits by expelling a volume-excluding ion in the opposite direction.²⁶² They demonstrated that the collective responses that determine solvation free energy would resolve very differently in the non-uniform environments than in bulk. It is commonly assumed that ion behavior at the air/water interface is a net effect of competition between electrostatic forces and hydrophobic forces, and a positive adsorption enthalpy associated with electrostatic forces and a positive adsorption entropy associated with hydrophobic forces.²⁶⁸ Later, Otten et al. determined that the adsorption enthalpy and entropy changes of aqueous thiocyanate ion from bulk solution to the liquid/vapor interface are both negative.²⁶⁸ They further highlighted the influence of nonlocal response of interfacial shape fluctuations on adsorption entropy. They also proposed that the position of an ion in the Hofmeister series could be determined by a combination of driving forces associated with the pinning of capillary wave and with a competition between ion hydration energy and the neat

liquid's surface tension. However, such a predictive calculation accounting for capillary wave fluctuations has not yet been established for oxyanions.

Based on above discussion, although the adopted energy/forces vary significantly in different models, it is indicative that the ion distributions at air/salt solution interfaces is driven by the collective contributions of a combination of forces, rather than one or more specific ionic features. Otten et al. has suggested that there might be other means of determining the ion Hofmeister series, such as a combination of driving forces associated with the pinning of capillary wave and with a competition between ion hydration energy and the neat liquid's surface tension. Of course, this prediction need to be further validated for oxyanions, particularly the determination of hydration energy.

9.2.3 Examination of Specific Ion Properties

It has been mentioned above that the surface propensity of ions, particular halide ions, has been correlated with specific ion properties, such as size and polarizability.^{9,27,31,62} To verify the role of these ion properties in determining the interfacial distribution of oxyanions, the value of these factors is further compared. Considering that the oxyanions studied herein are non-spherical and some of them are divalent ions, hence a comparison of their geometry and charge/surface charge density is also necessary.

Polarizability has been suggested to be importance key factor for the surface propensity of anions.^{9,169} For example, Jungwirth and Tobias found that the varying surface propensity of halide ions is largely due to ion polarizability although ion size appears to be critical as well.^{27,31} Their results showed that the larger more polarizable I

ion demonstrates a stronger surface propensity while the smaller less polarizable F^- ion is repelled from the interface. In contrast, Dang suggested that the interactions between the anions and the bare air/aqueous interface are mainly caused by differences in the ion polarizability rather than ion size.²⁰⁷ In fact, there is also some indication that inclusion of the solvent (water) polarizability is also crucial for theoretical calculation.^{27,58} In addition to halide ions, different treatments of the NO_3^- ion polarizability in the polarizable MD simulations also lead to apparent contradictory results regarding surface propensity.^{64,65} Moreover, upon examining the interfacial distribution of CO_3^{2-} ions, Mason et al. suggested that the polarizability indeed exerts a significant impact and needs to be taken into account in simulations of aqueous electrolytes, in particular when multivalent ions are present.²⁶⁵ However, a question regarding whether ion polarizability is the most importance ion property for determining oxyanions' surface propensity has not yet been answered. According to Pyper et al., the value of polarizability decreases in the order $SO_4^{2-} > ClO_4^- > CO_3^{2-} > NO_3^-$,²⁹⁰ while Parsons and Ninham adopted a similar ranking except for a reversal of CO_3^{2-} and ClO_4^- .²⁹¹ Although ion polarizability values given in the literature vary to some extent, the overall trend that SO_4^{2-} has the largest value while NO_3^- exhibits the smallest one remains unchanged. It is clear that the polarizability of oxyanions depicts a very different trend compared to the surface propensity proposed above, which follows the order of $ClO_4^- > NO_3^- > CO_3^{2-} > SO_4^{2-}$. Therefore, one can expect that there are other dominating ion properties in addition to polarizability accounting for the interfacial distribution of oxyanions.

The critical role of ion size in driving surface propensity has been highlighted in a

growing body of evidence.^{27,31,84,246,263} For instance, Mucha et al. have shown that surface propensity of halide ions for the air/aqueous interface is primarily correlated with ion size.³¹ The simulation results of Eggimann and Siepmann also indicated that ion size plays an importance role in driving monovalent inorganic ions to the surface.²⁶³ Moreover, the cavitation energy discussed above is intimately related to the ion size.²⁴⁶ To explore the impact of ion size of oxyanions on their interfacial distribution, their respective hydrated ionic radius is then compared. The value of hydrated ionic radius decreases in the order of SO_4^{2-} (2.78 Å) > ClO_4^- (2.69 Å) > CO_3^{2-} (2.54 Å) > NO_3^- (2.23 Å).²⁸⁴ Despite that the value and trend differ to some extent compared to the ones given by Nightingale and dos Santos et al.,^{165,292} the radius of hydrated ClO_4^- ion is always smaller than that of SO_4^{2-} ion, thus opposing the trend of surface propensity. As a result, one could propose that the surface propensity of oxyanions cannot be explained only based on ionic size or polarizability but that other factors must come to play. This postulate is consistent with the one made from simulations on alkali and halide ions;²⁶⁷ however, such an analysis for oxyanions is still very limited.

Along with ion polarizability and size, the charge effect (or surface charge density) and the associated electrostatic penalty is found to be of paramount importance in governing surface propensity of ions. For small water droplets, it has been shown that surface charge density is the most important ion property that determines the surface activity of a monoatomic ion.²⁹³ It has also been demonstrated that the surface charge density exerts a significant impact on the Hofmeister effects.^{211,294} By comparison of a series of sodium salts, Tarbuck and Richmond found that anions with greater charge

affect the hydrogen-bonding region of VSFG spectra to a greater extent.⁸⁴ Moreover, the simulations results indicate that CO_3^{2-} ions have strong polarizing effects on surrounding water molecules.²⁶⁵ This is in accordance with the results obtained from the present work that, at a constant anion concentration (1 M), divalent anions perturb interfacial water organization to a greater extent. Despite the fact that SO_4^{2-} and CO_3^{2-} ions are large and polarizable (comparable with I^- and Br^- ions),^{284,290} both of them are suggested to have very weak surface preference.^{56,57,59,70,84,124,125} Although it may be oversimplified, this can be rationalized by having the strong bulk-driving electrostatic forces induced by the high charge density overwhelming the surface-favoring forces, probably a combination of polarization interactions and cavitation energy.

Last but not least, owing to the fact that all the oxyanions studied here are non-spherical, this provides an opportunity to further explore the impact of ionic geometry on anion surface propensity. It has been suggested that the geometry (electronic distribution) of ions exerts a substantial impact on their surface propensity;⁸⁴ however, whether it could play a dominant role is so far not known. As already discussed in the previous section, ClO_4^- and NO_3^- exhibit surface enhancement while SO_4^{2-} and CO_3^{2-} show very weak surface propensity. Note that although ClO_4^- and SO_4^{2-} ions both have tetrahedral structure, these two anions show opposing surface preference. Similarly, two planar oxyanions, NO_3^- and CO_3^{2-} ions also display very different distributions in the interfacial region. Recall that the anisotropic solvation has been predicted to be a major factor driving surface propensity of spherical Cl^- and I^- ions.²⁷⁶ It is thus highly possible that these large non-spherical oxyanions may induce an equivalent or even more pronounced

anisotropy in the interfacial solvation structure due to their intrinsic unique geometry. Moreover, it is likely that the non-spherical ClO_4^- and NO_3^- ions may interact with the non-flat surface of aqueous salt solution and further complicates the picture. In addition, the asymmetric geometry of the oxyanions studied in the present work may result in an uneven distribution of charge on their hydration shells, which further gives rise to intricate scenarios. Upon examination of our results, it is apparent that geometry cannot serve as a simple indicator to predict the surface propensity of oxyanions; however, this specific ion property does contribute substantially to the overall determination of interfacial anion distributions.

The discussion above shows clearly that qualitative and quantitative errors could occur when attempting to interpret the surface preference of oxyanions simply based on one or more ion properties, prompting a paradigm shift in chemistry away from such simplifications. However, in comparison to other ion properties charge effects seem to exert a greater impact on the distributions of polyatomic ions, that is, oxyanions with higher charge/surface charge density reside deeper in the interfacial region while the ones exhibiting lower charge/surface charge density approach closer to the surface. Owing to the non-spherical geometry of oxyanions, a precise calculation of their hydration size and hence a corresponding surface charge density becomes difficult. Additionally, as shown by Noah-Vanhoucke and Geissler for small ions, strong surface enhancement can be accentuated or suppressed by modest changes in either solutes' size or charge. Therefore, the results of theoretical predictions may be highly sensitive to the parameters adopted in the calculation, which call for special caution.

9.3 Conclusions

From the HD-VSFG data, it is evident that oxyanions play a crucial role for the ion distributions at the air/aqueous interface of sodium salt solutions, and in the perturbation of the interfacial water network. Perchlorate and nitrates ions reside preferentially above their counter cations. This was inferred from the directly determined net transition dipole orientation of interfacial water molecules with their hydrogen atoms pointing on average more towards the surface relative to neat water. Similarly, the enhanced negative magnitudes of $\text{Im } \chi^{(2)}$ spectra of sulfate and carbonate salt solutions indicate that these anions are buried well below sodium ions in the interfacial region. Moreover, sodium salts perturb the interfacial water network to different extents depending on the identity of the oxyanion. Chemical identity and concentration lead to a change of the sign of the $\text{Im } \chi^{(2)}$ spectra, that is, the reversal of the direction of the net interfacial electric field. A tentative surface propensity sequence is given, following the order of $\text{ClO}_4^- > \text{NO}_3^- > \text{CO}_3^{2-} > \text{SO}_4^{2-}$, which follows an inverse Hofmeister series with the exception of CO_3^{2-} and SO_4^{2-} ions. The existence of these oxyanions at the interface may have potentially important implications for atmospheric and oceanic chemistry and thundercloud electrification as discussed in previous chapters.

To my knowledge, the work presented in this dissertation is the first systematic demonstration of the polyatomic anion effect employed by conventional VSFG and HD-VSFG spectroscopy. A series of energy/forces, including dehydration energy, electrostatic energy, cavitation energy, anisotropic solvation, and dispersion forces, as well as interfacial flexibility, has been discussed to analyze their potential contributions

to oxyanion interfacial solvation. The proposed order of oxyanions' surface propensity agrees well with their dehydration free energy and with predictions from the current surface-bulk partitioning model. To this end, further theoretical exploration would be helpful to decipher the microscopic picture of how oxyanions and their accompanying counter cations are distributed in the interface and to determine which energy/forces substantially drive interfacial solvation of oxyanions. An advanced generic model that could successfully elucidate surface propensity for all anions, in particular polyatomic anions, is pressingly needed. We hope that the present contribution will stimulate further theoretical work in this direction.

Also shown here, specific ion properties, such as polarizability and size, which successfully explained the relative surface propensity of halide ions, cannot solely account for the interfacial distribution of oxyanions. Two other ion properties, charge (surface charge density) and geometry (shape), were also examined. Although all these properties are partially responsible for determining interfacial ion distributions, charge (or surface charge density) affects the collective response of all involved factors to a greater extent compared to the others. An accurate quantification of these ion properties is of critical importance for simulations since their results could be highly sensitive to the values of these parameters. Future HD-VSFG work on non-spherical and/or polyvalent anions would help further assessing the influence of ion properties, in particular charge, in governing ion interfacial behavior.

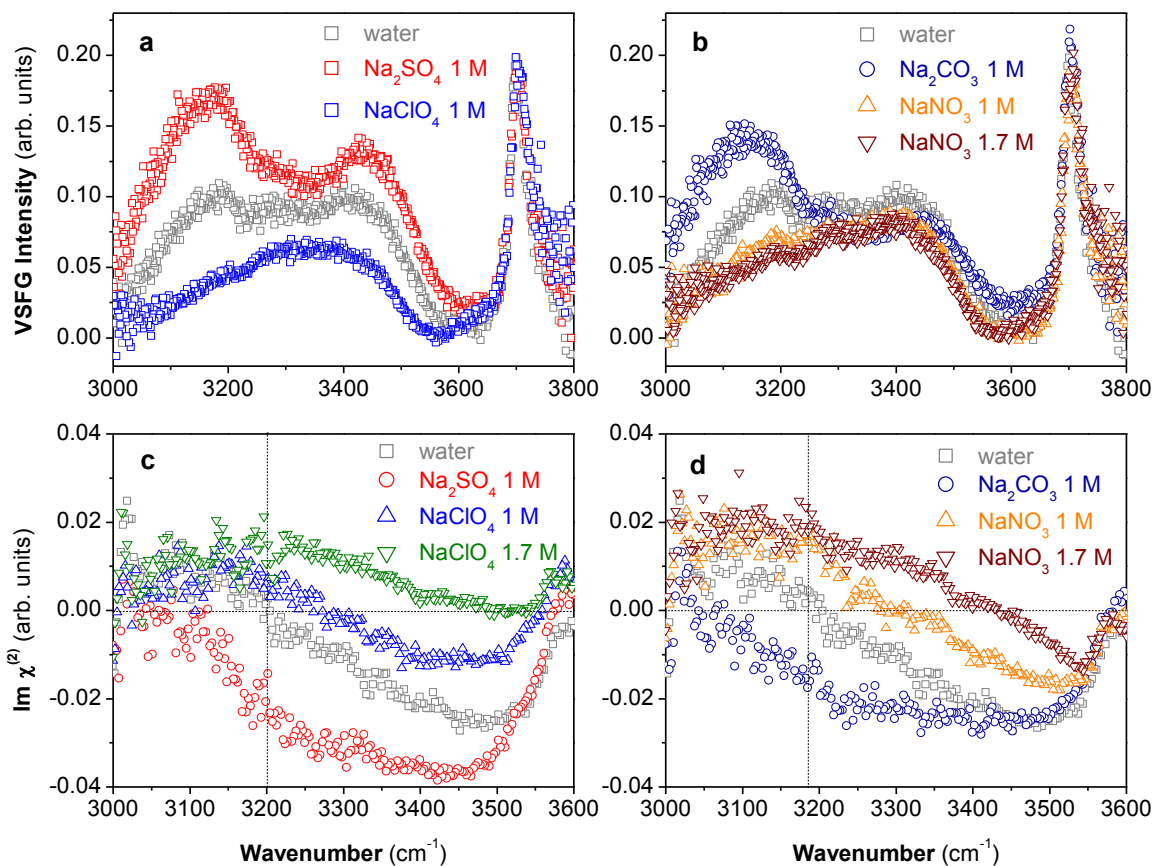


Figure 9.1 Conventional VSGF $|\chi_{\text{eff}}^{(2)}|^2$ spectra of air/aqueous interfaces of (a) 1 M Na₂SO₄ and 1 M NaClO₄, (b) 1 M Na₂CO₃, and 1 M and 1.7 M NaNO₃ salts solutions over the entire OH stretching region (3000–3800 cm⁻¹); HD-VSGF Im χ⁽²⁾ spectra of air/aqueous interfaces of (c) 1 M Na₂SO₄, and 1 M and 1.7 M NaClO₄, (d) 1 M Na₂CO₃, and 1 M and 1.7 M NaNO₃ salt solutions. Neat water spectrum is shown as a reference.

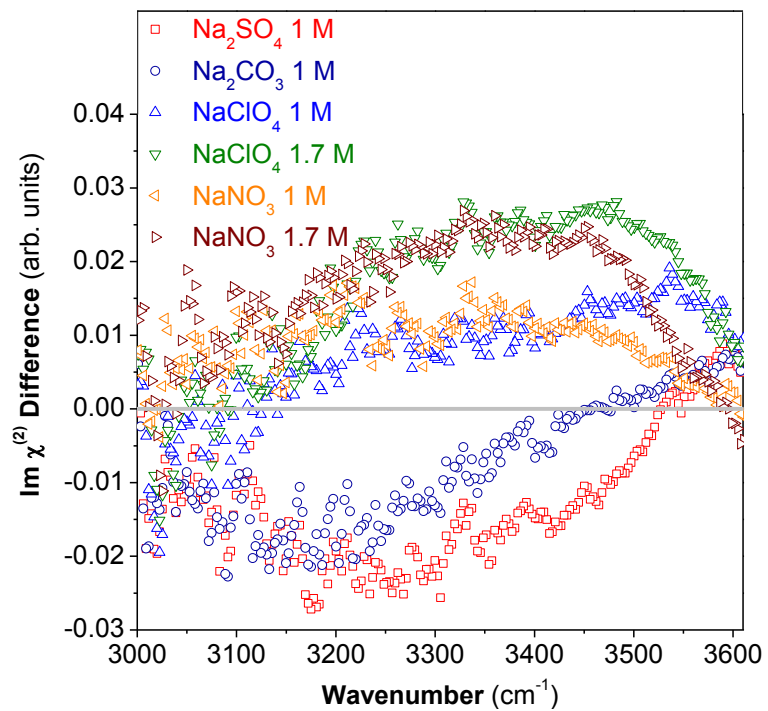


Figure 9.2 HD-VSFG $\text{Im } \chi^{(2)}$ difference spectra ($\text{Im } \chi^{(2)}$ salt spectrum minus $\text{Im } \chi^{(2)}$ water spectrum) for the indicated salts. Neat water spectrum is shown as a reference (zero line).

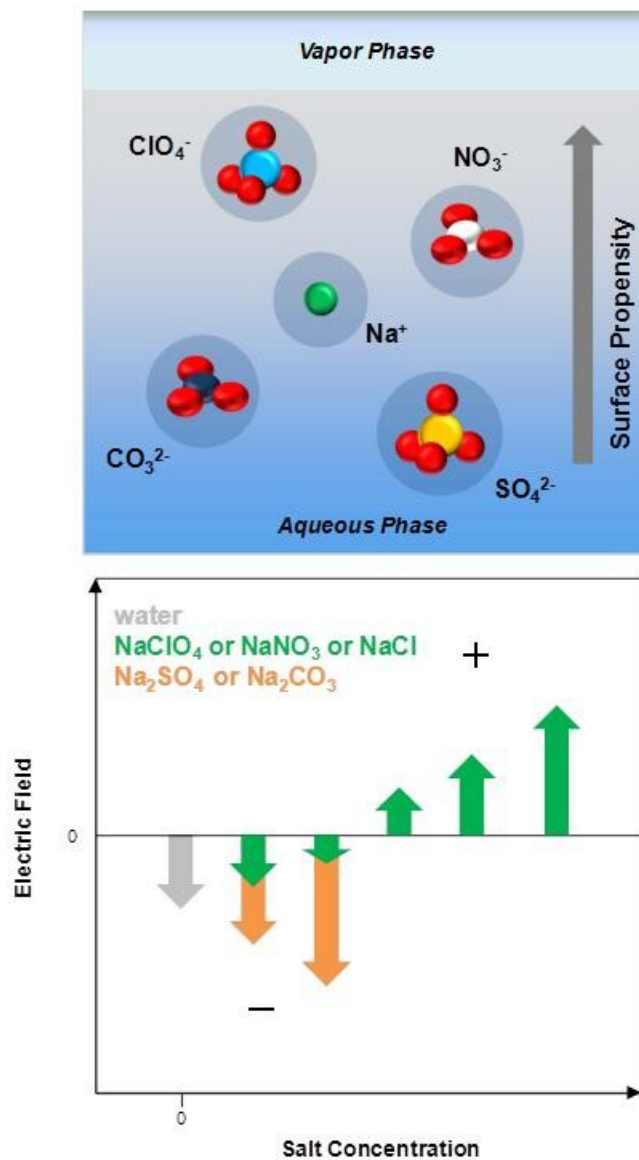


Figure 9.3 (a) Illustration of the relative location for oxyanions ($\text{ClO}_4^- > \text{NO}_3^- > \text{CO}_3^{2-} > \text{SO}_4^{2-}$) and its counter Na^+ ions at the air/aqueous interfaces. (b) Diagram qualitatively demonstrating the salt concentration dependence of the magnitude and direction of the overall electric field.

Chapter 10 Implications and Future Work

10.1 Implications

The work presented in this dissertation was motivated by the growing interest for the understanding of the molecular organization and interaction at environmental and atmospheric relevant interfaces. Interfacial water organization and inferred ion distributions obtained from this work could shed light on atmospheric aerosol chemistry,⁶⁻¹¹ in addition to ice/snowpack chemistry,¹²⁻¹⁵ thundercloud electrification,¹⁶ geochemistry,¹⁷⁻²¹ and ocean surface processes,²² among others. In this chapter, several examples will be given to illustrate these environmental and/or atmospheric implications.

The results regarding interfacial distributions of CO_3^{2-} and HCO_3^- ions have implications for atmospheric aerosol and ocean surface chemistry. Aqueous phase aerosols and the ocean's surface absorb atmospheric gaseous CO_2 and given its solubility into water, carbonate concentrations of 1 to 10 μM and bicarbonate concentrations of 0.4 to 1.6 mM (calculated temperature range of 0 to 25 °C) currently exist¹⁴² as calculated for the pH of sea water (7.75 to 8.2).⁵² Given the increasing concentration of CO_2 in the atmosphere, interfacial residence and chemistry of atmospheric aerosol and ocean surface water is important in considering the reactivity and uptake by these aqueous surfaces. Here we have shown that carbonate creates an increase in the interfacial thickness and generates a subsurface electric field by maintaining a charge separation between Na^+ and

the less surface active carbonate. In contrast, bicarbonate and its Na^+ counter cation, intercalate in the dynamic matrix of the hydrogen bonding network within the first few layers of the water surface. Although beyond the scope of this work, it is likely that the charge separation induced by carbonate will be maintained by sodium and carbonate ions even in the presence of bicarbonate. This suggests that the surface of aerosol and of the ocean will be impacted by changing ratios of carbonate to bicarbonate as atmospheric CO_2 concentrations continue to increase.

The existence of nitrate and chloride ions in the interfacial regions proposed by this work has implications for atmospheric chemistry. Nitrate ions are commonly found in atmospheric aerosols, sea ice, and snowpacks through heterogeneous reactions and direct deposition.^{6,41-44} It is evident that both the kinetics and mechanisms of interfacial reactions are different from those in the isotropic bulk phase.²⁻⁵ Hence, the indirect experimental evidence of the presence of NO_3^- and Cl^- ions within the air/aqueous solution interfaces inferred from our HD-VSFG results may provide more insight for atmospheric chemistry. For instance, it may help to understand the currently underestimated photolysis rates of NO_3^- ions in the polar snowpack in the absence of bromide and chloride ions.^{13,295} This enhanced photochemistry, the production of NO_x and OH radicals and the generation of gas-phase halogens through photolysis in the presence of bromide and/or chloride ions, may influence the oxidizing capacity of the atmosphere and atmospheric aerosols aging.

The surface propensity of SO_4^{2-} , NO_3^- and Cl^- ions and their counter cations may also shed some light on charge transfer in thundercloud electrification processes.

Thunderclouds are electrified when charge is transferred between small and large ice particles colliding in a cloud that contains strong updrafts. The small ice particles rise with positive charge and the large ice particles (graupels) fall and carry with them downward the negative charge, or vice versa in some rare conditions (e.g. smoke rich in NO_3^- and Cl^- ions), so that normally lightning lowers negative charge from cloud to the ground. It is found in a large range of observations that the enhanced positive lightning is associated with smoke, rich in nitrates and chlorides, yet the origin of this phenomenon is not fully understood.¹⁶ The findings presented here on the ion distributions and the presence of NO_3^- and Cl^- ions in the interface may help provide a physical explanation for the enhanced positive lightning, the net transfer of positive charge from the cloud to the ground. For instance, NO_3^- and Cl^- ions residing closer to the surface of the larger falling ice particles in thunderclouds could be preferentially transferred to the surface of the quasi-liquid layer of the small rising ice crystals during collisions between ice crystals and graupels, resulting in the positive charging of the falling graupels (Figure 10.1a). Considering that under normal conditions sulfate ions are more dominant in aerosols and cloud droplets, the negative lightning could be rationalized by having their counter cations being preferentially transferred to the surface of the quasi-liquid layer of the small rising ice crystals (Figure 10.1b).

Moreover, the ion distributions proposed in this dissertation may serve as a step toward better understanding the mechanism of water evaporation and the impact of ions on the evaporation rate. It was shown that the presence of ClO_4^- ions affects the evaporation kinetics at the air/aqueous interface of concentrated NaClO_4 solutions.⁵⁵ It is

found that atmospherically relevant solutes (ammonium sulfate, sodium chloride) have minimal effects on the evaporation kinetics of water,²⁹⁶ while 25% smaller evaporation rates were determined in concentrated (4 M) sodium perchlorate surface layers. This serves as an indication that direct interactions between surface-active perchlorate ions and evaporating water molecules are affecting the evaporation kinetics. However, the molecular mechanism relating to anion-water interactions and evaporation rate is not well understood to date.⁵⁵ It was predicted by Saykally and co-workers that the reduced evaporation rate in the presence of NaClO₄ may be related to the suppression of water surface fluctuations (or capillary waves) in the presence perchlorate ions.²⁹⁷ Other theorists have recently proposed that it might be caused by the change in the number and strength of water hydrogen bonds in the presence of surface-active ions.²⁹⁸

The distributions of hydronium (H₃O⁺) ions and their counter anions (e.g. sulfate, bisulfate and bicarbonate) may be important for the formation of secondary sulfate and potentially in the aging (growth) of atmospheric organic aerosols. The surface prevalence of hydronium ions has been suggested by previous studies.^{81-83,93,296} First, in the presence of water, SO₂ and CO₂ can easily undergoes chemical transformation and be converted into HSO₃⁻ and HCO₃⁻ and generate hydronium ions; HSO₃⁻ could be further oxidized by atmospheric oxidants such as hydrogen peroxides into HSO₄⁻ and SO₄²⁻ ions. Second, with the increase of hydronium ions derived from the above reactions, organic compounds could be effectively oxidized by hydrogen peroxides into water-soluble organic compounds (WSOC) via acid-catalyzed heterogeneous reactions.^{299,300} In this step, the surface prevalence of hydronium ions are of great importance, while the bulk-

favoring nature of SO_4^{2-} ion demonstrated in this dissertation may also play a role in prompting the SO_2 absorption reactions moving forward. Third, the formation of WSOC will increase the hygroscopicity of aerosols which, in turn, results in an increase of SO_2 oxidation by increasing the aqueous phase.³⁰¹ Although the reaction pathway proposed above is somewhat speculative, it still indicates that the knowledge of ion distributions may facilitate a better understanding of atmospheric aerosol chemistry and may need to be considered in current atmospheric models.

10.2 Future Work

The work presented in this dissertation covers a variety of environmentally and atmospherically relevant inorganic ions; however, in the real systems, the compositions of the aqueous phase are much more complicated, and the temperature and pH values may vary to different extent. It would be beneficial to mimic more sophisticated real environmental conditions in future work.

It has been suggested that the interfacial water organization and ion concentration in real aqueous phase will change dramatically by varying temperature.^{100,302,303} For instance, it is found that the interfacial water organization exhibits a substantial temperature dependency.¹⁰⁰ Also a significant enhancement in the adsorption of SO_2 to the water surface occurs when cooling the formaldehyde solution to an atmospherically relevant temperature.³⁰³ In addition, the impact of hydronium ions exert on the interfacial water organization has been investigated,^{81-83,93,296} however, in more complicated real systems, how the varying of pH value influences the net interfacial water organization and ion distributions and their potential significance for environmental chemistry is not

still not well known. Hence, the study of temperature and pH effects could be helpful to understand real environmental systems.

In addition to explore inorganic mixture systems, the role of organic components needs to be addressed as well. For instance, in marine aerosols, sea salts and organic compounds are the main components, with organics being the more abundant constituent. The concentration and composition of organic components plays an important role in determining the morphological, optical, and chemical properties of the aerosols which may further affects the aerosol's ability to act as a cloud condensation nuclei or its efficiency at scattering light.^{36,304} Although surface organics (organic coating) mostly acts as a barrier between the aerosol and its surrounding environment, they may facilitate uptake via cooperative interactions with absorbing compounds.³⁰³ To reflect the chemistry that occurs in real environment, the presence and role of different organics need to be taken into account in future work.

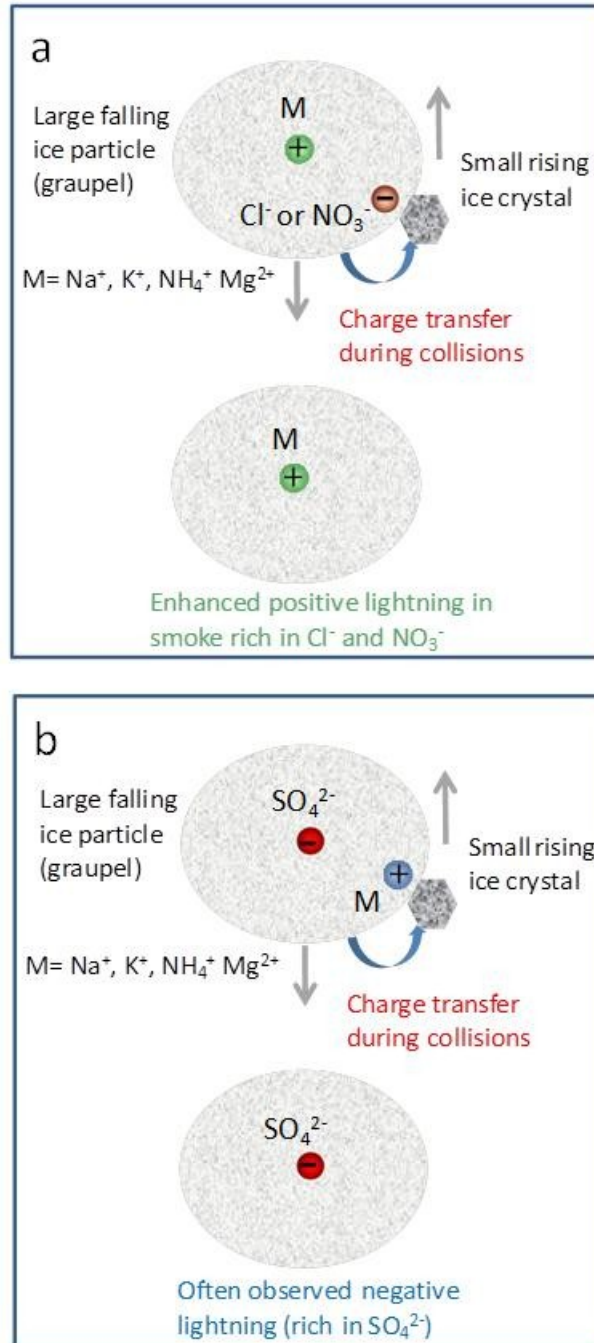


Figure 10.1 Illustration of the molecular-level charge transfer mechanism in thundercloud electrification. (a) Smoke rich in NO₃⁻ and Cl⁻ ions results in enhanced positive lightning. (b) Negative lightning under normal conditions.

References

- (1) Jamtveit, B.; Meakin, P., Eds. *Growth, Dissolution and Pattern Formation in Geosystems*; Kluwer Academic: Boston, 1999.
- (2) Knipping, E. M.; Lakin, M. J.; Foster, K. L.; Jungwirth, P.; Tobias, D. J.; Gerber, R. B.; Dabdub, D.; Finlayson-Pitts, B. J. *Science* **2000**, *288*, 301.
- (3) Hunt, S. W.; Roeselova, M.; Wang, W.; Wingen, L. M.; Knipping, E. M.; Tobias, D. J.; Dabdub, D.; Finlayson-Pitts, B. J. *J. Phys. Chem. A* **2004**, *108*, 11559.
- (4) Hanson, D. R.; Ravishankara, A. R. *J. Phys. Chem.* **1994**, *98*, 5728.
- (5) Nissenon, P.; Knox, C. J. H.; Finlayson-Pitts, B. J.; Phillips, L. F.; Dabdub, D. *Phys. Chem. Chem. Phys.* **2006**, *8*, 4700.
- (6) Finlayson-Pitts, B. J.; Pitts Jr., J. N. *Chemistry of the Upper and Lower Atmosphere: Theory, Experiments and Applications*; Academic Press: San Diego, CA, 2000.
- (7) Finlayson-Pitts, B. J. *Chem. Rev.* **2003**, *103*, 4801.
- (8) Gopalakrishnan, S.; Liu, D. F.; Allen, H. C.; Kuo, M.; Shultz, M. J. *Chem. Rev.* **2006**, *106*, 1155.
- (9) Jungwirth, P.; Tobias, D. J. *Chem. Rev.* **2006**, *106*, 1259.
- (10) Jungwirth, P.; Winter, B. *Annu. Rev. Phys. Chem.* **2008**, *59*, 343.
- (11) Tobias, D. J.; Stern, A. C.; Baer, M. D.; Levin, Y.; Mundy, C. J. *Annu. Rev. Phys. Chem.* **2013**, *64*, 339.

- (12) Finlayson-Pitts, B. J.; Wingen, L. M.; Sumner, A. L.; Syomin, D.; Ramazan, K. A. *Phys. Chem. Chem. Phys.* **2003**, *5*, 223.
- (13) Richards, N. K.; Wingen, L. M.; Callahan, K. M.; Nishino, N.; Kleinman, M. T.; Tobias, D. J.; Finlayson-Pitts, B. J. *J. Phys. Chem. A* **2011**, *115*, 5810.
- (14) Boxe, C. S.; Colussi, A. J.; Hoffmann, M. R.; Perez, I. M.; Murphy, J. G.; Cohen, R. C. *J. Phys. Chem. A* **2006**, *110*, 3578.
- (15) Dominé, F.; Shepson, P. B. *Science* **2002**, *297*, 1506.
- (16) Jungwirth, P.; Rosenfeld, D.; Buch, V. *Atmos. Res.* **2005**, *76*, 190.
- (17) Zhang, L.; Tian, C. S.; Waychunas, G. A.; Shen, Y. R. *J. Am. Chem. Soc.* **2008**, *130*, 7686.
- (18) Jubb, A. M.; Allen, H. C. *J. Phys. Chem. C* **2012**, *116*, 9085.
- (19) Brown, G. E.; Parks, G. A. *Int. Geol. Rev.* **2001**, *43*, 963.
- (20) Michot, L. J.; Villiéras, F.; François, M.; Bihannic, I.; Pelletier, M.; Cases, J. M. C. *R. Geosci.* **2002**, *334*, 611.
- (21) Schrödle, S.; Richmond, G. L. *J. Phys. D: Appl. Phys.* **2008**, *41*, 033001/1.
- (22) Laß, K.; Kleber, J.; Friedrichs, G. *Limnol. Oceanogr. Meth.* **2010**, *8*, 216.
- (23) Onsager, L.; Samaras, N. N. T. *J. Chem. Phys.* **1934**, *2*, 528.
- (24) Wagner, C. *Phys. Z.* **1924**, *25*, 474.
- (25) Tobias, D. J.; Hemminger, J. C. *Science* **2008**, *319*, 1197.

- (26) Gibbs, J. W. *The Collected Works of J. Willard Gibbs*; Longmans: New York, 1928; Vol. 1.
- (27) Jungwirth, P.; Tobias, D. J. *J. Phys. Chem. B* **2001**, *105*, 10468.
- (28) Bian, H.-t.; Feng, R.-r.; Xu, Y.-y.; Guo, Y.; Wang, H.-f. *Phys. Chem. Chem. Phys.* **2008**, *10*, 4920.
- (29) Ji, N.; Ostroverkhov, V.; Tian, C. S.; Shen, Y. R. *Phys. Rev. Lett.* **2008**, *100*, 096102.
- (30) Liu, D.; Ma, G.; Levering, L. M.; Allen, H. C. *J. Phys. Chem. B* **2004**, *108*, 2252.
- (31) Mucha, M.; Frigato, T.; Levering, L. M.; Allen, H. C.; Tobias, D. J.; Dang, L. X.; Jungwirth, P. *J. Phys. Chem. B* **2005**, *109*, 7617.
- (32) Raymond, E. A.; Richmond, G. L. *J. Phys. Chem. B* **2004**, *108*, 5051.
- (33) Salcedo, D.; Onasch, T. B.; Dzepina, K.; Canagaratna, M. R.; Zhang, Q.; Huffman, J. A.; DeCarlo, P. F.; Jayne, J. T.; Mortimer, P.; Worsnop, D. R.; Kolb, C. E.; Johnson, K. S.; Zuberi, B.; Marr, L. C.; Volkamer, R.; Molina, L. T.; Molina, M. J.; Cardenas, B.; Bernabe, R. M.; Marquez, C.; Gaffney, J. S.; Marley, N. A.; Laskin, A.; Shutthanandan, V.; Xie, Y.; Brune, W.; Leshner, R.; Shirley, T.; Jimenez, J. L. *Atmos. Chem. Phys.* **2006**, *6*, 925.
- (34) Keene, W. C.; Sander, R.; Pszenny, A. A. P.; Vogt, R.; Crutzen, P. J.; Galloway, J. N. *J. Aerosol Sci.* **1998**, *29*, 339.
- (35) Seinfeld, J. H.; Pandis, S. N. *Atmospheric Chemistry and Physics: From Air Pollution to Climate Change*; John Wiley & Sons: New York, 1998.
- (36) Andreae, M. O.; Crutzen, P. J. *Science* **1997**, *276*, 1052.
- (37) Fahey, D. W.; Kawa, S. R.; Woodbridge, E. L.; Tin, P.; Wilson, J. C.; Jonsson, H. H.; Dye, J. E.; Baumgardner, D.; Borrmann, S.; Toohey, D. W.; Avallone, L. M.; Proffitt,

M. H.; Margitan, J.; Loewenstein, M.; Podolske, J. R.; Salawitch, R. J.; Wofsy, S. C.; Ko, M. K. W.; Anderson, D. E.; Schoeberl, M. R.; Chan, K. R. *Nature* **1993**, *363*, 509.

(38) Hu, J. H.; Abbatt, J. P. D. *J. Phys. Chem. A* **1997**, *101*, 871.

(39) Robinson, G. N.; Worsnop, D. R.; Jayne, J. T.; Kolb, C. E.; Davidovits, P. J. *Geophys. Res.-Atmos.* **1997**, *102*, 3583.

(40) Roberts, J. M.; Osthoff, H. D.; Brown, S. S.; Ravishankara, A. R. *Science* **2008**, *321*, 1059.

(41) Boxe, C. S.; Colussi, A. J.; Hoffmann, M. R.; Murphy, J. G.; Wooldridge, P. J.; Bertram, T. H.; Cohen, R. C. *J. Phys. Chem. A* **2005**, *109*, 8520.

(42) Gard, E. E.; Kleeman, M. J.; Gross, D. S.; Hughes, L. S.; Allen, J. O.; Morrical, B. D.; Fergenson, D. P.; Dienes, T.; Galli, M. E.; Johnson, R. J.; Cass, G. R.; Prather, K. A. *Science* **1998**, *279*, 1184.

(43) Honrath, R. E.; Peterson, M. C.; Guo, S.; Dibb, J. E.; Shepson, P. B.; Campbell, B. *Geophys. Res. Lett.* **1999**, *26*, 695.

(44) Logan, J. A. *J. Geophys. Res.-Oc. Atm.* **1983**, *88*, 785.

(45) Finlayson-Pitts, B. J.; Hemminger, J. C. *J. Phys. Chem. A* **2000**, *104*, 11463.

(46) Gibson, E. R.; Hudson, P. K.; Grassian, V. H. *J. Phys. Chem. A* **2006**, *110*, 11785.

(47) Charlson, R. J.; Schwartz, S. E.; Hales, J. M.; Cess, R. D.; Coakley, J. A.; Hansen, J. E.; Hofmann, D. J. *Science* **1992**, *255*, 423.

(48) Soli, A. L.; Byrne, R. H. *Mar. Chem.* **2002**, *78*, 65.

(49) Millero, F. J.; Pierrot, D.; Lee, K.; Wanninkhof, R.; Feely, R.; Sabine, C. L.; Key, R. M.; Takahashi, T. *Deep-Sea. Res. Pt. I* **2002**, *49*, 1705.

- (50) Meng, Z. Y.; Seinfeld, J. H.; Saxena, P.; Kim, Y. P. *Aerosol Sci. Technol.* **1995**, *23*, 131.
- (51) Rudolph, W. W.; Fischer, D.; Irmer, G. *Appl. Spectrosc.* **2006**, *60*, 130.
- (52) Logan, C. A. *Bioscience* **2010**, *60*, 819.
- (53) Parker, D. R.; Seyfferth, A. L.; Reese, B. K. *Environ. Sci. Technol.* **2008**, *42*, 1465.
- (54) Urbansky, E. T. *Environ. Sci. Pollut. Res.* **2002**, *9*, 187.
- (55) Drisdell, W. S.; Saykally, R. J.; Cohen, R. C. *J. Phys. Chem. C* **2010**, *114*, 11880.
- (56) Jungwirth, P.; Curtis, J. E.; Tobias, D. J. *Chem. Phys. Lett.* **2003**, *367*, 704.
- (57) Gopalakrishnan, S.; Jungwirth, P.; Tobias, D. J.; Allen, H. C. *J. Phys. Chem. B* **2005**, *109*, 8861.
- (58) Wernersson, E.; Jungwirth, P. *J. Chem. Theory Comput.* **2010**, *6*, 3233.
- (59) Imamura, T.; Mizukoshi, Y.; Ishiyama, T.; Morita, A. *J. Phys. Chem. C* **2012**, *116*, 11082.
- (60) Ishiyama, T.; Morita, A.; Miyamae, T. *Phys. Chem. Chem. Phys.* **2011**, *13*, 20965.
- (61) Ishiyama, T.; Morita, A. *J. Phys. Chem. C* **2011**, *115*, 13704.
- (62) Pegram, L. M.; Record, M. T. *J. Phys. Chem. B* **2007**, *111*, 5411.
- (63) Pegram, L. M.; Record, M. T. *Proc. Natl. Acad. Sci. U. S. A.* **2006**, *103*, 14278.
- (64) Salvador, P.; Curtis, J. E.; Tobias, D. J.; Jungwirth, P. *Phys. Chem. Chem. Phys.* **2003**, *5*, 3752.

- (65) Dang, L. X.; Chang, T.-M.; Roeselova, M.; Garrett, B. C.; Tobias, D. J. *J. Chem. Phys.* **2006**, *124*, 066101.
- (66) Thomas, J. L.; Roeselova, M.; Dang, L. X.; Tobias, D. J. *J. Phys. Chem. A* **2007**, *111*, 3091.
- (67) Minofar, B.; Vacha, R.; Wahab, A.; Mahiuddin, S.; Kunz, W.; Jungwirth, P. *J. Phys. Chem. B* **2006**, *2006*, 15939.
- (68) Hua, W.; Verreault, D.; Allen, H. C. *In preparation*.
- (69) Callahan, K. M.; Richards, N. K.; Anderson, C.; Finlayson-Pitts, B. J.; Tobias, D. J. *In preparation* **2013**.
- (70) Du, H.; Liu, J.; Ozdemir, O.; Nguyen, A. V.; Miller, J. D. *J. Colloid Interface Sci.* **2008**, *318*, 271.
- (71) Baer, M. D.; Kuo, I. F. W.; Bluhm, H.; Ghosal, S. *J. Phys. Chem. B* **2009**, *113*, 15843.
- (72) Cheng, J.; Vecitis, C. D.; Hoffmann, M. R.; Colussi, A. J. *J. Phys. Chem. B* **2006**, *110*, 25598.
- (73) Wren, S. N.; Donaldson, D. J. *Chem. Phys. Lett.* **2012**, *522*, 1.
- (74) Goebbert, D. J.; Garand, E.; Wende, T.; Bergmann, R.; Meijer, G.; Asmis, K. R.; Neumark, D. M. *J. Phys. Chem. A* **2009**, *113*, 7584.
- (75) Bush, M. F.; Saykally, R. J.; Williams, E. R. *J. Am. Chem. Soc.* **2007**, *129*, 2220.
- (76) Zhou, J.; Santambrogio, G.; Brummer, M.; Moore, D. T.; Meijer, G.; Neumark, D. M.; Asmis, K. R. *J. Chem. Phys.* **2006**, *125*.
- (77) Wang, X. B.; Yang, X.; Nicholas, J. B.; Wang, L. S. *Science* **2001**, *294*, 1322.

- (78) Brown, M. A.; Winter, B.; Faubel, M.; Hemminger, J. C. *J. Am. Chem. Soc.* **2009**, *131*, 8354.
- (79) Otten, D. E.; Petersen, P. B.; Saykally, R. J. *Chem. Phys. Lett.* **2007**, *449*, 261.
- (80) Fordyce, A. J.; Bullock, W. J.; Spencer-Smith, R. D.; Frey, J. G. *Phys. Chem. Chem. Phys.* **2004**, *6*, 2415.
- (81) Baldelli, S.; Schnitzer, C.; Shultz, M. J.; Campbell, D. J. *J. Phys. Chem. B* **1997**, *101*, 10435.
- (82) Radüge, C.; Pflumio, V.; Shen, Y. R. *Chem. Phys. Lett.* **1997**, *274*, 140.
- (83) Baldelli, S.; Schnitzer, C.; Campbell, D. J.; Shultz, M. J. *J. Phys. Chem. B* **1999**, *103*, 2789.
- (84) Tarbuck, T. L.; Richmond, G. L. *J. Am. Chem. Soc.* **2006**, *128*, 3256.
- (85) Miyamae, T.; Morita, A.; Ouchi, Y. *Phys. Chem. Chem. Phys.* **2008**, *10*, 2010.
- (86) Jubb, A. M.; Allen, H. C. *J. Phys. Chem. C* **2012**, *116*, 13161.
- (87) Schnitzer, C. S.; Baldelli, S.; Shultz, M. J. *J. Phys. Chem. B* **2000**, *104*, 585.
- (88) Xu, M.; Spinney, R.; Allen, H. C. *J. Phys. Chem. B* **2009**, *113*, 4102.
- (89) Xu, M.; Tang, C. Y.; Jubb, A. M.; Chen, X. K.; Allen, H. C. *J. Phys. Chem. C* **2009**, *113*, 2082.
- (90) Soule, M. C. K.; Blower, P. G.; Richmond, G. L. *J. Phys. Chem. A* **2007**, *111*, 3349.
- (91) Nihonyanagi, S.; Yamaguchi, S.; Tahara, T. *J. Chem. Phys.* **2009**, *130*, 204704.

- (92) Stiopkin, I. V.; Weeraman, C.; Pieniazek, P. A.; Shalhout, F. Y.; Skinner, J. L.; Benderskii, A. V. *Nature* **2011**, *474*, 192.
- (93) Tian, C. S.; Ji, N.; Waychunas, G. A.; Shen, Y. R. *J. Am. Chem. Soc.* **2008**, *130*, 13033.
- (94) Koelsch, P.; Viswanath, P.; Motschmann, H.; Shapovalov, V. L.; Brezesinski, G.; Mohwald, H.; Horinek, D.; Netz, R. R.; Giewekemeyer, K.; Alditt, T. S.; Schollmeyer, H.; von Klitzing, R.; Daillant, J.; Guenoun, P. *Colloids Surf., A* **2007**, *303*, 110.
- (95) Miranda, P. B.; Shen, Y. R. *J. Phys. Chem. B* **1999**, *103*, 3292.
- (96) Shen, Y. R.; Ostroverkhov, V. *Chemical Reviews* **2006**, *106*, 1140.
- (97) Wang, H. F.; Gan, W.; Lu, R.; Rao, Y.; Wu, B. H. *Int. Rev. Phys. Chem.* **2005**, *24*, 191.
- (98) Lambert, A. G.; Davies, P. B. *Appl. Spectrosc. Rev.* **2005**, *40*, 103.
- (99) Shen, Y. R. *The Principles of Nonlinear Optics*; 1st ed.; John Wiley & Sons: New York, 1984.
- (100) Du, Q.; Superfine, R.; Freysz, E.; Shen, Y. R. *Phys. Rev. Lett.* **1993**, *70*, 2313.
- (101) Du, Q.; Freysz, E.; Shen, Y. R. *Science* **1994**, *264*, 826.
- (102) Shultz, M. J.; Schnitzer, C.; Simonelli, D.; Baldelli, S. *Int. Rev. Phys. Chem.* **2000**, *19*, 123.
- (103) Richmond, G. L. *Chem. Rev.* **2002**, *102*, 2693.
- (104) Shen, Y. R.; Ostroverkhov, V. *Chem. Rev.* **2006**, *106*, 1140.

- (105) Fan, Y. B.; Chen, X.; Yang, L. J.; Cremer, P. S.; Gao, Y. Q. *J. Phys. Chem. B* **2009**, *113*, 11672.
- (106) Shen, Y. R. *Ann. Rev. Phys. Chem.* **1989**, *40*, 327.
- (107) Feng, R.-r.; Guo, Y.; Lue, R.; Velarde, L.; Wang, H.-f. *J. Phys. Chem. A* **2011**, *115*, 6015.
- (108) Lambert, A. G.; Davies, P. B.; Neivandt, D. J. *Appl. Spectrosc. Rev.* **2005**, *40*, 103.
- (109) Tian, C. S.; Shen, Y. R. *Chem. Phys. Lett.* **2009**, *470*, 1.
- (110) Sovago, M.; Campen, R. K.; Bakker, H. J.; Bonn, M. *Chem. Phys. Lett.* **2009**, *470*, 7.
- (111) Levering, L. M.; Sierra-Hernandez, M. R.; Allen, H. C. *J. Phys. Chem. C* **2007**, *111*, 8814.
- (112) Tarbuck, T. L.; Ota, S. T.; Richmond, G. L. *J. Am. Chem. Soc.* **2006**, *128*, 14519.
- (113) de Beer, A. G. F.; Samson, J. S.; Hua, W.; Huang, Z. S.; Chen, X. K.; Allen, H. C.; Roke, S. *J. Chem. Phys.* **2011**, *135*, 224701/1.
- (114) Sovago, M.; Vartiainen, E.; Bonn, M. *J. Chem. Phys.* **2009**, *131*, 161107.
- (115) Chen, X. K.; Hua, W.; Huang, Z. S.; Allen, H. C. *J. Am. Chem. Soc.* **2010**, *132*, 11336.
- (116) Kemnitz, K.; Bhattacharyya, K.; Hicks, J. M.; Pinto, G. R.; Eisenthal, K. B.; Heinz, T. F. *Chem. Phys. Lett.* **1986**, *131*, 285.
- (117) Superfine, R.; Huang, J. Y.; Shen, Y. R. *Chem. Phys. Lett.* **1990**, *172*, 303.

- (118) Tian, C. S.; Shen, Y. R. *J. Am. Chem. Soc.* **2009**, *131*, 2790.
- (119) Tian, C. S.; Shen, Y. R. *Proc. Natl. Acad. Sci. U. S. A.* **2009**, *106*, 15148.
- (120) Stiopkin, I. V.; Jayathilake, H. D.; Bordenyuk, A. N.; Benderskii, A. V. *J. Am. Chem. Soc.* **2008**, *130*, 2271.
- (121) Nihonyanagi, S.; Yamaguchi, S.; Tahara, T. *J. Am. Chem. Soc.* **2010**, *132*, 6867.
- (122) Nihonyanagi, S.; Mondal, J. A.; Yamaguchi, S.; Tahara, T. In *Annu. Rev. Phys. Chem.*; Johnson, M. A., Martinez, T. J., Eds. 2013; Vol. 64, p 579.
- (123) Pool, R. E.; Versluis, J.; Backus, E. H. G.; Bonn, M. *J. Phys. Chem. B* **2011**, *115*, 15362.
- (124) Hua, W.; Chen, X. K.; Allen, H. C. *J. Phys. Chem. A* **2011**, *115*, 6233.
- (125) Hua, W.; Jubb, A. M.; Allen, H. C. *J. Phys. Chem. Lett.* **2011**, *2*, 2515.
- (126) Hua, W.; Verreault, D.; Adams, E. M.; Huang, Z. S.; Allen, H. C. *J. Phys. Chem. C* **2013**, *117*, 19577.
- (127) Hua, W.; Verreault, D.; Allen, H. C. *J. Phys. Chem. Lett.* **2013**, *accepted*.
- (128) Jubb, A. M.; Hua, W.; Allen, H. C. *Acc. Chem. Res.* **2012**, *45*, 110.
- (129) Jubb, A. M.; Hua, W.; Allen, H. C. *Annu. Rev. Phys. Chem.* **2012**, *63*, 6.1.
- (130) Verreault, D.; Hua, W.; Allen, H. C. *J. Phys. Chem. Lett.* **2012**, *3*, 3012.
- (131) Nihonyanagi, S.; Yamaguchi, S.; Tahara, T. *J. Chem. Phys.* **2009**, *130*, 204704/1.
- (132) Yamaguchi, S.; Tahara, T. *J. Chem. Phys.* **2008**, *129*, 101102.

- (133) Gan, W.; Wu, D.; Zhang, Z.; Feng, R. R.; Wang, H. F. *J. Chem. Phys.* **2006**, *124*, 114705.
- (134) Hommel, E. L.; Ma, G.; Allen, H. C. *Anal. Sci.* **2001**, *17*, 1325.
- (135) Ma, G.; Allen, H. C. *J. Phys. Chem. B* **2003**, *107*, 6343.
- (136) Allen, H. C.; Casillas-Ituarte, N. N.; Sierra-Hernandez, M. R.; Chen, X. K.; Tang, C. Y. *Phys. Chem. Chem. Phys.* **2009**, *11*, 5538.
- (137) Tang, C.; Allen, H. *J. Phys. Chem. A* **2009**, *113*, 7383.
- (138) Tian, C. S.; Byrnes, S. J.; Han, H. L.; Shen, Y. R. *J. Phys. Chem. Lett.* **2011**, *2*, 1946.
- (139) Kane, S. M.; Caloz, F.; Leu, M. T. *J. Phys. Chem. A* **2001**, *105*, 6465.
- (140) Sabine, C. L.; Feely, R. A.; Gruber, N.; Key, R. M.; Lee, K.; Bullister, J. L.; Wanninkhof, R.; Wong, C. S.; Wallace, D. W. R.; Tilbrook, B.; Millero, F. J.; Peng, T. H.; Kozyr, A.; Ono, T.; Rios, A. F. *Science* **2004**, *305*, 367.
- (141) McGillis, W. R.; Edson, J. B.; Zappa, C. J.; Ware, J. D.; McKenna, S. P.; Terray, E. A.; Hare, J. E.; Fairall, C. W.; Drennan, W.; Donelan, M.; DeGrandpre, M. D.; Wanninkhof, R.; Feely, R. A. *J. Geophys. Res.-Oceans* **2004**, *109*, 1.
- (142) McGillis, W. R.; Wanninkhof, R. *Mar. Chem.* **2006**, *98*, 100.
- (143) Buch, V.; Milet, A.; Vacha, R.; Jungwirth, P.; Devlin, J. P. *Proc. Natl. Acad. Sci. U. S. A.* **2007**, *104*, 7342.
- (144) Superfine, R.; Huang, J. Y.; Shen, Y. R. *Phys. Rev. Lett.* **1991**, *66*, 1066.
- (145) Richmond, G. L. *Chem. Rev.* **2002**, *102*, 2693.

- (146) Shultz, M. J.; Baldelli, S.; Schnitzer, C.; Simonelle, D. *J. Phys. Chem. B* **2002**, *106*, 5313.
- (147) Liu, D. F.; Ma, G.; Levering, L. M.; Allen, H. C. *J. Phys. Chem. B* **2004**, *108*, 2252.
- (148) Chen, X. K.; Allen, H. C. *J. Phys. Chem. B* **2010**, *114*, 14983.
- (149) Ishiyama, T.; Morita, A. *J. Phys. Chem. C* **2009**, *113*, 16299.
- (150) Ishiyama, T.; Morita, A. *J. Chem. Phys.* **2009**, *131*, 244714.
- (151) Ozdemir, O.; Karakashev, S. I.; Nguyen, A. V.; Miller, J. D. *Int. J. Miner. Process.* **2006**, *81*, 149.
- (152) Finlayson-Pitts, B. J.; Pitts, J. N. *Chemistry of the Upper and Lower Troposphere*; Academic Press: San Diego, CA, 2000.
- (153) Ma, G.; Liu, D.; Allen, H. C. *Langmuir* **2004**, *20*, 11620.
- (154) Liu, D.; Ma, G.; Allen, H. C. *Environ. Sci. Technol.* **2005**, *39*, 2025.
- (155) Casillas-Ituarte, N. N.; Allen, H. C. *Chem. Phys. Lett.* **2009**, *483*, 84.
- (156) Xu, M.; Liu, D. F.; Allen, H. C. *Environ. Sci. Technol.* **2006**, *40*, 1566.
- (157) Zhu, X. D.; Suhr, H.; Shen, Y. R. *Phys. Rev. B: Condens. Matter Mater. Phys.* **1987**, *35*, 3047.
- (158) Petersen, P. B.; Saykally, R. J. *J. Phys. Chem. B* **2005**, *109*, 7976.
- (159) Ghosal, S.; Hemminger, J. C.; Bluhm, H.; Mun, B. S.; Hebenstreit, E. L. D.; Ketteler, G.; Ogletree, D. F.; Requejo, F. G.; Salmeron, M. *Science* **2005**, *307*, 563.

- (160) Finlayson, A. C. *J. Chem. Educ.* **1992**, *69*, 559.
- (161) Raymond, E. A.; Tarbuck, T. L.; Brown, M. G.; Richmond, G. L. *J. Phys. Chem. B* **2003**, *107*, 546.
- (162) Auer, B. M.; Skinner, J. L. *J. Phys. Chem. B* **2009**, *113*, 4125.
- (163) Ishiyama, T.; Morita, A. *J. Phys. Chem. C* **2007**, *111*, 738.
- (164) Casillas-Ituarte, N. N.; Callahan, K. M.; Tang, C. Y.; Chen, X. K.; Roeselova, M.; Tobias, D. J.; Allen, H. C. *Proc. Natl. Acad. Sci. U. S. A.* **2010**, *107*, 6616.
- (165) dos Santos, A. P.; Diehl, A.; Levin, Y. *Langmuir* **2010**, *26*, 10778.
- (166) Bush, M. F.; Saykally, R. J.; Williams, E. R. *J. Am. Chem. Soc.* **2008**, *130*, 15482.
- (167) Finlayson-Pitts, B. J. *Phys. Chem. Chem. Phys.* **2009**, *11*, 7760.
- (168) Usher, C. R.; Michel, A. E.; Grassian, V. H. *Chem. Rev.* **2003**, *103*, 4883.
- (169) Chang, T. M.; Dang, L. X. *Chem. Rev.* **2006**, *106*, 1305.
- (170) Petersen, P. B.; Saykally, R. J. *Annu. Rev. Phys. Chem.* **2006**, *57*, 333.
- (171) Jungwirth, P. *Faraday Disc.* **2009**, *141*, 9.
- (172) Zhang, Z.; Piatkowski, L.; Bakker, H. J.; Bonn, M. *J. Chem. Phys.* **2011**, *135*, 021101/1.
- (173) Zhang, Z.; Piatkowski, L.; Bakker, H. J.; Bonn, M. *Nat. Chem.* **2011**, *3*, 888.
- (174) Singh, P. C.; Nihonyanagi, S.; Yamaguchi, S.; Tahara, T. *J. Chem. Phys.* **2012**, *137*, 094706/1.

- (175) Feng, R.-r.; Bian, H.-t.; Guo, Y.; Wang, H.-f. *J. Chem. Phys.* **2009**, *130*, 134710/1.
- (176) Sloutskin, E.; Baumert, J.; Ocko, B. M.; Kuzmenko, I.; Checco, A.; Tamam, L.; Ofer, E.; Gog, T.; Gang, O.; Deutsch, M. *J. Chem. Phys.* **2007**, *126*, 054704/1.
- (177) Lunkenheimer, K.; Pergande, H. J.; Kruger, H. *Rev. Sci. Instrum.* **1987**, *58*, 2313.
- (178) Pieniazek, P. A.; Tainter, C. J.; Skinner, J. L. *J. Am. Chem. Soc.* **2011**, *133*, 10360.
- (179) Okur, H. I.; Kherb, J.; Cremer, P. S. *J. Am. Chem. Soc.* **2013**, *135*, 5062.
- (180) Kherb, J.; Flores, S. C.; Cremer, P. S. *J. Phys. Chem. B* **2012**, *116*, 7389.
- (181) Huang, Z. S.; Hua, W.; Verreault, D.; Allen, H. C. *submitted*.
- (182) Watry, M. R.; Tarbuck, T. L.; Richmond, G. L. *J. Phys. Chem. B* **2003**, *107*, 512.
- (183) Keil, O.; Dahmen, J.; Volmer, D. A. *Fresenius J. Anal. Chem.* **1999**, *364*, 694.
- (184) Maeda, S.; Pham, H. Q.; Young, T. C.; Young, T.; Pham, H.; Ha Kyu, P.; Shuuji, M.; U. S. Patent Application 2010331494-A1: 2009.
- (185) Kikuchi, T.; Furusho, S.; Sato, Y.; WO2007122781-A1: 2008.
- (186) Gurau, M. C.; Kim, G.; Lim, S. M.; Albertorio, F.; Fleisher, H. C.; Cremer, P. S. *Chemphyschem* **2003**, *4*, 1231.
- (187) Collins, K. D. *Proc. Natl. Acad. Sci. U. S. A.* **1995**, *92*, 5553.
- (188) Collins, K. D. *Biophys. Chem.* **2006**, *119*, 271.
- (189) Kherb, J.; Flores, S. C.; Cremer, P. S. *J. Phys. Chem. B* **2012**, *116*, 7389.

- (190) Okur, H. I.; Kherb, J.; Cremer, P. S. *J. Am. Chem. Soc.* **2013**, *135*, 5062.
- (191) Tang, C. Y.; Allen, H. C. *J. Phys. Chem. A* **2009**, *113*, 7383.
- (192) Aziz, E. F.; Ottosson, N.; Eisebitt, S.; Eberhardt, W.; Jagoda-Cwiklik, B.; Vacha, R.; Jungwirth, P.; Winter, B. *J. Phys. Chem. B* **2008**, *112*, 12567.
- (193) Hajari, T.; Ganguly, P.; van der Vegt, N. F. A. *J. Chem. Theory Comput.* **2012**, *8*, 3804.
- (194) Uejio, J. S.; Schwartz, C. P.; Duffin, A. M.; Drisdell, W. S.; Cohen, R. C.; Saykally, R. J. *Proc. Natl. Acad. Sci. U. S. A.* **2008**, *105*, 6809.
- (195) Vrbka, L.; Vondrasek, J.; Jagoda-Cwiklik, B.; Vacha, R.; Jungwirth, P. *Proc. Natl. Acad. Sci. U.S.A.* **2006**, *103*, 15440.
- (196) *Biological Membrane Ion Channels Dynamics, Structure, and Applications*; Chung, S.-H., Andersen, O. S., Krishnamurthy, V., Ed.; Springer: New York, 2007.
- (197) Clausen, T. *Acta Physiologica* **2008**, *192*, 339.
- (198) Collins, K. D.; Neilson, G. W.; Enderby, J. E. *Biophys. Chem.* **2007**, *128*, 95.
- (199) Jagoda-Cwiklik, B.; Vacha, R.; Lund, M.; Srebro, M.; Jungwirth, P. *J. Phys. Chem. B* **2007**, *111*, 14077.
- (200) Ma, G.; Allen, H. C. *Langmuir* **2007**, *23*, 589.
- (201) Kaganer, V. M.; Mohwald, H.; Dutta, P. *Rev. Mod. Phys.* **1999**, *71*, 779.
- (202) Tang, C. Y.; Huang, Z. S. A.; Allen, H. C. *J. Phys. Chem. B* **2010**, *114*, 17068.
- (203) Chen, X. K.; Hua, W.; Huang, Z. S.; Allen, H. C. *J. Am. Chem. Soc.* **2010**, *132*, 11336.

- (204) Sovago, M.; Wurpel, G. W. H.; Smits, M.; Muller, M.; Bonn, M. *J. Am. Chem. Soc.* **2007**, *129*, 11079.
- (205) Tang, C. Y.; Huang, Z. S.; Allen, H. C. *J. Phys. Chem. B* **2011**, *115*, 34.
- (206) Miranda, P. B.; Du, Q.; Shen, Y. R. *Chem. Phys. Lett.* **1998**, *286*, 1.
- (207) Dang, L. X. *J. Phys. Chem. B* **2002**, *106*, 10388.
- (208) Ji, N.; Ostroverkhov, V.; Tian, C. S.; Shen, Y. R. *Phys. Rev. Lett.* **2008**, *100*, 096102/1.
- (209) Cheng, M. H.; Callahan, K. M.; Margarella, A. M.; Tobias, D. J.; Hemminger, J. C.; Bluhm, H.; Krisch, M. J. *J. Phys. Chem. C* **2012**, *116*, 4545.
- (210) Zhang, Y. J.; Cremer, P. S. *Annu. Rev. Phys. Chem.* **2010**, *61*, 63.
- (211) Parsons, D. F.; Bostrom, M.; Lo Nostro, P.; Ninham, B. W. *Phys. Chem. Chem. Phys.* **2011**, *13*, 12352.
- (212) Randles, J. E. B. *Discuss. Faraday Soc.* **1957**, *24*, 194.
- (213) Gurau, M. C.; Lim, S.-M.; Castellana, E. T.; Albertorio, F.; Kataoka, S.; Cremer, P. S. *J. Am. Chem. Soc.* **2004**, *126*, 10522.
- (214) *Perchlorate: Environmental Occurrence, Interactions and Treatment*; Gu, G.; Coates, J. D., Eds.; Springer New York, 2006.
- (215) Dasgupta, P. K.; Dyke, J. V.; Kirk, A. B.; Jackson, W. A. *Environ. Sci. Technol.* **2006**, *40*, 6608.
- (216) Rajagopalan, S.; Anderson, T.; Cox, S.; Harvey, G.; Cheng, Q.; Jackson, W. A. *Environ. Sci. Technol.* **2009**, *43*, 616.

- (217) Dasgupta, P. K.; Martinelango, P. K.; Jackson, W. A.; Anderson, T. A.; Tian, K.; Tock, R. W.; Rajagopalan, S. *Environ. Sci. Technol.* **2005**, *39*, 1569.
- (218) Rao, B.; Anderson, T. A.; Redder, A.; Jackson, W. A. *Environ. Sci. Technol.* **2010**, *44*, 2961.
- (219) Huang, Z. S.; Hua, W.; Verreault, D.; Allen, H. C. *J. Phys. Chem. A* **2013**, *117*, 6346.
- (220) Morita, A.; Hynes, J. T. *Chem. Phys.* **2000**, *258*, 371.
- (221) Walrafen, G. E. *J. Chem. Phys.* **1970**, *52*, 4176.
- (222) Rodgers, G. E.; Plane, R. A. *J. Chem. Phys.* **1975**, *63*, 818.
- (223) Stangret, J.; Kostrowicki, J. *J. Solution Chem.* **1988**, *17*, 165.
- (224) Rull, F. *Pure Appl. Chem.* **2002**, *74*, 1859.
- (225) Saitow, K.; Kobayashi, K.; Nishikawa, K. *J. Solution Chem.* **2004**, *33*, 689.
- (226) Chen, Y.; Zhang, Y. H.; Zhao, L. *J. Phys. Chem. Chem. Phys.* **2004**, *6*, 537.
- (227) Frumkin, A. Z. *Phys. Chem.* **1924**, *109*, 34.
- (228) Verreault, D.; Allen, H. C. *Chem. Phys. Lett.* **2013**, *586*, 1.
- (229) Viswanath, P.; Motschmann, H. *J. Phys. Chem. C* **2008**, *112*, 2099.
- (230) Millero, F. J. *Chemical Oceanography*; 3rd ed.; CRC Press: Boca Raton, FL, 2005.
- (231) Chu, L.; Anastasio, C. *J. Phys. Chem. A* **2003**, *107*, 9594.

- (232) Honrath, R. E.; Guo, S.; Peterson, M. C.; Dziobak, M. P.; Dibb, J. E.; Arsenault, M. A. *J. Geophys. Res.-Atmos.* **2000**, *105*, 24183.
- (233) Honrath, R. E.; Peterson, M. C.; Dziobak, M. P.; Dibb, J. E.; Arsenault, M. A.; Green, S. A. *Geophys. Res. Lett.* **2000**, *27*, 2237.
- (234) Mack, J.; Bolton, J. R. *J. Photoch. Photobio. A* **1999**, *128*, 1.
- (235) Lihavainen, H.; Kerminen, V. M.; Komppula, M.; Hyvarinen, A. P.; Laakia, J.; Saarikoski, S.; Makkonen, U.; Kivekas, N.; Hillamo, R.; Kulmala, M.; Viisanen, Y. *Atmos. Chem. Phys.* **2008**, *8*, 6925.
- (236) Talbot, R. W.; Dibb, J. E.; Loomis, M. B. *Geophys. Res. Lett.* **1998**, *25*, 1367.
- (237) Bush, M. F.; O'Brien, J. T.; Prell, J. S.; Wu, C.-C.; Saykally, R. J.; Williams, E. R. *J. Am. Chem. Soc.* **2009**, *131*, 13270.
- (238) Du, H.; Rasaiah, J. C.; Miller, J. D. *J. Phys. Chem. B* **2007**, *111*, 209.
- (239) Allen, H. C.; Casillas-Ituarte, N. N.; Sierra-Hernandez, M. R.; Chen, X. K.; Tang, C. Y. *Phys. Chem. Chem. Phys.* **2009**, *11*, 5538.
- (240) Skinner, J. L.; Pieniazek, P. A.; Gruenbaum, S. M. *Acc. Chem. Res.* **2012**, *45*, 93.
- (241) Callahan, K. M.; Casillas-Ituarte, N. N.; Roeselova, M.; Allen, H. C.; Tobias, D. J. *J. Phys. Chem. A* **2010**, *114*, 5141.
- (242) Ishiyama, T.; Morita, A. *J. Phys. Chem. A* **2007**, *111*, 9277.
- (243) Bock, C. W.; Markham, G. D.; Katz, A. K.; Glusker, J. P. *Theor. Chem. Acc.* **2006**, *115*, 100.
- (244) Shannon, R. D. *Acta Crystallogr., Sect. A* **1976**, *32*, 751.

- (245) Persson, I. *Pure Appl. Chem.* **2010**, *82*, 1901.
- (246) Levin, Y. *Phys. Rev. Lett.* **2009**, *102*, 147803/1.
- (247) Slavchov, R. I.; Novev, J. K. *J. Colloid Interface Sci.* **2012**, *387*, 234.
- (248) Mahler, J.; Persson, I. *Inorg. Chem.* **2012**, *51*, 425.
- (249) Miller, D. J.; Lisy, J. M. *J. Am. Chem. Soc.* **2008**, *130*, 15393.
- (250) Markham, G. D.; Glusker, J. P.; Bock, C. W. *J. Phy. Chem. B* **2002**, *106*, 5118.
- (251) Martinez, J. M.; Pappalardo, R. R.; Marcos, E. S. *J. Am. Chem. Soc.* **1999**, *121*, 3175.
- (252) Varma, S.; Rempe, S. B. *Biophys. Chem.* **2006**, *124*, 192.
- (253) Hashimoto, K.; Kamimoto, T. *J. Am. Chem. Soc.* **1998**, *120*, 3560.
- (254) Marcus, Y. *Chem. Rev.* **2009**, *109*, 1346.
- (255) Smirnov, P. R.; Trostin, V. N. *Russ. J. Gen. Chem.* **2006**, *76*, 175.
- (256) Funkner, S.; Niehues, G.; Schmidt, D. A.; Heyden, M.; Schwaab, G.; Callahan, K. M.; Tobias, D. J.; Havenith, M. *J. Am. Chem. Soc.* **2012**, *134*, 1030.
- (257) Omta, A. W.; Kropman, M. F.; Woutersen, S.; Bakker, H. J. *J. Chem. Phys.* **2003**, *119*, 12457.
- (258) Collins, K. D.; Washabaugh, M. W. *Q. Rev. Biophys.* **1985**, *18*, 323.
- (259) Hofmeister, F. *Arch. Exp. Pathol. Pharmacol* **1888**, *24*, 247.

- (260) Kunz, W.; Henle, J.; Ninham, B. W. *Curr. Opin. Colloid. Interface. Sci.* **2004**, *9*, 19.
- (261) Levin, Y.; dos Santos, A. P.; Diehl, A. *Phys. Rev. Lett.* **2009**, *103*, 257802/1.
- (262) Noah-Vanhoucke, J.; Geissler, P. L. *Proc. Natl. Acad. Sci. USA* **2009**, *106*, 15125.
- (263) Eggimann, B. L.; Siepmann, J. I. *J. Phys. Chem. C* **2008**, *112*, 210.
- (264) Wick, C. D.; Kuo, I. F. W.; Mundy, C. J.; Dang, L. X. *J. Chem. Theory. Comput.* **2007**, *3*, 2002.
- (265) Mason, P. E.; Wernersson, E.; Jungwirth, P. *J. Phys. Chem. B* **2012**, *116*, 8145.
- (266) Ahn-Ercan, G.; Krienke, H.; Kunz, W. *Curr. Opin. Colloid Interface Sci.* **2004**, *9*, 92.
- (267) Caleman, C.; Hub, J. S.; van Maaren, P. J.; van der Spoel, D. *Proc. Natl. Acad. Sci. USA* **2011**, *108*, 6838.
- (268) Otten, D. E.; Shaffer, P. R.; Geissler, P. L.; Saykally, R. J. *Proc. Natl. Acad. Sci. U. S. A.* **2012**, *109*, 701.
- (269) Arslanargin, A.; Beck, T. L. *J. Chem. Phys.* **2012**, *136*, 104503/1.
- (270) Bostrom, M.; Kunz, W.; Ninham, B. W. *Langmuir* **2005**, *21*, 2619.
- (271) Bostrom, M.; Ninham, B. W. *Langmuir* **2004**, *20*, 7569.
- (272) Bostrom, M.; Williams, D. R. M.; Ninham, B. W. *Phys. Rev. Lett.* **2001**, *87*, 168103/1.
- (273) Parsons, D. F.; Ninham, B. W. *Langmuir* **2010**, *26*, 6430.

- (274) Baer, M. D.; Stern, A. C.; Levin, Y.; Tobias, D. J.; Mundy, C. J. *J. Phys. Chem. Lett.* **2012**, *3*, 1565.
- (275) Horinek, D.; Herz, A.; Vrbka, L.; Sedlmeier, F.; Mamatkulov, S. I.; Netz, R. R. *Chem. Phys. Lett.* **2009**, *479*, 173.
- (276) Wick, C. A.; Xantheas, S. S. *J. Phys. Chem. B* **2009**, *113*, 4141.
- (277) Collins, K. D.; Neilson, G. W.; Enderby, J. E. *Biophys. Chem.* **2007**, *128*, 95.
- (278) Stuart, S. J.; Berne, B. J. *J. Phys. Chem. A* **1999**, *103*, 10300.
- (279) Sachs, J. N.; Woolf, T. B. *J. Am. Chem. Soc.* **2003**, *125*, 8742.
- (280) Buchner, R.; Chen, T.; Hefter, G. *J. Phys. Chem. B* **2004**, *108*, 2365.
- (281) Archontis, G.; Leontidis, E. *Chem. Phys. Lett.* **2006**, *420*, 199.
- (282) Wachter, W.; Kunz, W.; Buchner, R.; Hefter, G. *J. Phys. Chem. A* **2005**, *109*, 8675.
- (283) Marcus, Y. *Ion properties*; Marcel Dekker: New York, 1997.
- (284) Marcus, Y. *Biophys. Chem.* **1994**, *51*, 111.
- (285) Perera, L.; Berkowitz, M. L. *J. Chem. Phys.* **1991**, *95*, 1954.
- (286) Tobias, D. J.; Jungwirth, P.; Parrinello, M. *J. Chem. Phys.* **2001**, *114*, 7036.
- (287) Yang, X.; Kiran, B.; Wang, X. B.; Wang, L. S.; Mucha, M.; Jungwirth, P. *J. Phys. Chem. A* **2004**, *108*, 7820.
- (288) Ninham, B. W.; Yaminsky, V. *Langmuir* **1997**, *13*, 2097.

- (289) Parsons, D. F.; Ninham, B. W. *Langmuir* **2010**, *26*, 1816.
- (290) Pyper, N. C.; Pike, C. G.; Edwards, P. P. *Mol. Phys.* **1992**, *76*, 353.
- (291) Parsons, D. F.; Ninham, B. W. *J. Phys. Chem. A* **2009**, *113*, 1141.
- (292) Nightingale, E. R. *J. Phys. Chem.* **1959**, *63*, 1381.
- (293) Hagberg, D.; Brdarski, S.; Karlstrom, G. *J. Phys. Chem. B* **2005**, *109*, 4111.
- (294) Nucci, N. V.; Vanderkooi, J. M. *J. Mol. Liq.* **2008**, *143*, 160.
- (295) Richards, N. K.; Finlayson-Pitts, B. J. *Environ. Sci. Technol.* **2012**, *46*, 10447.
- (296) Drisdell, W. S.; Saykally, R. J.; Cohen, R. C. *Proc. Natl. Acad. Sci. U. S. A.* **2009**, *106*, 18897.
- (297) Saykally, R. J. *67th International Symposium on Molecular Spectroscopy - The Ohio State University* **2012**.
- (298) Musolino, N.; Trout, B. L. *J. Chem. Phys.* **2013**, *138*, 134707/1.
- (299) Claeys, M.; Wang, W.; Ion, A.; Kourtchev, I.; Gelencser, A.; Maenhaut, W. *Atmos. Environ.* **2004**, *38*, 4093.
- (300) Claeys, M.; Graham, B.; Vas, G.; Wang, W.; Vermeylen, R.; Pashynska, V.; Cafmeyer, J.; Guyon, P.; Andreae, M.; Artaxo, P.; Maenhaut, W. *Science* **2004**, *303*, 1173.
- (301) Hua, W.; Chen, Z. M.; Jie, C. Y.; Kondo, Y.; Hofzumahaus, A.; Takegawa, N.; Chang, C. C.; Lu, K. D.; Miyazaki, Y.; Kita, K.; Wang, H. L.; Zhang, Y. H.; Hu, M. *Atmos. Chem. Phys.* **2008**, *8*, 6755.

- (302) Koop, T.; Kapilashrami, A.; Molina, L. T.; Molina, M. J. *J. Geophys. Res.* **2000**, *105*, 26393.
- (303) Ota, S. T.; Richmond, G. L. *J. Am. Chem. Soc.* **2012**, *134*, 9967.
- (304) Lohmann, U.; Feichter, J. *Atmos. Chem. Phys.* **2005**, *5*, 715.

Appendix B Performance Test of the Broad Bandwidth VSFG Spectrometer

As mentioned in Chapter 2, the intensity of the generated sum frequency signal is proportional to the intensity of the incident infrared and visible beams. To delineate the performance of the broad bandwidth VSFG system used for this work and to examine the impact of visible and infrared energy on the intensity and spectral lineshape on the resulting conventional VSFG spectra, a series of energy tests were conducted using GaAs and nitrate salt solutions. To ensure the validity of the tests, the stability of VSFG system during the entire experiments was monitored by measuring the GaAs profile and the conventional VSFG spectrum of neat water in the OH stretching region ($3000\text{--}3800\text{ cm}^{-1}$) (Figure A.1).

1. Visible energy test.

It can be seen from Figure A.2 that the VSFG signal intensity is proportional to visible energy as expected.

2. Infrared energy test

To test the influence of infrared energy on the resulting VSFG spectra, a neutral density filter was placed between the TOPAS and NDFG. The infrared energy were $\sim 9\ \mu\text{J}$ and $\sim 6.9\ \mu\text{J}$, respectively, before and after energy attenuation. The GaAs profiles and the

corresponding VSFG counts on the low and high frequency sides in each spectrum are given in Figure A.3. It is clear that the VSFG signal intensity is not proportional to the infrared energy as seen in the visible energy test. The intensity of the VSFG signal dropped to less than half of its original response. In addition, the overall spectral lineshape altered unevenly over the entire OH stretching region. By adjusting the time delay (in the visible beam propagating path), the VSFG intensity obtained by using a lower infrared energy increased dramatically; however, the lineshape of GaAs profile differs significantly. The raw and normalized final conventional VSFG spectra of neat water, 1.6 M NH_4NO_3 and 2.3 M $\text{Mg}(\text{NO}_3)_2$ salt solutions before and after energy attenuation are demonstrated in Figure A.4.

In summary, the resulting VSFG signal intensity is proportional to the incident visible energy as expected. In contrast, a reduction of the incident infrared energy would result in non-uniform decrease of VSFG intensity in both GaAs profile and sample spectra, with more pronounced reduction on the edges of the spectra and less reduction in the center of the spectral region. Decreased infrared energy does cause slight distortion of the overall spectral lineshape of spectra; however, the relative differences between various sample systems are not affected by the lower incident infrared (see Figure A.5).

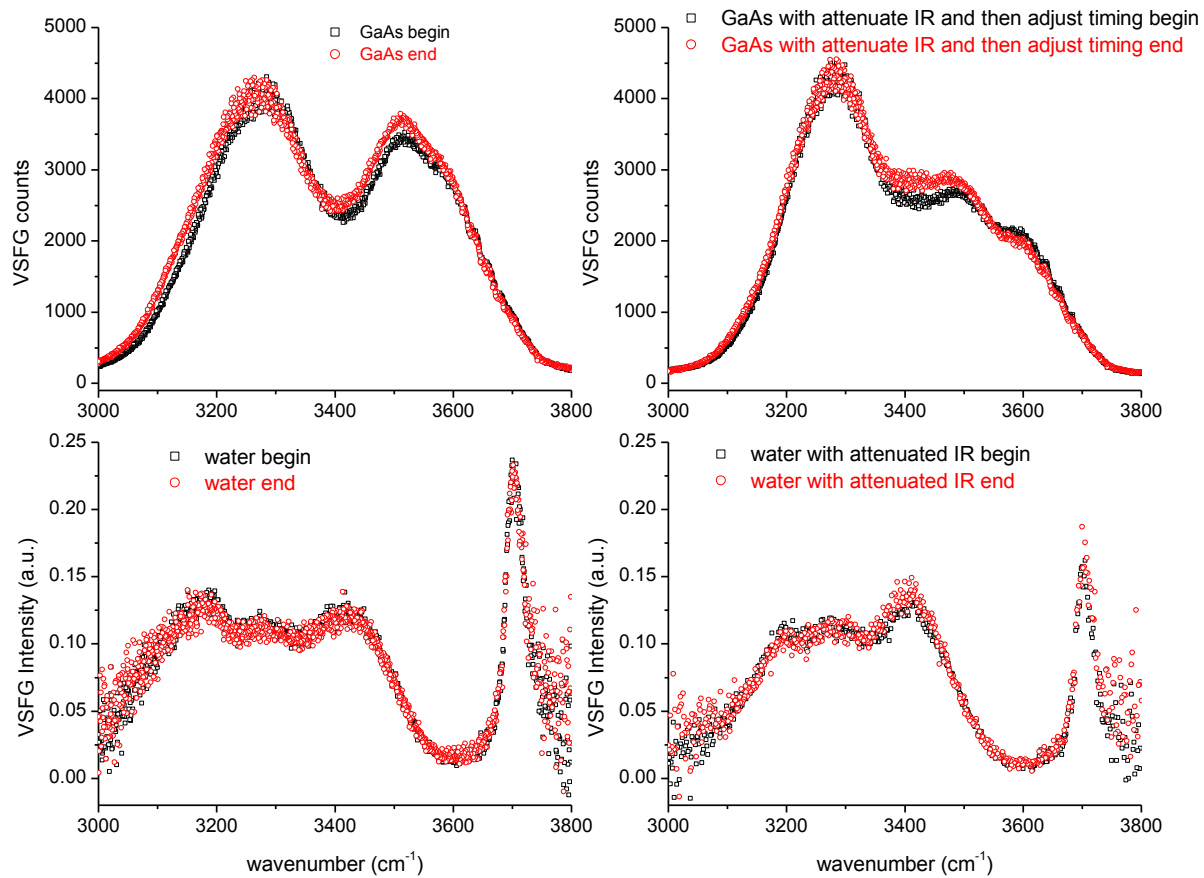


Figure B.1 Stability of the VSFG system shown by the GaAs profile and the conventional VSFG spectrum of neat water in the OH stretching region ($3000\text{--}3800\text{ cm}^{-1}$) before and after infrared energy attenuation.

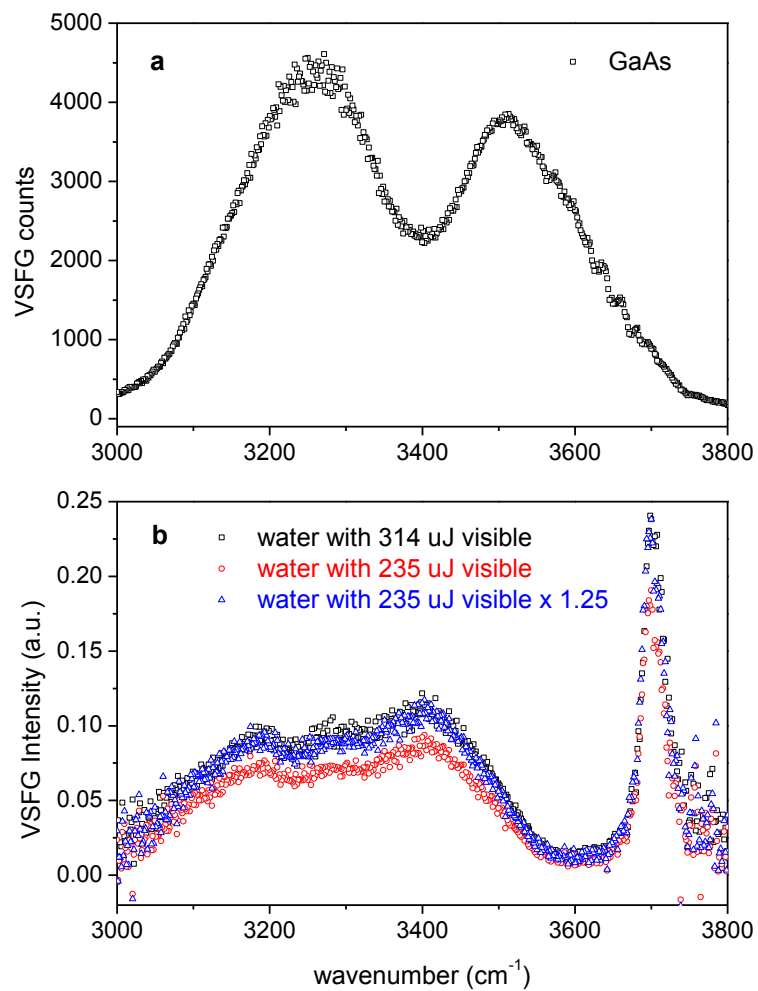


Figure B.2 (a) GaAs profile and (b) conventional VSFG spectra of neat water in the OH stretching region measured using different visible energy.

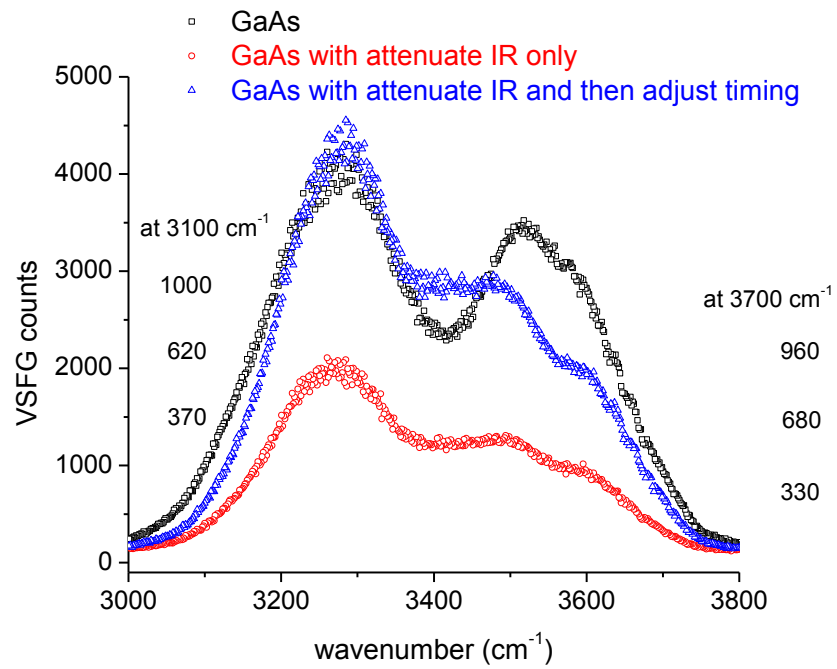


Figure B.3 GaAs profiles measured with original infrared energy ($\sim 9 \mu\text{J}$), attenuated infrared energy ($\sim 6.9 \mu\text{J}$), and attenuated infrared energy with timing adjustment.

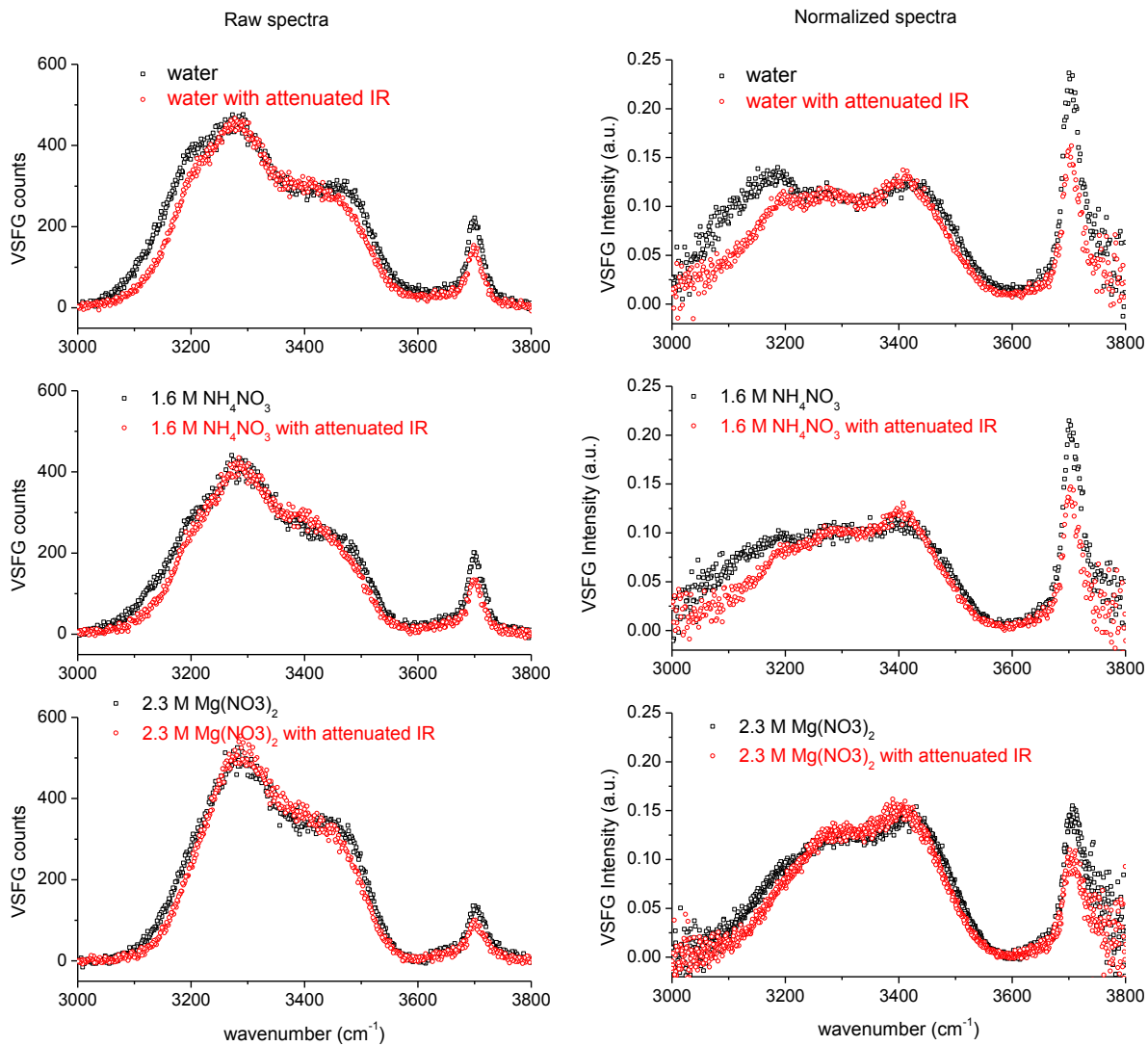


Figure B.4 Raw and normalized final conventional VSFG spectra of neat water, 1.6 M NH_4NO_3 and 2.3 M $\text{Mg}(\text{NO}_3)_2$ salt solutions before and after energy attenuation.

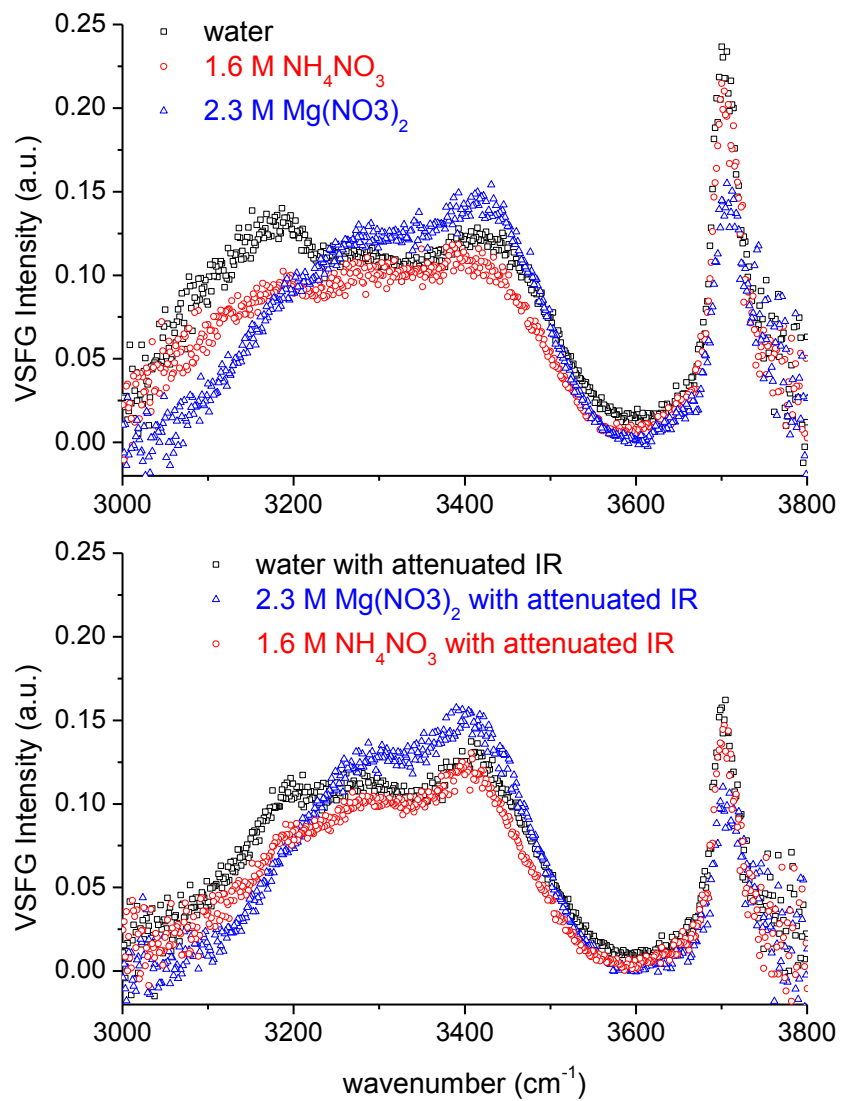


Figure B.5 An example showing that the relative spectral differences between various samples are not affected by the incident energy utilized.

Appendix C Permissions

Chapter 1: No previously published material.

Chapter 2:

Section 2.2: Reproduced in part with permission from Hua, W; Jubb, A.M.; and Allen, H.C. “Electric Field Reversal of Na_2SO_4 , $(\text{NH}_4)_2\text{SO}_4$, and Na_2CO_3 relative to CaCl_2 and NaCl at the Air/Aqueous Interface revealed by Phase-Sensitive Sum Frequency” *J. Phys. Chem. Lett.*, **2011**, 2, 2515-2520. Copyright 2011 American Chemical Society.

- **From www.acs.org** – *Reuse/Republication of the Entire Work in Theses or Collections: Authors may reuse all or part of the Submitted, Accepted or Published Work in a thesis or dissertation that the author writes and is required to submit to satisfy the criteria of degree-granting institutions.*
- RightsLink permissions provided below.

Chapter 3: Reproduced in part with permission from Hua, W; Jubb, A.M.; and Allen, H.C. “Electric Field Reversal of Na_2SO_4 , $(\text{NH}_4)_2\text{SO}_4$, and Na_2CO_3 relative to CaCl_2 and NaCl at the Air/Aqueous Interface revealed by Phase-Sensitive Sum Frequency” *J. Phys. Chem. Lett.*, **2011**, 2, 2515-2520. Copyright 2011 American Chemical Society.

- **From www.acs.org** – *Reuse/Republication of the Entire Work in Theses or Collections: Authors may reuse all or part of the Submitted, Accepted or*

Published Work in a thesis or dissertation that the author writes and is required to submit to satisfy the criteria of degree-granting institutions.

- RightsLink permissions are the same as Chapter 2.

11/4/13 RightsLink® by Copyright Clearance Center

Copyright Clearance Center
ACS Publications
high quality. high impact.

Electric Field Reversal of Na₂SO₄, (NH₄)₂SO₄, and Na₂CO₃ Relative to CaCl₂ and NaCl at the Air/Aqueous Interface Revealed by Heterodyne Detected Phase-Sensitive Sum Frequency

Authors: Wei Hua, Aaron M. Jubb, and Heather C. Allen

Publication: Journal of Physical Chemistry Letters

Publisher: American Chemical Society

Date: Oct 1, 2011

Copyright © 2011, American Chemical Society

Home Create Account Help

User ID
Password
 Enable Auto Login
LOGIN
[Forgot Password/User ID?](#)
If you're a copyright.com user, you can login to Rightslink using your copyright.com credentials. Already a Rightslink user or want to learn more?

Quick Price Estimate

Permission for this particular request is granted for print and electronic formats, and translations, at no charge. Figures and tables may be modified. Appropriate credit should be given. Please print this page for your records and provide a copy to your publisher. Requests for up to 4 figures require only this record. Five or more figures will generate a printout of additional terms and conditions. Appropriate credit should read: "Reprinted with permission from {COMPLETE REFERENCE CITATION}. Copyright {YEAR} American Chemical Society." Insert appropriate information in place of the capitalized words.

I would like to... reuse in a Thesis/Dissertation

Requester Type Author (original work)

Portion Full article

Format Print

Will you be translating? No

Select your currency USD - \$

Quick Price Click Quick Price

This service provides permission for reuse only. If you do not have a copy of the article you are using, you may copy and paste the content and reuse according to the terms of your agreement. Please be advised that obtaining the content you license is a separate transaction not involving Rightslink.

QUICK PRICE **CONTINUE**

To request permission for a type of use not listed, please contact [the publisher directly](#).

Copyright © 2013 Copyright Clearance Center, Inc. All Rights Reserved. [Privacy statement](#).
Comments? We would like to hear from you. E-mail us at customercare@copyright.com



RightsLink®

[Home](#)
[Create Account](#)
[Help](#)


High quality. High impact.

Title: Electric Field Reversal of Na₂SO₄, (NH₄)₂SO₄, and Na₂CO₃ Relative to CaCl₂ and NaCl at the Air/Aqueous Interface Revealed by Heterodyne Detected Phase-Sensitive Sum Frequency

Author: Wei Hua, Aaron M. Jubb, and Heather C. Allen

Publication: Journal of Physical Chemistry Letters

Publisher: American Chemical Society

Date: Oct 1, 2011

Copyright © 2011, American Chemical Society

User ID

Password

Enable Auto Login

[LOGIN](#)

[Forgot Password/User ID?](#)

If you're a copyright.com user, you can login to RightsLink using your copyright.com credentials. Already a RightsLink user or want to [learn more?](#)

PERMISSION/LICENSE IS GRANTED FOR YOUR ORDER AT NO CHARGE

This type of permission/license, instead of the standard Terms & Conditions, is sent to you because no fee is being charged for your order. Please note the following:

- Permission is granted for your request in both print and electronic formats, and translations.
- If figures and/or tables were requested, they may be adapted or used in part.
- Please print this page for your records and send a copy of it to your publisher/graduate school
- Appropriate credit for the requested material should be given as follows: "Reprinted (adapted) with permission from (COMPLETE REFERENCE CITATION). Copyright (YEAR) American Chemical Society." Insert appropriate information in place of the capitalized words.
- One-time permission is granted only for the use specified in your request. No additional uses are granted (such as derivative works or other editions). For any other uses, please submit a new request.

[BACK](#)
[CLOSE WINDOW](#)

Copyright © 2013 Copyright Clearance Center, Inc. All Rights Reserved. [Privacy statement.](#)
Comments? We would like to hear from you. E-mail us at customer@copyright.com

Chapter 4: Reproduced in part with permission from Hua, W.; Chen, X.K.; and Allen, H.C. "Phase-Sensitive Sum Frequency Revealing Accommodation of Bicarbonate Ions, and Charge Separation of Sodium and Carbonate Ions within the Air/Water Interface" *J. Phys. Chem. A*, **2011**, 115, 6233-6238. Copyright 2011 American Chemical Society.

- From www.acs.org – *Reuse/Republication of the Entire Work in Theses or Collections: Authors may reuse all or part of the Submitted, Accepted or Published Work in a thesis or dissertation that the author writes and is required to submit to satisfy the criteria of degree-granting institutions.*
- RightsLink permissions provided below.

11/1/13 RightsLink® by Copyright Clearance Center

Copyright Clearance Center **RightsLink®** Home Create Account Help

ACS Publications **Title:** Phase-Sensitive Sum Frequency Revealing Accommodation of Bicarbonate Ions, and Charge Separation of Sodium and Carbonate Ions within the Air/Water Interface

Author: Wei Hua, Xiangke Chen, and Heather C. Allen

Publication: The Journal of Physical Chemistry A

Publisher: American Chemical Society

Date: Jun 1, 2011
Copyright © 2011, American Chemical Society

User ID
Password
 Enable Auto Login
LOGIN
[Forgot Password/Username ID?](#)
If you're a copyright.com user, you can login to RightsLink using your copyright.com credentials. Already a RightsLink user or want to learn more?

Quick Price Estimate

Permission for this particular request is granted for print and electronic formats, and translations, at no charge. Figures and tables may be modified. Appropriate credit should be given. Please print this page for your records and provide a copy to your publisher. Requests for up to 4 figures require only this record. Five or more figures will generate a printout of additional terms and conditions. Appropriate credit should read: "Reprinted with permission from (COMPLETE REFERENCE CITATION). Copyright (YEAR) American Chemical Society." Insert appropriate information in place of the capitalized words.

I would like to... reuse in a Thesis/Dissertation

Requestor Type Author (original work)

Portion Full article

Format Print

Will you be translating? No

Select your currency USD - \$

Quick Price Click Quick Price

This service provides permission for reuse only. If you do not have a copy of the article you are using, you may copy and paste the content and reuse according to the terms of your agreement. Please be advised that obtaining the content you license is a separate transaction not involving Rightslink.

QUICK PRICE **CONTINUE**

To request permission for a type of use not listed, please contact [the publisher](#) directly.

Copyright © 2013 Copyright Clearance Center, Inc. All Rights Reserved. [Privacy statement](#). Comments? We would like to hear from you. E-mail us at customerservice@copyright.com



RightsLink®

[Home](#)
[Create Account](#)
[Help](#)

ACS Publications
High quality. High impact.

Title: Phase-Sensitive Sum Frequency Revealing Accommodation of Bicarbonate Ions, and Charge Separation of Sodium and Carbonate Ions within the Air/Water Interface

Author: Wei Hua, Xiangke Chen, and Heather C. Allen

Publication: The Journal of Physical Chemistry A

Publisher: American Chemical Society

Date: Jun 1, 2011

Copyright © 2011, American Chemical Society

User ID

Password

Enable Auto Login

[Forgot Password/User ID?](#)

If you're a copyright.com user, you can login to RightsLink using your copyright.com credentials. Already a RightsLink user or want to [learn more?](#)

PERMISSION/LICENSE IS GRANTED FOR YOUR ORDER AT NO CHARGE

This type of permission/license, instead of the standard Terms & Conditions, is sent to you because no fee is being charged for your order. Please note the following:

- Permission is granted for your request in both print and electronic formats, and translations.
- If figures and/or tables were requested, they may be adapted or used in part.
- Please print this page for your records and send a copy of it to your publisher/graduate school
- Appropriate credit for the requested material should be given as follows: "Reprinted (adapted) with permission from (COMPLETE REFERENCE CITATION). Copyright (YEAR) American Chemical Society." Insert appropriate information in place of the capitalized words.
- One-time permission is granted only for the use specified in your request. No additional uses are granted (such as derivative works or other editions). For any other uses, please submit a new request.

Copyright © 2013 Copyright Clearance Center, Inc. All Rights Reserved. [Privacy statement.](#)
 Comments? We would like to hear from you. E-mail us at customercare@copyright.com

Chapter 5: Reproduced in part with permission from Hua, W; Jubb, A.M.; and Allen, H.C. "Electric Field Reversal of Na₂SO₄, (NH₄)₂SO₄, and Na₂CO₃ relative to CaCl₂ and NaCl at the Air/Aqueous Interface revealed by Phase-Sensitive Sum Frequency" *J. Phys. Chem. Lett.*, **2011**, 2, 2515-2520. Copyright 2011 American Chemical Society.

- **From www.acs.org** – *Reuse/Republication of the Entire Work in Theses or Collections: Authors may reuse all or part of the Submitted, Accepted or Published Work in a thesis or dissertation that the author writes and is required to submit to satisfy the criteria of degree-granting institutions.*
- RightsLink permissions are the same as Chapter 2.

Chapter 6:

Section 6.1: Reproduced in part with permission from Hua, W.; Verreault, D; Adams, E.M.; Huang, Z.S.; and Allen, H.C. “Impact of Salt Purity on Interfacial Water Organization Revealed by Conventional and Heterodyne-Detected Vibrational Sum Frequency Generation Spectroscopy” *J. Phys. Chem. C*, **2013**, 117, 19577-19585. Copyright 2013 American Chemical Society.

- **From www.acs.org** – *Reuse/Republication of the Entire Work in Theses or Collections: Authors may reuse all or part of the Submitted, Accepted or Published Work in a thesis or dissertation that the author writes and is required to submit to satisfy the criteria of degree-granting institutions.*
- RightsLink permissions are the same provided below.

Section 6.2: Reproduced in part with permission from Huang, Z.S.; Hua, W.; Verreault, D; and Allen, H.C. “Influence of Salt Purity on Na⁺ and Palmitic Acid Interactions” *J. Phys. Chem. A*, Accepted – In Press. Copyright 2013 American Chemical Society.



RightsLink®

[Home](#)
[Create Account](#)
[Help](#)

ACS Publications Titles
High quality. High impact.

Title: Impact of Salt Purity on Interfacial Water Organization Revealed by Conventional and Heterodyne-Detected Vibrational Sum Frequency Generation Spectroscopy

Author: Wei Hua, Dominique Verreault, Ellen M. Adams, Zishuai Huang, and Heather C. Allen

Publication: The Journal of Physical Chemistry C

Publisher: American Chemical Society

Date: Sep 1, 2013

Copyright © 2013, American Chemical Society

User ID

Password

Enable Auto Login

[Forgot Password/User ID?](#)

If you're a copyright.com user, you can login to Rightslink using your copyright.com credentials. Already a Rightslink user or want to learn more?

Quick Price Estimate

Permission for this particular request is granted for print and electronic formats, and translations, at no charge. Figures and tables may be modified. Appropriate credit should be given. Please print this page for your records and provide a copy to your publisher. Requests for up to 4 figures require only this record. Five or more figures will generate a printout of additional terms and conditions. Appropriate credit should read: "Reprinted with permission from {COMPLETE REFERENCE CITATION}. Copyright {YEAR} American Chemical Society." Insert appropriate information in place of the capitalized words.

I would like to...	reuse in a Thesis/Dissertation	This service provides permission for reuse only. If you do not have a copy of the article you are using, you may copy and paste the content and reuse according to the terms of your agreement. Please be advised that obtaining the content you license is a separate transaction not involving Rightslink.
Requestor Type	Author (original work)	
Portion	50% or more of original article	
Format	Print	
Select your currency	USD - \$	
Quick Price	Click Quick Price	
<input type="button" value="QUICK PRICE"/> <input type="button" value="CONTINUE"/>		

To request permission for a type of use not listed, please contact [the publisher directly](#).

Copyright © 2013 Copyright Clearance Center, Inc. All Rights Reserved. [Privacy statement](#).
 Comments? We would like to hear from you. E-mail us at customerservice@copyright.com.



RightsLink®

[Home](#)
[Create Account](#)
[Help](#)


ACS Publications
High quality. High impact.

Title: Impact of Salt Purity on Interfacial Water Organization Revealed by Conventional and Heterodyne-Detected Vibrational Sum Frequency Generation Spectroscopy

Author: Wei Hua, Dominique Verreault, Ellen M. Adams, Zishuai Huang, and Heather C. Allen

Publication: The Journal of Physical Chemistry C

Publisher: American Chemical Society

Date: Sep 1, 2013

Copyright © 2013, American Chemical Society

User ID

Password

Enable Auto Login

[Forgot Password/User ID?](#)

If you're a copyright.com user, you can login to RightsLink using your copyright.com credentials. Already a RightsLink user or want to [learn more?](#)

PERMISSION/LICENSE IS GRANTED FOR YOUR ORDER AT NO CHARGE

This type of permission/license, instead of the standard Terms & Conditions, is sent to you because no fee is being charged for your order. Please note the following:

- Permission is granted for your request in both print and electronic formats, and translations.
- If figures and/or tables were requested, they may be adapted or used in part.
- Please print this page for your records and send a copy of it to your publisher/graduate school
- Appropriate credit for the requested material should be given as follows: "Reprinted (adapted) with permission from (COMPLETE REFERENCE CITATION). Copyright (YEAR) American Chemical Society." Insert appropriate information in place of the capitalized words.
- One-time permission is granted only for the use specified in your request. No additional uses are granted (such as derivative works or other editions). For any other uses, please submit a new request.

[BACK](#)
[CLOSE WINDOW](#)

Copyright © 2013 [Copyright Clearance Center, Inc.](#) All Rights Reserved. [Privacy statement.](#)
Comments? We would like to hear from you. E-mail us at customer@copyright.com

Chapter 7: Reproduced in part with permission from Hua, W.; Verreault, D.; and Allen, H.C. "Surface Prevalence of Perchlorate Anions at the Air/Aqueous Interface" *J. Phys. Chem. Lett.*, Accepted. Copyright 2013 American Chemical Society.

Chapter 8: No previously published material.

Chapter 9: No previously published material.

Chapter 10: No previously published material.